7
CHAPTER 7
SSC MODEL: SEISMOTECTONIC ZONES BRANCH

As discussed in Section 4.2.1, the conceptual framework for assessing the CEUS SSC model is characterized by two alternative branches of the master logic tree: the Mmax zones branch and the seismotectonic zones branch. The seismotectonic zones branch subdivides the CEUS SSC region according to differences in the seismic source assessment criteria described in Section 4.1.3.3. A common element of both the Mmax zones and the seismotectonic zones branches is the RLME sources. Because the paleoearthquake data that indicate the presence, location, and size of the RLMEs are essentially independent from data used to assess seismotectonic sources, the RLME branch is present in both models. The seismotectonic zones approach allows the incorporation of additional information related to the characteristics of future earthquakes. Therefore, this approach is assessed a higher weight than the Mmax zones approach in the master logic tree, as discussed in detail in Section 4.2.1. An overview of the factors used to identify and characterize the seismotectonic zones is given in Sections 7.1 and 7.2, followed by a detailed discussion of each of these zones in Section 7.3.

7.1 Approaches and Data Used to Define Seismotectonic Zones

The conceptual basis for the seismotectonic zones branch of the master logic tree is that regional differences in characteristics related to recurrence rates, Mmax, future earthquake characteristics, and/or the probability of activity of tectonic features are best addressed by identifying a source zone (see Section 4.1.3.3). Likewise, the regional differences in these characteristics provide the bases for defining individual seismotectonic zones. Although the recurrence rates within the zones are allowed to vary according to the smoothing of observed seismicity, the other characteristics are assumed to be uniform within the zone. For example, a seismotectonic zone may possess characteristics that would lead to a different Mmax than adjacent zones, including a different prior distribution or different maximum observed earthquake. A seismotectonic zone might also be characterized by earthquakes resulting from reverse fault displacement, while adjacent zones might be characterized by larger components of strike-slip displacement. Likewise, a seismotectonic zone might best be characterized as having thicker seismogenic crust than adjacent zones. A seismotectonic zone may also be defined if tectonic features or groups of tectonic features are identified that have a significant probability of activity, but as discussed in Section 4.1.3.3, such features have not been identified on a regional basis as part of this study.

The geometries of the seismotectonic zones are largely a function of the major tectonic domains within which a given SSC characteristic is assessed to be relatively uniform (Figures 7.1-1 through 7.1-4) and different from the characteristics of adjacent zones. In most cases, the characteristics that define the zones are expected differences in future earthquake characteristics

such as rupture orientation, depth distribution, and style of faulting. A summary of the future earthquake characteristics for each seismotectonic zone is given in Table 5.4-2. The boundaries of the seismotectonic zones are derived from interpretations in the literature of regional geophysical, geologic, and tectonic data sets. In addition, data developed as part of the CEUS SSC Project, such as magnetic and gravity data (Figures 7.1-5 and 7.1-6), were examined for defining the zones. As discussed in Section 5.4.7, zone boundaries are defined as being either "leaky" or "strict" with respect to whether future earthquake ruptures are assessed to extend across a zone boundary.

As described in Section 4.1.2.2 and included in Appendices C and D, Data Evaluation and Data Summary tables have been developed for each of the seismotectonic zones. These tables are an important resource for the reader, as they supplement the discussions of each zone given in this section. The Data Summary tables specify the various data sets that were reviewed and considered by the TI Team during the course of its assessments. The Data Evaluation tables provide an evaluation of the quality of the data and the degree of reliance placed by the team on the data during the assessment process. The reader is advised to consult both tables when reviewing the descriptions to better understand how the available data were applied to define the characteristics of each seismotectonic zone. Tables developed for RLME sources are also relevant for some of the seismotectonic zones. Table 7.1-1 shows which table numbers are associated with each of the seismotectonic zones.

To illustrate the definition of a seismotectonic zone by way of a specific example, the St. Lawrence Rift (SLR) seismotectonic zone (discussed in Section 7.3.1 and shown on Figures 7.1-1 and 7.3.1-1) is outlined by the region assessed to be a terrane of known and inferred northeast-trending normal faults that formed parallel to the passive margin of Laurentia during the late Proterozoic–early Paleozoic opening of the Iapetus Ocean and underwent continental extension during the most recent extensional tectonic episode in the Mesozoic. The data considered in the identification and characterization of this zone are presented in Data Summary Table D-7.3.1 (Appendix D), and the data evaluated to provide a basis for characterizing the zone are given in Data Evaluation Table C-7.3.1 (Appendix C). The detailed assessments of the available data for the SLR zone are given in Section 7.3.1, including the basis for identifying the SLR as a seismotectonic zone and the location of the zone boundary (Section 7.3.1.2). The set of future earthquake characteristics for the SLR zone is given in Table 5.4-2. This zone is adjacent to the Northern Appalachian zone to the south and differs from it in the expected strikes of future ruptures and in the thickness of the seismogenic crust. The boundaries to the SLR zone are assessed to be "leaky," such that future earthquake epicenters would lie within the zone, but ruptures, the strike of which is given in Table 5.4-2 and the length and width of which are magnitude-related (as discussed in Section 5.4), could extend beyond the zone boundaries.

Given the regional nature of the CEUS SSC model and the need for it to be reviewed for possible local refinement for site-specific application (see discussion in Section 4.1.3), the sensitivity to the exact location of seismotectonic zone boundaries is not expected to be large. Therefore, explicit quantification of the uncertainty in zone boundary location is included in the model for only a couple of cases, such as the western boundary of the Paleozoic Extended Crust (PEZ narrow or wide) and the inclusion or exclusion of the Rough Creek graben in the Reelfoot Rift seismotectonic zone (RR-RCG).

It is important to note that, in the discussion of the seismotectonic zones, the TI Team was well aware of previous SSC models developed for the CEUS through the years for both site-specific and regional hazard evaluations. Some of these studies relied on different approaches and criteria for identifying seismic source zones from those used in this study (Section 4.1.3). As a result, it may appear that some of the "tried-and-true" approaches to drawing seismic source zone boundaries have been ignored or not considered in the CEUS SSC Project. For example, the spatial distribution of seismicity is decidedly non-uniform in the CEUS (Figure 7.1-7), and a common approach to identifying seismic sources in some past studies was to enclose zones of concentrated seismicity. Specific examples include the Central Virginia seismic zone and the Eastern Tennessee seismic zone (ETSZ). Acknowledging that these zones of elevated seismicity in the historical period of observation likely represent zones of future elevated rates, the method of implementing this concept in the CEUS SSC model is spatial smoothing of *a*- and *b*-values, rather than drawing source zone boundaries. Further, both the Mmax zones and the seismotectonic zones branches of the master logic tree provide for such smoothing regardless of where source zone boundaries are drawn. Therefore, given that some seismotectonic zones show spatial variations in observed rates of past earthquakes (Figure 7.1-8), these variations are accounted for in the smoothing model.

Another common characteristic of previous SSC models is identifying prominent tectonic features as potential seismic source zones. Examples include the Midcontinent rift, which displays strong gravity and magnetic anomalies, or the numerous Mesozoic extensional faults and basins along the eastern margin of the CEUS. In a general sense, the seismotectonic zones accommodate the regional tectonic domains within which these types of tectonic features occur, provided that they meet the criteria for identifying a seismic source (Section 4.1.3.3). The SLR is defined by a different prior distribution for estimating Mmax from that of some adjacent regions, and the zone encloses the major Paleozoic extensional features of the St. Lawrence rift system. However, the zone boundary is drawn not because it is a tectonic feature, but because of expected differences with adjacent zones in Mmax, as well as other future earthquake characteristics (e.g., style of faulting, rupture orientation, thickness of seismogenic crust).

In contrast, features such as the Midcontinent rift are not assessed to lead to different Mmax or future earthquake characteristics from adjacent regions, nor does the feature have a high probability of activity ($P_a > 0.5$) that could lead to a significant potential hazard. Therefore, using the hazard-informed approach discussed in Section 4.1.3, these types of tectonic features are not called out in the SSC model. Other types of tectonic features that are not identified explicitly are faults and other features that might have local significance, unless there is a clear consensus within the technical community that the feature should be assessed a high P_a and considered seismogenic. For example, recent and ongoing studies of faults in the vicinity of the ETSZ postulate that these faults are related to the zone either as causative faults or as secondary faults resulting from displacement on faults at depth (see Section 7.3.4). However, these postulated associations are judged to lack definitive support for use in this SSC model as a result of the preliminary nature of the studies. Even the Charleston RLME source characterization does not rely on an individual fault or faults as seismic sources, given the lack of definitive geologic evidence for young faulting in the Charleston area. However, the range of hypotheses for the location of the Charleston source fault is encompassed by the source zones as they are currently defined.

7.2 RLME Sources in the Seismotectonic Zones Branch

The RLME sources are described in Section 6.1 under the Mmax zones branch of the master logic tree. Because the RLME sources are defined and characterized by independent paleoseismic data that are not affected by the presence or absence of seismotectonic zones or Mmax zones, they are assumed to exist in exactly the same manner as on the Mmax zones branch of the master logic tree.

7.3 Seismotectonic Source Zones

The logic tree structure for the seismotectonic source zones is shown on Figure 7.3-1. The first two levels of the logic tree address the basic source zoneation. The first level addresses the location of the boundary between the PEZ and the Midcontinent-Craton (MidC) zone. Characterization of the uncertainty in this boundary parallels the uncertainty in the MESE/NMESE boundary for the Mmax zones and arises from uncertainty in characterizing the western extent of Mesozoic extension. The second level of the logic tree addresses the uncertainty in the eastern extent of the RR zone—whether or not it includes the Rough Creek graben. These two logic tree branches lead to the four alternative seismotectonic zonation configurations shown on Figures 7.1-1 through 7.1-4.

The next level of the logic tree addresses uncertainty in the choice of weights on magnitude ranges used in computing the seismicity rates. These are discussed in Section 7.5.

Descriptions of the individual seismotectonic zones are presented below.

7.3.1 St. Lawrence Rift Zone (SLR)

The SLR seismotectonic zone consists of crust initially rifted during the late Proterozoic–early Paleozoic opening of the Iapetus Ocean; faults within the rifted crust were subsequently reactivated during the Paleozoic and Mesozoic. This seismotectonic zone is characterized by elevated rates of seismicity and contains significant historical earthquakes, including the 1935 Timiskaming **M** 6.2 (E[**M**] 6.02)[1] earthquake, the 1988 Saguenay **M** 5.9 (E[**M**] 5.84) earthquake, and historical earthquakes from Charlevoix (Figure 7.3.1-1). Historical earthquakes and paleoseismic evidence suggest that the entire rift system is capable of generating moderate- to large-magnitude earthquakes. Compressional reactivation of favorably oriented Iapetan faults has been postulated as the causal mechanism for several seismically active regions in eastern North America, including the SLR, Charlevoix, and the lower St. Lawrence Valley in Quebec, Canada (Adams and Basham, 1991). As the result of an analysis of earthquakes in stable continental regions (SCRs) worldwide, Johnston et al. (1994) determined that zones of rifted crust in SCRs correlate directly with increased earthquake activity when compared to zones of nonrifted SCRs in regard to number and maximum magnitude of earthquakes. The seismic source

[1] Magnitudes are reported in magnitude scale as designated in the cited publication. E[**M**] denotes the value of the expected moment magnitude listed in the CEUS SSC catalog for an earthquake. It is reported to two decimal places to indicate that it is a calculated value. See the discussion in Section 3.3.1.

characterization of the SLR seismotectonic zone is based on a review of published material that is summarized in the Data Summary table for the SLR zone (Appendix Table D-7.3.1). Explicit references and data that were used as the basis for source characteristics of SLR are identified in the Data Evaluation table (Appendix Table C-7.3.1).

7.3.1.1 Background

7.3.1.1.1 Iapetan Rifting

Breakup of the Mesoproterozoic supercontinent of Rodinia occurred as diachronous rifting along the margins of Laurentia. Rifting began on the western margin of Laurentia between 780 and 680 Ma, and continued to the eastern margin between 620 and 550 Ma from Newfoundland into the southern Appalachian Mountains (Whitmeyer and Karlstrom, 2007), resulting in the opening of the Iapetus Ocean (Faill, 1997a). Kumarapeli (1985) proposed that a mantle plume initiated Iapetan rifting along the Sutton Mountains triple junction, resulting in the development of the St. Lawrence valley system and aulacogens of the Ottawa-Bonnechere and Saguenay grabens (Kumarapeli and Saull, 1966; Kumarapeli, 1985, 1993). Based on geochronological studies of the Sutton Mountains volcanics, Kumarapeli (1993) established the following sequence: (1) rifting initiated at 590 Ma and continued for 35 Myr; (2) rifting ceased about 554 Ma after an outburst of alkaline to transitional basalts at the Sutton Mountains triple junction; and (3) a period of rift-facies clastic sedimentation followed until the rift-drift transition at 550 Ma. Rift-related lava flows (Figure 7.3.1-2) are observed along the entire eastern margin of Laurentia now preserved in Appalachian thrust sheets, including the Skinner Cove Formation of western Newfoundland (McCausland and Hodych, 1998); the Mont St-Anselme Formation and Lac Matapédia flows of Quebec (Hodych and Cox, 2007); the Tibbit Hill Formation of Vermont and Quebec (Kumarapeli et al., 1988); the Pinney Hollow metarhyolite of central Vermont (Walsh and Aleinikoff, 1999); the Caldwell Group lavas of southern Quebec (Bedard and Stevenson, 1999); and the Nassau Formation of eastern New York and western Massachusetts (Ratcliffe, 1987). Major and trace element studies of the lava rocks confirm a mantle source consistent with plume activity (St. Seymour and Kumarapeli, 1995; Abdel-Rahman and Kumarapeli, 1998). Puffer (2002) compiled a database of high field-strength elements for late Neoproterozoic to early Paleozoic flood basalts, revealing that superplume activity peaked at 550 Ma at the Sutton Mountains triple junction. The 564 Ma Catoctin Formation of southeastern Pennsylvania and central Virginia and the 758 Ma Mount Rogers Formation of southwestern Virginia and North Carolina and Tennessee record a more complex history of Iapetan rifting in the southeastern United States (Aleinikoff et al., 1995) and are discussed in Section 7.3.4.1.

Iapetan rifting is also recorded by widespread dikes and intrusions throughout the SLR and the Ottawa-Bonnechere and Saguenay aulacogens (Figure 7.3.1-2). The Grenville dike swarm of the Ottawa-Bonnechere graben (Kamo et al., 1995) and the Adirondack dike swarm of New York (Abdel-Rahman and Kumarapeli, 1998) are coeval with the 590 Ma Sutton Mountains volcanism, implying that the dike swarms were emplaced within a relatively short time span at the onset of rifting. Alkalic intrusions within the Ottawa-Bonnechere graben yielding an early Cambrian age of approximately 565 Ma and syn-rift carbonatite complexes of the Saguenay graben dated at 565 Ma support the view that these aulacogens formed as part of a single event (Kumarapeli, 1985). This interpretation is supported by subsequent ages of the 577 Ma Callander

Complex near Lake Nipissing in the western end of the Ottawa-Bonnechere graben (Kamo et al., 1995) and the 564 Ma Mt. Rigaud syenite of Quebec (McCausland and Hodych, 1998). Higgins and van Breemen (1998) attribute the 565 ± 4 Ma Sept Iles layered mafic intrusion of the Gulf of St. Lawrence to emplacement of plume melts along rift faults that developed after emplacement of dike swarms. Additional details are provided in Appendix Table D-7.3.1. This rifted margin is expressed as promontories and embayments defined by northeast-striking normal faults and northwest-striking transform faults along the margins of Laurentia (Thomas, 1991; 2006; Lavoie et al., 2003).

In southeastern Canada, Iapetan rifting is expressed along the St. Lawrence River valley (Section 7.3.1.1.2) and associated with the Ottawa (Section 7.3.1.1.4) and Saguenay (Section 7.3.1.1.5) failed arms, or aulacogens, that formed transverse to the faulted edge of the ancient continental margin (Adams et al., 1995). These aulacogens are defined by zones of approximately east-west-trending normal faults that extend into the Canadian Shield and have not undergone significant total extension (Adams et al., 1995). Large-magnitude earthquakes located within the Charlevoix area (Figure 6.1.1-1) are characterized as part of the Charlevoix RLME seismic source zone (Sections 6.1.1 and 7.3.1.1.3), whereas the moderate-magnitude seismicity at Charlevoix is characterized as part of the SLR seismotectonic zone. Adams et al. (1995) argue that seismicity clusters observed throughout the Iapetan margin are a temporal artifact and characterize the possible future activity of the region by incorporating these clusters into a regional zone. The following subsections address the geologic, geophysical, and seismic characteristics of the crust within the SLR seismotectonic zone, which exhibits variable rates of seismicity.

7.3.1.1.2 St. Lawrence Rift

The late Proterozoic–early Paleozoic St-Laurent fault, which is attributed to opening of the Iapetus Ocean, forms a northeast-trending, southeast-dipping half graben lying along the main axis of the SLR system (Tremblay and Lemieux, 2001). High-resolution seismic profiles in the St. Lawrence estuary indicate that the Laurentian Channel trough transitions from a half graben to a graben structure from southwest to northeast (Tremblay et al., 2003). The St-Laurent fault trends N20 to 50E, dips 60–70 degrees to the southeast (Tremblay and Lemieux, 2001; Tremblay et al., 2003), and is crosscut by the Cap-Tourmente fault at Cap-Tourmente, Quebec. West of Cap-Tourmente, the Montmorency Falls fault occupies the same structural position as the St-Laurent fault, suggesting that they formed as en echelon faults oblique to the axis of the SLR (Tremblay and Lemieux, 2001). The Cap-Tourmente fault possibly represents a transfer fault acting as an oblique relay structure between two longitudinal normal faults (Tremblay and Lemieux, 2001). St. Julien and Hubert (1975) observe that east-west and N30E steeply southeast-dipping normal faults active between late Precambrian and the Late Ordovician times cut Cambrian and Ordovician platform rocks in southwestern Quebec. Results of the Quebec-Maine seismic reflection surveys provide evidence of closely spaced en echelon normal faults with displacements between 200 and 1,000 m (656 and 3,280 ft.), interpreted as fossilized Iapetan growth faults below the Appalachian detachment surface (Spencer et al., 1989). These normal faults are imaged on the northwestern portion of seismic line QM2001 northwest of the Baie-Vert–Brompton line (Spencer et al., 1989).

Multiple phases of reactivation of the SLR are in evidence. The St-Laurent fault crosses the Devonian Charlevoix impact crater without major deflection, suggesting post-impact reactivation (Lemieux et al., 2003). The St-Laurent fault influenced the deposition of Ordovician sediments during late stages of the Taconian orogeny by syndepositional faulting, preserved as major lateral thickness variations within these platform rocks, presence of slump deformation in almost all stratigraphic units, preservation of pseudotachylyte within synsedimentary breccias, and occurrence of fault breccia clasts (Lemieux et al., 2003). Truncation of Devonian impact-related structures by northeast-southwest and northwest-southeast fault sets is consistent with Mesozoic fault reactivation due to rifting of the North Atlantic region (Lemieux et al., 2003). Tremblay et al. (2003) attribute some fault throw along the SLR fault system to opening of the Central Atlantic in the Jurassic and/or seafloor spreading of the North Atlantic during the Cretaceous. Faults located in Quebec near Montreal, where the southern portion of the SLR approaches the Ottawa-Bonnechere graben, provide evidence for northwest-southeast extension associated with the opening of the Iapetus Ocean; west-northwest/east-southeast compression followed by minor north-northwest compression associated with Appalachian thrusting; northeast-southwest and north-northwest/south-southeast extension associated with the opening of the Atlantic-Labrador Ocean; and northeast-southwest compression postdating these events (Rocher et al., 2003).

In addition to large-magnitude historical earthquakes located within the Charlevoix RLME source area (Sections 6.1.1 and 7.3.1.1.3), the September 16, 1732, modified Mercalli intensity (MMI) VIII (E[**M**] 6.25) Montreal earthquake (Leblanc, 1981) and the September 5, 1944, **M** 5.8 (E[**M**] 5.71) Cornwall-Massena earthquake (Bent, 1996b) are also located along the main axis of the SLR.

7.3.1.1.3 Charlevoix RLME Source

Adams and Basham (1991) attribute seismicity of the SLR system to earthquakes occurring on rift structures in the regional stress field of southeast-to-east compression, recognizing that a Devonian impact structure also exists in the general area and may be related to the spatial concentration of seismicity in the Charlevoix area. Two major fault orientations (N40-70W and N20-40E) are found outside the Charlevoix impact zone, with minor fault sets trending east to west to N80W and north to south to N20E (Lemieux et al., 2003). Lemieux et al. (2003) observed the largest variation in fault trends within the central portion of the impact crater, which still displayed a dominant northeast-southwest orientation. Lamontagne and Ranalli (1997) attribute large-magnitude Charlevoix earthquakes to reactivation of rift faults in response to the regional stress field. They interpret variations in orientation and style of faulting for small-magnitude earthquakes to reactivation of impact-related faults and fractures in response to local stress and/or strength conditions. In another paper, Lamontagne and Ranalli (1996) attribute earthquakes in the Charlevoix seismic zone to some or all of the following circumstances:

- Fracturing above the brittle-ductile transition at depths of at least 25 km (15.5 mi.).
- High pore-fluid pressure at mid- to lower crustal depths where hydration reactions are not favored.
- Low coefficients of friction related to highly fractured zones at depth, as opposed to thick fault gouges made of clay minerals.

Results of two-dimensional stress modeling account for the spatial pattern of observed seismicity as stress concentration due to the interaction of the crater (local zone of weakness) and rift faults (large-scale weak zone; Baird et al., 2009). Smaller-magnitude, more frequent seismicity occurs within the impact crater, and infrequent larger-magnitude earthquakes are localized along rift faults (Baird et al., 2009). Tuttle and Atkinson (2010) observed paleoliquefaction features in the Charlevoix area—but not to the south in Trois Rivières, Quebec—that suggest stationarity of large-magnitude earthquakes within the Charlevoix RLME seismic source zone. Although the February 5, 1663, **M** 7 (E[**M**] 7.00) and October 20, 1870, **M** 6.5 (E[**M**] 6.55) earthquakes are modeled as RLME in Section 6.1.1, the December 6, 1791, **M** 5.8 (E[**M**] 5.50); October 17, 1860, **M** 6 (E[**M**] 6.08); and March 1, 1925, **M** 6.3 (E[**M**] 6.18) earthquakes do not meet the RLME criterion of exceeding **M** 6.5 and are thus assigned to the SLR seismotectonic zone. The Charlevoix Data Summary and Data Evaluation tables (Tables D-6.1.1 and C-6.1.1) present additional details about the Charlevoix RLME zone.

7.3.1.1.4 Ottawa-Bonnechere Graben

The Ottawa-Bonnechere graben extends for approximately 700 km (435 mi.) into the Canadian Shield (Kumarapeli and Saull, 1966; Kumarapeli, 1985, 1993) from the Sutton Mountains salient of the central Appalachian orogen. The graben is inferred to extend eastward beneath the Appalachian thrust sheets for approximately 30 km (19 mi.) by Kumarapeli (1993), based on observations that the Early Cretaceous Monteregian intrusions reported by Foland et al. (1986) are emplaced along the graben faults. Alkalic intrusions within the Ottawa-Bonnechere graben yield an early Cambrian age of approximately 565 Ma (Kumarapeli, 1985). A tholeiitic diabase dike swarm associated with the graben is dated at 590 Ma, implying that the initiation of rifting was a late Proterozoic event (Kumarapeli, 1985).

The faults defining the Ottawa-Bonnechere graben generally strike west-northwest and offset Silurian strata (Forsyth, 1981). Rimando and Benn (2005) report three periods of faulting in Cambro-Ordovician sedimentary rocks within the eastern end of the Ottawa-Bonnechere graben, near Ottawa, Ontario, Canada, as follows:

- The oldest generation of faults, formed in response to a horizontal maximum principal compressive stress (σ_1) oriented northwest, are kinematically congruent with the compression direction associated with closing of the Iapetus Ocean.
- A second generation of faults, which indicate a west-northwest-oriented σ_1, coincide with emplacement of Cretaceous carbonatite dikes.
- A third generation of faults indicate a southwest-oriented σ_1 consistent with the post-Cretaceous stress field for eastern North America.

The Ottawa-Bonnechere graben and associated basement faults acted as localized zones of weakness in the early stage of Cretaceous extension, resulting in reorientation of the regional stress field and formation of the localized zone of north-south-directed extension (Faure et al., 1996b). Results of the 1982 Canadian Consortium for Crustal Reconnaissance Using Seismic Techniques (COCRUST) long-range seismic refraction experiment show a sharp, step-like displacement of the Moho beneath the south shoulder of the Ottawa-Bonnechere graben,

confirming the deep-seated nature of the faults associated with the graben and penetration of mantle melts into the crust (Mereu et al., 1986). In addition, the COCRUST surveys show a poorly defined Moho at unusually shallow depths beneath the graben (Mereu et al., 1986).

Adams and Basham (1991) recognized two distinct bands of seismicity within the Western Quebec seismic zone. They attribute the west-northwest-trending band of seismicity along the Ottawa River between Ottawa, Ontario, and Lake Timiskaming to rift faults of the Ottawa-Bonechere graben and the more northern band to the Great Meteor hotspot (Section 7.3.2). The second band of seismicity in the Western Quebec seismic zone trends north-northwest, extends from Montreal to the Baskatong Reservoir, and is attributed to crustal fracturing associated with the passage of a Cretaceous hot spot track as discussed in Section 7.3.3. Adams et al. (1995) consider the 1935 **M** 6.2 (E[**M**] 6.02) Timiskaming earthquake, which occurred at a depth of 10 km (6 mi.) near the Quebec-Ontario border, the paradigm earthquake for the Ottawa-Bonnechere graben. The January 1, 2000, M_N 5.2 (E[**M**] 4.62) Kipawa earthquake is located near the 1935 epicenter and exhibits northwest-southeast-striking reverse faults that may be associated with northwest-trending lineaments under Lake Kipawa that have been interpreted as faults (Bent et al., 2002).

In the western portion of the Ottawa-Bonnechere graben, Doig (1991) interprets two paleoearthquakes based on inferred landslide deposits in lakes located near the epicenter of the 1935 Timiskaming earthquake. As discussed in Section 6.1.1.5, this method of interpreting earthquake-induced landslide deposits cannot distinguish between local small-magnitude earthquakes and distant large-magnitude earthquakes, but these results qualitatively suggest that the Ottawa-Bonnechere graben has experienced recurring moderate-magnitude earthquakes. Aylsworth et al. (2000) attribute widespread landsliding and irregular subsidence along the Ottawa River in the eastern portion of the graben to two paleoearthquakes occurring at about 7,060 and 4,550 BP that could be as large as the 1663 Charlevoix (**M** 7) earthquake (Section 7.3.1.3).

7.3.1.1.5 Saguenay Graben

The Saguenay graben, which also represents a failed arm of the Iapetan passive margin (Kumarapeli, 1985), extends into the Precambrian Canadian Shield for approximately 300 km (186 mi.) northwest from the St. Lawrence Valley. The graben margins are defined by the Lac Tchitogama, Ste-Marguerite River, and Lake Kenogami east-west-striking normal faults (Du Berger et al., 1991). Syn-rift carbonatite complexes dated at 565 Ma suggest an early Cambrian age for the Saguenay graben (Kumarapeli, 1985). Some of the graben-bounding faults offset Ordovician limestone by as much as 500 m (1,640 ft.) and are marked by prominent topographic scarps with 100–300 m (328-984 ft.) of relief (Du Berger et al., 1991). Lavoie et al. (2003) attribute middle to late Cambrian debris flow units preserved in southern Quebec and western Newfoundland to reactivation of the Saguenay graben. Longuépée and Cousineau (2005) interpret the Anse Maranda Formation as sediments deposited in deep subbasins along a narrow shelf south of the Saguenay graben. Roden-Tice, Brandt, and Tremblay (2009) observe apatite fission-track age discontinuities across the Sainte-Marguerite and Lac Kenogami faults, suggesting Late Triassic to Early Jurassic and Middle Jurassic reactivation, respectively, across the faults. Adams et al. (1995) characterized the 1988 Saguenay **M** 5.9 (E[**M**] 5.84) earthquake,

which occurred at a depth of 27 km (17 mi.), as the paradigm earthquake for the Saguenay graben. Prior to this earthquake, seismicity rates for the Saguenay graben were extremely low (Adams et al., 1995). Paleoliquefaction investigations conducted by Tuttle et al. (1990, 1992) and Tuttle (1994) in the Saguenay graben area revealed liquefaction features within 26 km (16 mi.) of the epicenter of the 1988 Saguenay earthquake, and included evidence for an older earthquake of unknown magnitude occurring at AD 1420 ± 200 yr.

Other investigations also provide geologic evidence for repeated earthquakes in Saguenay. Doig (1998) determined a recurrence interval ranging from 350 to 1,000 years based on evidence of earthquake-induced landslide deposits within lakes near the epicenter of the 1988 Saguenay earthquake. As discussed in Sections 6.1.1.5 and 7.3.1.1.4, these observations are difficult to quantitatively incorporate within recurrence calculations because silt layers may be due to nontectonic landslides, and if they are tectonic, these silt layers can be attributed to either local moderate-sized earthquakes or distant large-magnitude earthquakes. These results do, however, suggest that the Saguenay graben has experienced recurring moderate-magnitude earthquakes. Recent work by Locat (2008) places the 1663 **M** 7 earthquake near Saguenay, based on the distribution of largely undated landslide deposits throughout the region and subaqueous mass movements in the St. Lawrence estuary, Saguenay fjord (Syvitski and Schafer, 1996; Urgeles et al., 2002; St-Onge et al., 2004), and nearby lakes. These studies by Doig (1998), Locat (2008), Syvitski and Schafer (1996), Urgeles et al. (2002) and St-Onge et al. (2004) illustrate the role of landsliding, in addition to liquefaction, as a mechanism for recording paleoearthquakes in the region. As discussed in Section 6.1.1.3, better constraints on timing of earthquakes are required for correlating deformation with specific earthquakes and determining location and magnitude of those earthquakes.

7.3.1.1.6 Lower St. Lawrence

Adams et al. (1995) attribute aseismic regions that clearly separate seismicity of the Lower St. Lawrence from that in the Charlevoix area as temporal artifacts, and relate the Lower St. Lawrence cluster of seismicity to a separate seismic source zone, the Bas St. Laurent zone in the GSC H model (Adams et al., 1996; Adams and Halchuk, 2003). Lamontagne et al. (2003) propose that this localized Lower St. Lawrence cluster of seismicity occurs in Precambrian basement where intersecting faults may be weakened by crustal fluids, hydrostatic pressure, or fault gouge, and that emplacement of the Sept-Iles layered igneous complex may have further fractured this portion of crust. Lamontagne et al. (2004) attribute the March 16, 1999, M_N 5.1 (E[**M**] 4.45) Côte-Nord earthquake, whose focal mechanisms exhibited northwest-trending nodal planes to rupture of northwest-striking faults associated with magnetic and gravimetric lineaments, as opposed to northeast-southwest-trending rift faults.

7.3.1.1.7 Adirondack Mountains

Kumarapeli and Saull (1966) interpret fault scarps along the western margin of the Champlain Valley to St. Lawrence rifting. Iapetan normal faults within the Adirondack Mountains occur within the Adirondack dike swarm (Kamo et al., 1995; Figure 7.3.1-2). Kamo et al. (1995) established that the Grenville dike swarm of the Ottawa-Bonnechere graben is coeval with the

590 Ma Sutton Mountains triple junction, and Abdel-Rahman and Kumarapeli (1998) determined that the Adirondack dike swarm of New York is geochemically similar to the Grenville dike swarm, implying that both swarms are coeval and comagmatic with Sutton Mountains volcanism. Focal mechanism interpretations for the April 20, 2002, **M** 5.0 (E[**M**] 4.91) Au Sable Forks, New York, earthquake show reverse faulting consistent with reactivation of a north-south-striking structure (Pierre and Lamontagne, 2004; Seeber et al., 2002). The October 7, 1983, m_b 5.1 (E[**M**] 4.84) Goodnow, New York, earthquake also is related to reverse faulting oriented north-south (Nábělek and Suárez, 1989). North-south-trending structures in the Lake Champlain area include normal faults associated with Iapetan rifting and high-angle reverse faults associated with Taconic compression (Seeber et al., 2002). Roden-Tice et al. (2000) inferred Late Jurassic exhumation of the High Peaks section of the Adirondack Mountains, which continued along the northern, northwestern, and southwestern margins of the Adirondack Mountains into the Cretaceous, with a suggestion of renewed unroofing in the Eocene. This exhumation is thought to have been accommodated by reverse-slip reactivation of north-northeast-trending normal faults (Roden-Tice et al., 2000). Subsequent work by Roden-Tice and Tice (2005) indicates that differential unroofing in the southeastern Adirondack Mountains and central New England may have been accommodated by Late Cretaceous fault reactivation.

7.3.1.2 Basis for Defining Seismotectonic Zone

The SLR seismotectonic zone delineates crust initially rifted during the late Proterozoic–early Paleozoic opening of the Iapetus Ocean and subsequently reactivated during the Mesozoic opening of the Atlantic Ocean, meeting the criterion for separating crust of the SLR on the basis of maximum earthquake magnitude. As discussed in Section 7.3.1.1, although the rates of seismicity vary throughout the rift, moderate- to large-magnitude earthquakes are observed throughout the seismotectonic zone. Previous interpretations of the Iapetan rifted margin (IRM; Wheeler, 1995; Adams et al., 1995) have included crust that is characterized as part of the Northern Appalachian (Section 7.3.3) and Paleozoic Extended Zone (Section 7.3.4) seismotectonic zones. Crust of the SLR seismotectonic zone is distinguished from these two zones on the basis of age, history of reactivation, and earthquake characteristics.

The SLR seismotectonic zone is defined by mantle plume–initiated Iapetan rifting along the Sutton Mountains triple junction (Kumarapeli, 1985, 1993) that resulted in normal faulting along the main axes of the St. Lawrence rift and the Ottawa-Bonnechere and Saguenay grabens (Kumarapeli and Saull, 1966; Kumarapeli, 1985, 1993; Tremblay et al., 2003; Lemieux et al., 2003). The IRM extends south of the SLR and lies buried beneath the Northern and Southern Appalachian Mountains (Wheeler, 1995). Compressional reactivation of favorably oriented Iapetan faults has been postulated as the causal mechanism for several seismically active regions in eastern North America (Adams and Basham, 1991). Adams et al. (1995) observe that seismicity of the IRM is largely expressed as reverse-slip faulting mechanisms in Canada and strike-slip mechanisms in the United States. Faults exposed within the SLR exhibit multiple phases of reactivation, including during the Mesozoic (Tremblay et al., 2003; Lemieux et al., 2003; Rocher et al., 2003; Rimando and Benn, 2005). Faure et al. (2006) observe east-west- and northwest-southeast-oriented extensional stress regions in Quebec based on stress tensor analysis of regional- and mesoscopic-scale faults, which indicate that Mesozoic extension was

widespread and extended at least 400 km (250 mi.) from the Atlantic margin. Apatite fission-track ages from the Adirondack Mountains and New England indicate widespread Mesozoic uplift and erosion that locally display age discontinuities, suggesting reactivation of preexisting structures (Roden-Tice et al., 2000; Roden-Tice and Tice, 2005; Roden-Tice, West, et al., 2009). As presented in Section 7.3.1.1, the presence of moderate- to large-magnitude historical earthquakes and paleoseismic data indicate that the entire rift system is capable of generating moderate to large earthquakes.

7.3.1.3 Basis for Zone Geometry

The geometry for the SLR seismotectonic zone incorporates crust exhibiting evidence of Iapetan rifting, either by faulting or intrusion of rift-related volcanic rocks. The spatial extent of dikes and intrusions is generally larger than graben-bounding normal faults (Figure 7.3.1-2). Therefore, the geometry for SLR is modified from the IRM and Adirondack source zones of the GSC regional model (Adams et al., 1996; Adams and Halchuk, 2003) and the IRM boundary by Wheeler (1995) to incorporate the following data sets. The SLR seismic source zone boundary along the Adirondack Mountains and Ottawa-Bonnechere graben incorporates the Sutton Mountains triple junction, Grenville and Adirondack dike swarms, and Iapetan normal faults as mapped by Kamo et al. (1995).

Mapped locations of Iapetan lava flows (McCausland and Hodych, 1998; Hodych and Cox, 2007; Kumarapeli et al., 1988; Walsh and Aleinikoff, 1999; Bedard and Stevenson, 1999; Ratcliffe, 1987) are preserved within Appalachian thrust sheets and therefore do not provide a reliable eastern boundary for the SLR seismotectonic zone. The eastern boundary of the zone coincides with the Baie Verte–Brompton line of Moench and Aleinikoff (2003) to capture normal growth faulting observed below the Appalachian detachment in the northern Appalachians by Spencer et al. (1989). These boundaries are not well-imaged in potential field data (Figure 7.3.1-3). Du Berger et al. (1991) observed that the 1988 Saguenay earthquake is located outside the Saguenay graben. Therefore, the geometry of this graben is modified from that proposed by Higgins and van Breeman (1998) based on the spatial distribution of small-magnitude earthquakes in the dependent earthquake catalog. The main axis of the SLR seismotectonic zone was drawn to include these small-magnitude earthquakes. The northeastern portion of zone is also truncated beyond the edge of the project boundary.

7.3.1.4 Basis for Zone Mmax

A paleoseismic study conducted by Aylsworth et al. (2000) in the eastern portion of the Ottawa-Bonnechere graben provides evidence for two moderate- to large-magnitude Holocene earthquakes. Landslide deposits occurring in the Leda Clay, which was deposited in the Champlain Sea, have normalized radiocarbon ages between 1,870 and 5,130 yr BP, with the majority of ages clustering at 4,550 yr BP. This age is significantly younger than paleochannel abandonment, so these landslides deposits are attributed to a paleoearthquake. Disturbed, hummocky terrain exhibiting local relief between 3 and 8 m (9.8 and 26 ft.) is located east of these landslide deposits within the flat erosional plane of the Ottawa River, and is likely related to landsliding. Faulted, upturned, and warped sediment is also exposed for 500 m (1,640 ft.)

along a ditch, and nearby excavations contain sand lenses, a small flame structure, and a sand boil feature. Large patches of sand occur randomly on the surface. All these features have a radiocarbon age of 7,060 ± 80 yr BP.

Based on analogy to the 1663 Charlevoix earthquake, these earthquakes were estimated to represent a magnitude of **M** ≥ 7 (Aylsworth et al., 2000). Subsequent trenching by Aylsworth and Lawrence (2003) documented lateral spreading and deformation of sediments and surface subsidence within a deep bedrock basin (180 m [590 ft.]) at 7,060 yr BP. In one location, 2 m (6.5 ft.) of fluidized sand is interpreted to have been emplaced along a sand dike during an earthquake associated with either ground cracking due to lateral spreading or in situ block rotation (Aylsworth and Lawrence, 2003). Assessing the magnitude and location of the earthquake causing these features is complicated by the observations that fine sand interbedded with the Leda Clay induces lower cyclic resistance and that deep, steep-sided basins amplify ground motions. A comparison with other earthquakes led Aylsworth and Lawrence (2003) to estimate the magnitude of the earthquake to which these features are related to be at least **M** ≥ 6.2, and likely **M** ≥ 6.5. The field observations conducted for these studies are consistent with appropriate evidence for paleoliquefaction as outlined in Appendix E. However, geotechnical investigations to constrain the cyclic stress ratio for these materials are required for constraining magnitude and location of these paleoearthquakes. It is also important to understand that these features could be caused by a paleoearthquake located in the SLR or Great Meteor Hotspot (GMH) seismotectonic zones, or that they could be caused by larger, more distant earthquakes associated with the Charlevoix RLME source. Future research may provide information to update the maximum magnitude distributions for these zones.

Given that the magnitude of the largest observed earthquake lies within the range of uncertainty of the magnitudes estimated by Aylsworth and Lawrence (2003), Mmax for the SLR seismic source zone was assessed using historical seismicity. The largest observed earthquakes in SLR include the September 16, 1732, E[**M**] 6.25; March 1, 1925, E[**M**] 6.18; and November 1, 1935, E[**M**] 6.08 earthquakes. As part of the EPRI study on earthquakes in SCRs, Kanter (1994) classified the St. Lawrence–Ottawa domain (Domain 227) as a Paleozoic rift that was reactivated in the Cretaceous. Therefore, the maximum magnitude distribution for the SLR seismotectonic zone was determined by applying a Mesozoic and younger prior to the largest observed earthquake. The resulting Mmax distribution is presented in Section 7.4.2.

7.3.1.5 Future Earthquake Characteristics

Earthquakes in southeastern Canada are classified as mainly thrust earthquakes (Adams et al., 1995; Du et al., 2003). Bent et al. (2003) determined focal mechanisms for **M** > 4 earthquakes occurring in eastern Canada between 1994 and 2000 and documented the mechanisms as predominantly reverse. Bent (1996a) determined a reverse mechanism for the November 1, 1935, m_b 6.1 Timiskaming earthquake (Figure 7.3.1-1) and preferred a moderately dipping northwest-striking plane. The January 1, 2000, M_N 5.2 (E[**M**] 4.62) Kipawa earthquake (Figure 7.3.1-1) is located near the 1935 epicenter and exhibits northwest-southeast reverse faults dipping to the northeast (Bent et al., 2002). Du et al. (2003) determined thrust motion along either a southwesterly steeply dipping (68 degrees) or northeasterly dipping (30 degrees) nodal plane for

the Kipawa earthquake. Bent et al. (2003) observed that focal mechanisms in the Western Quebec seismic zone have a strong component of thrust faulting, with at least one nodal plane striking northwest-southeast, consistent with reactivation of the Ottawa-Bonnechere graben. Bent (1996b) determined an oblique thrust mechanism for the September 5, 1944, **M** 5.8 (E[**M**] 5.71) Cornwall-Massena earthquake (Figure 7.3.1-1), located at the eastern edge of the Ottawa-Bonnechere graben along the St. Lawrence River. Bent (1996b) could not determine which nodal plane was the fault plane, given that the regional seismicity trend is consistent with the northwest plane, and mapped faults are more consistent with the northeast plane.

Bent et al. (2003) report that mechanisms for the October 22, 1998, and March 16, 1999, Lower St. Lawrence earthquakes (Figure 7.3.1-1) exhibit evidence for oblique-thrust faulting over a wide range of possible dips (30–68 degrees). Lamontagne et al. (2004) favor the northwest nodal plane of the March 16, 1999, M_N 5.1 (E[**M**] 4.45) Côte-Nord earthquake based on agreement with an alignment of aftershocks. The focal mechanism determined by Du et al. (2003) for this earthquake favors northeast- and southwest-trending nodal planes for this earthquake.

Focal mechanisms for two earthquakes in the Adirondack Mountains indicate north-south-striking nodal planes. Focal mechanisms for the April 20, 2002, **M** 5.0 (E[**M**] 4.91) Au Sable Forks, New York, earthquake (Figure 7.3.1-1) show reverse faulting along a north-south-striking nodal plane, with aftershocks indicating an intermediate dip to the west (Seeber et al., 2002). The October 7, 1983, m_b 5.1 (E[**M**] 4.84) Goodnow, New York, earthquake (Figure 7.3.1-1) also exhibits north-south-striking reverse faults dipping 60 degrees to the west (Nabelek and Suarez, 1989).

Adams and Basham (1991) report that structural complexity in the form of distributed fracturing and ring faulting within the Charlevoix impact crater may be responsible for more varied focal mechanisms within the Charlevoix RLME source. Focal mechanisms for earthquakes of magnitude $\geq$3 show reverse faulting, whereas smaller-magnitude earthquakes indicate some strike-slip and normal faulting, suggesting that local stress conditions may affect rupture style (Lamontagne and Ranalli, 1997). Fault plane solutions for recent small earthquakes located within the Charlevoix RLME source are predominantly thrust earthquakes on steeply dipping planes, but there are also a number of earthquakes with a significant strike-slip component, some on northwest-striking planes and some on more shallowly dipping planes (Lamontagne, 1987; Adams et al., 1989; Wetmiller and Adams, 1990). Analysis of rupture directions for two **M** 4 earthquakes by Li et al. (1995) indicate that focal mechanisms have east-dipping planes. Bent (1992) determined a thrust mechanism for the 1925 M_S 6.2 (E[**M**] 6.18) Charlevoix earthquake with a strike of N42° ± 7°E, a dip 53° ± 7°, and rake 105° ± 10°, and favors a southeast-dipping solution based on observed seismicity and mapped faults. Dips for fault surfaces related to the January 11, 1986, M_N 4.0 (E[**M**] 3.40) and the March 18, 1987, M_N 3.3 (E[**M**] 2.79) earthquakes range between 42 and 59 degrees to the south (Lamontagne and Ranalli, 1997).

Future ruptures occurring in the SLR seismotectonic zone are modeled with two-thirds weight as reverse mechanisms and one-third weight as strike-slip. Given the wide variability in structural orientations and focal mechanisms, the strike of future ruptures contains northeast, northwest, north-south, and east-west alternative orientations with the following percentages: N25E (20%), N40E (20%), N70E (20%), N50W (15%), N70W (15%), N-S (5%), and E-W (5%).

Earthquakes within eastern Canada can have anomalously deep hypocenters compared to the adjacent craton. Bent and Perry (2002) relocated earthquakes in eastern Canada occurring between 1992 and 2000 and concluded that moderate-magnitude earthquakes in the Ottawa-Bonnechere graben have depths in the 11–16 km (7–10 mi.) range but may occur at variable depths in the crust. Hypocentral depths for the 1935 Timiskaming and 1944 Cornwall-Massena earthquakes are 10 and 20 km (6 and 12.5 mi.), respectively (Bent 1996a, 1996b). Bent and Perry (2002) also observed that earthquakes in the Lower St. Lawrence extend to 27 km (17 mi.) in depth. The 1988 Saguenay earthquake was anomalously deep, occurring at a depth of 28 km (17.5 mi.; Somerville et al., 1990). Based on the above information, thickness of seismogenic crust for the SLR seismic source zone is modeled with equal weights at 25 and 30 km (15.5 and 18.5 mi.).

7.3.2 Great Meteor Hotspot Zone (GMH)

The Great Meteor Hotspot (GMH) seismotectonic zone lies within the Western Quebec seismic zone as defined by Adams and Basham (1991). This seismotectonic zone is characterized by moderate seismicity, including the 1975 **M** 4.2 (E[**M**] 4.17) Maniwaki and 1978 **M** 4.1 (E[**M**] 3.82) St. Donat earthquakes (Adams and Basham, 1991); the October 19, 1990, **M** 4.6 (E[**M**] 4.53) Mont-Laurier earthquake (Lamontagne et al., 1994; Du et al., 2003); and the February 10, 1914, M_L 5.5 (E[**M**] 5.10) Saint-André-Avellin earthquake (Bent, 2009; Figure 7.3.2-1). Adams and Basham (1991) have suggested that the band of seismicity north of the Ottawa River within the Western Quebec seismic zone is due to crustal fractures that formed as the North American Plate rode over a Cretaceous hotspot (Crough, 1981).

Section 7.3.2.1.1 presents alternative hypotheses for Cretaceous volcanism, including mantle plume, lithospheric processes, and/or small convection cells. Regardless of the mechanism for Cretaceous volcanism, Sections 7.3.2.1.2 and 7.3.2.1.3 also present evidence of faulting, uplift, and geophysical anomalies associated with Cretaceous alkaline rocks. Ma and Eaton (2007) propose that seismicity of the Western Quebec seismic zone represents blind intrusions associated with entrapment of mantle-derived melt at the transition from kimberlite dikes to plutons of the Monteregian Hills. Modern seismicity may be localized along these intrusions either by weakened faults and shear zones as a result of reheating of the crust by the hotspot track, or by stress concentrations associated with the emplacement of major bodies in more felsic crust (Ma and Eaton, 2007). Elevated seismicity rates are present within Grenville-age crust that lacks Iapetan rifting but exhibits Cretaceous volcanism and reactivation, and these form the basis of the GMH seismotectonic zone.

The source characterization of the GMH seismotectonic zone is based on a review of published material that is summarized in the Data Summary table for the GMH zone (Appendix Table D-7.3.2). Explicit references and data that were used as the basis for source characteristics of GMH are identified in the Data Evaluation table (Appendix Table C-7.3.2).

7.3.2.1 Background

7.3.2.1.1 Geological Evidence

Cretaceous volcanism in eastern Canada and New England has been attributed to intrusions along preexisting zones of weakness (McHone, 1996) and movement of the Great Meteor hotspot track (Morgan, 1983; Crough, 1981; Sleep, 1990) beneath eastern North America. (The Great Meteor hotspot is named after the Great Meteor seamount in the central Atlantic Ocean [Morgan, 1983]). Morgan (1983) attributed the age distribution of these rocks to two hotspot tracks passing through New England at different times: the Verde hotspot track at 160 Ma and the Meteor hotspot at about 120 Ma (Figure 7.3.2-2). Geologic evidence for the hotspot (see Appendix Table D-7.3.2) consists of an alignment of mapped alkalic intrusions from the Monteregian Hills of Quebec (Poole, 1970) through the White Mountain magma series in New Hampshire (Zartman, 1977), the Cretaceous seamounts of offshore New England (Duncan, 1984), the Corner Rise (recorded when the Mid-Atlantic Ridge crossed over the hotspot), to the Great Meteor seamount (11–17 Ma) in the Central Atlantic (Morgan, 1983; Figure 7.3.2-2). Rock types and chronology of igneous activity related to the GMH can be summarized as follows:

- Alkaline intrusive rocks of the Monteregian Hills form circular plugs with steep walls and lacoliths within a 241.5 km (150 mi.) long west-trending line between Montreal and Lake Megantic of Quebec (Poole, 1970). These intrusions range in age from 84 to 123 Ma, with many dates falling between 100 and 115 Ma (Poole, 1970).
- Alkaline rocks of the White Mountain plutonic suite were emplaced over three rather broad pulses of magmatism at 220–235 Ma, 155–200 Ma, and 95–125 Ma, but lack any regular time-transgressive pattern of ages (Zartman, 1977; Figure 7.3.2-2).
- Duncan (1984) observed that radiometric ages for dredged volcanic rocks from seven of the New England seamounts increase in age from the southeast (82.9 Ma for the Nashville seamount) to the northwest (103 Ma for the Bear seamount; Figure 7.3.2-2) and fall within a longer age progression to the Corner seamounts (70–75 Ma).
- Subsequent mapping by Heaman and Kjarsgaard (2000) extended the GMH track to the Rankin Inlet on the west side of James Bay. They identified four periods of kimberlite magmatism (at 196, 180–176, 148–146, and 142–134 Ma) along a northwest-southeast trend from Rankin Inlet through to the Attawapiskat, Kirkland Lake, and Timiskaming fields (Figure 7.3.2-2). These results support a single hotspot track.

McHone (1996) concluded that lithospheric processes were necessary to start and stop the generation of magma from the same source in the mantle. He proposed that heterogeneous source areas, coupled with tectonic reactivation of crustal structures, were required to explain the wide distribution of intrusions in space and time and the different styles of igneous activity expressed onshore and offshore. Heaman and Kjarsgaard (2000) proposed that interaction of the hotspot with thinned continental lithosphere toward the continental margin can account for the transition from kimberlitic dikes to alkaline intrusions east of Montreal. Subsequent synthesis by McHone (2000) attributes Cretaceous magmatism to shallow linear upwelling and convection following Jurassic rifting. Matton and Jebrak (2009) propose that periodic reactivation of deep-

seated preexisting zones of weakness during major stages of Atlantic tectonic evolution, combined with coeval asthenospheric upwelling due to edge-driven convection and continental insulation flow, enhanced the ascent of alkaline magmas. Shallow, small-scale upwelling during periodic structural reactivation provides a better mechanism for Cretaceous alkaline magmas than a mantle plume model (Matton and Jebrak, 2009).

7.3.2.1.2 Evidence for Reactivation

Faure et al. (1996b) recognize two distinct phases of Cretaceous extension based on paleostress analysis of Cretaceous dike trends and regional- and mesoscopic-scale faults from the Monteregian plutons that differ from regional stress fields related to opening of the Atlantic ocean (Faure et al., 2006). Paleostress analysis of Jurassic normal faults and dike trends in the Quebec and New England Appalachian Mountains distinguishes east-west- and northwest-southeast-oriented extensional stress regimes (Faure et al., 2006). Fault stress tensors indicate that most east-west to east/southeast–west/northwest–oriented stress is found in the Montreal and Gaspe area, possibly related to regional partitioning of stress along north-south-trending structures in the Champlain Lake valley and the northeast-southwest-trending structures of the St. Lawrence rift basin (Faure et al., 2006). An initial Late Triassic east-west extension related to the formation of rift basins in the Bay of Fundy and South Georgia and a later Early Jurassic east/southeast–west/northwest-oriented extension related to the central Atlantic rift system is more consistent with the two-phase rifting models for the opening of the Atlantic Ocean (Faure et al., 2006). Subsequent Cretaceous extension consists of an older widespread northeast-southwest-trending extension and a younger north-south-oriented extension restricted to the Montreal area (Faure et al., 1996b).

Northwest-southeast- to west-northwest-/east-southeast-trending normal faults trend obliquely to the Ottawa-Bonnechere graben and have stress orientations that vary between north/northeast–south/southwest near Ottawa and Montreal and east/northeast–west/southwest in southern Quebec (Faure et al., 1996b). East-west-trending normal faults are predominantly found in the Montreal area and along the axis of the Monteregian Hills, have similar orientations to regional Cretaceous dikes, and have crosscutting relationships indicating they are younger than northwest-southeast-trending faults (Faure et al., 1996b). The Ottawa-Bonnechere graben and associated basement faults may have acted as localized zones of weakness in the early stage of Cretaceous extension, resulting in reorientation of the regional stress field and formation of the localized north-south-directed extension (Faure et al., 1996b). Although Faure et al. (1996b) attribute these two Cretaceous extensions to an initial northeast-southwest extension event associated with rifting between Labrador and Greenland at 140 Ma and opening of the South Atlantic at 130 Ma and a subsequent north-south-oriented extension corresponding to global fragmentation of Pangaea when Iberia separated from Newfoundland, Faure et al. (2006) recognize that the lack of Mesozoic rift basins in central New England and Quebec may be due to high topographic elevation induced by a regional thermal event.

Crough (1981) suggests that the passage of the GMH caused a 600 km (373 mi.) wide zone of epeirogeny (broad regional vertical motion) during the Cretaceous and early Tertiary in southeastern Canada and New England, resulting in erosion of at least 1 km (0.6 mi.) in Montreal and as much as 6–7 km (3.7–4.3 mi.) in New England. Recent thermochronology studies provide

evidence for epeirogeny that was accompanied by Late Cretaceous reactivation of faults. Roden-Tice et al. (2000) interpreted two periods of unroofing of the Adirondack Mountains from apatite fission-track dating that must be explained by tectonic denudation processes: Late Jurassic–Early Cretaceous (160–120 Ma) throughout the region and Early–Late Cretaceous (~110–80 Ma) in the southeast. Roden-Tice et al. (2000) support the hypothesis that this Early–Late Cretaceous uplift, contemporaneous with intrusion of the Monteregian Hills plutons, can be attributed to differential unroofing resulting from reactivation normal faults. Roden-Tice and Tice (2005) attribute the widespread unroofing during the Middle Jurassic–Late Cretaceous to remnant heating from the GMH track, accommodated by extensional reactivation of faults in the Adirondack Mountains and New Hampshire. Roden-Tice, West, et al. (2009) integrate these results with apatite fission-track ages from northeastern Vermont, New Hampshire, and western Maine and conclude that normal reactivation of orogen-parallel faults accommodating northwest-southeast extension is associated with remnant heating from passage of the GMH during the Late Cretaceous.

7.3.2.1.3 Geophysical Evidence

A remnant thermal anomaly is inferred to exist in the upper mantle and lower lithosphere, based on several types of geophysical evidence. Travel-time inversions of teleseismic results from southern Ontario image a low-velocity corridor between 50 and 300 km (31 and 186.5 mi.) depth that crosscuts regional structures of the Grenville province (Rondenay et al., 2000). These results are attributed to a zone of contrasting thermal-compositional-anisotropic properties related to the GMH (Rondenay et al., 2000). Subsequent work by Li et al. (2003) using Rayleigh wave paths confirms the presence of a broad, low-velocity layer in the upper mantle beneath eastern New York and central New England between depths of 60 and 140 km (37 and 225 mi.). This anomaly is interpreted as the lateral contrast between relatively thick lithosphere beneath western New York and Pennsylvania and the warm asthenosphere beneath the thinned New England lithosphere, caused by thermal erosion associated with the Cretaceous hotspot (Li et al., 2003). Crustal thickness and average P-wave and S-wave velocity (V_p/V_s) ratio maps derived from teleseismic receiver functions illustrate thin crust (Figure 7.3.2-3) and variable V_p/V_s ratio northeast of the Ottawa-Bonnechere graben coincident with the Western Quebec seismic zone (Eaton et al., 2006), possibly indicating mafic intrusions within felsic crust (Ma and Eaton, 2007).

7.3.2.2 Basis for Defining Seismotectonic Zone

Ma and Eaton (2007) recognize that seismicity cannot be easily correlated with Grenville or Iapetan structures within this zone and conclude that the GMH provides the only compelling explanation for seismicity within the Western Quebec seismic zone. Seismicity may result from either weakened crust caused by reheating or from stress concentrations caused by strength contrasts between mafic and felsic crust (Ma and Eaton, 2007), as indicated by the variable V_p/V_s observed by Eaton et al. (2006). Crust of the GMH seismotectonic zone is distinguished from the adjacent craton on the basis of Cretaceous volcanism and extension, meeting the criterion for separating crust of the GMH on the basis of maximum earthquake magnitude. GMH crust lacks Iapetan-age faulting and the repeated reactivation expressed within the St. Lawrence rift (SLR)

seismotectonic zone (Section 7.3.1). Additionally, the earthquakes within this seismotectonic zone have a depth distribution similar to the SLR seismotectonic zone. However, earthquakes of the GMH seismotectonic zone exhibit thrust mechanisms with predominantly northwest-striking nodal planes, whereas those of the SLR seismotectonic zone generally exhibit greater variability in the strike of nodal planes and a component of strike-slip faulting. Earthquakes of the Northern Appalachian and Extended Continental Crust–Atlantic Margin seismotectonic zones have shallower depth distributions than the GMH zone.

7.3.2.3 Basis for Zone Geometry

The GMH seismotectonic zone lies within the Western Quebec seismic zone, as defined by Adams and Basham (1991), who recognized two distinct bands of seismicity within the Western Quebec zone. One band trends west-northwest along the Ottawa River between Ottawa and Lake Timiskaming, is associated with rift faults of the Ottawa-Bonnechere graben, and is interpreted to be part of the SLR seismotectonic zone (Section 7.3.1). The second band trends north-northwest, extends from Montreal to the Baskatong Reservoir, and is attributed to crustal fracturing associated with the passage of a Cretaceous hotspot track. Ma and Eaton (2007) propose that seismicity of the Western Quebec seismic zone represents blind intrusions associated with entrapment of mantle-derived melt at the transition from kimberlite dikes to plutons of the Monteregian Hills. The geometry for the GMH source zone is adopted from the Gatineau (GAT) source zone of the GSC H model (Adams et al., 1996; Adams and Halchuk, 2003) and was compared to data sets listed in the Data Evaluation table (Appendix Table C-7.3.2). Given the uncertainty in a plume model as a mechanism for the cause of Cretaceous volcanism presented in Section 7.3.2.1.1, alternative geometries based on segments of the proposed hotspot track were not considered in the CEUS SSC model.

The geometry of the GMH zone is consistent with a region of thinner crust northeast of the Ottawa-Bonnechere graben observed by Eaton et al. (2006) and with the progressive change from kimberlitic melts in the interior of the craton to more voluminous crustal magmatism as the hotspot interacted with a progressively thinner lithosphere (Ma and Eaton, 2007). Earthquakes of the Kapuskasing cluster, located 100 km (62 mi.) northwest of the zone and separated by an aseismic area, have focal depths (4–20 km [2.5–12.4 mi.]; Figure 7.3.2-3) and mechanisms (reverse with northwest-striking nodal planes) located along strike of the kimberlite dike portion of the hotspot track (Ma et al., 2008). Adams and Basham (1991) postulate that elevated rates of seismicity in western Quebec are due to thermally stressed and fractured crust, whereas plutonism in New England may have healed deep crustal fractures. Therefore, the geometry for the GMH seismotectonic zone encompasses the volume of crust likely to produce frequent moderate earthquakes associated with thermally stressed crust. Gravity and magnetic maps do not correlate well with seismicity and seismogenic structures (Figure 7.3.2-4) given that the mechanisms for earthquakes associated with the GMH track involve thermal weakening.

7.3.2.4 Basis for Zone Mmax

No paleoseismic investigations have been performed within the GMH seismotectonic zone. A paleoseismic study conducted by Aylsworth et al. (2000; Figure 7.3.2-1), located south of the

GMH within the SLR seismotectonic zone (Section 7.3.1.3), provided evidence for two moderate- to large-magnitude paleoearthquakes in the Holocene. Subsequent trenching by Aylsworth and Lawrence (2003) documented lateral spreading, surface subsidence, and sediment deformation occurring at 7,060 yr BP. As discussed in Section 7.3.1.3, additional research is required to constrain the location and magnitude of earthquakes causing this deformation. Ma and Eaton (2007) observe that the Mont-Laurier earthquake clusters are located near the paleoseismic investigations along the Ottawa River documented by Aylsworth et al. (2000) and Aylsworth and Lawrence (2003) and may represent persistent aftershocks of past large earthquakes. The maximum observed earthquake for the GMH seismotectonic zone is therefore derived from historical and instrumental earthquakes. The largest observed earthquake within the zone is the February 1914 E[**M**] 5.10 Saint-André-Avellin earthquake.

Kanter (1994) classified crust of the GMH seismotectonic zone as exposed middle Proterozoic non-extended crust. However, as described above, Cretaceous uplift (Roden-Tice and Tice, 2005; Roden-Tice, West, et al., 2009) and Cretaceous mesoscopic-scale normal faulting (Faure et al., 1996) provide evidence for Mesozoic extension. Therefore, the maximum magnitude distribution for this zone was determined by applying the likelihood function based on the largest observed earthquake to the Mesozoic and younger prior distribution.

7.3.2.5 Future Earthquake Characteristics

The GMH has been associated with clusters of midcrustal seismicity by Ma and Eaton (2007). Ma and Atkinson (2006) attribute the wide hypocentral depth distribution (2–25 km [1.2–15.5 mi.]) for relocated earthquakes in the Western Quebec seismic zone to faults of through-going crustal extent or faults of varying depths in the crust. Ma and Atkinson (2006) also note that the clustering of focal depths at 5, 8, 12, 15, and 22 km (3, 5, 7.5, 9.3, and 13.7 mi.) may reflect layering related to different seismogenic properties within the crust. Ma and Eaton (2007) report that shallow earthquakes with relocated depths less than 8 km (5 mi.) are randomly distributed, with reverse mechanisms that can be attributed to glacial isostatic adjustment. Ma and Eaton (2007) also note that earthquakes with intermediate depths define a linear band of earthquakes, and deep earthquakes (greater than 17 km [10.5 mi.] in depth) are localized as clusters at Maniwaki and Mont-Laurier. Focal depths for this deep zone extend to 30 km (18.5 mi.; CEUS SSC Project earthquake catalog). Seismogenic thickness for the GMH seismotectonic zone is modeled with equal weight for 25 and 30 km (15.5 and 18.5 mi.).

Earthquakes within the GMH seismotectonic zone exhibit reverse mechanisms. Bent et al. (2003) observe that focal mechanisms can be classified as either thrust or oblique-thrust in response to northeast compression. Ma and Eaton (2007) note that these reverse mechanisms have southwest-trending P-axes that change to east-west-trending P-axes in the southern portion of the zone. Bent (1996a) acknowledges that interpreting which nodal plane for mechanisms within the Western Quebec seismic zone corresponds to the fault plane is ambiguous, given that seismicity trends northwest and some mapped structures trend northeast. Mechanisms in the southern part of the Western Quebec seismic zone, corresponding to the Ottawa graben of the SLR seismotectonic zone, display more variability in strike and exhibit more strike-slip behavior (Bent, 1996a) compared to mechanisms of the GMH seismotectonic zone. Lamontagne et al.

(1994) determined a steeply north-dipping, east-west-oriented nodal plane with a reverse mechanism for the October 19, 1990, Mont-Laurier earthquake. Du et al. (2003) observe that mechanisms for earthquakes in the Western Quebec seismic zone have strikes of one of their nodal planes parallel to the general trend of seismicity. Future ruptures are modeled as 100 percent reverse faulting. The strike of ruptures is modeled with three orientations consisting of N50W (0.4), N20W (0.4), and EW (0.2). The dip of ruptures consists of the default characteristics for both styles. Ruptures are allowed to extend beyond the zone boundary. These characteristics are presented in Table 5.4.2.

7.3.3 Northern Appalachian Zone (NAP)

The Northern Appalachian (NAP) seismotectonic zone (Figures 7.3.3-1 and 7.3.3-2), which is characterized by moderate-magnitude, shallow seismicity (Adams et al., 1995), contains crust assembled outboard of the Laurentian margin in the Taconic, Salinian, and Acadian orogenies and deformed by these events and the subsequent Alleghanian orogeny and Mesozoic extension associated with opening of the Atlantic Ocean (see the data summary in Appendix Table D-7.3.2). This seismicity occurs above the continental margin within crust of Appalachian terranes (Spencer et al., 1989).

7.3.3.1 Background

7.3.3.1.1 Geological Evidence

Crust of the NAP seismotectonic zone postdates Iapetan rifting. The late Cambrian–Middle Ordovician Penobscottian orogeny amalgamated composite terranes within arcs of the Iapetus Ocean (Murphy and Keppie, 2005). These magmatic arcs, which developed in the late Cambrian within the Theic Ocean, were obducted to the Laurentian margin during the Middle–Late Ordovician Taconic orogeny (Faill, 1997a; Moench and Aleinikoff, 2003). This deformation produced north-south- to northeast-southwest-trending reverse conjugated brittle faults under a pure compressional stress regime late in the development of the orogeny (Faure et al., 2004). This Taconic compressional event also resulted in reactivation of Iapetan faults in the SLR seismotectonic zone as east-northeast/west-southwest dextral and northwest-southeast sinistral faults (Rocher et al., 2003; Faure et al., 2004).

The Late Ordovician–Silurian Salinic orogeny accreted the Gander, Avalon, Nashoba, and Carolina terranes to Laurentia during the closing of the Iapetus Ocean during the Laurentia-Avalonia collision (Murphy and Keppie, 2005). Silurian metamorphism (430–410 Ma) in the northern Appalachian Mountains is attributed to retrograde metamorphism following the main compression event (Tremblay and Castonguay, 2002). Compression of the Salinian orogeny involved southeast-directed transport of the Taconian crustal wedge followed by normal faulting (Saint-Joseph and Baie Verte–Brompton faults) and development of the fault-bounded sedimentary basins of the Connecticut Valley–Gaspé trough (Tremblay and Castonguay, 2002). Tremblay and Pinet (2005) attribute the late-stage extension to supracrustal extensional collapse caused by late-stage delamination of the lithospheric mantle in a southeast-dipping subduction zone.

The Devonian Acadian orogeny has been attributed to either the collision of Avalonia with Laurentia or the accretion of the Meguma terrane; however, recent work indicates that the Meguma terrane is the passive margin on the southern margin of Avalonia (Murphy and Keppie, 2005). Murphy and Keppie (2005) interpreted the Acadian orogeny as forming along an Andean-type margin that possibly overrides a plume and swell. Acadian metamorphism is well dated as 385–375 Ma in the southern part of the Dunnage zone (Tremblay et al., 2000). Deformation from the Acadian orogeny is expressed as east-southeast/west-northwest compression in a transpressional regime producing east-northeast/west-northwest dextral and northwest-southeast sinistral strike-slip faults that crosscut Taconian thrust faults in the Appalachian Mountains of Quebec and New Brunswick (Faure et al., 2004). This deformation also resulted in reactivation of Iapetan structures in the SLR seismotectonic zone (Faure et al., 2004; Rocher et al., 2003).

There is general consensus that the late Carboniferous–Permian Alleghany orogeny was due to terminal collision between Gondwana and Laurentia-Baltica that closed the Rheic Ocean and resulted in the formation of Pangaea (Murphy and Keppie, 2005). The Alleghanian orogeny produced decollement tectonism in the central and southern Appalachian Mountains along with early penetrative shortening, late low-angle thrusts, low-grade metamorphism, and transpressional shear zones. Rocks of the northern Appalachians exhibit relatively high-grade metamorphism of Taconic and Acadian crust and deformation of Appalachian deposits near the Hudson Valley (Faill, 1998). Although no structures within the northern Appalachians have been unequivocably assigned to Alleghanian deformation, brittle faults of the northern Appalachians exhibit three phases of compression: an early north-northwest/south-southeast compression, a north-northeast/south-southwest compression, and a late west-northwest/east-southeast compression (Faure et al., 1996a).

Mesozoic rifting resulted in the breakup of Pangaea. This rifting is associated with the separation of the North American and African plates and produced rift basins along the Atlantic seaboard that are situated landward of the hinge zone of the continental margin. This landward region experienced considerably less crustal thinning than did the region seaward of the hinge zone that includes the deeper marginal sedimentary basins (Klitgord et al., 1988). Faure et al. (2006) identified two phases of extension: an initial Late Triassic east-west extension related to the formation of rift basins in the Bay of Fundy and South Georgia, and Early Jurassic east-southeast/west-northwest extension related to the central Atlantic rift system.

Apatite fission-track ages across the Norumbega fault zone in southern coastal Maine reveal a 30–50 Myr discontinuity, suggesting that this fault shows 2 km (1.2 mi.) of vertical offset in the Late Cretaceous (West and Roden-Tice, 2003). Roden-Tice and Tice (2005) attribute the widespread unroofing during the Middle Jurassic–Late Cretaceous, accommodated by northwest-southeast extensional reactivation of faults in the Adirondack Mountains and New Hampshire, to remnant heating from the Great Meteor hotspot track.

7.3.3.1.2 Geophysical Data

Refraction studies across northern New England image crust between 36 and 40 km (22 and 25 mi.) thick from Maine to Vermont (Hughes and Luetgert, 1991; Taylor and Toksöz, 1982), to 44 km (27 mi.) thick in New Brunswick and southeastern Quebec (Taylor and Toksöz, 1982).

Regional seismic profiles of the Quebec-Maine transect image normal faults in the passive margin beneath the master decollement overlain by the St. Lawrence platform and allochthonous continental margin sediments and volcanics accreted during the Taconic orogeny (Stewart et al., 1993). These normal faults do not appear to extend east of the Baie Verte–Brompton line (Stewart et al., 1993).

7.3.3.1.3 Seismicity

Various special studies provide better constraints for historical earthquakes: Leblanc and Burke (1985) determined the location for the March 21, 1904, m_{bLg} 5.9 (E[**M**] 5.73) Passamaquoddy Bay earthquake and three other earthquakes. Burke (2004) revised magnitudes and locations for historical earthquakes within the Central Highlands, Moncton, and Passamaquoddy Bay subzones. He also later provided complete documentation, with felt areas, for all historical earthquakes in New Brunswick (Burke, 2009). Ruffman and Peterson (1988) researched historical earthquakes in Nova Scotia under contract with the Geological Survey of Canada and provided lists of new and fictitious earthquakes. Unfortunately, this study did not provide intensity or felt-area information for determining magnitudes and locations of historical earthquakes, and it could be improved upon with further research.

Ebel (1996) reviewed felt reports in Trois Rivières, Quebec, and Boston, Massachusetts, for the June 11, 1638, earthquake and placed the epicenter within the seismically active part of central New Hampshire with a magnitude of 6.5 ± 0.5 (E[**M**] 5.32). Ebel et al. (1986) analyzed historical seismograms for two earthquakes occurring in December 1940 near Ossipee, New Hampshire: the December 20 M_L 5.3 (E[**M**] 5.08) and December 24 M_L 5.4 (E[**M**] 5.13) earthquakes. Instrumental seismicity consists of small- to moderate-magnitude earthquakes, including the January 19, 1982, M_C 4.7 (E[**M**] 4.23) Gaza, New Hampshire, earthquake (Brown and Ebel, 1985) and the January 9, 1982, m_{bLg} 5.7 (E[**M**] 5.47) Miramichi earthquake (Wetmiller et al., 1984).

7.3.3.2 Basis for Defining Seismotectonic Zone

Crust of the NAP seismotectonic zone postdates Iapetan rifting and therefore should be excluded from the SLR and PEZ seismotectonic zones. Terranes of this zone formed outboard of the Laurentian margin after Iapetan rifting and were subsequently accreted to the passive margin. Normal faulted basement underlying the Taconic master decollement (St. Julien and Hubert, 1975; Spencer et al., 1989) exhibits en echelon normal faults associated with development of the Iapetan passive margin as interpreted from seismic profiles (Spencer et al., 1989). These normal faults are depicted at the base of the aulochthonous continental margin sediments northwest of the Baie Verte–Brompton line. This crust is included within the SLR seismotectonic zone (Section 7.3.1).

Crust of the NAP seismotectonic zone formed in the Paleozoic and experienced multiple phases of extension, including normal faulting in the late stages of the Salinian orogeny (Tremblay and Castonguay, 2002) and extensional reactivation of both the Ammonoosuc fault in the Mesozoic (Moench and Aleinikoff, 2003) and the Norumbega fault zone in the Late Cretaceous (Stewart et

al., 1993; West and Roden-Tice, 2003). Therefore, the NAP seismotectonic zone meets the criterion for application of a Mesozoic and younger prior distribution for maximum earthquake magnitude. Crust of the NAP seismotectonic zone is separated from the Extended Continental Crust–Atlantic Margin (ECC-AM) seismotectonic zone on the basis of lack of Alleghanian structure and Mesozoic rift basins.

The style of extension within the NAP seismotectonic zone differs from the ECC-AM seismotectonic zone (Section 7.3.7) by exhibiting a lack of fault-bounded rift basins. This difference has been attributed to Early Jurassic pluton emplacement associated with the White Mountain magma series in central New England, which created a topographic high that resisted extension (Faure et al., 2006). Roden-Tice, West, et al. (2009) attribute this topographic elevation to regional unroofing during the Cretaceous. Additionally, fault rupture characteristics for the NAP seismotectonic zone are predominantly reverse (Du et al., 2003; Bent et al., 2003), and seismicity of the NAP seismotectonic zone occurs in the upper 10 km (6 mi.) of the crust.

7.3.3.3 Basis for Zone Geometry

The geometry for the NAP seismotectonic zone is modified from the Northern Appalachians source zone of the GSC (Adams et al., 1996; Adams and Halchuk, 2003). Adams et al. (1995) characterized this source zone for use in Canadian seismic hazard maps (Adams et al., 1996; Adams and Halchuk, 2003) as extending from the landward limit of Mesozoic extensional faulting to the seaward limit of thinned Grenville crust of the Iapetan passive margin. The northwestern boundary of NAP coincides with the Baie Verte–Brompton line of Moench and Aleinikoff (2003) to restrict Iapetan normal faults below the Taconic decollement to the SLR seismotectonic zone. The southeastern boundary follows the Cobequid-Chedabucto fault system in Nova Scotia (Pe-Piper and Piper, 2004) and the northern limit of the Fundy Basin and Gulf of Maine along coastal Maine (Klitgord et al., 1988), which exhibit clear Mesozoic activity. The southwestern boundary was drawn to exclude the Hartford basin, which falls within the ECC-AM seismotectonic zone. The northeastern boundary of the NAP seismotectonic zone follows the project boundary.

7.3.3.4 Basis for Zone Mmax

As part of the EPRI study on earthquakes of stable continental regions, Kanter (1994) classified crust of the NAP seismotectonic zone as exposed Paleozoic non-extended crust. However, as described above, the NAP seismotectonic zone has experienced several contrasting stress regimes, including several phases of extension: Cambrian growth faulting beneath the master decollement (St. Julien and Hubert, 1975; Stewart et al., 1993; Spencer et al., 1989); normal faulting in the late stages of the Salinian orogeny (Tremblay and Castonguay, 2002); extensional reactivation of the Ammonoosuc fault in the Mesozoic (Moench and Aleinikoff, 2003); and recurring movement along the Norumbega fault zone (Stewart et al., 1993; West and Roden-Tice, 2003). Because extension has occurred since the Mesozoic, the maximum magnitude distribution for this zone was determined by applying a Mesozoic and younger extension prior, updated by a likelihood function based on the largest observed earthquake.

There is some uncertainty about the largest observed earthquake within the NAP seismotectonic zone. The largest observed earthquakes include the March 21, 1904, E[**M**] 5.73, followed by the June 11, 1638, E[**M**] 5.32 and December 24, 1940, E[**M**] 5.6 earthquakes. There is also some possibility that the largest observed earthquake in the ECC-AM seismotectonic zone (1755 E[**M**] 6.10 Cape Ann earthquake) applies to the NAP seismotectonic zone. Bakun et al. (2003) have a preferred location for the 1755 E[**M**] 6.10 Cape Ann earthquake near the boundary between ECC-AM and NAP, with the area defining 95 percent confidence level for the earthquake location spread across both seismotectonic zones. Ebel (2006a) estimates the location within ECC-AM farther southeast than the Bakun et al. (2003) location based on attenuation of felt effects. Therefore, the probability that the 1755 Cape Ann earthquake modifies the prior for the NAP seismotectonic zone is assigned a weight of 0.4. The resulting Mmax distributions are presented in Section 7.4.2.

7.3.3.5 Future Earthquake Characteristics

As noted by Adams et al. (1995), all earthquakes in the NAP seismotectonic zone with known depths are relatively shallow (less than 10 km, or 6 mi.), the prime example being the Miramichi earthquake sequence of 1982 (Wetmiller et al., 1984). Ebel et al. (1986) determined depths of 8 km (5 mi.)for both 1940 earthquakes. Relocating depths of earthquakes within the NAP seismotectonic zone has not been as active an area of research as other seismically active regions of Eastern Canada and the northeastern United States. The default depth distribution as described in Section 5.4 is applied to the NAP seismotectonic zone.

Ebel and Bouck (1988) present focal mechanisms for small to moderate earthquakes occurring in New England between 1981 and 1987. These mechanisms are predominantly reverse with a component of strike-slip. These mechanisms have variable strike directions, including northeast-southwest, northwest-southeast, north-south, and east-west. Synthetic seismograms for the December 20, 1940, Ossipee earthquake provide evidence for a predominantly thrust mechanism with either a north-south- or east-west-striking nodal plane (Ebel et al., 1986). Bent et al. (2003) observe a combination of thrust and strike-slip faulting in mechanisms for the July 14, 1994, and July 15, 1998, New Brunswick earthquakes. Bent et al. (2003) do not observe a consistent trend in stress axes orientation. Both solutions exhibit one west-southwest- to west-striking plane (Bent et al., 2003)—and the 1994 earthquake has one near north-south nodal plane. The June 16, 1995, Lisbon, New Hampshire, M_w 3.7 (E[**M**] 3.17) and August 21, 1996, Berlin, New Hampshire, M_w 3.4 (E[**M**] 3.45) earthquakes have predominantly reverse mechanisms with northwest-striking nodal planes. The Lisbon earthquake contains an oblique component (Du et al., 2003). Future ruptures within the NAP seismotectonic zone are modeled with 1/3 weight as strike-slip and 2/3 weight as reverse with default dip characteristics. The distribution for rupture strike is modeled as N50W (20%), NS (20%), N35E (40%), N60E (10%), and EW (10%).

7.3.4 Paleozoic Extended Crust (PEZ)

The concept that extended crust may have different seismogenic characteristics (i.e., maximum magnitude and related moment rate) than non-extended or Precambrian rifted crust in SCRs has been applied to the identification and characterization of regional seismic source zones. Based on

a global analysis of earthquakes in SCRs, Johnston et al. (1994) concluded that zones of rifted crust in SCRs exhibit a higher rate of seismic activity, normalized to a given unit area of crust, than nonrifted crust and Precambrian rifts; these zones also have different maximum magnitude priors (see discussion in Section 5.2).[2] This interpretation by Johnston et al. (1994) resulted in efforts to characterize the limit of early Paleozoic (Iapetan) extension within the craton in the CEUS by defining the margin of Iapetan rifting. As characterized by Wheeler (1995), the Iapetan rifted margin (IRM) encompasses that portion of continental crust that includes known and inferred normal faults that formed parallel to the passive margin of Laurentia during the late Proterozoic–early Paleozoic opening of the Iapetus Ocean. Compressional reactivation of favorably oriented Iapetan faults has been suggested as the causal mechanism for several seismically active regions in eastern North America, including Giles County, Virginia, and eastern Tennessee (Bollinger and Wheeler, 1988; Wheeler, 1995; Powell et al., 1994). Adams et al. (1995) observe that seismicity of the IRM is largely expressed as reverse-slip faulting mechanisms in Canada and strike-slip mechanisms in the United States. The IRM concept is incorporated in source characterization for the national seismic hazard maps for the United States (Petersen et al., 2008) and Canada (Adams et al., 1995).

For the CEUS SSC Project, crust of the IRM source zone of Wheeler (1995) and Adams et al. (1995) has been divided into the St. Lawrence rift (SLR; Section 7.3.1); Northern Appalachian (NAP; Section 7.3.3); and Paleozoic Extended Crust (PEZ; this section) seismotectonic zones according to geologic criteria established by this project for separating crust on the basis of Mmax and future earthquake characteristics. The following discussion addresses the geologic, geophysical, and seismic characteristics of the PEZ seismotectonic zone (Figure 7.3.4-1). This discussion, as well as the seismic source characterization of the PEZ, is based on a review of published material, summarized in the Data Summary table for the PEZ (Appendix Table D-7.3.4). Explicit references and data that were used as the basis for source characteristics of PEZ are identified in the Data Evaluation table (Appendix Table C-7.3.4).

7.3.4.1 Background

As discussed in Section 7.3.1.1, breakup of the Mesoproterozoic supercontinent of Rodinia occurred as diachronous rifting along the margins of Laurentia. Rifting began on the western margin of Laurentia between 780 and 680 Ma during opening of the paleo-Pacific Ocean, and resulted in the separation of Australia, Antarctica, south China, and Siberia from Laurentia (Whitmeyer and Karlstrom, 2007). This event also resulted in failed rifting along the eastern margin of Laurentia (Whitmeyer and Karlstrom, 2007), as evidenced by both the continental rift-facies volcanic Mount Rogers Formation of the Virginia/North Carolina Blue Ridge and the largely nonvolcanic Ocoee rift deposits farther to the southwest (Faill, 1997a). Successful rifting of the eastern margin of Laurentia occurred between 620 and 550 Ma and culminated in the rifting of the Argentina Precordillera terrane from the Ouachita embayment (Whitmeyer and Karlstrom, 2007). This second phase of rifting is recorded by the volcanic rocks of the Catoctin

[2] As discussed in Section 5.2, analysis of the updated worldwide data set completed for this study suggests that crust extended during the Paleozoic cannot be differentiated from non-extended or Precambrian rifted crust and that the more statistically significant difference is between Mesozoic and younger crust and older extended/nonextended crust.

Formation; sedimentary clastics of the Chilhowee group of Virginia, Maryland, and Pennsylvania (Faill, 1997a); and lavas, dikes, and intrusions formed along the eastern margin of Laurentia extending north to Labrador (Kumarapeli et al., 1988; Kamo et al., 1995; Higgins and van Breemen, 1998; McCausland and Hodych, 1998; Bédard and Stevenson, 1999; Walsh and Aleinikoff, 1999; Hodych and Cox, 2007). Within the PEZ seismotectonic zone, these events occurred 758 Ma for the Mount Rogers Formation and 564 Ma for the Catoctin rift (Aleinikoff et al., 1995; Figure 7.3.4-1).

The IRM is expressed as promontories and embayments defined by northeast-striking normal faults and northwest-striking transform faults along the margins of Laurentia (Thomas, 1991; 2006; Lavoie et al., 2003). The Peters Creek Formation of southeastern Pennsylvania and northern Maryland (Figure 7.3.4-1) may represent deposits transported along an Iapetan rift–related transform fault linking the southern Lynchburg rift basin with a comparable rift basin in southern New England (Valentino and Gates, 1995). The IRM influenced the location of salients and angular recesses during subsequent Appalachian orogenesis and Atlantic rifting (Thomas, 2006). A master detachment separates overthrusted Paleozoic Appalachian terranes from the relatively intact continental crust of North America that includes IRM structures (Spencer et al., 1989; Cook et al., 1979; McBride et al., 2005). In the southern Appalachians, the Consortium for Continental Reflection Profiling (COCORP) seismic-reflection data in Tennessee and Georgia show the master detachment to be ~6 km (3.5 mi.) deep at the western flank of the Appalachians and ~10 km (6 mi.) deep in the Piedmont zone, then quickly steepening to ~35 km (22 mi.) deep beneath the peri-Gondwanan Carolina terrane to the east, where it merges with the Moho (Cook et al., 1979; McBride et al., 2005).

The western extent of significant extensional structures associated with the IRM is not well defined. The IRM exhibits some tectonic inheritance from Grenville structures. For example, the trace of the Alabama-Oklahoma transform corresponds to the probable location of a large-scale dextral bend in the Grenville front that subsequently localized the Ouachita salient and Mississippi embayment (Thomas, 2006). The New York–Alabama (NY-AL) lineament represents a crustal-scale right-lateral strike-slip fault that may have formed during either a late postcontractional stage of the Grenville orogeny, Iapetan rifting, or Appalachian orogenesis (Steltenpohl et al., 2010). The NY-AL lineament locally parallels and coincides with linear fault segments that border the Rome trough (Steltenpohl et al., 2010). Rift-parallel graben systems of the Rome trough formed inboard from the rifted margin during late synrift extension (Thomas, 2006) and may represent inboard extension of Iapetan rifting along the Mesoproterozoic East Continent rift basin (Drahovzal, 1997; Stark, 1997). It appears that a part of the fault along the southern margin of the trough was reactivated as a normal fault that underwent west-side-down dip-slip displacement during the formation of the Rome trough (Steltenpohl et al., 2010). To the north, crust northwest of the NY-AL lineament appears to have behaved as a coherent block (Steltenpohl et al., 2010). The Michigan basin experienced late Cambrian–Early Ordovician subsidence that evolved into different styles and geometry of subsidence in response to subsequent Appalachian tectonic events, indicating that Iapetan rifting did not affect the Michigan basin (Howell and van der Pluijm, 1999).

The following subsections present geologic and seismic information for zones of elevated seismicity within the continental crust of the PEZ seismotectonic zone.

7.3.4.1.1 Giles County, Virginia, Seismic Zone (GCVSZ)

Earthquake foci at Giles County in southwestern Virginia define a tabular zone that strikes N44°E and dips steeply to the southeast within Precambrian basement lying beneath Appalachian thrust sheets (Bollinger and Wheeler, 1983, 1988). This zone, referred to as the Giles County, Virginia, seismic zone (GCVSZ), is about 40 km (25 mi.) long, 10 km (6 mi.) wide, and 5–25 km (3–15.5 mi.) deep (Bollinger and Wheeler, 1982, 1983; Bollinger et al., 1991). The zone is oriented about 20 degrees counterclockwise from the east-northeasterly trend of the overlying structures in the Valley and Ridge province and subparallel to the northeasterly trend of the central Appalachian structures in the northern part of the state (Bollinger et al., 1991).

Possible differential uplift of Tertiary and younger New River fluvial terraces in southwestern Virginia in the area of the GCVSZ has been postulated as resulting from movement on a series of small faults exposed in the terraces (i.e., the high-angle Pembroke faults of Law et al., 1993). The location and relative displacement of the Pembroke faults is consistent with orientation of the GCVSZ and principal-stress estimates from focal-mechanism studies (Mills, 1986). The Pembroke faults and a broad antiformal fold exposed in unconsolidated fluvial deposits have raised questions about the possibility of surface tectonic faulting that may be related to seismic activity in this region (Bollinger et al., 1992; Law et al., 1993; Robinson et al., 1993). The age of the deformed sediments, which lie at 55 m (180 ft.) above the current level of the New River, is estimated as 1.5 ± 0.4 Ma or 2.0 ± 0.4 Ma based on analysis of cosmogenic ^{26}Al and ^{10}Be present in the deposits (Granger et al., 1997; Law et al., 1998). Therefore, the age of this deformation, whether tectonic or nontectonic in nature, is latest Pliocene to Pleistocene.

The east-northeast-/west-southwest-trending antiform in these sediments extends over a horizontal distance of at least 95 m (312 ft.) from limb to limb and plunges 70 degrees toward N64°E. Two grabens are associated with the antiform, one in the hinge zone and one on the south-southeast-dipping limb. The grabens are downward-narrowing structures defined by at least five extensional faults having apparent dip-slip offsets of 1–2.8 m (3.3–9.2 ft.). These faults are marked by 10–20 cm (4–7.8 in.) wide zones of clay-rich infilling. Based on the orientation of striae on surfaces within the fault zones, displacements of 11.4 m (37.4 ft.), 1.84 m (6 ft.), 1.1 m (3.6 ft.), and 3 m (9.8 ft.) are indicated for four of these faults. Judging from electrical resistivity surveys, the major graben is a linear feature that can be traced for a distance of 100–130 m (300–400 ft.). Recent geophysical investigations (Robinson et al., 1993), however, have not been successful in imaging anything below a depth of approximately 35 m (115 ft.), and thus the downdip extent of these structures is unknown. Law et al. (1994) presented three models to explain the formation of the fold and fault structures at this site: landsliding, solution collapse, and basement faulting of tectonic origin. Although some researchers have noted that the correlation between surface faults and subdetachment seismogenic structures may be tenuous or completely lacking (e.g., Chapman and Krimgold, 1994), Law et al. (1994, 1997) concluded from a review of the available data and interpretations that a tectonic origin cannot be ruled out.

Additional geophysical and subsurface investigations of these structures provide further constraints on the origin of the fold and faults. Robinson et al. (2000) show that voids occurring in the terrace sediments may result from cavity collapse in the underlying limestone, and that no

features occur in the limestone basement that correspond to the fold and graben structure in the terrace deposits. Williams et al. (2000) map a linear depression in the limestone bedrock surface that corresponds to the graben in the terrace deposits, and note that the fold and graben structure has a linear nature that is not consistent with a subcircular sinkhole. Law et al. (2000) show that the nature of fine structure in some of the terrace deposits is consistent with sedimentation in a depression formed by limestone solution, followed by inversion to form the anticlinal structure.

These observations appear to indicate that some or all of the observed deformation is nontectonic in origin. Additional surficial mapping by Anderson and Spotila (2001) of fractures in bedrock outcrops shows that the orientation of many small fractures is not consistent with topography or with karst-related subsidence. Anderson and Spotila (2001) note that one set of northeast-trending fractures crosscuts the regional structural trend, is oriented consistent with the trend of the underlying seismic zone, and may be a surface manifestation of rupture in the seismic zone. None of the field evidence, however, provides any direct evidence for Quaternary displacement on these fractures.

7.3.4.1.2 Eastern Tennessee Seismic Zone (ETSZ)

The Eastern Tennessee seismic zone (ETSZ) is a well-defined, northeasterly trending belt of seismicity, 300 km (186 mi.) long by less than 100 km (62 mi.) wide, within the Valley and Ridge and Blue Ridge physiographic provinces of eastern Tennessee and parts of North Carolina, Georgia, and Alabama (Johnston et al., 1985, Bollinger et al., 1991; Powell et al., 1994; Chapman et al., 2002). This area is one of the most active seismic regions in eastern North America in terms of the rate of small (i.e., $\mathbf{M} < 5$) earthquakes.

The earthquakes are spatially associated with major potential field anomalies (King and Zietz, 1978; Johnston et al., 1985; Bollinger et al., 1991; Powell et al., 1994; Kaufmann and Long, 1996; Vlahovic et al., 1998; Chapman et al., 2002). For example, the western margin of the ETSZ is associated with a prominent gradient in the total intensity magnetic field marking the NY-AL lineament (Chapman et al., 2002). Alternative structural models have also been postulated to explain the association of seismicity with these anomalies. Powell et al. (1994) proposed that the ETSZ is an evolving seismic zone in which slip on north- and east-striking surfaces is slowly coalescing into a northeast-trending strike-slip zone running along or near the northwest boundary of the Ocoee block in eastern Tennessee. Strike-slip motion would be consistent with both the sharp nature of this boundary, as inferred from its magnetic signature, and the orientation of the boundary in the contemporary stress field. Powell et al. (1994) suggested that the ETSZ seismic activity results from the regional stress field, and the activity is coalescing near the juncture between a relatively weak, seismogenic block (the Ocoee block of Johnston et al., 1985) and the relatively strong crust to the northwest, which may be strengthened by mafic rocks associated with an inferred Keweenawan-age rift (1,100 Ma; Keller et al., 1982). Powell et al. (1994) also noted that the densest seismicity and the largest of the instrumentally located epicenters in the ETSZ generally lie close to and east of the NY-AL magnetic lineament between latitudes 34.3°N and 36.5°N, and west of the Clingman magnetic lineament.

Based on detailed analyses of the pattern and focal mechanisms of earthquakes in the ETSZ, Chapman (1996) and Chapman et al. (1997) present a more refined picture of the nature of

faulting in the region. Using a revised velocity structure model (Vlahovic et al., 1996), focal mechanisms and hypocentral locations were updated. Statistical analysis of trends in the earthquake focal mechanisms suggests that earthquakes occur primarily by left-lateral strike-slip on east-west-trending faults, and to a lesser degree by right-lateral slip on north- and northeast-trending faults. The hypocenters suggest that possible east-west-trending fault sources are up to 50–100 km (31–62 mi.) long and lie east of, but adjacent to, the NY-AL lineament. This more refined picture is consistent with a tectonic model in which seismogenic faulting is localized along a sharp contrast in crustal strength, reflecting competency as represented by the NY-AL lineament.

An alternative model to explain the localization of seismicity in the eastern Tennessee region is given by Long and Kaufmann (1994). After an analysis of the velocity structure of the region, they conclude that the seismically active areas are not apparently constrained by the crustal blocks defined by the NY-AL lineament, but rather their locations are determined by low-velocity regions at midcrustal depths. They suggest that the data support the conjecture that intraplate earthquakes occur in crust that may be weakened by the presence of anomalously high fluid pressures. Their data suggest that only a portion of the NY-AL lineament is consistent with the interpretation of this lineament as a contact between two crustal blocks having different properties.

Steltenpohl et al. (2010) propose in recent work that seismicity of the ETSZ may be localized along a N15°E-trending magnetic low anomaly in the Ocoee block. They observe that seismicity occurs south of the NY-AL lineament and follows this trend within the magnetic anomalies. This anomaly coincides with the subsurface extension of the Amish anomaly beyond the NY-AL lineament and is interpreted to represent metasedimentary gneissic rocks. The modern stress field is compatible with that which initiated dextral motion along the NY-AL lineament. The magnetic grain of the gneissic rocks and depositional anisotropies could control the spatial pattern of modern seismicity, given the lack of known faults.

Chapman et al. (2002) conclude that the linear segments, and the locations of their terminations, may reflect a basement fault structure being reactivated in the modern stress field. They state that physical processes for reactivation of basement faults could involve a weak lower crust and/or increased fluid pressures within the upper to middle crust. There may be a marginal correlation between the seismicity and major drainage pattern and general topography of the region, suggesting a possible hydrological element linkage (Chapman et al., 2002).

7.3.4.1.3 Clarendon-Linden Fault System

The Clarendon-Linden fault system is located in upstate New York south of Lake Ontario (Figure 7.3.4-1) and comprises a broad zone of faults with small displacements in lower Paleozoic bedrock. The fault system is at least 77 km (48 mi.) long and 7–17 km (4–10.5 mi.) wide and is spatially coincident with a north-trending geophysical (combined magnetic and gravity) lineament within the basement rock (Fakundiny and Pomeroy, 2002). The fault system extends for approximately 150 km (93 mi.) from just north of the Pennsylvania border (Jacobi and Fountain, 1993) to the north shore of Lake Ontario (Hutchinson et al., 1979).

Closely spaced small-offset step faults characterize the Clarendon-Linden fault system in outcrops of Devonian rocks (Jacobi and Fountain, 1993, 1996, 2002). By integrating surface stratigraphy, structure, soil gas, and lineaments, Jacobi and Fountain (2002) recognized as many as 10 parallel, segmented faults across the fault system in southwestern New York State. The main strand of the Clarendon-Linden fault system is highly segmented, steeply east-dipping in the north and west-dipping in the south, and displays a maximum vertical displacement of about 80 m (262 ft.; Jacobi and Fountain, 1993). Cumulative offset across the Clarendon-Linden fault system is as high as 130–200 m (426–656 ft.), according to well log, outcrop, and seismic data (Jacobi and Fountain, 1996). Forsyth, Milkereit, Zelt, et al. (1994); Milkereit et al. (1992); and Zelt et al. (1994) suggested that the Clarendon-Linden fault system is part of a wider zone of small Paleozoic faults that lie above the crest of a northeast-trending Precambrian bedrock high (i.e., the Iroquoian high).

The Clarendon-Linden fault system is inferred to extend northeastward beneath Lake Ontario, coincident with a bathymetric lineament known as the Scotch Bonnet Rise (Hutchinson et al., 1979). The Scotch Bonnet Rise is a west-facing bedrock ridge that exhibits approximately 20 m (66 ft.) of relief and may be related to faulting (Anderson and Lewis, 1975). Hutchinson et al. (1979) collected seismic data across the Scotch Bonnet Rise and, within the resolution of their data (approximately 2–3 m [6.6–9.8 ft.]), observed no evidence for postglacial Holocene faulting across this feature. Both the Clarendon-Linden fault system and the Scotch Bonnet Rise coincide with the east flank of a magnetic anomaly and the west edge of a series of Bouguer gravity anomalies, both of which can be traced from west-central New York to the north shore of Lake Ontario (Hutchinson et al., 1979).

Deep seismic-reflection data suggest that the Clarendon-Linden fault system is coincident with structures associated with the Elzevir-Frontenac terrane boundary zone of the Grenville province (Milkereit et al., 1992; Zelt et al., 1994; Forsyth, Milkereit, Zelt, et al., 1994; Easton and Carter, 1995). Seismic-reflection profiles show the gently east-dipping ductile thrusts of the Elzevir-Frontenac boundary zone extending up to the Precambrian/Paleozoic contact in the region of the Clarendon-Linden fault system (Forsyth, Milkereit, Zelt, et al., 1994; Jacobi and Fountain, 1996). However, the Precambrian structures do not lead directly to individual Clarendon-Linden faults (Jacobi and Fountain, 1996). The Salmon River fault, which is exposed approximately 30 km (18.5 mi.) north of Lake Ontario, is believed to be the northern extension of the Clarendon-Linden fault system (McFall, 1993). Farther north, the projection of the Clarendon-Linden fault system and Salmon River faults coincide with the Robertson Lake mylonite zone in the Canadian Shield (McFall, 1993; Easton and Carter, 1995). The surface continuity of inferred faults constituting the Clarendon-Linden fault system is not strongly supported by the reprocessed seismic data examined by Ouassaa and Forsyth (2002). Ouassaa and Forsyth (2002) also noted that north-northeast-trending curvilinear magnetic and gravity anomalies parallel, but are not restricted to, the principal trend of the postulated Clarendon-Linden fault system.

The Clarendon-Linden fault system probably represents brittle reactivation of a major Grenville structure (Hutchinson et al., 1979; Seeber and Armbruster, 1995). The detailed map pattern of the Clarendon-Linden fault system shows that the north-south-trending faults comprise numerous short segments connected by oblique northwest-trending transfer faults, similar to that in rift settings (Jacobi and Fountain, 1996). This geometry suggests that the underlying east-dipping

Precambrian thrusts could have acted as a detachment surface, possibly during Iapetan rifting (Jacobi and Fountain, 1996). Culotta et al. (1990) correlated the Clarendon-Linden fault system with a continental-scale magnetic lineament, the Amish anomaly, which is crosscut by the NY-AL lineament (Culotta et al., 1990). This anomaly is interpreted as a major Grenville terrane boundary that separates the Elzevir and Frontenac tectonic blocks (Culotta et al., 1990).

The Clarendon-Linden fault system is associated with a well-defined cluster of seismicity, which is referred to as the Attica seismic zone (Seeber and Armbruster, 1995). This zone contains the 1929 m_b 5.2 (E[**M**] 4.72**)** Attica earthquake, numerous natural small-magnitude earthquakes, and several induced earthquakes associated with salt brine recovery at Dale, New York (Fletcher and Sykes, 1977). Seeber and Armbruster (1995) suggest that the 1929 earthquake may have been artificially triggered, as the brine fields in Dale were already active in 1929. Dineva et al. (2004) relocated hypocenters from earthquakes occurring between 1990 and 2001 that delineate clusters of earthquakes beneath Lake Ontario. They report that their cluster C is parallel to the Clarendon-Linden fault system but shifted slightly to the southeast by about 4 km (2.5 mi.). During the 1990–2001 recording period for their analysis, Dineva et al. (2004) note that little seismic activity occurred along the Clarendon-Linden fault system, with only two earthquakes near the southern end.

7.3.4.2 Basis for Defining Seismotectonic Zone

As described in Section 7.3.4.1, reactivation of Iapetan rift–related structures has been postulated as a causal mechanism for localizing seismicity in the Appalachian Mountains, St. Lawrence, and eastern Great Lakes regions. Well-documented Iapetan faults that were reactivated during the Mesozoic are included in the SLR seismotectonic zone (Section 7.3.1). Likewise, thinned Iapetan crust under the Atlantic coastal plain that experienced significant extension during the Mesozoic is included in the ECC seismotectonic zone (Section 7.3.7). Postulated Iapetan structures beneath the Appalachian detachment west of the Piedmont gravity anomaly gradient are not easily identified and are interpreted only from limited seismic and borehole information. The PEZ seismotectonic zone encompasses IRM crust in that region, which exhibits some evidence of early Paleozoic rifting or extension.

Extended crust of the PEZ seismotectonic zone does not exhibit clear evidence of rift faulting. The deep seismic data collected in Lakes Ontario and Erie (e.g., Milkereit et al., 1992; Forsyth, Milkereit, Davidson, et al., 1994; Forsyth, Milkereit, Zelt, et al., 1994; Zelt et al., 1994; White et al., 1994) do not show high-angle extensional structures or extensional deformation within the PEZ seismotectonic zone on the scale of the Ottawa graben faults or the St. Lawrence rift faults, providing very strong evidence that a failed rift arm does not extend into the lake. Faulted lower Paleozoic rocks in the northeastern Lake Ontario region (e.g., Grier, 1995; Williams, 1991) generally exhibit maximum offsets on the order of several tens of meters. Normal faulting within the PEZ seismotectonic zone is associated with the Rome trough, Clarendon-Linden fault system, and CMBBZ, which represent extensional reactivation of Grenville structures, as opposed to rift structures.

Because Mesozoic extension within the PEZ seismotectonic zone is equivocal, crust of the SLR, ECC-AM, and ECC-GC seismotectonic zones is separated from the PEZ seismotectonic zone based on the more definitive evidence of Mesozoic extension in those zones. However, it is difficult to preclude that subdetachment structures within the PEZ seismotectonic zone that are currently active were not also reactivated during Mesozoic opening of the Atlantic Ocean (Swanson, 1986; Williams, 1978; Pratt et al., 1988; Cook et al., 1979; McBride et al., 2005). Therefore, the PEZ seismotectonic zone is differentiated from the adjacent Midcontinent-Craton (MidC) seismotectonic zone to accommodate alternative Mmax priors (see discussion in Section 7.3.4.4).

7.3.4.3 Basis for Zone Geometry

The PEZ seismotectonic zone characterizes crust extended in the Paleozoic inboard of the rifted margin. Iapetan normal faults likely decrease in size, abundance, and slip gradually and irregularly northwestward into the North American craton over a distance of perhaps 100–200 km (60–120 mi.; Bollinger and Wheeler, 1988). The eastern margin of the Paleozoic Appalachian terranes beneath the detachment corresponds to a gravity anomaly gradient underlying the Piedmont that is inferred to represent thinning of crust (Pratt et al., 1988) (Figure 7.3.4-2). Bollinger and Wheeler (1988) suggested that the steep eastward rise in the Bouguer gravity anomaly field is the eastern limit for the Iapetan normal faults and that most of the faults occur in the relatively intact continental crust of North America west of the gravity anomaly gradient. This gravity anomaly gradient, referred to as the Appalachian (Piedmont) gravity gradient, is interpreted to mark the transition from thick continental to less thick, and possibly more mafic (transitional), crust to the east (James et al., 1968; Kane and Long, 1981; Hatcher and Zietz, 1980; Hutchinson et al., 1983). Wheeler (1996) interprets this boundary as the hinge zone of the IRM. Two alternative geometries are considered for PEZ, namely, the PEZ Narrow and PEZ Wide. The criteria for defining these two alternatives are discussed below.

7.3.4.3.1 PEZ Narrow

The PEZ Narrow (PEZ-N) geometry is defined based on structural and seismologic evidence that provides the most convincing evidence for the presence of Iapetan faults or rift sediments below the detachment (Wheeler et al., 1995). This alternative is given the highest weight (0.8) because of the strength of this evidence. The western boundary of the PEZ-N alternative geometry follows the Birmingham basement fault system in Alabama and the NY-AL lineament to the northeast. Crust northwest of the NY-AL lineament appears to have behaved as a rigid, somewhat coherent block, and its sharp boundary against the anomaly implies the edge of this competent block (Steltenpohl et al., 2010). King and Zeitz (1982) suggested that the lineament acted as buttress during the Paleozoic and limited Appalachian deformation east of it. Seismicity is observed below the detachment in Giles County and eastern Tennessee, supporting the concept that these earthquakes involve reactivation of Iapetan structures below the detachment surface.

7.3.4.3.2 PEZ Wide

The PEZ Wide (PEZ-W) geometry extends to the west to capture additional crust that was extended to a lesser degree during opening of the Iapetan Ocean. Given that Iapetan rift structures and significant extension are assumed to decrease to the west, and the evidence for extensional reactivation is limited, a low weight (0.2) is assigned to the PEZ-W alternative.

The western boundary of the PEZ-W alternative geometry follows the Rome trough in Kentucky and West Virginia and the CMBBZ in Ontario. Wheeler (1995) interpreted the Clarendon-Linden fault system of upstate New York as the westernmost limit of Iapetan faulting in the vicinity of the Great Lakes. The Clarendon-Linden fault system appears to be associated with a Grenville shear zone at depth. Movement along the Clarendon-Linden fault system records Iapetan reactivation (Seeber and Armbruster, 1995) of the Grenville Elzevir-Frontenac boundary zone, indicating the extent of the extensional stress field and not the location of through-going rift faults. Lower Paleozoic extensional reactivation also is exhibited farther west on the CMBBZ (Milkereit et al., 1992; Forsyth, Milkereit, Davidson, et al., 1994). Recent interpretation of seismic lines and regional magnetic data place the western boundary of the CMBBZ on the west side of the Mississauga domain as defined by O'Dowd et al. (2004).

The western boundary of the PEZ-W continues southward to the western margin of the Rome trough, following the Kentucky River fault system (Van Arsdale, 1986, Potter et al., 1995; Steltenpohl et al., 2010). Subsidence of the Rome trough may represent inboard extension of Iapetan rifting along the Mesoproterozoic East Continent rift basin (Drahovzal, 1997). Stark (1997) attributes development of the Rome trough and reactivation of the Kentucky River fault system to reactivation of the East Continent rift complex during Iapetan extension. The western boundary of the Rome trough coincides with the western limit of Grenvillian contractional deformation (i.e., Grenville front) and the eastern boundary of the East Continent rift basin (Drahovzal et al., 1992).

7.3.4.4 Basis for Zone Mmax

Paleoseismic investigations from the Rome trough, eastern Tennessee, and the vicinity of the Clarendon-Linden fault system do not provide evidence for large-magnitude earthquakes in these areas of historically higher seismicity. Van Arsdale and Sergeant (1992) trenched terrace materials along the Kentucky River fault system, which forms the northern boundary of the Rome trough, and observed evidence for folding and faulting within the last five million years, and probably within the last million years. The absence of post-Paleozoic deposits prevents the determination of Mesozoic or Tertiary reactivation (Van Arsdale and Sergeant, 1992). Whisner et al. (2003) performed paleoseismic reconnaissance investigations in a 300 km^2 (186 $mi.^2$) area within the most active part of the ETSZ and found no evidence of large prehistoric earthquakes.

An NRC-sponsored research effort was initiated in the ETSZ in the last half of 2009 to help clarify the late Quaternary earthquake history and hazard potential of this seismic zone. At locations east to northeast of Knoxville, Tennessee, with late Quaternary terrace deposits, Vaughn et al. (2010) report the occurrence of outcrop-scale strike-slip, reverse, and normal faults and prevalent fractures; minor paleoliquefaction features; and anomalous fractured and disrupted

features attributed to liquefaction and forceful expulsion of groundwater during one or more major late Quaternary earthquakes. These preliminary observations suggest that the ETSZ has produced surface faulting and generated one or more strong earthquakes during late Quaternary time. However, these preliminary results could not qualify that RLMEs had occurred in the ETSZ, and were therefore insufficient to determine whether the ETSZ could be considered an RLME zone and treated accordingly in the CEUS SSC Project.

A paleoliquefaction study of the Clarendon-Linden fault system was conducted by Tuttle et al. (2002). These investigations observed a lack of earthquake-induced liquefaction features in geologic units susceptible to liquefaction, suggesting that the fault system did not generate large M > 6 earthquakes during the past 12,000 years. Tuttle et al. (2002) conclude that the fault system could have produced small and moderate earthquakes, but probably not large earthquakes during the late Wisconsinan and Holocene. Because this lack of evidence for paleoliquefaction features may not indicate an absence of past earthquakes, the maximum magnitude for the PEZ seismotectonic zone is modeled by historical seismicity.

Paleoseismic investigations in other areas of the PEZ seismotectonic zone have not been carried out. Therefore, the maximum magnitude for PEZ-N and PEZ-W is assessed using historical earthquakes. The largest observed earthquake in the PEZ seismotectonic zone is the 1897 Giles County earthquake (MMI = VIII, m_b = 5.7; E[**M**] 5.91), which occurred within this zone near the Virginia–West Virginia border (Bollinger and Hopper, 1971). The next largest earthquakes are also located near Giles County and include the 1861 E[**M**] 5.63 and 1852 E[**M**] 5.21 earthquakes. The largest recorded earthquakes associated with the ETSZ are the 1973 M_S 4.6[3] (E[**M**] 4.01) Maryville, Tennessee, earthquake (Stover and Coffman, 1993) (m_b 4.6; Bollinger et al., 1991) and the April 2003 **M** 4.6 (E[**M**] 4.53) Fort Payne earthquake that occurred in northeastern Alabama near the Georgia border.

A likelihood function based on the moment magnitude of the 1897 Giles County earthquake is used to update two prior distributions representing alternative interpretations of the age of most recent activation of extensional features in the PEZ seismotectonic zone (NMESE and MESE, see Section 5.2). The geometries of the PEZ seismotectonic zone are defined largely by the limit of Iapetan rifting in the late Precambrian and early Cambrian. However, some researchers have suggested thatMesozoic extension continued west into crust of the PEZ seismotectonic zone. Faure et al. (2006) performed paleostress analysis of mesoscopic faults and emplacement of Jurassic dikes in Quebec and New Brunswick and concluded that preexisting Neoproterozoic, Taconic, Acadian, and Alleghanian structures within this zone were reactivated during the opening of the Atlantic Ocean and are kinematically linked to faults bounding Mesozoic basins. This work suggests that Atlantic rifting was a widespread extensional event extending as far as 400 km (244 mi.) into the plate (Faure et al., 2006). Pliocene and younger deformation within Giles County (Law et al., 1993, 1998) and the Rome trough (Van Arsdale and Sergeant, 1992) can be considered a proxy for Mesozoic activity. Therefore, some weight is given to a Mesozoic and younger prior for the PEZ seismotectonic zone. The resulting Mmax distributions are presented in Section 7.4.2.

[3] M_S = surface-wave magnitude.

7.3.4.5 Future Earthquake Characteristics

Earthquakes within the PEZ seismotectonic zone exhibit predominantly strike-slip focal mechanisms with a variety of orientations. Therefore, default characteristics for fault orientation are used, but style of faulting parameters is modified to give a higher weight to strike-slip (0.80) than to reverse (0.20) faulting based on the focal mechanism information described below. The default orientations are therefore modeled with the default characteristics for future earthquakes.

Bollinger and Wheeler (1988) propose that earthquakes in Giles County consist of strike-slip faulting below the Appalachian detachment on steeply dipping (>70 degrees) planes. They attribute right-lateral slip on northerly striking nodal planes or left-lateral slip on easterly striking nodal planes (Bollinger and Wheeler, 1988) to a series of down-to-the-east, subdetachment faults associated with Iapetan rifting (Gresko, 1985). The P-axis estimates (i.e., maximum compressive stress axes) are uniformly of a northeasterly (north-northeast to east-northeast) trend with subhorizontal inclination, and are similar to the orientation of P-axis estimates elsewhere in the region (Bollinger and Wheeler, 1988).

Focal mechanisms in eastern Tennessee indicate strike-slip faulting on steeply dipping planes and a uniform regional stress field with horizontal maximum compression trending N70E (Chapman et al., 2002). Most mechanisms involve either right-lateral motion on north-south-oriented planes or left-lateral slip on east-west-oriented planes (Chapman et al., 1997). Chapman et al. (2002) also note that a smaller population shows right-lateral motion on northeasterly trending planes, parallel to the overall trend of the seismicity. The seismicity is not uniformly distributed; rather, epicenters form northeasterly trending en echelon segments (Chapman et al., 2002).

Focal mechanisms near the Great Lakes are also predominantly strike-slip. Herrmann (1978) reported that focal mechanism studies of two shallow (2–3 km, or 1.2–1.9 mi.) earthquakes in 1966 and 1967 in the Attica area suggested that seismicity occurs along approximately north-northeast-trending Clarendon-Linden faults. The 1966 earthquake (m_b = 4.6 [E[**M**] 4.26]) yielded solutions with one nodal plane striking north-northeast and dipping steeply to the east, and a second striking west-northwest and dipping steeply to the south. If the north-northeast solution is accepted, then the fault motion was primarily right-lateral strike-slip with a reverse component. The 1967 earthquaket (m_b = 4.4 [E[**M**] 4.07]) yielded solutions with one nodal plane striking north-northeast and dipping steeply to the east, and a second west-northwest-striking plane dipping moderately to the south. Again, accepting the north-northeast solution indicates right-lateral and reverse slip on the fault. Herrmann (1978) selected the north-northeast nodal plane as the most likely fault plane solution, based on the well log data (Van Tyne, 1975) indicating north-northeast-trending Clarendon-Linden faults. He noted, however, that the west-northwest trend could not be totally discounted. Kim et al. (2006) determined a predominantly strike-slip double-couple moment tensor with a strike of 8 degrees east of north and dipping to the east (50 degrees) for the August 4, 2004, Lake Ontario earthquake.

Kim et al. (2006) determined a precise hypocentral depth of 4 ± 2 km (2.4 ± 1.2 mi.) mechanism for the August 4, 2004, M_w 3.1(E[**M**] 3.11) earthquake located in Lake Ontario. This shallow depth is consistent with other well-located earthquakes near Lakes Erie and Ontario, including

the 1966 Attica earthquake (2 km [1.2 mi.]); the 1967 Attica earthquake (3 km [1.8 mi.]); the 1998 Pymatuning, Pennsylvania, earthquake (2 km [1.2 mi.]; Du et al., 2003); the 2001 Ashtabula, Ohio, earthquake (2 km [1.2 mi.]); and the 1986 Perry, Ohio, earthquake. These observations suggest a broad-scale strike-slip faulting stress regime with a shallow seismogenic layer in the Erie-Ontario Lowlands. Dineva et al. (2004) provide the depth distribution for relocated hypocenters in the Great Lakes region. These data are consistent with the shallow hypocentral depths mentioned above. However, the entire distribution has a 95th percentile depth of approximately 16 km (10 mi.). Ma and Atkinson (2006) determined focal depths for small to moderate earthquakes in southern Ontario and northern New York that range from 2 to 15 km (1.2 to 9 mi.). Focal depths of most earthquakes in ETSZ range from 5 to 22 km (3 to 13.4 mi.) and lie beneath detached Alleghanian thrust sheets (Vlahovic et al., 1998; Chapman et al., 2002). Therefore, the thickness of seismogenic crust is modeled using the default alternatives.

7.3.5 Ilinois Basin Extended Basement Zone (IBEB)

Southern Indiana and southern Illinois are characterized by higher rates of seismicity than adjacent craton regions. Braile et al. (1984) proposed that two branches or arms of the Reelfoot rift, the Wabash Valley and St. Louis arms, extend into southern Indiana and southeast Missouri, respectively. Although subsequent studies (e.g., Wheeler and Cramer, 2002) have demonstrated that highly extended rifted crust does not extend into these regions as far as Braile et al. (1984) proposed, the interpretation of seismic profiles and the mapping and dating of paleoliquefaction features in the southern Illinois basin provide evidence for multiple paleoearthquakes having magnitudes larger than historical earthquakes that have occurred in this region. The two largest paleoearthquakes that appear to be localized within the Wabash Valley are included in the Wabash Valley RLME source zone (Section 6.1.9). Four additional paleoearthquakes estimated to be approximately **M** 6.2–6.3 are recorded by more widely distributed liquefaction features and inferred energy centers for moderate-sized earthquakes beyond the limits of the Wabash Valley RLME source (Table 6.1.9-1; Figures 7.3.5-1, 7.3.5-2, and 7.3.5-3). These earthquakes are considered in the characterization of the Illinois Basin Extended Basement (IBEB) seismotectonic zone.

An additional energy center near St. Louis, referred to as the Meramec River energy center, is not included in the IBEB zone. The Meramec energy center lies outside the areas of extended Precambrian basement used to define the zone boundaries (Section 7.3.5.3); it has been postulated that paleoliquefaction features here could be the result of smaller (**M** < 6.0) local earthquakes or larger earthquakes (**M** 7.0–7.5) originating on structures in the southern Illinois region (e.g., the Du Quoin monocline/Centralia fault that lies within the IBEB) (Tuttle, Chester et al., 1999; Tuttle, 2005b). The Wabash Valley RLME source zone as described in Section 6.1.9 is an independent zone that characterizes only RLMEs. Earthquakes of magnitudes less than the RLME maximum magnitude are modeled based on recurrence parameters for the IBEB seismotectonic zone.

7.3.5.1 Background

McBride, Hildenbrand, et al. (2002) and McBride et al. (2007) have completed integrated analyses of geophysical, industry seismic reflection profile, and well data to evaluate possible fault sources for historical earthquakes in the southern Illinois basin. These studies suggest that both Precambrian basement and Paleozoic structures within the southern Illinois basin have been reactivated by recent moderate-sized earthquakes, and that to a large degree, Paleozoic structures may be decoupled from deeper seismogenic Precambrian basement structures. Although some historical earthquakes, such as the 1987 m_b 5.2 (E[**M**] 4.95) earthquake, may be associated with a fault-propagation fold representing possible reactivation of a basement fault that originated during the Laramide orogeny), McBride et al. (2007) suggest that a clear association of seismicity with mapped structural trends is not well documented throughout the southern Illinois basin.

McBride et al. (2007) note that the post-Mississippian structure and stratigraphy of the Illinois basin's thick Paleozoic sedimentary section have been investigated using petroleum industry boreholes and limited seismic reflection profiles (e.g., Sexton et al., 1986; Kolata and Nelson, 1991; Bear et al., 1997; McBride and Nelson, 1999). The seismic stratigraphy and composition of the Precambrian basement upper crust have been less well characterized (Pratt et al., 1992; Van Schmus et al., 1996; Potter et al., 1997; McBride and Kolata, 1999; McBride et al., 2003), and thus the deep structure of the basin remains poorly understood.

Historical epicenter relocation studies by the USGS, based on the method of Bakun and Wentworth (1997), have repositioned moderate- to large-magnitude earthquakes over or near major structural axes in the southern Illinois basin (e.g., Du Quoin monocline; Cottage Grove fault system; La Salle anticlinal belt) (Bakun et al., 2003; Bakun and Hopper, 2004a).

The Du Quoin monocline has been suggested by some researchers (Su and McBride, 1999; Tuttle, Chester, et al., 1999; Tuttle, Schweig, et al., 2005) as a possible causative source for the earthquake that resulted in the paleoliquefaction features in the Shoal Creek–Kaskaskia River region of south-central Illinois.

Other prehistoric earthquakes, such as the Springfield paleoearthquake, cannot be readily correlated to mapped structures in the Paleozoic cover rocks, but may be associated with a magnetic anomaly (Figure 7.3.5-3).

7.3.5.2 Basis for Defining Seismotectonic Zone

The following observations suggest that there are fundamental differences in the crust underlying the southern Illinois basin that will influence the maximum magnitude and future earthquake characteristics relative to the surrounding regions:

- There is evidence of several moderate-sized paleoearthquakes and higher rates of instrumental seismicity in parts of this region that are not recognized in the adjoining craton regions.

- The southern part of the Illinois basin is one of the most structurally complex areas of the Midcontinent (McBride et al., 2007). McBride et al. (2007) note that (1) Proterozoic rift faults distinct from those bounding the Grayville graben (in the Wabash Valley RLME source zone [Section 6.1.9]) are imaged in Precambrian basement rock below a thick sequence of Precambrian layered volcanic rocks; (2) the circular to oval pattern of the sequences in plan view argue against a linear rift geometry and and is instead suggestive of a large rhyolitic collapsed caldera complex; and (3) newly observed mantle reflectivity beneath the Illinois basin indicates significant upper-mantle heterogeneity compared with other parts of the United States studied using reflection methods. These observations suggest that crust beneath the Illinois basin is distinct from that of the neighboring craton.
- An extensive series of moderately dipping reflectors interpreted to be faults is present in the basement. The 1968 m_b 5.5 earthquake may have occurred in response to reactivation of one of these inferred faults.
- Association of dipping crustal reflectors and gently arched Paleozoic strata suggests an additional, but limited, degree of Phanerozoic (post-Precambrian) reactivation of structures spatially associated with the strongly deformed deep structure. Moderate-sized historical earthquakes that appear to be spatially associated with Precambrian basement faults and with Paleozoic faults suggest continued reactivation of older basement features as well as younger Paleozoic structures (McBride et al., 2007).
- Stresses induced by Mesozoic rifting possibly extended into the southern Illinois basin, resulting in reactivation of deep structures. This concept was initially postulated by Braile et al. (1984). Although evidence for Mesozoic rifting is primarily limited to reactivation of basement structures in the Grayville graben (included in the Wabash Valley RLME source, Section 6.1.9), more distal effects cannot be ruled out. The IBEB is defined in part to allow for use of both the non-Mesozoic and younger extended (NMESE) and the Mesozoic and younger extended (MESE) Mmax prior distributions in the assessment of maximum magnitude.

Multiple hypotheses have been presented to explain the localization and high rates of Holocene activity within the adjacent Reelfoot rift and the New Madrid region to the south (see Section 6.1.5). Some of these mechanisms may also apply to the southern Illinois and southern Indiana region, as follows:

- The presence of intrusive rocks in the Precambrian basement may cause a local stress concentration.
- Glacial unloading at the close of the Wisconsinan increased seismic strain rates in the region.
- Descent of the ancient Farallon slab into the deep mantle beneath central North America as inferred from high-resolution seismic tomography induces a highly localized flow and stresses in the Midcontinent.
- This region, like the NMSZ, may be a lithospheric weak zone on the edge of a high-velocity lithospheric block that transfers stress to the upper crust when loaded, thus leading to repeated shallow earthquakes.

None of the individual characteristics alone are sufficient to define the IBEB as a separate seismotectonic zone. However, when considered in combination, they support the contention that the IBEB has different seismogenic characteristics and possibly a different Mmax prior compared with the neighboring regions.

The IBEB source zone is defined to characterize sources of moderate- to large-magnitude earthquakes (excluding those attributed to the Wabash RLME source) that may occur on deep structures in the Precambrian basement and in as Paleozoic faults that extend into the overlying Paleozoic sedimentary rocks.

7.3.5.3 Basis for Zone Geometry

The roughly oval-shaped Illinois basin, overlying parts of Illinois, Indiana, western Kentucky, and southeastern Missouri, contains as much as 7,000 m of Cambrian through Pennsylvanian sedimentary rock units (Buschbach and Kolata, 1991; Nelson, 1995; Figure 7.3.5-2). The basin is bisected by the La Salle anticlinal belt and the Wabash Valley fault system, both of which have expression in the Paleozoic strata.

The extent of the older Precambrian basement structural features is less well known. McBride, Hildenbrand, et al. (2002) identify a proto-Illinois basin based on interpretation of geopotential field data; petroleum industry borehole logs (Buschbach and Kolata, 1991); and deep crustal seismic data. McBride et al. (2001) report that the first vertical derivative of the reduced-to-pole magnetic intensity anomaly map shows a subdued magnetic intensity character associated with the Proterozoic rifting and/or layered volcanic sequences in Precambrian basement as inferred from deep seismic reflection profiles. The pattern continues to the north and east beyond the limits of the deep reflection profile data. The margins of the layered volcanic sequences, especially to the south and west, are marked by prominent coincident closed-contour magnetic and gravity anomalies, which reflect, at least in part, mafic igneous source intrusions that may be related to the original thermal event that produced the Proterozoic Eastern Granite-Rhyolite province (1,480–1,450 Ma; McBride et al., 2001) (Figure 7.3.5-3). Other researchers (e.g., Pratt et al., 1992; Baranoski et al., 2009, Drahovzal, 2009) have identified rift basin sediments in the Precambrian basement below the Paleozoic cover rocks in southern Illinois and southern Indiana. Drahovzal et al. (1992) characterize these basement rocks as the western part of the East Continent rift basin. Baranoski et al. (2009) also interpret clastic rift basins associated with the East Continent rift basin under most of the southern Illinois basin and a basaltic rift basin extending into northern Illinois (Figure 7.3.5-2).

The boundaries of the IBEB are drawn to roughly encompass the various interpretations of basement rift sediments and the areas where moderate-sized prehistoric earthquakes have been identified from paleoliquefaction studies. Because the boundary of the IBEB is not well defined by these data and its exact geographic location is uncertain, it is treated as “leaky,” such that ruptures that nucleate within the zone may also propagate outside the uncertain geographic boundary of the source zone.

7.3.5.4 Basis for Zone Mmax

The Mmax distribution for the IBEB uses only the Bayesian approach, as outlined in Section 5.2. The three largest historical earthquakes recorded within the zone are the September 27, 1891, E[**M**] 5.52; August 15, 1891, E[**M**] 4.97; and April 18, 2008, E[**M**] 5.30 earthquakes. Four prehistoric earthquakes inferred from the paleoliquefaction studies have estimated magnitudes that are larger than the historical earthquakes. These are the ~**M** 6.3 Vallonia, ~**M** 6.2 Shoal Creek, ~**M** 6.2 Springfield, and **M** 6.2 Waverly earthquakes (Figure 7.3.5-1; Table 6.1.9-1).

For the Bayesian approach, three alternative priors are considered: COMP, a composite (weight of 0.4); NMESE, non-Mesozoic and younger extended (weight of 0.48); and MESE, Mesozoic and younger extended (weight of 0.12). The NMESE prior is given a high weight (0.48) based on the lack of evidence for Mesozoic mafic intrusions and significant Mesozoic or younger extension throughout the IBEB zone. Less weight is given to the possibility that stresses associated with Mesozoic extension in the adjacent Reelfoot rift may have propagated into the IBEB zone, giving rise to some reactivation of structures in both the Precambrian basement and the overlying Paleozoic cover. The COMP prior also is given a relatively high weight (0.4) based on the uncertainty in the characteristics that influence maximum magnitude. The prior distribution in each case is truncated and modified based on the evidence for the four moderate-sized paleoearthquakes (**M** 6.2–6.3) in the zone that are not modeled as RLMEs. Due to the uncertainty in the sizes of these paleoearthquakes, which are based primarily on the magnitude-bound curve presented by Olson et al. (2005b), a sigma of 0.25-magnitude units is used in the development of an updated likelihood function. The derived Mmax distribution for IBEB is presented in Section 7.4.2.

7.3.5.5 Future Earthquake Characteristics

Characteristics for future earthquake ruptures in the IBEB source zone are given in Table 5.4-2. The aleatory variability in the future earthquake characteristics assigned to the IBEB is based on the following:

- Consideration of focal mechanisms in the southern Illinois basin region, which are a mixture of interpreted north-northeast-trending strike-slip and reverse mechanisms (Taylor et al., 1989; McBride, Hildenbrand, et al., 2002; McBride et al., 2007; Larson, 2002; Hamburger et al., 2008; Larson et al., 2009; Withers et al., 2009; Yang et al., 2009).
- Orientations of mapped Paleozoic structures (Nelson, 1995).
- Orientations of Precambrian basement faults and inferred structures (McBride et al., 2007).

The expected style of faulting and fault dip vary with the fault orientation and are inferred based on comparison to focal mechanisms and fault geometry, which is also inferred based on analysis of seismic profiles and seismicity data. The majority of earthquakes having well-constrained focal mechanisms show strike-slip movement. Therefore, strike-slip behavior overall is judged to be more likely. However, reverse faulting mechanisms for historical earthquakes also have been associated with reactivated Precambrian basement and Paleozoic structures (McBride et al., 2007).

The depth of future ruptures is based on reported depths of seismicity within the IBEB (Taylor et al., 1989; McBride, Hildenbrand, et al., 2002; McBride et al., 2007; Hamburger et al., 2008; and Yang et al., 2009). The deepest well-constrained earthquake hypocenters in the Fairfield basin, a relatively deep part of the Illinois basin, are located at depths of 20–22 km (12.4–13.7 mi.; (McBride et al., 2007; Yang et al., 2009). However, the average depth throughout the IBEB zone based on other historical earthquakes may be less. Therefore, a range of values from 13 to 22 km (8 to 13.7 mi.) is used to model the average seismogenic depth within the zone.

7.3.6 Reelfoot Rift Zone (RR)

The Reelfoot Rift (RR) seismotectonic zone beneath the northern Mississippi embayment is interpreted as a Cambrian aulacogen (Ervin and McGinnis, 1975; Thomas, 1991). The crystalline basement rocks defining the rift have been mapped from gravity, magnetic, and seismic refraction and reflection data, as well as from subsurface information derived from a few deep petroleum exploration wells (Hildenbrand, 1982; Mooney et al., 1983; Hildenbrand and Hendricks, 1995; Langenheim and Hildenbrand, 1997; Dart and Swolfs, 1998; Parrish and Van Arsdale, 2004; Csontos et al., 2008; Csontos and Van Arsdale, 2008). The RR zone includes the Reelfoot graben as defined by gravity, magnetic, and seismic data, as well as the regions marginal to the rift graben where crustal extension also is indicated by secondary structures and Mesozoic mafic and ultramafic plutons (Hildenbrand and Hendricks, 1995).

RLME sources within the RR zone are independent sources that characterize only RLMEs; these sources include the New Madrid Fault System (NMFS; Section 6.1.5), Eastern Rift Margin (ERM; Section 6.1.6), Marianna (MAR; Section 6.1.7), and Commerce Geophysical Lineament (CGL; Section 6.1.8) RLMEs.

The source characterization of the RR described in the following text is based on a review of published material outlined in the Data Summary table for the Reelfoot Rift–New Madrid Fault System (Appendix Table D-6.1.5-1). Explicit references that were used as the basis for source characteristics are identified in the Data Evaluation table for the RR zone (Appendix Table C-7.3.6).

7.3.6.1 Background

7.3.6.1.1 Evolution of the Reelfoot Rift

Csontos et al. (2008) outline the major tectonic events and evolution of the Reelfoot rift. The following observations are primarily summarized from Csontos et al. (2008) and cited references:

- The Reelfoot rift graben structures are part of the Reelfoot rift–Rough Creek graben–Rome trough intracratonic rift zone that formed during the disassembly of Rodinia and opening of the Iapetus Ocean in late Proterozoic time (Thomas, 1976; 2006). Rifting may have been initiated by an upwelling mantle plume that developed along terrane boundaries (Dart and Swolfs, 1998). Alternatively, the Reelfoot rift may be a consequence of right-lateral strike-

slip motion along a northwest-oriented transform fault that formed the Paleozoic continental margin of southeastern Laurentia (Thomas, 1991).

- An anomalously dense layer is present at the base of the crust and thickens beneath a broad northeast-trending graben that formed during the initial stages of Iapetan rifting. The thickest part of the anomalous crust underlies the region of greatest seismic activity within the geographic limits of the Reelfoot rift (Hildenbrand, 1982).
- Cambrian Reelfoot rifting occurred primarily along large normal faults that appear to become listric with depth (Nelson and Zhang, 1991). However, the straight margin faults suggest that the northeast-trending rift structures originated as strike-slip faults (Hildenbrand, 1985).
- A maximum of 7 km (4.3 mi.) of sediment accumulated in the Reelfoot graben during rifting that continued into middle Cambrian time, while outside the rift only 1.5 km (0.9 mi.) of contemporary sediments accumulated. Regional subsidence and sedimentation continued during the late Cambrian–Middle Ordovician time (Dart and Swolfs, 1998). From Middle Ordovician to Pennsylvanian time, subsidence and uplift alternated due to distal effects of the Taconic, Acadian, and Alleghanian orogenies.
- Structural reactivation of the Reelfoot rift began during the late Paleozoic with the assembly of Pangaea (Thomas, 1985). An unconformity atop the Paleozoic rock units represents mid-Cretaceous uplift and erosion. Sense of slip along many preexisting normal faults within the Central United States was inverted to reverse slip during the Paleozoic collisional processes (Marshak and Paulsen, 1996).
- Cox and Van Arsdale (1997, 2002) proposed that the regional mid-Cretaceous uplift and subsequent subsidence of the Mississippi embayment occurred as the North America Plate drifted over the Bermuda hotspot.
- Late Cretaceous and Cenozoic sediments record transgressive-regressive sequences within the Mississippi embayment trough (Thomas, 1985).
- Fluvial erosion and deposition during the Pliocene resulted in deposition of the Upland Complex, a terrace of the ancestral Mississippi-Ohio River system (Van Arsdale et al., 2007). Crowley's Ridge formed from erosion of the Western Lowlands by the ancestral Mississippi River, erosion of the Eastern Lowlands by the ancestral Ohio River, and Quaternary reactivation of ridge-bounding faults (Van Arsdale et al., 1995).
- Repeated periods of glacial meltwater escape, sea-level change, loess deposition, and structural deformation have produced various river terraces, river courses, lakes, and areas of warping during the Quaternary (Autin et al., 1991; Schweig and Van Arsdale, 1996). Four processes affected base level through the Quaternary: glacio-eustatic sea-level changes, variations in rates and patterns of sediment yield, climatic changes, and tectonic activity.
- The principal seismic activity within the upper Mississippi embayment currently is interior to the Reelfoot rift along the NMSZ.

7.3.6.1.2 Major Structures

Major basement structures and tectonic features associated with the Reelfoot rift graben are shown on Figure 7.3.6-1; structural and tectonic features inferred from interpretation of geopotential field data (gravity and magnetic) are shown on Figure 7.3.6-2. Using a structure-contour map and a three-dimensional computer model of the top of the Precambrian crystalline basement, Csontos et al. (2008) show the Reelfoot rift to consist of two major basins, separated by an intrarift uplift, that are further subdivided into eight subbasins bounded by northeast- and southeast-striking rift faults, some of which have been reactivated as reverse or oblique-slip faults.

Tectonic landforms within the central Mississippi River valley are directly linked to the underlying Reelfoot rift faults (Figure 7.3.6-1; Mihills and Van Arsdale, 1999; Csontos et al., 2008; Csontos and Van Arsdale, 2008). Recent seismologic, geologic, and geophysical studies have associated some of these basement faults within the NMSZ with large-magnitude historical earthquakes that occurred in 1811 and 1812. These faults are referred to as the New Madrid fault system (NMFS). Quaternary displacement also has been documented along the Eastern Rift margin (Cox, Van Arsdale, and Harris, 2001; Cox, Van Arsdale, et al., 2001; Cox et al., 2006); Western Rift Margin (Van Arsdale et al., 1995; Baldwin et al., 2005); Axial fault (Van Arsdale, 1998; Guccione et al., 2000); Reelfoot fault (Russ, 1982; Kelson et al., 1996; Mueller et al., 1999; Van Arsdale et al., 1999; Champion et al., 2001); and Fluorspar Area fault complex (Nelson et al., 1997; Nelson, Denny et al. 1999; McBride, Nelson, and Stephenson, 2002; SAIC, 2002; Woolery et al., 2009). In addition, the Lake County uplift, which is essentially coincident with the seismicity between the central and northern 1811-1812 earthquakes shown on Figure 7.3.6-1, the Reelfoot Lake basin, the southern half of Crowley's Ridge, the Big Lake and Lake Saint Francis Sunklands area, and Joiner Ridge are interpreted to be tectonic or tectonically influenced landforms (Csontos et al., 2008).

NMSZ faults have also modified Mississippi River gradients and influenced sedimentary processes during the Quaternary (Schumm and Spitz, 1996; Spitz and Schumm, 1997; Guccione, Mueller, et al., 2002; Guccione, 2005; Holbrook et al., 2006). Johnston and Schweig (1996) have proposed that the Bootheel lineament produced one of the major earthquakes of the 1811-1812 sequence. Guccione et al. (2005) confirmed Quaternary displacement along the Bootheel lineament and suggested the feature should be referred to as a fault. However, Csontos (2007) mapped the Precambrian basement unconformity and the Pliocene-Pleistocene unconformity surfaces within the Reelfoot rift, and sees no evidence of vertical displacement or hypocenter alignment along the Bootheel fault. This lack of vertical displacement may be due to a very young Bootheel fault with relatively minor displacement, or the actual fault displacement may be primarily strike-slip.

The NMFS, Quaternary active faults along the northwestern and southeastern margins of the zone (i.e., the ERM and CGL fault zones, respectively), and unknown structures in the southern part of the rift near Marianna, Arkansas, are characterized as RLME sources (NMFS, ERM, MAR , and CGL RLME sources; Figure 6.1-1). Section 6.1 provides a detailed description of these RLME sources.

The Fluorspar Area fault complex (FAFC) structures, which originated as normal faults during latest Proterozoic and early Cambrian time coincident with the formation of the northeast-trending faults associated with the Reelfoot rift, have experienced periodic reactivation in post-Pennsylvanian, pre-Cretaceous, and late Neogene–Quaternary time (Nelson, Denny, et al., 1999; McBride, Nelson, and Stephenson, 2002). The FAFC structures were very active, with evidence for large-magnitude earthquakes as reflected by surface manifestation of faulting as far back as latest Pleistocene (Nelson, Denny, et al., 1999; McBride, Nelson, and Stephenson, 2002). Despite efforts to identify and document evidence for Holocene activity on several of the FAFC structures, no convincing evidence of Holocene activity has been identified on any of the faults (E. Woolery, pers. comm., February 9, 2010). Reported evidence supporting Holocene displacement on one of the major faults within this system, the Barnes Creek fault (SAIC, 2002), is very equivocal based on the following observations:

- There is an apparent absence of faulting observed in the upper younger deposits (i.e., presence of only a fracture).
- The origin of the observed fracture is uncertain (e.g., possibly related to roots).
- There is an absence of distinct stratigraphic evidence for Holocene displacement on this fault and other faults within the FAFC (WLA, 2006; E. Woolery, pers. comm., February 9, 2010).

There also is a general lack of paleoliquefaction evidence for large-magnitude earthquakes in the northern Reelfoot rift that cannot be attributed to the New Madrid earthquakes. Older, weathered paleoliquefaction features in western Kentucky to the east of the FAFC appear to have formed within the past 4,850 years (WLA, 2006; Appendix E). An older earthquake, the source of which has not been determined, is recorded by older paleoliquefaction features dated at 11,300 yr BP ± 200 yr (Appendix E). Rupture along the northern Eastern Rift margin fault, or along one of the Wabash Valley fault zone structures (e.g., the Hovey Lake fault) that exhibit evidence for possible latest Pleistocene displacement, is considered to be a likely source of the earthquake that produced these older paleoliquefaction features.

Because of the lack of definitive evidence for Holocene or latest Pleistocene faulting of the FAFC, McBride, Nelson, and Stephenson (2002) propose a dynamic structural model that suggests a mechanism by which seismicity and active (Holocene) faulting have shifted within the central Mississippi Valley, away from the FAFC, over the last several ten thousand years. There is no evidence to indicate that the FAFC should be modeled as an RLME source, and a seismicity-based estimate of recurrence on the FAFC is consistent with the latest Pleistocene/Holocene record.

Quaternary reactivation of faults bounding Crowley's Ridge, a topographic ridge that spans the western margin of the Reelfoot rift in northeastern Arkansas and southeastern Missouri, is inferred from interpretation of high-resolution geophysical data and geomorphic relationships (Van Arsdale et al., 1992, 1995). Van Arsdale et al. (1995) infer that the faults bounding the ridge likely are right-lateral strike-slip faults that appear to have been active in late Wisconsinan time. This ridge, which is subparallel to the CGL in northeastern Missouri, diverges in trend from the CGL in northeastern Arkansas (Figure 7.3.6-1). Because no definitive evidence for recurrent late Pleistocene deformation has been identified along Crowley's Ridge, if faults

bounding this ridge are active, they may have much lower slip rates than faults identified in the Thebes Gap/Benton Hill region. Therefore, potential slip on faults along Crowley's Ridge is represented by earthquakes occurring in the RR seismotectonic or Mmax zone.

Other structures postulated as potential Quaternary neotectonic features (e.g., Joiner Ridge [Csontos et al., 2008] and a north-northwest-trending Meeman-Shelby fault–Joiner Ridge boundary fault [Odum et al., 2010]) also do not offer sufficient evidence to be modeled as RLME sources.

7.3.6.2 Basis for Defining Seismotectonic Zone

The following observations suggest that there are fundamental differences in the crust underlying the RR that will influence maximum magnitude and future earthquake characteristics relative to the surrounding regions:

- The RR graben structures were reactivated during Mesozoic rifting and experienced Mesozoic and younger plutonic activity. The extended crust within and adjacent to the central rift basin contrasts with the surrounding, more stable non-extended crust.
- The higher rate of seismicity within the RR and the occurrence of multiple Quaternary active faults and tectonic landforms within the RR, in addition to the identified RLME sources, suggest that tectonic strain has been localized within and adjacent to the rift. Multiple hypotheses have been presented to explain the localization and high rates of Holocene activity within the rift and the New Madrid region (see Section 6.1.5).
- The RR is expected to have distinct differences in future earthquake characteristics compared to surrounding regions. For example, focal depths for a well-located earthquake in the RR show that the seismogenic crust is not as deep as in parts of the Illinois Basin Extended Basement (IBEB) seismotectonic zone to the north. Detailed seismic surveys (e.g., Pratt, 2009), studies of the crustal architecture of the basin, and deformation of the Pliocene-Pleistocene unconformity surface (Csontos et al., 2008) provide specific information about the orientation of structures that may have experienced Quaternary reactivation, and this information can be used to differentiate the earthquake characteristics for the RR (Section 7.3.6.5) from the default values used for the adjacent Midcontinent-Craton (MidC) and Extended Continental Crust–Gulf Coast (ECC-GC) zones.

7.3.6.3 Basis for Zone Geometry

The first branch of the RR logic tree (Figure 7.3-1) addresses the uncertainty about the inclusion of the Rough Creek graben (RCG) into the RR source zone. The RCG represents the eastward extension of extensional deformation related to formation of the intracontinental rift system during Precambrian to earliest Cambrian rifting of North America (Braile et al., 1982, 1986; Kolata and Nelson, 1991). Initial development involved strike-slip and extensional faulting related to the development of the Reelfoot rift, probably in latest Proterozoic or early Cambrian time. Some of the structures may have been reactivated in post-Pennsylvanian time, probably during the late Paleozoic Ouachita orogeny (Kolata and Nelson, 1991). The RCG is bounded on

the north by the south-dipping, listric Rough Creek fault and on the northwest by the Shawneetown fault (Nelson and Lumm, 1987; Kolata and Nelson, 1991). The southern boundary approximately follows the Pennyrile fault system (Nelson and Lumm, 1987), which forms the southern margin to the Paleozoic syn-rift deposits (Kolata and Nelson, 1991). The RCG in western Kentucky is structurally connected to the northern portion of the RR that includes the Fluorspar area of southern Illinois (Soderberg and Keller, 1981; Kolata and Nelson, 1991; Potter and Drahovzal, 1994). Wheeler (1997), however, defines a boundary in this region between the RCG and the Reelfoot rift/Fluorspar area based on changes in the strikes of single large faults, the location of a Cambrian transfer zone, and the geographic extent of alkaline igneous rocks that provide three independent estimates of the location of a structural boundary between the rift and graben.

Faults associated with the RCG show strong evidence for initiation during late Proterozoic–Cambrian Iapetan-phase rifting and reactivation during the mid to late Paleozoic Appalachian-Ouachita orogeny (Heyl, 1972; Soderberg and Keller, 1981; Thomas, 1991; Noger, 1988, Kolata and Nelson, 1991; Potter et al., 1995). Mesozoic activity on RCG faults also is suggested by post-Permian displacements and regional correlation of extensional deformation associated with post-Permian to pre-Cretaceous rifting of the Pangaea continental landmass (Kolata and Nelson, 1991). However, the lack of clearly associated alkaline igneous rocks of Mesozoic age in the RCG (Wheeler, 1997) suggests that Mesozoic reactivation of deep-penetrating faults was limited.

Based on these observations, lower weight (0.333) is given to the inclusion of the RCG in the RR zone and higher weight (0.667) is given to limiting the RR to the more seismically active part of the rift that also experienced greater Mesozoic extension.

7.3.6.4 Basis for Zone Mmax

The Mmax distribution for the RR is based on the two approaches outlined in Section 5.2: the Bayesian approach and the Kijko [2004] approach. For the Bayesian approach, the Mesozoic and younger prior is used in addition to the composite prior. The prior is truncated by the two largest historical earthquakes recorded within the zone: the January 5, 1843, and October 31, 1895 earthquakes, which are interpreted to be **M** 6 (E[**M**] 6.00) earthquakes (Bakun et al., 2003). The 1811-1812 sequence of earthquakes and other large-magnitude prehistoric earthquakes recognized in the RR are included in the characterization of the RR RLME sources (NMFS, ERM, MAR, and CGL).

The weights for the Bayesian and Kijko approaches for the RR zone and the weighted composite posterior maximum-magnitude probability distribution for the RR zone are presented in Section 7.4.2.

7.3.6.5 Future Earthquake Characteristics

Characteristics for future earthquake ruptures in the RR source zone are given in Table 5.4-2. The aleatory variability in the future earthquake characteristics assigned to the RR is based on the following:

- Consideration of focal mechanisms (Zoback, 1992; Shumway, 2008).
- Orientations of RLME fault sources and faults that do not meet the criteria for RLME sources but have evidence of reactivation in the Quaternary (e.g., the north-northeast-trending FAFC faults, the north-trending faults bounding the southern part of Crowley's Ridge).
- Orientations of basement faults and inferred structures that deform the Pliocene-Pleistocene unconformity (Csontos et al., 2008).

The expected style of faulting varies with fault strike and is inferred based on comparison to focal mechanism and fault geometry interpreted from seismic profiles and seismicity data. The majority of earthquakes having well-constrained focal mechanisms show strike-slip movement (Zoback, 1992; Shumway, 2008). Therefore, strike-slip behavior is judged to be more likely. Faults and postulated structures with trends subparallel to the Reelfoot thrust fault, however, are expected to behave as reverse faults in the present tectonic stress environment.

Seismogenic depth is based on reported depths of seismicity within the RR (Zoback, 1992; Chiu et al., 1992, 1997; Herrmann and Ammon, 1997; Mueller and Pujol, 2001; Shumway, 2008; Csontos and Van Arsdale, 2008). In the central and northern part of the rift, seismicity is observed at depths between 5 and 15 km (3.1 and 9.3 mi.); (Chiu et al., 1992; Shumway, 2008). Along the southeastern margin of the rift, seismicity is slightly deeper, with earthquakes recorded between 13.9 and 22.8 km (8.6 and 14.2 mi.). The average depth of seismicity across the entire zone, which takes into account uncertainties in the velocity model and measurements, is considered to range from 13 to 17 km (8 to 10.6 mi.).

Specific parameters and weights used to characterize future ruptures in the RR are given in Table 5.4-2.

7.3.7 Extended Continental Crust–Atlantic Margin Zone (ECC-AM)

The Extended Continental Crust–Atlantic Margin (ECC-AM) seismotectonic zone was defined to include the region characterized by the presence of extended continental crust developed during Mesozoic rifting along the Atlantic Ocean basin margin. This seismotectonic zone extends from Georgia to Nova Scotia and includes onshore portions of the Piedmont and Coastal Plain provinces as well as most of the offshore continental shelf region (Figures 7.3.7-1 and 7.3.7-2).

Breakup of the supercontinent of Pangaea and formation of the Atlantic Ocean basin in the Triassic and Jurassic produced the present-day passive Atlantic margin, which can be divided into three general zones based on several characteristics, including crustal structure, composition, and thickness. These zones, from west to east are (1) rifted and extended continental crust

beneath the Piedmont, Coastal Plain, and continental shelf; (2) a 50–100 km wide (31–62 mi.) zone of highly extended transitional crust; and (3) mafic oceanic crust lying beneath the continental rise (Klitgord et al., 1988; Holbrook, Reiter, et al., 1994). The ECC-AM seismotectonic zone includes only the rifted and extended portion of the continental crust. The narrow zone of highly extended transitional crust is included in the AHEX seismotectonic zone (see Section 7.3.8).

This chapter discusses the geologic, seismic, and geophysical characteristics of the ECC-AM seismotectonic zone. The information presented is based on a review of the published material summarized in the Data Summary table for the ECC-AM and the AHEX seismotectonic zones (Appendix D, Table D-7.3.7). Explicit references and data that were used as the basis for source characteristics of the ECC-AM are identified in the Data Evaluation table of Appendix C (Table C-7.3.7).

7.3.7.1 Background

7.3.7.1.1 Crustal Structure

A distinguishing structural feature of the Mesozoic extended crust within the ECC-AM is that it includes an older, east-dipping Paleozoic master basal detachment surface separating overthrusted Paleozoic Appalachian terranes from the underlying rocks of the North American craton. For example, in the southern Appalachian Mountains, the Consortium for Continental Reflection Profiling (COCORP) seismic reflection data from Tennessee and Georgia show the master detachment to be ~6 km (~3.5 mi.) deep at the western flank of the mountains (west of ECC-AM), ~10 km (~6 mi.) deep in the Piedmont, and then quickly steepening to ~35 km (~22 mi.) depth beneath the peri-Gondwanan Carolina terrane to the east, where it merges with the Moho (Cook et al., 1979; McBride et al., 2005). In general, therefore, Paleozoic thrust sheets above the master detachment surface change across the Appalachian orogenic belt in the ECC-AM from dominantly “thin-skinned” in the west over the North American craton, to dominantly “thick-skinned” in the accreted terranes to the east over the cratonic margin (Klitgord et al., 1988).

The formation of the Appalachian orogen in the Paleozoic was followed in the Mesozoic by extension that resulted in formation of the present-day Atlantic Ocean. Extension occurred primarily in the eastern foothills of the Appalachian Mountains, the Piedmont, and Coastal Plain regions as the rifting propagated southward, initiating the separation of North America and Africa in Late Permian time. Continued rifting in the Late Triassic created elongate, northeast-trending rift basins, primarily as half grabens, from the Gulf of Mexico to the Grand Banks (Figure 7.3.7-1). A second phase of rifting in the Early Jurassic opened extensional marginal basins, such as the offshore Carolina and Baltimore Canyon troughs, as the extensional onshore basins ceased to be active (Klitgord et al., 1988). Generally, bounding faults of Mesozoic extensional basins follow the crustal fabric of the Paleozoic orogenies, and several Mesozoic normal faults have been demonstrated to be reactivated Paleozoic thrust faults (Withjack et al., 1998).

During most of the Late Triassic, onshore half grabens were created that are bounded by faults extending into the lower crust, except along the northeast Atlantic margin, where rift basins tend to be local, rather than widespread, and bounded by listric normal faults (Manspeizer et al., 1989; Withjack et al., 1998). This difference between basins in the northeast and southeast of the ECC-AM has been attributed to Early Jurassic pluton emplacement associated with the White Mountain Magma Series in central New England, which created a topographic high that may have resisted extension (Faure et al., 2006). Roden-Tice, West, et al. (2009) attribute this topographic elevation to regional unroofing during the Cretaceous, resulting from passage of the Great Meteor hotspot (see Section 7.3.2). As a result, the southeast portion of the ECC-AM underwent a relatively greater degree of extension, and faults extended to lower crustal levels.

7.3.7.1.2 Geophysical Anomalies

Given the presence of the relatively shallow Appalachian thrust sheets in the western parts of the ECC-AM, geophysical markers may provide the best means to define deep structural boundaries along the Atlantic margin and the ECC-AM. Gravity anomaly profiles across the Appalachian Mountains show a gravity anomaly low in the Valley and Ridge province, with a parallel gravity anomaly high in the Piedmont (Hutchinson et al., 1983; Karner and Watts, 1983; Cook, 1984). Pratt et al. (1988) concluded that this gravity anomaly gradient, when combined with geophysical data documenting an eastward-shallowing Moho and east-dipping reflectors, represents a thinning of continental crust toward the inferred late Precambrian–early Paleozoic continental margin lying beneath the Piedmont and marks the location of a Taconic collision zone at depth. Pratt et al. (1988) propose that this buried margin has persisted as a zone of weakness, which could explain the spatial correlation of the Piedmont gravity anomaly high with Mesozoic rift basins from Massachusetts to southern Georgia (Swanson, 1986; Hutchinson et al., 1986; Williams, 1978; Pratt et al., 1988). In either case, the Appalachian gravity anomaly gradient appears to define a fundamental structural boundary that is the western limit of thinned, extension-dominated crust lying east of the Appalachian Mountains.

The East Coast magnetic anomaly (ECMA) is a major geophysical feature of the North American Atlantic margin, extending from Georgia to Nova Scotia (Figure 7.3.7-3). Combined multichannel and wide-angle seismic studies of the Atlantic margin have shown that the ECMA is spatially correlated with a zone of transitional igneous crust, largely comprised of basalts and mafic intrusions, marking the seaward transition from rifted continental crust to mafic oceanic crust that extends along the entire Atlantic margin (Austin et al., 1990; Holbrook, Purdy, et al., 1994; Holbrook, Reiter, et al., 1994; LASE Study Group, 1986; Trehu et al., 1989). The magnetic anomaly that defines the ECMA changes trend offshore of Georgia. This east-west-trending onshore portion of the magnetic anomaly has been identified as the Brunswick magnetic anomaly (BMA; Figure 7.3.7-3). The BMA cuts across the South Georgia rift, as well as several other pre-Cretaceous features, suggesting that it must be related to a deeper and older structure (Daniels et al., 1983). COCORP seismic reflection data, combined with magnetic anomaly modeling results, suggest that this structure is either a subducted slab, or subcontinental mantle, trapped during the Alleghanian collision (McBride and Nelson, 1988). The BMA therefore demarcates the structural boundary between the North American craton and the Florida–South Georgia microcontinent, known as the Suwannee, or Wiggins-Suwannee, suture.

7.3.7.1.3 Major Structures

The ECC-AM includes an abundance of major shear zones and faults, most of which are related to the Paleozoic accretion of terranes during the Appalachian orogenies. Prominent examples are the Brevard fault zone, a largely strike-slip fault in Georgia, South Carolina, and North Carolina that transported west-directed thrusts to the southwest along the Inner Piedmont during the Neoacadian and Alleghanian orogenies; the Central Piedmont suture of Georgia, the Carolinas, and Virginia that was the possible Alleghanian thrust ramp for the Carolina terrane; and the East Piedmont fault system, which bounds the Alleghanian metamorphic core of the southern Appalachian Mountains (Hatcher et al., 2007).

Mesozoic normal faults bound the rift basins throughout the ECC-AM (Figure 7.3.7-1). The location and geometry of these rift basins are interpreted to have been controlled mainly by existing Paleozoic structures, which were reactivated as brittle normal faults when the Mesozoic extension direction was at a high angle to the preexisting fault (Cook et al., 1981; Schlische, 1993). The East Piedmont fault system, for example, was the dominant structure controlling basin development in the southern Appalachians, forming the Danville, Farmville, and Richmond basins (Swanson, 1986). Rift basins of the northern Appalachian Mountains, such as the Gulf of Maine and Fundy Basin, can be similarly correlated with specific reactivated Paleozoic faults (Swanson, 1986).

Cretaceous and younger faults within the ECC-AM are predominantly oriented north-south to northeast-southwest (Prowell, 1988). Prowell (1988) indicates that post-Cretaceous movement on these faults is reverse slip, with limited evidence for strike-slip movement. Within the ECC-AM source zone, several northeast-striking reverse fault zones in fault systems have experienced Cenozoic activity (Prowell, 1983, 1988; Wentworth and Mergner-Keefer, 1983). Some of these include the Stafford fault system in northeastern Virginia (Mixon and Newell, 1977; Newell, 1985; Pavich et al., 1989); the subsurface Brandywine fault system in southwestern Maryland (Jacobeen, 1972); the Belair fault zone in eastern Georgia (Prowell and O'Connor, 1978; Bramlett et al., 1982); the Everona–Mountain Run fault zone and the Dutch Gap fault in Virginia (Pavlides et al., 1983; Prowell, 1988; Pavlides, 1994); the Hares Crossroads fault in North Carolina (Prowell, 1983); and the Cooke and offshore Helena Banks faults (Behrendt et al., 1983) near Charleston, South Carolina. These faults typically strike north to northeast, exhibit steep dips, and displace sedimentary rocks of Late Cretaceous–Miocene (100–5.3 Ma) age. Individual vertical fault zone displacements generally are tens of meters, with a maximum cumulative offset of as much as 80 m (262.5 ft; Prowell, 1988). The available stratigraphic data generally show greater displacement on older units, indicating progressive displacement through time. Vertical slip rates range from 0.0003 to 0.0015 meters per thousand years (m/ka) during the past 110 Ma, averaging 0.0005 m/ka (Prowell, 1988).

The occurrence of late Cenozoic movement along the faults mapped in the ECC-AM is difficult to assess because of poor exposure, lack of suitable stratigraphy, relatively small displacements, and low slip rates on these faults. Possible Quaternary displacement on north- and northeast-striking faults appears to be reverse slip. However, the available evidence for postulated Quaternary movement provides little constraint on possible strike-slip movement. For example, possible Pleistocene (1.8 Ma to 11 ka) activity is suggested on the Everona–Mountain Run fault

zone in central Virginia based on displacement of gravel deposits considered to be of late Cenozoic or Pleistocene age (Pavlides et al., 1983; Pavlides, 1994; Crone and Wheeler, 2000). Geomorphic relationships (Mayer and Wentworth, 1983) and possible faulted fluvial terraces at Fredricksburg, Virginia, along an extension of the Stafford fault system (Darton, 1950) may indicate post-Pliocene movement (post–1.8 Ma). There is no direct evidence, however, for Quaternary movement on any of the strands of the Stafford fault system. Furthermore, activity of these north- to northeast-striking reverse faults is difficult to reconcile with the observed northeast-southwest orientation of contemporary maximum horizontal compressive stress for the Atlantic Coastal Plain defined by Zoback and Zoback (1989) and Zoback (1992).

7.3.7.1.4 Seismicity

Like most of the CEUS, seismicity within the ECC-AM is spatially variable, with moderate concentrations of earthquake activity separated by areas of very low seismicity. The most prominent of these zones of seismicity are located in the Central Virginia seismic zone and the greater New York City–Philadelphia area. To a lesser degree, these prominent zones include clusters of seismicity in the Charleston, South Carolina, area; the Piedmont region of South Carolina and Georgia; and New England (Figure 7.3.7-2). As characterized by Bollinger et al. (1991), hypocenters in the Atlantic Coastal Plain are distributed throughout the upper 13 km (8 mi.) of crust where focal mechanisms indicate a north-northeast maximum horizontal compressive stress. The largest earthquake within the ECC-AM is the 1886 Charleston earthquake. Due to the strong paleoliquefaction evidence for RLMEs in the Charleston area, a separate RLME seismic source zone is defined for Charleston (see Section 6.1.2).

The Central Virginia seismic zone (CVSZ) is an area of persistent seismic activity in the Piedmont province of Virginia, extending approximately 120–150 km (75–93 mi.) west of Richmond with a north-south width of about 100 km (62 mi.). The relative paucity of paleoliquefaction features along the coastlines and riverways of Virginia makes it unlikely that the CVSZ has produced M > 7 earthquakes in the last 5,000 years (Obermeier and McNulty, 1998). The largest historical earthquake in this zone is the 1875 Goochland County earthquake, with a reported intensity of MMI VII and an estimated magnitude of m_b 5.0 (Bollinger and Hopper, 1971). In general, however, the CVSZ is defined by small, shallow earthquakes, three-quarters of which occur at depths <11 km (7 mi.; Bollinger and Sibol, 1985). As the southern Appalachian detachment is at least 12 km (7.5 mi.) deep in this part of the Piedmont (Keller et al., 1985; de Witt and Bayer, 1986), CVSZ seismicity is interpreted to occur on the Paleozoic and Mesozoic faults that lie above the Precambrian basement. Outside the CVSZ, the broad pattern of seismicity in eastern North America suggests an aseismic upper crust and the occurrence of strike-slip faulting below the Appalachian detachment, with focal mechanisms yielding a northeast-southwest orientation for the maximum horizontal compressive stress. This stress orientation is consistent with the ridge-push forces resulting from continuous seafloor spreading at the mid-Atlantic ridge, which Zoback and Zoback (1989) proposed as the origin of the contemporary regional stress field in the CEUS.

For the New York–Philadelphia region, Sykes et al. (2008) used historical earthquake catalogs with their own instrumentally located earthquake database to compile a history of seismicity covering the years 1677–2006. Sykes et al. (2008) find earthquakes to be concentrated in mid-

Proterozoic to Ordovician terranes bordering the Newark basin, with hypocenters tracing out northeasterly swaths that roughly parallel the trend of the Appalachian Mountains. The most active of these zones is a 35 km (22 mi.) wide belt east and southeast of the Newark basin, which is the location for the largest historical earthquake in this region (i.e., a magnitude 5.25, a felt magnitude of Sykes that relates felt area to m_{bLg}). Of the 383 earthquakes in the Sykes et al. (2008) local catalog, 95 percent occurred at depths shallower than 12.5 km (8 mi.). Both the New York–Philadelphia region and CVSZ are characterized by a majority of earthquakes occurring at depths shallower than the Appalachian detachment, in contrast to the deeper levels of seismicity in the Eastern Tennessee and Giles County seismic zones, which occur nearly exclusively below the detachment surface. Both of these seismic zones are located within the Paleozoic Extended Crust (PEZ) seismotectonic source (see Section 7.3.4). As is the case in the CVSZ, specific faults responsible for seismicity around the Newark basin are not well defined. However, focal mechanisms around the Newark basin conform to the broad stress field found throughout the Atlantic margin and are consistent with a N64°E orientation of maximum horizontal compressive stress (Sykes et al., 2008).

Northeastern Massachusetts, southeastern New Hampshire, and southernmost Maine have experienced many small, and several moderate, earthquakes during the past 400 years. The two most notable earthquakes, the 1727 felt-area magnitude 5.5 Newburyport and the 1755 **M** 6.1 (E[**M**] 6.10) Cape Ann earthquakes in Massachusetts, induced liquefaction and caused damage to buildings (Ebel, 2000, 2001). During a paleoseismology study in the Newburyport area in the late 1980s, Tuttle and Seeber (1991) found both historical and prehistoric liquefaction features. The historical features were attributed to the 1727 earthquake, and the prehistoric features were estimated to have formed during the past 4,000 years. More recent searches for earthquake-induced liquefaction features in the region yielded only one small sand dike (Tuttle, 2007, 2009). The limited paleoliquefaction features in New England, which do not provide sufficient information to characterize the recurrence, geometry, or Mmax parameters of the ECC-AM seismotectonic source, are further discussed in Appendix E.

7.3.7.2 Basis for Defining Seismotectonic Zone

The basis for defining the ECC-AM seismotectonic zone centers primarily on the assessments of Johnston et al. (1994) that Mesozoic and younger extended crust has produced all $\mathbf{M} \geq 7$ stable craton earthquakes worldwide, and that extended or rifted crust may provide a basis for differentiating Mmax. In this study of global earthquakes and SCR tectonic domains, Johnston et al. (1994) found that the subdivision between rifted and nonrifted crust is significant and that SCR earthquake activity is concentrated in extended crust. As presented in Section 5.2, the SCR database and analysis of the data given in Johnston et al. (1994) was updated as part of the CEUS SSC Project. This updated analysis supports the basis for separating Mesozoic and younger extended crust to establish a prior distribution of Mmax. The statistical significance for this separation, however, is not strong.

Defining the ECC-AM as a seismic source also differentiates it from adjoining regions of the crust that appear capable of producing different Mmax earthquakes or future earthquake rupture characteristics. For example, the ECC-AM is separated from the ECC-GC (Gulf Coast) because

the structural grain of the two seismotectonic zones is different and will likely give rise to different future rupture characteristics (e.g., particularly rupture orientation). Crust of the ECC-AM seismotectonic zone is separated from Mesozoic extended crust of the Northern Appalachian (NAP) seismotectonic zone (Section 7.3.3) because of both the lack of rift basins expressed in the NAP and the multiple phases of reactivation and differences in future earthquake rupture characteristics.

7.3.7.3 Basis for Geometry

The geometry of the ECC-AM is based on the concept of including those portions of crust that underwent significant Mesozoic extension expressed as rifting. The geometry of the ECC-AM zone is similar to the Eastern Seaboard domain defined by Kanter (1994), which includes extended Paleozoic basement of the eastern United States and Nova Scotia as well as the continental shelf. The western boundary of the ECC-AM, which is defined by the Piedmont (Appalachian) gravity anomaly gradient (e.g., Bollinger and Wheeler, 1988; Figure 7.3.7-3) and corresponds closely to the Piedmont/Avalon terrane boundary of Williams and Hatcher (1983), generally follows the western edge of the Triassic-Jurassic onshore basins or the boundaries of the structural blocks in which they occur. In New England and eastern New York, the western boundary of the ECC-AM incorporates crust that has experienced Cretaceous uplift west of the Hartford basin (Roden-Tice and Tice, 2005) and deep-velocity anomalies associated with the Cretaceous Great Meteor hotspot (Li et al., 2003). Across Nova Scotia, the ECC-AM western boundary generally follows the Cobequid-Chedabucto fault system (Pe-Piper and Piper, 2004; Murphy and Keppie, 2005). The eastern boundary of the ECC-AM follows the western margin of the ECMA. The southern boundary of the ECC-AM generally follows the Brunswick magnetic anomaly (BMA), which marks the Wiggins-Suwannee suture (Hatcher et al., 2007).

7.3.7.4 Basis for Mmax

As with all seismotectonic zones defined for the CEUS-SSC Project, the Mmax distribution for the ECC-AM is derived using two different approaches (see Section 5.2). For the Bayesian approach, both the Mesozoic and younger extended (MESE) and composite (COMP) priors are used for this seismotectonic zone because the zone is defined by the presence of extended continental crust that was rifted during Mesozoic extension. The Kijko method was also used to assess Mmax for the ECC-AM. These methods are discussed further in Section 5.2, and the Mmax distributions and weighting schemes for ECC-AM are presented in Section 7.4.

The largest observed earthquake in the ECC-AM seismotectonic zone is the 1755 **M** 6.1 (E[**M**] 6.10) Cape Ann, Massachusetts, earthquake. However, there is some uncertainty as to whether this earthquake occurred in the ECC-AM since it lies near the boundary between the ECC-AM and the NAP zones. As shown on Figure 7.3.7-4, the location preferred by Bakun et al. (2003) lies within the ECC-AM, but the area defining a 95 percent confidence level for the earthquake location straddles the seismotectonic boundary. A study by Ebel (2006a) estimates the location within the ECC-AM farther southeast from the Bakun et al. (2003) preferred location (Figure 7.3.7-4). The Bakun et al. (2003) model addresses uncertainty by mapping the 67 percent and 95

percent confidence levels for its location, whereas the Ebel study (2006a) provides only an estimated epicentral area.

The uncertainty in location of the 1755 Cape Ann earthquake is included in this assessment of Mmax by assigning a 0.6 weight for a location within the ECC-AM, and a corresponding 0.4 weight that the earthquake is located not in the ECC-AM but farther north in the NAP. The higher weight is assigned for the location within the ECC-AM since the more recent study by Ebel (2006a) places the earthquake within the ECC-AM. Therefore, the Cape Ann earthquake is used (with a weight of 0.6) to represent the largest earthquake within the ECC-AM. The next largest earthquake within the ECC-AM is the E[**M**] 5.32 earthquake that occurred on June 11, 1638. This earthquake, which is located farther offshore than the 1755 Cape Ann earthquake, is also used (with a weight of 0.4) to represent the largest earthquake within the zone.

7.3.7.5 Future Earthquake Characteristics

The future rupture characteristics assigned to the ECC-AM seismotectonic zone are listed in Table 5.4-2. For the ECC-AM, the sense of slip, rupture dip, and source boundaries are assigned default characteristics (Tables 5.4-1 and 5.4-2). The characteristics of seismogenic crustal thickness and rupture orientation are assigned unique values for ECC-AM. The extended continental crust within the ECC-AM is assigned a greater seismogenic thickness than the more highly extended transitional crust of AHEX because the crustal thickness defined by depth to the Moho is distinctly greater in the ECC-AM. Seismogenic thickness values of 13, 17, and 22 km (8, 10.5, and 13.5 mi.) are assigned weights of 0.6, 0.3, and 0.1, respectively, for the ECC-AM. In contrast, the adjacent highly extended AHEX is assigned seismogenic thickness values of 8 and 15 km (5 and 9.5 mi.) with equal weights as discussed in Section 7.3.8. The ECC-AM distribution reflects a greater seismogenic thickness than the AHEX, but a slightly lesser thickness than most of the more cratonward seismotectonic zones which have default seismogenic thickness distributions of 13, 17, and 22 km (8, 10.5, and 13.5 mi.), with weights of 0.4, 0.4, and 0.2, respectively (Table 5.4-1). The rupture orientation distribution assigned to the ECC-AM modifies the weights of the default orientations of N50°W, N-S, N35°E, N60°E, and E-W (Table 5.4-1) such that most of the weight is given to the north and northeast orientations. For the ECC-AM, the individual weights assigned to the rupture orientations of N50°W, N-S, N35°E, N60°E, and E-W are 0.1, 0.2, 0.4, 0.2, and 0.1, respectively (Table 5.4-2).

7.3.8 Atlantic Highly Extended Crust Zone (AHEX)

The Atlantic highly extended crust (AHEX) seismotectonic zone represents the region of highly extended crust that is the transition between the extended, thick continental crust of the ECC-AM and the significantly thinner mafic oceanic crust of the Atlantic Ocean basin. This zone lies entirely offshore and approximately follows the continental shelf edge from Georgia to Nova Scotia (Figure 7.3.7-1).

Extension during the Triassic and Jurassic rifting of the Atlantic Ocean basin produced the relatively broad zone of extended continental crust of the ECC-AM and the adjacent narrow AHEX zone of highly extended transitional crust that was more intensely modified by rifting.

The greater amount of rifting in the 50–100 km (31–62 mi.) wide AHEX zone resulted in a greater thinning of the crust and the introduction of significant components of new igneous material, largely basalts, and mafic intrusions (Klitgord et al., 1988; Holbrook, Reiter, et al., 1994).

This chapter discusses the geologic, seismic, and geophysical characteristics of the AHEX seismotectonic zone. The information presented is based on a review of the published material summarized in the Data Summary table for both the ECC-AM and AHEX seismotectonic zones (Appendix D, Table D-7.3.7). Explicit references and data that were used as the basis for source characteristics in the AHEX are identified in the Data Evaluation table of Appendix C (Table C-7.3.7).

7.3.8.1 Basis for Defining Seismotectonic Zone

Following the methodology for defining seismotectonic zones (see Chapter 4), the AHEX seismotectonic zone is included as a zone distinct from the ECC-AM zone because the AHEX zone is expected to exhibit a lesser seismogenic thickness to influence future earthquake characteristics. The sparse seismicity in the AHEX does not allow seismogenic thickness, and hence, dimensions of future ruptures, to be characterized directly from the depths of recorded earthquakes. Rather, the crustal thickness defined by depth to the Moho provides the best proxy for assessing seismogenic thickness compared with that of the adjacent extended continental crust. The eastward-thinning wedge of highly extended transitional crust that characterizes the AHEX zone is significantly thinner than the approximately 35–40 km thick (21.5–25 mi.) extended continental crust of the adjacent ECC-AM seismotectonic zone. Crustal-scale seismic-reflection profiles derived from multichannel and wide-angle seismic studies offshore of South Carolina (Holbrook, Purdy, et al., 1994), Virginia (Holbrook, Reiter, et al., 1994), and Nova Scotia (Funck et al., 2004) indicate that the AHEX zone ranges in thickness from about 15 to 30 km (9.5 to 18.5 mi.). The decreasing crustal thickness away from the continent strongly argues that the seismogenic thickness (typically thinner than the crust or depth to the Moho) should also be thinner in the AHEX than in the ECC-AM. These same studies also reveal that the zone of transitional crust of the AHEX zone corresponds to the strong positive East Coast magnetic anomaly (ECMA). As shown on Figure 7.3.8-1, Holbrook, Purdy, et al. (1994) and Holbrook, Reiter, et al. (1994) interpret the eastern limit of rifted continental crust to correspond to the western margin of the ECMA, and the western limit of oceanic crust to correspond to the eastern margin of the ECMA. In seismic Line 801 from Holbrook, Reiter, et al. (1994), located on Figure 7.3.8-1, the AHEX zone beneath the ECMA is interpreted as comprising rift-related basalts and mafic intrusive rocks up to 25 km (15.5 mi.) thick (Holbrook, Reiter, et al., 1994, Figure 15).

Crust of the AHEX seismotectonic zone is also compositionally different than the extended continental crust of the ECC-AM. The more mafic composition of the AHEX is defined by the ECMA, a major geophysical feature of the North American Atlantic margin, extending from Georgia to Nova Scotia (Figure 7.3.7-3). Combined multichannel and wide-angle seismic studies of the Atlantic Ocean margin have shown that the ECMA is spatially correlated with a zone of transitional igneous crust, marking the seaward transition from rifted continental crust to mafic

oceanic crust that extends along the entire Atlantic margin (Austin et al., 1990; Holbrook, Purdy, et al., 1994; Holbrook, Reiter, et al., 1994; LASE Study Group, 1986; Trehu et al., 1989), implying that the basalts and underlying mafic intrusives produce the high magnetic values of the anomaly (Talwani et al., 1992). The ECMA is interpreted as the result of rift-related magmatism during the first pulse of seafloor spreading (Sheridan et al., 1993; Holbrook, Purdy, et al., 1994; Holbrook, Reiter, et al., 1994; Talwani et al., 1995; Oh et al., 1995; Talwani and Abreau, 2000). The ECMA therefore marks a profound geological boundary beyond which very little continental crust occurs (Holbrook, Reiter, et al., 1994).

7.3.8.2 Basis for Geometry

The boundary of the AHEX was largely defined based on the location of the ECMA. This magnetic anomaly corresponds to the highly extended transitional crust comprising the AHEX (Figure 7.3.8-1). The western margin of the AHEX corresponds to the seaward extent of continental crust that was rifted and extended in the Mesozoic, and the eastern margin of AHEX corresponds to the landward extent of oceanic crust. Although the boundary of the AHEX is generally well defined by high total magnetic values (Figure 7.3.8-1), the boundary is gradational, and thus local uncertainty about the location of the boundary between AHEX and ECC-AM seismotectonic zones could be on the order of tens of kilometers.

7.3.8.3 Basis for Mmax

The Mmax distribution for the AHEX was developed using the Bayesian approach, which uses global prior distributions developed for SCRs (see Section 5.2). Because the AHEX is defined as highly extended transitional crust that was rifted during Mesozoic extension, the Mesozoic and younger extended prior (MESE) is used for this zone with the composite prior (COMP). The Kijko method was not used for the AHEX due to the low number of earthquakes observed within the zone. The largest observed earthquake within the AHEX is the September 24, 1996, E[**M**] 2.89 earthquake. The derived Mmax distributions for the AHEX are presented in Section 7.4.

7.3.8.4 Future Earthquake Characteristics

The future rupture characteristics assigned to the AHEX seismotectonic zone are listed in Table 5.4-2 and, with the exception of seismogenic thickness and rupture orientation, are the same as those assigned to the ECC-AM. The more highly extended transitional crust within the AHEX is assigned two equally weighted seismogenic thicknesses of 8 and 15 km (5 and 9.5 mi.), which reflects a shallower seismogenic thickness than that for the ECC-AM. These values are estimates of seismogenic thickness that are not well constrained by data. Because large faults within this zone likely formed during extension and are therefore likely to be oriented parallel to the long axis of the zone and perpendicular to the maximum extension direction, a distribution of rupture directions that are asymmetrically weighted in favor of northeast-striking (i.e., N25°E and N60°E) ruptures was assigned for the AHEX, while also allowing for ruptures striking north-south, east-west, and N50°W (Table 5.4-2).

7.3.9 Extended Continental Crust–Gulf Coast Zone (ECC-GC)

The breakup of the supercontinent of Pangaea and the formation of the Gulf of Mexico in the Triassic and Jurassic resulted in the development of three large crustal domains in the Gulf of Mexico region. From north to south, these domains are thick transitional crust, thin transitional crust, and newly formed oceanic crust (Buffler and Sawyer, 1985; Marton and Buffler, 1994; Salvador, 1991a, b; Sawyer et al., 1991). The Extended Continental Crust–Gulf Coast (ECC-GC) seismotectonic zone is the thick transitional crust domain (Figure 7.3.9-1). The thin transitional crust domain, the Gulf Highly Extended Crust (GHEX) seismotectonic zone, is discussed in Section 7.3.10.

The thick transitional crust domain within the Gulf of Mexico region represents continental crust that was thinned during the opening of the Gulf of Mexico. In general, the thick transitional crust is characterized by basement highs (e.g., Sarasota arch, Middle Ground arch, Wiggins uplift, Monroe uplift, Sabine uplift) and intervening lows (e.g., South Florida basin, Tampa embayment, Apalachicola basin, Mississippi Salt basin, North Louisiana Salt basin, East Texas basin) that occur along the Gulf margin from Florida to Texas (Sawyer et al., 1991). Crustal thicknesses within the thick transitional crust vary between approximately 20 and 40 km (12 and 25 mi.), with the thinnest crust occurring within the basement lows, and the thicker, relatively less extended crust occurring in association with the basement highs.

Most of the mid-Jurassic and younger subsidence and sedimentation within the thick transitional crust domain occurred in the basement lows, as reflected by the thick salt deposits that occur in many of these basins (Buffler and Sawyer, 1985; Marton and Buffler, 1994; Sawyer et al., 1991). Combined with the thin transitional crust to the south (discussed in Section 7.3.10), the total amount of thinning of continental crust in Gulf region is thought to have accommodated 50 percent of the relative plate motion during the rifting of Pangaea and opening of the Gulf of Mexico (Dunbar and Sawyer, 1987). Despite the significant amount of extension that has occurred in the thick transitional crust domain, very few accommodating structures have been identified, in part due to masking by the thick sedimentary sequence that overlies the area of extended crust (Buffler and Sawyer, 1985; Marton and Buffler, 1994; Sawyer et al., 1991).

The source characterization of the ECC-GC described in the following text is based on a review of published material (see Appendix Table D-7.3.9). Explicit references that were used as the basis for source characteristics are identified in Appendix Table C-7.3.9.

7.3.9.1 Basis for Defining Seismotectonic Zone

Following the methodology for defining seismotectonic zones presented in Chapter 4, the ECC-GC is defined as a distinct seismotectonic zone because it is anticipated that this zone will have an Mmax distribution different from that of neighboring zones. In particular, the ECC-GC has experienced Mesozoic extension and thus the appropriate Mmax prior is different from that applicable to other regions of the CEUS that have not experienced Mesozoic extension. The ECC-GC zone is defined as distinct from the equivalent zone along the Atlantic margin (i.e., the Extended Continental Crust–Atlantic Margin seismotectonic zone, or ECC-AM, as discussed in

Section 7.3.7), based on differences in expected future rupture characteristics. In particular, the dominant structural grain for the ECC-AM is roughly north-northeast and subparallel to the margin of Mesozoic extension along the East Coast, regional structures in the Appalachian orogen, and the modern Atlantic coastline. There is no preferred dominant structural grain in the ECC-GC because there is considerable variability and uncertainty in the orientation of structures that accommodated the opening of the Gulf of Mexico (see Section 7.3.9.4).

The ECC-GC is also distinguished from the highly extended crust to the south, which lies within the GHEX zone, as discussed in Section 7.3.10, based on a difference in expected future earthquake characteristics. This difference is related to the interpretation that the GHEX seismotectonic zone is characterized by a thinner seismogenic crust than the ECC-GC zone because the GHEX zone is more highly extended (see Sections 7.3.7.10.4 and 7.3.7.9.4).

7.3.9.2 Basis for Zone Geometry

7.3.9.2.1 Southern Boundary

Most of the southern boundary of the ECC-GC zone, from west Texas to the eastern Gulf of Mexico, is defined as the transition between thick and thin transitional crust domains (Figure 7.3.9-1). In general, the boundary between these domains is not well defined because of the lack of a clear distinction in geologic characteristics of the two domains, and because of the difficulty in observing geologic differences between the zones due to the thick accumulation of sediment deposited atop the rifted Mesozoic crust. Some of the fundamental geologic differences between the thick and thin transitional crust domains are as follows:

- The thin transitional crust has undergone more extension.
- The thin transitional crust has been thinned more uniformly, as opposed to the basin-and-uplift style of extension in the thick transitional crust.
- The pattern of magnetic anomaly trends within the thin transitional crust are roughly margin-parallel, as opposed to margin-perpendicular in the thick transitional crust domain (e.g., Figure 7.1-5; Buffler and Sawyer, 1985; Marton and Buffler, 1994; Sawyer et al., 1991).

In many places along the Gulf margin, these geologic contrasts are coincident with a hinge zone in the basement topography, marking where the shallow-dipping basement of the less subsided, thick transitional crust abuts the more subsided and more steeply dipping thin transitional crust. This hinge zone correlates with the location of an Early Cretaceous carbonate platform that rimmed the Gulf of Mexico basin (Buffler and Sawyer, 1985; Harry and Londono, 2004; Sawyer et al., 1991). Presumably, the location of the platform reflects the contrast in subsidence between the thick and thin transitional crust domains. This platform has been called upon by many authors to infer the location of the boundary between thick and thin transitional crust (Buffler and Sawyer, 1985; Ewing and Lopez, 1991; Harry and Londono, 2004; Marton and Buffler, 1994; Sawyer et al., 1991).

Given the lack of readily identifiable and distinct geologic differences between the thick and thin transitional crust domains, there is considerable uncertainty in the location of this boundary.

Therefore, the interpretation of the thick to thin transitional crust boundary presented by Sawyer et al. (1991) is used for defining the southern boundary of the ECC-GC; the uncertainty in the location of this boundary is on the order of 50–100 km (31–62 mi.).

South of Florida, the southern boundary of the ECC-GC zone is defined by the location of the Nortecubana fault along the north coast of Cuba. This fault marks the former suture zone of the Caribbean and North American plates and thus delineates the southern limit of Mesozoic extension within the Gulf of Mexico at this longitude (Kanter, 1994). This fault system was active until about Middle Eocene time, and it accommodated relative convergence of the Bahama platform and Cuba (Gordon et al., 1997). The current boundary between the Caribbean and North American plates is on the southern side of Cuba.

7.3.9.2.2 Western Boundary

The western boundary of the ECC-GC zone is defined as the easternmost extent of the Gulf of Mexico coastal plain as determined by the onset of topographic relief associated with the Sierra Madre Oriental, the Coahuila folded province, and other topographic features of the eastern Mexico peninsula (Figure 7.3.9-1). Uncertainty in this boundary is on the order of several to tens of kilometers (several to tens of miles) at most, given that it is relatively well defined based on topography. The Sierra Madre Oriental and the Coahuila folded province are structural domains produced by Laramide-age fold-and-thrust tectonics, and they exhibit some evidence of Tertiary extension associated with development of the Basin and Range and the Rio Grande rift (Cook et al., 1979; Dickerson and Muehlberger, 1994; Gray et al., 2001; Murray, 1961).

7.3.9.2.3 Eastern Boundary

Some researchers consider the eastern limit of transitional crust associated with the opening of the Gulf of Mexico to be delineated by the northwest-trending Bahamas fracture zone that extends from roughly the southeastern tip of the Florida peninsula to the northwest part of the Gulf of Mexico. This interpretation is largely based on (1) the extent of Mesozoic volcanic rocks observed in wells in southern Florida; (2) distinct boundaries seen in the gravity and magnetic anomalies of Florida; and (3) the presence of the Suwannee terrane, a relatively unextended portion of the African continent that was accreted to North America during the rifting that formed the Atlantic Ocean and Gulf of Mexico, between the Bahamas fracture zone and southern Georgia (Marton and Buffler, 1994; Salvador, 1991a; Sawyer et al., 1991; Thomas, 2006).

In spite of this tectonic interpretation, the eastern boundary of the ECC-GC zone is defined as the edge of the Atlantic margin continental shelf and the Blake plateau (Figure 7.3.9-1), and thus includes the Suwannee terrane within the ECC-GC. The decision to include the Suwannee terrane, all of Florida, and parts of southern Georgia in the ECC-GC is based on the following considerations:

- Mesozoic extension is documented within these regions (e.g., rifted crust off eastern Florida, the Apalachicola basin, and the South Georgia rift) (Daniels et al., 1983; Kanter, 1994; Klitgord et al., 1984).

- A boundary between the ECC-GC and ECC-AM occurs along the Wiggins-Suwannee suture that represents the late Alleghanian suture separating the southern Appalachians from Gondwana (African-affinity rocks). This suture marks the southern termination of the dominant Appalachian structural grain and subsequent northeasterly striking structures that formed or reactivated during Mesozoic rifting of the Atlantic.

Given the different orientations of spreading between the Atlantic and Gulf and the dominant northeast structural grain of the Appalachians, it is anticipated that the Suwannee terrane, all of Florida, and parts of southern Georgia will likely have future earthquake rupture characteristics more similar to other portions of the ECC-GC than to the ECC-AM (see Section 7.3.9.2.4).

7.3.9.2.4 Northern Boundary

The northern boundary of the ECC-GC is intended to represent the northernmost extent of Mesozoic crustal thinning associated with the rifting of Pangaea and the opening of the Gulf of Mexico. The northernmost extent of Mesozoic extension is roughly coincident with the edge of Iapetan margin that formed during Paleozoic extension (within approximately 100 km, or 62 mi.; Thomas, 1988, 2006). However, there is considerable variability in the relative location of the Paleozoic and Mesozoic extensional boundaries. In Texas, the location of both boundaries is not well defined. Faulting of Mesozoic-aged basement is hypothesized by some to have extended as far north as the Balcones fault zone in central Texas (Collins, 2004; Pindell et al., 2000; Sawyer et al., 1991), but some interpretations of the edge of Iapetan margin are gulfward of this fault zone (see Wheeler and Frankel, 2000, and references therein). In this region, the northern edge of the ECC-GC is defined as the edge of the Iapetan margin by the USGS in its national seismic hazard maps (Petersen et al., 2008; Wheeler and Frankel, 2000) for the following reasons:

- There is considerable uncertainty in the boundary of Mesozoic rifting in the region.
- In many other locations along the Gulf of Mexico, structures associated with the Iapetan margin localized Mesozoic extension (Sawyer et al., 1991; Thomas, 1988).
- This boundary lies within the zone of Mesozoic rifting proposed by different researchers (e.g., Kanter, 1994; Pindell and Kennan, 2001; Pindell et al., 2000; Sawyer et al., 1991).

At the longitude of Arkansas and Louisiana, the Southern Arkansas fault zone is commonly interpreted as the northern extent of transitional crust, based on the presence of Triassic-age red beds that fill grabens associated with the fault zone (Sawyer et al., 1991; Thomas, 1988). In this region, however, the northern boundary of the ECC-GC zone is drawn farther north, encompassing more of southern Arkansas and abutting the southern extents of the Oklahoma Aulacogen (OKA) and RR seismotectonic zones. The source zone is extended north of the South Arkansas fault zone for several reasons:

- There is evidence of Late Cretaceous volcanism north of the fault zone and south of the Reelfoot rift that, while not related to the Mesozoic opening of the Gulf of Mexico, suggests that this region has undergone deformation more recently than the Midcontinent-Craton seismotectonic zone to the north (Baksi, 1997; Byerly, 1991; Hendricks, 1988; Hildenbrand and Hendricks, 1995).

- It does not seem tectonically reasonable to have a relatively thin sliver of crust without Mesozoic extension sandwiched between the northern extent of the ECC-GC zone and the southern extent of the Reelfoot rift zone, both of which are zones with Mesozoic extension.
- It does not seem appropriate to include the potential liquefaction features discussed by Cox and other researchers (Cox, 2009; Cox et al., 2007; Cox, Larsen, Forman, et al., 2004) within the Midcontinent-Craton seismotectonic zone when, if these features represent actual paleoseismic earthquakes, they may be related to reactivation of Mesozoic and Paleozoic structures (e.g., Alabama-Oklahoma transform fault; see Section 7.3.9.5; Gordon and Cox, 2008; Thomas, 1988; Thomas, 2006).

From Mississippi to western Alabama, the boundary of the ECC-GC zone is defined by the location of the Alabama-Oklahoma transform, a transform fault originally formed during the opening of the Iapetus Ocean and later reactivated during the Mesozoic opening of the Gulf of Mexico and the Atlantic Ocean (Sawyer et al., 1991; Thomas, 1988). The location of this boundary is relatively well known based on its expression in magnetic anomaly data.

From Alabama to Georgia, the northern boundary of the ECC-GC is defined by the late Alleghanian Wiggins-Suwannee suture, which underlies the South Georgia rift basin and approximately coincides with the Brunswick magnetic anomaly (BMA; McBride and Nelson, 1988; McBride et al., 2005; Hatcher et al., 2007). This suture represents the southern termination of the dominant Appalachian structural grain and subsequent structures that formed or reactivated during Mesozoic rifting of the Atlantic.

In general, the entire northern boundary of the ECC-GC is not well defined, and uncertainty in the location of the boundary is on the order of 50–100 km (31–62 mi.).

7.3.9.3 Basis for Zone Mmax

As with all the seismotectonic zones, the Mmax distribution for the ECC-GC is derived using two different approaches (see Section 5.2). For the Bayesian approach, the MESE and COMP priors are used for this seismotectonic zone because the zone geometry is defined by the extent of Mesozoic extension. For both approaches, three weighted alternative characterizations are used to represent uncertainty in the largest observed earthquake within the zone, as follows:

- Alternative 1: The largest observed earthquake is the October 22, 1882, E[**M**] 5.58 earthquake.
- Alternative 2: The largest observed earthquake is the October 24, 1997, **M** 4.9 E[**M**] 4.88 earthquake.
- Alternative 3: The largest observed earthquake is the potential paleoearthquake identified from the studies of Cox and other researchers and is characterized with a potential magnitude distribution of 5.0 (0.1), 5.5 (0.4), 6.0 (0.4), and 6.5 (0.1) (see discussion in Section 7.3.9.5).

Alternative characterizations 1 and 2 represent the use of historical and instrumental seismicity to define the largest observed earthquake, and Alternative 3 represents the use of paleoseismicity

to define the largest observed earthquake within the zone. For this project, 0.2 weight is given to using the potential paleoearthquake as the largest observed earthquake within the zone (see Section 5.2), so Alternative 3 is given 0.2 weight in truncating the prior. Alternatives 1 and 2 combined are given the remaining 0.8 weight, and individually they are weighted 0.4 each. The October 22, 1882, E[**M**] 5.58 earthquake is the largest earthquake in the zone, and the October 24, 1997, E[**M**] 4.884.9 earthquake is the second largest earthquake within the zone. The even weighting between the two alternative characterizations reflects the observation that the October 22, 1882, E[**M**] 5.58 earthquake occurs close to the eastern edge of the OKA zone boundary (see Figure 7.3.11-1), and that there is significant uncertainty in its location because the location is based on historical accounts. Similar to the treatment of this earthquake for the OKA zone (see Section 7.3.11.3), the possibility that this earthquake occurred outside the ECC-GC zone is captured with the 0.4 weight on the October 24, 1997, E[**M**] 4.88 earthquake as the largest in the zone.

It should be noted that for the Alternative 3 case where the maximum observed magnitude is based on the potential paleoearthquake, the magnitude distribution for maximum observed earthquake needs to take into account the probability that the largest historical earthquake is either the 5.58 or 4.9. Taking this weighted historical earthquakes into account, the actual maximum observed magnitude distribution for Alternative 3 is 5.0 (0.05), 5.5 (0.2), 5.58 (0.25), 6.0 (0.4), 6.5 (0.1).

The final Mmax distribution for the zone is presented in Section 7.4

7.3.9.4 Future Earthquake Characteristics

Future earthquakes within the ECC-GC are modeled using the default characteristics for the CEUS, with the exception of the strike of fault ruptures and weighting of seismogenic thickness values. It is anticipated that future moderate to large earthquakes will most likely occur along preexisting basement structures associated with the opening of the Gulf of Mexico, and the two types of structures most likely to be reactivated are normal faults roughly perpendicular to the rifting direction that accommodated the extension, and transform faults subparallel to the rifting direction that accommodated differential spreading rates. However, there is considerable uncertainty in the orientation of these structures throughout the ECC-GC zone because there are several kinematic models for opening of the Gulf of Mexico, all of which imply different orientations for the two fault types, and, in general, each of the models has internal variation in orientation of the two fault types within different regions of the ECC-GC zone (e.g., the western vs. eastern Gulf of Mexico) (Anderson and Schmidt, 1983; Buffler and Sawyer, 1985; Buffler et al., 1980; Dunbar and Sawyer, 1987; Hall et al., 1982; Hall and Najmuddin, 1994; Klitgord et al., 1984; Marton and Buffler, 1994; Pindell, 1985, 1993; Pindell and Kennan, 2001; Pindell et al., 2006; White, 1980). Combining the uncertainty from these two factors, it is difficult to identify a preferred range of orientations, so the expected strike of future ruptures within the ECC-GC is modeled as randomly oriented.

7.3.9.5 Possible Paleoliquefaction Features in Arkansas, Louisiana, and Mississippi

Cox and other researchers (Cox, 2002, 2009; Cox, Forman, et al., 2002; Cox, Harris, et al., 2004; Cox and Larsen, 2004; Cox, Larsen, Forman, et al., 2004; Cox, Larsen, and Hill, 2004; Garrote et al., 2006; Cox et al., 2007; Cox and Gordon, 2008; Gordon and Cox, 2008) have conducted several studies in the southeastern Arkansas, northeastern Louisiana, and western Mississippi (ALM) areas, investigating what they interpret to be paleoliquefaction features possibly related to moderate to large earthquakes occurring along the Saline River fault zone in southern Arkansas. Collectively, this group of proposed paleoliquefaction features is referred to as the ALM features. Briefly, the basis for the researchers' interpretation is as follows:

- They observed roughly circular sandy deposits in aerial photographs throughout the Arkansas and Mississippi river valleys between southeastern Arkansas and northeastern Louisiana that they interpret to be seismically induced sand blows.
- They trenched sandy deposits at seven locations, and within the trenches they interpret multiple sand-venting episodes that can be correlated between trench sites based on stratigraphic relationships observed in the trenches, and dating of the sand units.
- They proposed that there is evidence of Quaternary fault rupture in the Saline River area along the trend of the Oklahoma-Alabama transform, a transform boundary during the Paleozoic rifting related to opening of the Iapetus Ocean and the Mesozoic rifting that formed the Gulf of Mexico.

As part of the CEUS SSC Project, the results of the studies by Randel Cox (University of Memphis) and his colleagues were evaluated to determine whether there was evidence of either RLMEs, and thus evidence for a RLME source zone, or of a single Quaternary earthquake that would impact the determination of the maximum observed earthquake within the ECC-GC zone.

To establish whether the proposed ALM paleoliquefaction data supported the presence of an RLME source, criteria established as part of the CEUS SSC Project were used for identifying earthquake-induced liquefaction features. These criteria focus on the identification of sand blows, sand-blow craters, and sand dikes because these features are the only reliable indicators of earthquake-induced liquefaction. Characteristics of these liquefaction features are described in Appendix E. With these criteria, project team members evaluated in detail the ALM features presented by Cox and other researchers. This evaluation included reviews of published papers, including trench logs; conversations with Cox; and reviews of original field notes, field trench logs, and field photographs taken by Cox as part of the various studies.

The conclusions of the evaluation are as follows:

- There is no unequivocal evidence for repeated large earthquakes in the exposures.
- There is little, if any, unequivocal evidence for large ($M > 6$) earthquakes in the studied exposures.
- The best evidence for a paleoearthquake is a possible small (<6 cm wide) feeder dike shown in the field logs and on photographs of the Portland, Arkansas, trench site. It remains unclear

whether this possible small dike is the result of (1) a moderate-magnitude local earthquake, (2) a larger, more distant earthquake, or (3) non-earthquake processes. Other small sand dikes may occur in other trenches.

In summary, the conclusion was made that the paleoliquefaction data from the ALM region are preliminary and do not provide adequate evidence for a source of RLMEs in the ALM area. Therefore, an RLME source zone is not defined based on the ALM features.

The studies of Cox and other researchers were also evaluated to determine whether they provided evidence of any Quaternary paleoearthquakes that would impact the characterization of the ECC-GC zone. Following from the methodology of using the maximum observed earthquake within a seismotectonic zone in defining the Mmax distribution, a paleoearthquake magnitude could define the largest observed earthquake. As stated above, the possible sand dike in the Portland trench is the strongest evidence for a paleoearthquake within the ALM region. In general, the magnitude threshold for liquefaction is about **M** 5. The magnitude threshold in Holocene fluvial deposits in the Mississippi River floodplain is about **M** 6.3 (i.e., the magnitude of the 1895 Charleston, Missouri, earthquake). Therefore, a local earthquake in the magnitude range of **M** 5 to 6.5 could be responsible for the formation of the sand dike.

Based on our evaluation of the uncertainty in this possible magnitude, the magnitude of the paleoearthquake was characterized using the following magnitude distribution: **M** 5.0 (0.1), **M** 5.5 (0.4), **M** 6.0 (0.4), and **M** 6.5 (0.1). This magnitude distribution is one of the options used in truncating the Mmax prior for the zone (see Section 7.3.9.3). The apparent lack of unequivocal liquefaction features at other sites across the ALM region argues against a large local earthquake. Alternatively, the Portland sand dike could be the result of a large distant earthquake, perhaps centered near Marianna, Arkansas.

The Quaternary fault rupture in the Saline River area as proposed by Cox et al. (2000) was not considered in developing estimated paleoearthquake magnitudes because it is not thought that there is strong evidence for Quaternary fault rupture at that location. This appraisal of the evidence for Quaternary activity is based on (1) the fact that the faults described by Cox et al. (2000) are all relatively small displacement fault splays that have evidence of Eocene offsets, and at best equivocal evidence of Pliocene to Pleistocene offsets; and (2) the fact that there has been no additional published research conducted to support Quaternary offsets along these faults (e.g., Wheeler, 2005).

7.3.10 Gulf Coast Highly Extended Crust Zone (GHEX)

The breakup of the supercontinent of Pangaea and the formation of the Gulf of Mexico in the Triassic and Jurassic resulted in the development of three large crustal domains in the Gulf of Mexico region. From north to south, these domains are the thick transitional crust, the thin transitional crust, and the newly formed oceanic crust (Buffler and Sawyer, 1985; Marton and Buffler, 1994; Salvador, 1991a, 1991b; Sawyer et al., 1991). The Gulf Highly Extended Crust (GHEX) seismotectonic zone is the thin transitional crust domain (Figure 7.3.10-1).

The thin transitional crust within the Gulf of Mexico region represents continental crust that has undergone considerable thinning associated with the opening of the Gulf of Mexico. In contrast to the thick transitional crust that is 20–40 km (12.5–25 mi.) thick (see Section 7.3.9), the thin transitional crust is generally 8–15 km (5–9.3 mi.) thick (Sawyer et al., 1991). This relatively thin crust subsided more quickly than the thick transitional crust during and following the opening of the Gulf of Mexico allowing for the deposition of thick nonmarine and marine sediments, including the salt deposits that are characteristic of the Gulf of Mexico region. These thick sedimentary sequences—and in particular, the salt deposits—have made it difficult to seismically image geologic structures that may have accommodated the extension of the thin transitional crust (Buffler and Sawyer, 1985; Marton and Buffler, 1994; Sawyer et al., 1991). However, magnetic data suggests that structures within the thin transitional crust are generally oriented parallel to the trend of the Gulf margin (Sawyer et al., 1991).

The source characterization of the GHEX seismotectonic zone described in the following text is based on a review of published material; these same materials were also used for Section 7.3.9 Extended Continental Crust—Gulf Coast (see Appendix Table D-7.3.9). Explicit references that were used as the basis for source characteristics are identified in Appendix Table C-7.3.9.

7.3.10.1 Basis for Defining Seismotectonic Zone

Following the methodology for defining seismotectonic zones (see Chapter 4), the GHEX zone is included as a zone distinct from the ECC-GC zone because the GHEX zone is expected to have different future earthquake characteristics. In particular, based on the reduced crustal thickness of the GHEX zone (8–15 km [5–9.3 mi.]), the seismogenic thickness of the zone should be less than that of the ECC-GC zone.

7.3.10.2 Basis for Zone Geometry

The boundaries of the GHEX seismotectonic zone are defined by the boundary between the thin and thick transitional crust (see Section 7.3.9.2 for discussion of this boundary) and the boundary between the oceanic crust and the thin transitional crust (Figure 7.3.10-1). The oceanic-transitional crust boundary of Bird et al. (2005) defines the zone because it is one of the more recent interpretations of the crustal extent that takes into account the latest data, and because it is within the range of extents estimated by previous researchers (e.g., Buffler and Sawyer, 1985; Hall and Najmuddin, 1994; Marton and Buffler, 1994; Pindell et al., 2000; Sawyer et al., 1991).

7.3.10.3 Basis for Zone Mmax

As with all the seismotectonic zones, the Mmax distribution for the GHEX zone is derived using two different approaches (Section 5.2). However, the Kijko approach was given zero weight for this zone because of the low *P*-value (see Section 5.2.1.3). For the Bayesian approach, the MESE and COMP priors are used because the zone geometry is defined by the extent of Mesozoic extension. Two weighted magnitudes are used to represent uncertainty in the largest earthquake occurring within the zone.

The largest earthquake from the catalog within the zone is the February 10, 2006, E[**M**] 4.85 earthquake, referred to as the Green Canyon earthquake. The earthquake occurred along the Sigsbee escarpment off Louisiana. Nettles (2007) has interpreted this earthquake as a gravity-driven landslide based on the lack of high-frequency energy in the waveforms, slow rise time, preliminary focal mechanism determinations, and location on the Sigsbee escarpment. Preliminary conclusions of Dellinger et al. (2007a, b) also support this interpretation, but these studies acknowledge that neither a consensus nor conclusive interpretation of the earthquake mechanism has been determined. Furthermore, efforts to relocate the earthquake cannot constrain the depth of the earthquake to within the range expected for a landslide mechanism (Dewey and Dellinger, 2008), and there have been no peer-reviewed studies of the earthquake published in the scientific literature.

In addition to the February earthquake, the September 10, 2006, E[**M**]5.82 earthquake occurred just outside the zone by approximately 15 km (9 mi.; Figure 7.3.10-1). The magnitudes of these two earthquakes are equally weighted as the maximum observed earthquake within the zone for the following reasons:

- There is uncertainty in whether or not the February earthquake was caused by a landslide or discrete fault rupture.
- There is considerable uncertainty in the exact location of the oceanic-transitional crust boundary (e.g., Bird et al., 2005; Buffler and Sawyer, 1985; Hall and Najmuddin, 1994; Marton and Buffler, 1994; Pindell et al., 2000; Sawyer et al., 1991).
- Given that uncertainty, it is possible that the September earthquake occurred in transitional, and not oceanic, crust.

The final Mmax distribution for this zone is presented in Section 7.4.

7.3.10.4 Future Earthquake Characteristics

Future earthquakes within the GHEX seismotectonic zone are modeled with the default characteristics for the CEUS with the exception of the strike of fault ruptures and the seismogenic thickness of crust within the zone. Similar to the ECC-GC zone, it is likely that future moderate to large earthquakes will occur along preexisting basement structures associated with the opening of the Gulf of Mexico, and the structures most likely to be reactivated are normal faults roughly perpendicular to the rifting direction (i.e., roughly parallel to the coastline) that accommodated the extension and transform faults subparallel to the rifting direction (i.e., roughly perpendicular to the coastline) that accommodated differential spreading rates. However, there is considerable uncertainty in the orientation of these structures throughout the GHEX zone because there are several kinematic models for the opening of the Gulf of Mexico, all of which imply different orientations for the two fault types, and in general, each of the models has internal variation in the orientation of the two fault types within different regions of the ECC-GC zone (e.g., the western vs. eastern Gulf of Mexico) (Anderson and Schmidt, 1983; Buffler and Sawyer, 1985; Buffler et al., 1980; Dunbar and Sawyer, 1987; Hall et al., 1982; Hall and Najmuddin, 1994; Klitgord et al., 1984; Marton and Buffler, 1994; Pindell, 1985, 1993; Pindell and Kennan, 2001; Pindell et al., 2006; White, 1980). Combining the uncertainty from these two

factors, it is difficult to identify a preferred range of orientations, so the expected strike of future ruptures within the GHEX zone is modeled as randomly oriented.

The large amounts of crustal thinning in the GHEX zone has resulted in crustal thicknesses for the thin transitional crust that are generally between 8 and 15 km (5 and 9.3 mi.; Sawyer et al., 1991). Because of this thinning, the seismogenic thickness of the crust within the zone should be less than the default values for the CEUS. For the GHEX zone the seismogenic thickness is assumed to be limited by the approximate crustal thickness (i.e., 8–15 km [5–9.3 mi.]). For simplicity and because the crustal thickness is not uniformly known within the GHEX zone, these two end-member seismogenic thicknesses are weighted evenly.

7.3.11 Oklahoma Aulacogen Zone (OKA)

The Oklahoma aulacogen (OKA) seismotectonic zone (Figure 7.3.11-1) is interpreted as a failed rift arm that formed in the late Proterozoic to early Cambrian. Many of the original rift-related structures were subsequently reactivated and/or overprinted during the late Paleozoic Ouachita orogeny. The geologic history of the aulacogen generally is represented as consisting of four phases (Gilbert, 1983b; Keller and Stephenson, 2007; McConnell and Gilbert, 1990; Perry, 1989):

1. The initial late Proterozoic–early Cambrian rifting and associated magmatism.
2. A period of post-rift subsidence in the middle Paleozoic.
3. Compressional deformation associated with the late Paleozoic Ouachita orogeny.
4. Mesozoic and Cenozoic stability with the exception of the noted Quaternary slip observed on the Meers fault.

The main stage of rifting that led to the breakup of Rodinia along what is now the eastern margin of North America occurred between approximately 620 Ma and 550 Ma (Thomas, 2006; Whitmeyer and Karlstrom, 2007). Within this stage of large-scale rifting, the initiation of extension within the OKA is marked by the intrusion of rift-related basaltic magma at approximately 600 Ma (Gilbert, 1983b; McConnell and Gilbert, 1990). Magmatism associated with aulacogen formation continued until approximately 500 Ma (Gilbert, 1983b). The rifting presumably was accommodated along a series of normal faults approximately parallel to the trend of the aulacogen, but the original extensional faults have been either masked or reactivated during subsequent tectonic events, making identification of rift-related faults difficult (Brewer et al., 1983; Gilbert, 1982; Gilbert, 1983b; Keller and Stephenson, 2007; Perry, 1989).

During the middle Paleozoic (Cambrian through early Mississippian), the region surrounding the aulacogen was tectonically stable and characterized by subsidence that initiated significant basin deposition in the present-day Anadarko basin (Perry, 1989). This period of tectonic quiescence ended in the late Paleozoic during the Pennsylvania Ouachita orogeny that marked the closing of the Iapetus Ocean and the formation of the supercontinent Pangaea. In the region of the Oklahoma aulacogen, the Ouachita orogeny led to the formation of the Wichita, Arbuckle, and Amarillo uplifts, which partially were accommodated along reactivated normal faults from the original aulacogen formation. These uplifts and related structures now overprint the structural

expression of the aulacogen (Brewer, 1982; Brewer et al., 1981; Brewer et al., 1983; Good et al., 1984; Perry, 1989). Since the cessation of the Ouachita orogeny, the region surrounding the OKA has been tectonically stable with the exception of the Quaternary activity observed on the Meers fault (Crone and Luza, 1990; Gilbert, 1983a; Swan et al., 1993; see Section 6.1.4). No other faults associated with the Wichita, Arbuckle, and Amarillo uplifts or the OKA have demonstrated Quaternary activity.

The source characterization of the OKA described in the following text is based on a review of published material (see Appendix Table D-6.1.4). Explicit references that were used as the basis for source characteristics are identified in Appendix Table C-6.1.4.

7.3.11.1 Basis for Defining Seismotectonic Zone

Following the CEUS SSC methodology for defining seismotectonic zones (see Chapter 4), the OKA is included as a distinct zone because we expect it to have distinct differences in future earthquake characteristics compared to surrounding regions. Compared to the default future earthquake characteristics applied to the CEUS in our model, we expect the OKA to have the following differences:

- Style of faulting: Left-lateral oblique-reverse fault dominated by strike-slip motion based on the observed slip of the Meers fault (see Section 6.1.4).
- Strike of ruptures: N60°W ± 15° based on the observed strike of faults in the Wichita, Arbuckle, and Amarillo uplifts (e.g., Ham et al., 1964; Texas BEG, 1997).

The basis for defining the distinct future earthquake characteristics for the aulacogen is the observation of the characteristics of the Quaternary activity on the Meers fault, a fault within the Wichita frontal fault system (see Section 6.1.4). Despite the lack of evidence for any Quaternary activity on any other geologic structures within the aulacogen, the strong structural expression of the aulacogen and uplifts indicates that any future moderate to large earthquakes in the aulacogen are likely to have characteristics similar to those of the Meers fault.

7.3.11.2 Basis for Zone Geometry

The geometry of the OKA seismotectonic zone is defined to envelop the extent of (1) the aulacogen as defined by gravity and magnetic anomaly data (CEUS SSC gravity and magnetic anomaly data; Figure 7.3.11-1); and (2) mapped faults related to the Arbuckle, Amarillo, and Wichita uplifts (e.g., Ham et al., 1964; Texas BEG, 1997). The southeastern extent of the zone is defined by the limit of crustal thinning associated with the Mesozoic opening of the Gulf of Mexico. This envelope is meant to capture both the region of crust that was the center of rifting and magmatism during the opening of the aulacogen, and faults within this potentially weakened crust and associated with the Arbuckle, Amarillo, and Wichita uplifts and the Ouachita orogeny. Given the uncertainty in the extent of the aulacogen and the uplift-related faults, there is considerable uncertainty in the boundary of the OKA. It is not possible to quantify this uncertainty, but it is likely on the order of 50 km (31 mi.) or more.

It should be noted that the OKA zone was not extended into New Mexico, Colorado, and Utah despite evidence for magmatism and geopotential anomalies in these regions that have been attributed to the Cambrian rifting of the OKA (e.g., Keller and Stephenson, 2007; Larson et al., 1985). The decision to limit the OKA source zone to the extent presented here was based on the lack of evidence for Quaternary faulting within the New Mexico, Colorado, and Utah regions of Cambrian rifting; the fact that the Arbuckle, Amarillo, and Wichita uplifts do not extend that far; and the fact that most of these regions are outside of the study area.

7.3.11.3 Basis for Zone Mmax

As with all the seismotectonic zones, the Mmax distribution for the OKA zone is derived using two different approaches (see Section 5.2). However, for this zone, the Kijko approach was given zero weight because of the low *P*-value (see Section 5.2.1.3). For the Bayesian approach, the NMESE and COMP priors are used for this zone due to the absence of Mesozoic extension within the OKA. Two weighted scenarios are used to represent uncertainty in the largest earthquake observed within the zone. The largest earthquake within the zone is the July 30, 1925, E[**M**] 5.24 earthquake (Figure 7.3.11-1). However, the October 22, 1882, E[**M**] 5.58 earthquake is located just to the west of the zone and likely has significant uncertainty in its location because that location is based on historical accounts. To capture the possibility that the 1882 earthquake did occur within the OKA zone, two equally weighted options for the largest observed earthquake in the zone are considered: E[**M**] 5.58, based on the 1882 earthquake, and E[**M**]5.24, based on the 1925 earthquake. The final Mmax distribution for this zone is presented in Section 7.4.2.

7.3.11.4 Future Earthquake Characteristics

As described above, we model future earthquakes within the OKA seismotectonic zone using the default characteristics for the CEUS, as discussed in Section 5.4, with the exception of the style of faulting and rupture strike. Default values are used because there is little to no information to strongly support alternative values. Based on the observations of Quaternary slip on the Meers fault, the style of faulting for future earthquakes within the OKA is constrained to be left-lateral, oblique-reverse fault dominated by strike-slip motion (see Section 6.1.4). Based on the observed orientation of faulting associated with the Wichita, Arbuckle, and Amarillo uplifts, the strike of future ruptures within the OKA is constrained to be parallel to the long axis of the zone (e.g., Ham et al., 1964; Texas BEG, 1997).

7.3.12 Midcontinent-Craton Zone (MidC)

The continental interior (Midcontinent-Craton), which consists of those regions that have not been incorporated into Phanerozoic orogens of the continental margin, comprises two geologic provinces: the Canadian Shield, where Precambrian metamorphic and igneous basement rocks crop out at the ground surface, and the platform, where Precambrian basement rocks lie beneath a veneer of sedimentary strata (Marshak and Paulsen, 1997).

The following text provides a discussion of the geologic, seismic, and geophysical characteristics of the Midcontinent-Craton (MidC) seismotectonic zone. This discussion, as well as the seismic source characterization of the MidC, is based on a review of published material that is summarized in the Data Summary table for the MidC zone (Appendix Table D-7.3.12). Explicit references and data that were used as the basis for source characteristics of MidC are identified in the Data Evaluation table (Appendix Table C-7.3.12).

7.3.12.1 Background

7.3.12.1.1 Precambrian Crustal Basement Structure

The Central United States is underlain by several Precambrian terranes, including the Superior province (2,700 Ma); Penokean orogen (1,880–1,830 Ma); Northern Central Plains orogen (1,880–1,700 Ma); Southern Central Plains orogen (1,700–1,600 Ma); Eastern Granite-Rhyolite province (1,470 ± 30 Ma); Southern Granite-Rhyolite province (1,370 ± 30 Ma); Midcontinent rift system (1,100–1,000 Ma); and Grenville province (1,100–800 Ma; Atekwana, 1996; Van Schmus et al., 1996).

Whitmeyer and Karlstrom (2007) present a plate-scale model for the Precambrian growth and evolution of the North American continent. The core of the North American continent, including the Canadian Shield, was formed in the Paleoproterozoic (1,600–2,500 Ma) by plate collisions. The thick, buoyant, and compositionally depleted mantle lithosphere that now underlies North America, although dominantly of Archean (>2,500 Ma) age, took its present shape due to collisional orogenesis and likely has a scale of mantle heterogeneity similar to that exhibited in the overlying crust.

In marked contrast, the lithosphere of southern North America (i.e., much of the continental United States) was built by progressive addition of a series of dominantly juvenile volcanic arcs and oceanic terranes accreted along a long-lived southern (based on present coordinates) plate margin. The lithospheric collage that formed from dominantly juvenile terrane accretion and stabilization (1,800–1,000 Ma) makes up about half of the present-day North American continent. Throughout—and as a result of—this long-lived convergent cycle, mantle lithosphere below the accretionary provinces was more hydrous, fertile, and relatively weak compared to mantle lithosphere under the Archean core.

Mooney and Ritsema (2009) hypothesize that greater lithospheric strength correlates with lower rates of continental crustal seismicity and with lower maximum magnitude. They suggest that high lithospheric S-wave velocities that are typical of cratonic lithosphere correspond to high integrative lithospheric strength. By comparing global maps of S-wave velocity anomalies at a depth of 175 km (108 mi.) and the moment magnitudes of earthquakes in the overlying crust, Mooney and Ritsema (2009) conclude that the maximum magnitude for SCRs underlain by S-wave velocity anomalies of >3.5 percent, which includes a large portion of the Archean- and Neoproterozoic-age Precambrian continental interior of the CEUS, appears to be **M** 7. Analysis of the magnitudes of earthquakes in stable continental regions worldwide indicates that a broader range of magnitudes may better represent the uncertainty in maximum magnitude (Section 5.2).

7.3.12.1.2 Major Precambrian Basement Structures

Major Precambrian basement features have been interpreted by various workers based on interpretation of geologic data from drilling, deep crustal seismic profiles, and interpretation of geopotential field data (e.g., Braile et al., 1986; Pratt et al., 1989; Atekwana, 1996; Marshak and Paulsen, 1997). Sims et al. (2005) present a preliminary structure map of Precambrian basement rocks based on interpretation of geologic and magnetic data (Figure 7.3.12-1). They suggest that the systematics of major regional post-assembly Precambrian basement structures throughout the continental United States point to a common causal mechanism for their development. A major driving force for plate movement is deep-mantle flow resulting from seismic anisotropy beneath the continents and mechanical coupling and subsequent shear between the lithosphere and asthenosphere. Two orthogonal sets of shear zones and faults are predominant in the continent: (1) northeast-striking partitioned ductile shear zones and (2) northwest-trending strike-slip ductile-brittle faults (Sims et al., 2005).

The northeast-striking shear zones are interpreted by Sims et al. (2005) as resulting from northwest-southeast shortening, apparently formed during the interval 1,760–1,700 Ma. The northwest-trending (1,700–1,500 Ma) transcurrent fault system consists of west-northwest to northwest synthetic faults and northerly trending antithetic transfer faults. The deformation during this interval is attributed to transpressional-transtensional deformation (i.e., strike-slip deformation that deviates from simple shear because of a component of shortening or extension orthogonal to the deformation zone). The northeast- and northwest-oriented shears and faults mimic orthogonal teleseismic images of the upper mantle. These structures were reactivated during the Mesoproterozoic (1,000–1,600 Ma) and later times. The kinematics of regional Precambrian basement structures within the continental United States suggest that deformation since at least early Proterozoic time has been predominantly transpressional. Transcurrent lithospheric structures formed during Proterozoic mantle deformation are oriented obliquely to the southwestward (absolute) motion of the North American Plate. Stress caused by traction between the asthenosphere and lithosphere during the southwestward drift focused on preexisting block boundaries that have repeatedly reactivated basement zones of weakness, thus localizing sedimentation, magmatism, and generation of ore deposits (Sims et al., 2005).

Marshak and Paulsen (1997) identified similar north-northeast and west-northwest trends that break up the continental interior of the United States into roughly rectangular blocks. They refer to these as the Midcontinent fault and fold zones and suggest that the current intraplate stress field of North America is sufficient to cause slight movements of crustal blocks in the interior, thereby triggering seismicity. Marshak and Paulsen (1997) also note that differential epeirogenic movements (the gradual uplift, subsidence, or tilting of broad areas relative to their surroundings) have affected sedimentary thicknesses and facies throughout the region. These movements occurred episodically through the Phanerozoic (post-Precambrian), giving rise to reactivated regional-scale (>200 km [>124 mi.] diameter) basins, domes, and arches.

7.3.12.1.3 Geophysical Anomalies

As noted by Hinze and Hildenbrand (1988), information on the crystalline crust of the Eastern United States from direct observations, drilling, and sparse crustal seismic studies is limited.

Regional gravity and magnetic anomaly data provide more uniform coverage and can be used to estimate the strength of the crust and lithosphere and to map and characterize (1) zones of weakness such as paleorifts, sutures, and faults; (2) regions of potential stress amplifications such as plutons and irregularities in fault zones; and (3) basement terranes of generally consistent structural pattern that may delimit coherent regional seismic zones.

Some of the more prominent geophysical anomalies are shown on Figures 7.3.12-1 and 7.3.12-2, including the Midcontinent gravity high associated with the Midcontinent rift (Hinze et al., 1997); gravity and magnetic anomalies associated with the East Continent rift basin (Drahovzal et al., 1992); geophysical lineaments such as the Commerce geophysical lineament (CGL; Langenheim and Hildenbrand, 1997; Hildenbrand and Hendricks, 1995); the south-central magnetic lineament (SCML; Hildenbrand et al., 1983); and the neodymium (Nd) isotopic boundary (also referred to as the St. Charles lineament [SCL]), which probably represents the southeast limit of Paleoproterozoic crust (Van Schmus et al., 1996; Harrison and Schultz, 2002; Van Schmus et al., 2007); and sutures such as the Great Lakes tectonic zone (GLTZ), Spirit Lake tectonic zone (SLTZ), Eau Plain shear zone (EP), and Niagara fault zone (NF; Hinze, 1996; Van Schmus et al., 2007).

7.3.12.1.4 Seismicity

Seismicity within the MidC zone is spatially variable, with moderate concentrations of earthquake activity separated by areas of very low seismicity. Previously recognized zones of seismicity are the Anna seismic zone in Ohio, the Northeast Ohio seismic zone, and a zone of moderate seismicity in the vicinity of the Nemaha ridge in Kansas (Figure 7.3.12-3). Reconnaissance paleoliquefaction surveys conducted to date have not identified evidence for large-magnitude (**M** > 7) earthquakes in these zones. Preliminary conclusions from these studies, which are discussed in the following descriptions of the zones, are that **M** > 7 earthquakes probably have not occurred in these regions in the past few thousand years. Moderate-sized earthquakes (**M** 6 to < **M** 7), however, cannot be precluded based on the extent and completeness of the surveys and the existing geologic characteristics (e.g., liquefaction susceptibility, quality of exposure, age of deposits). The available information does not support defining RLME sources associated with these zones of more concentrated seismicity.

Anna Seismic Zone—This zone, also called the Western Ohio seismic zone, coincides with northwest-southeast-trending basement faults associated with the Fort Wayne rift (Figure 7.312-2) in Shelby, Auglaize, and nearby counties (Hansen, 1993; Baranoski, 2002). Ruff et al. (1994) attribute seismicity to the Anna-Champaign, Logan, and Auglaize faults. This zone has produced at least 40 felt earthquakes since 1875, including earthquakes in 1875, 1930, 1931, 1937, 1977, and 1986 that caused minor to moderate damage (Hansen, 1993). The July 12, 1986, earthquake near the town of St. Marys in Auglaize County was the largest earthquake to occur in the zone since 1937 (Hansen, 1993). For the 1986 magnitude (m_b) 4.5 (E[**M**] 4.37) earthquake, Schwartz and Christensen (1988) determined a hypocenter of 5 km (3 mi.) and a focal mechanism (strike = 25°, dip = 90°, rake = 175°) representing mostly strike-slip, with a small oblique component approximately parallel to the Anna-Champaign fault and a nearly horizontal *P*- (maximum compressive stress) axis oriented east-northeast. The earthquake produced a MMI VI intensity (Schwartz and Christiansen, 1988). Obermeier (1995) investigated stream banks in

the vicinity of Anna, Ohio, and portions of the Auglaize, Great Miami, Stillwater, and St. Marys rivers and found no evidence of paleoliquefaction features indicative of a magnitude 7 earthquake in the past several thousand years. Obermeier (1995) noted that although there was sufficient outcrop to preclude with some confidence an earthquake larger than magnitude 7, the paucity of outcrop did not preclude the possibility of prehistoric earthquakes of lower magnitudes. Crone and Wheeler (2000) designated the Anna seismic zone a Class C feature[4] based on the occurrence of significant historical earthquakes and the lack of paleoseismic evidence.

Northeast Ohio Seismic Zone—This zone, also called the Ohio-Pennsylvania seismic zone, defines an approximately 50 km (30.5 mi.) long, northeast-southwest-trending zone of earthquakes south of Lake Erie on the Ohio-Pennsylvania border (Dineva et al., 2004). The largest historical earthquake in this zone was the January 31, 1986, m_b 5.0 (E[**M**] 4.65) earthquake located about 40 km (25 mi.) east of Cleveland in southern Lake County, Ohio. The earthquake produced MMI VI to VII at distances of 15 km (9 mi.) from the epicenter (Nicholson et al., 1988). Aftershocks with magnitudes ranging from 0.5 to 2.5 and focal depths ranging from 2 to 6 km (1.2 to 3.7 mi.) occurred in a tight cluster about 1 km (0.6 mi.) wide and oriented north-northeast. Focal mechanisms represent predominantly oblique, right-slip motion on nearly vertical planes oriented N15° to 45°E, with a nearly horizontal *P*-axis consistent with the modern stress regime (Nicholson et al., 1988).

The January 31, 1986, earthquake and aftershocks were within 12 km (7.3 mi.) of deep waste-disposal injection wells, and the earthquake sequence is possibly due to injection activities at the wells that reactivated favorably oriented preexisting fractures (Nicholson et al., 1988). However, the relative distance of the wells from the earthquake cluster (12 km [7.3 mi.]), as well as the lack of large numbers of earthquakes that are typical of induced sequences, a history of small to moderate earthquakes in the region preceding well activities, and the attenuation of the pressure field with distance from the wells—all argue for a natural origin for the earthquakes (Nicholson et al., 1988).

Nicholson et al. (1988) observe that the 1986 cluster is coincident with a N40°E trending gravity and magnetic anomaly. Seeber and Armbruster (1993) and Dineva et al. (2004) also associate the Northeast Ohio seismic zone with the Akron magnetic boundary, which is also called the Akron magnetic anomaly or lineament (Figure 7.3.12-2). Seeber and Armbruster (1993) speculate that the Akron magnetic boundary may be associated with the Central Metasedimentary Belt boundary zone as a continental-scale Grenville-age structure. Since the Akron lineament is imaged as ductile shear zones on regional seismic lines and no structures are observed in the overlying Paleozoic sediments, Seeber and Armbruster (1993) acknowledge that the geometry of brittle faulting within or near this ductile deformation may have a complex relationship with the geometry of these shear zones.

In 1987, the first in a series of earthquakes continuing to 2003 occurred within the Northeast Ohio seismic zone near Ashtabula in Ashtabula County, Ohio, northeast of the 1986 earthquakes

[4] See Section 4.1.3.3 for definition of fault and feature categories used by the USGS to characterize Quaternary and possible Quaternary features in the CEUS.

(Nicholson et al., 1988; Seeber and Armbruster, 1993; Hansen et al., 2001; Seeber et al., 2004). The largest earthquakes in the sequence include an initial m_{bLg} 3.8 (E[**M**] 3.61) earthquake on July 13, 1987; a m_{bLg} 2.6 foreshock earthquake on January 19, 2001; a m_{bLg} 4.3 (E[**M**] 3.86) earthquake on January 26, 2001, which had an MMI of VI; followed by a m_{bLg} 3.0 (E[**M**] 2.92) earthquake on June 3, 2001, and a m_{bLg} 2.4 earthquake on June 5, 2001 (Hansen et al., 2001). The latest subsequence started in July 2003 with a m_{bLg} 2.5 earthquake (Seeber et al., 2004)

Seeber et al. (2004) discuss these fore-/main-/aftershock sequences and interpretations of these earthquakes using information obtained from three short-term deployments of portable seismographs (in 1987, 2001, and 2003) and from regional broadband seismograms. The main observations and conclusions from this analysis are as follows:

- A persistent earthquake sequence in northeast Ohio includes multiple, distinct fore-/main-/aftershock sequences that illuminate two nearly vertical, east-trending faults approximately 4 km (2.5 mi.) apart. The first motions are consistent with left-lateral strike-slip movement on an east-west-striking fault. The seismicity is closely associated with injection of waste fluid in the basal Paleozoic formation from 1986 to 1994.
- All the earthquakes originated from a relatively small area (~10 km [~6 mi.] wide) and are assumed to form a single sequence of casually related earthquakes.
- Felt earthquakes started in 1987, a year after the onset of injection. At that time, earthquakes were located 0.7–2.0 km (0.4–1.2 mi.) from the injection site. Seismicity continued and in 2001, five and a half years after the end of injection, hypocenters were then 5–9 km (3–5.6 mi.) from the injection site. The only known episode of seismicity in Ashtabula is closely associated with the 1986–1994 Class 1 injection, and the pattern of hypocenters is consistent with one expected for the high pore-pressure anomaly spreading from the injection site.
- This spatial and temporal correlation is strong evidence that the seismicity was triggered by the injection.

A paleoseismic liquefaction field study along two of the larger drainages in northeast Ohio, the Grand River and the Cuyahoga River, was conducted by Obermeier (1995) and involved reconnaissance along approximately 25 km (7.6 mi.) of stream bank. No evidence of liquefaction was observed along either transect. Although the scarcity of suitable exposures precludes definitive statements about prehistoric earthquakes, this led Crone and Wheeler (2000) to classify the Northeast Ohio seismic zone as a Class C feature. Conditions and ages of the sediment encountered along each of these rivers as noted by Obermeier (1995) were summarized in the report, as follows:

- Radiocarbon data from along the Grand River show that many of the exposures searched are at least 2,000 years old. Many others are probably mid-Holocene in age, based on depth and severity of weathering. A few scattered sites are earliest Holocene in age. Liquefaction susceptibility at many of the sites examined is at least moderate.
- Numerous exposures along the Cuyahoga River are at least a few thousand years in age, and scattered exposures are up to 8,000 years old, based on radiocarbon data. Conditions are favorable for forming liquefaction effects at many places.

- It is unlikely that sediments exposed in a sand pit near the Ashtabula-Trumbull county line experienced strong ground shaking through most or all of Holocene time. The groundwater table has probably been shallow enough through all or much of the Holocene to provide conditions favorable to liquefy the thick sand deposits overlain by a silt cap that are exposed in the quarry walls.

Nemaha Ridge–Humboldt Fault Seismic Zone—Historical felt earthquakes and instrumentally recorded microseismicity are loosely associated with basement structures in northeastern Kansas. Wheeler and Crone (2001) note that two damaging earthquakes in 1867 (Wamego earthquake) and 1952, which were assigned magnitudes of **M** 5.54 and **M** 5.66, respectively, by Johnston (1994), occurred in the vicinity of the Humboldt fault zone on the Nemaha uplift. Niemi et al. (2004) and Bakun and Hopper (2004a) also suggest a possible association of the 1867 Wamego earthquake with the basement Nemaha Ridge–Humboldt fault structures, which lie to the east and roughly parallel to the Proterozoic Midcontinent rift system. Seeber and Armbruster (1991) assigned the 1867 earthquake a magnitude of 5.2. Bakun and Hopper (2004a) assign a magnitude (2σ range) of $\mathbf{M}_{\mathrm{I}}$ 4.9 (4.5–5.2) to the earthquake. The 1867 and 1952 earthquakes are assigned magnitudes of E[**M**] 5.50 and E[**M**] 5.29 in the CEUS SSC Project catalog.

Niemi et al. (2004) conducted field reconnaissance investigations to evaluate evidence for paleoliquefaction in the epicentral region of the 1867 Wamego earthquake. Field investigations confirm that sedimentary deposits with moderate liquefaction susceptibility are present in the vicinity of Wamego and Wabaunsee, Kansas, the preferred source location of the 1867 Wamego earthquake. Soft-sediment deformation features, including flame and dish structures, are present in late Holocene floodplain deposits of the Kansas River and appear to be concentrated in the horseshoe bend region of the Kansas River near Wamego and Wabaunsee, Kansas. Results of the reconnaissance suggest that liquefaction features (e.g., clastic dikes), which may be attributed to seismically induced liquefaction, are present but may not be pervasive in this region. Niemi et al. (2004) concluded from the results of their reconnaissance that these data suggest that the 1867 Wamego earthquake with a reported magnitude of 5.2 (Seeber and Armbruster, 1991) may characterize the seismic source in this region. Although the available data suggest that the earthquake that triggered the paleoliquefaction features could have been close to the threshold-sized earthquake that may trigger paleoliquefaction (approximately **M** 5.4–5.8; Olson et al., 2005), the available data do not preclude the possibility that the earthquake was larger. There is not sufficient information at this time to characterize an RLME source associated with the Nemaha Ridge–Humboldt fault region.

7.3.12.2 Basis for Defining Seismotectonic Zone

The MidC seismotectonic zone represents continental crust that has not experienced Mesozoic or younger crustal extension. Defining the MidC seismotectonic zone centers primarily on the concept that continental crust that has not experienced Mesozoic or younger crustal extension will have a different maximum magnitude probability than crust that has experienced Mesozoic or younger extension (Johnston et al., 1994; see also updated analysis in Section 5.2).

The MidC zone is also defined as a seismic source in part to differentiate it from some adjoining regions of the crust that that are interpreted as producing different future rupture characteristics. For example, the trend of future ruptures in the adjoining Illinois Basin Extended Basement (IBEB), Reelfoot Rift (RR), and Oklahoma Aulacogen (OKA) seismotectonic zones reflects preferred orientations of structures in those zones, which differ from the trend of ruptures modeled for the MidC.

7.3.12.3 Basis for Zone Geometry

Four alternative geometries are considered based on alternative geometries of adjacent zones. These are shown on Figure 7.3.12-4. The northern and western boundaries of all alternative MidC zones are the study region boundaries. The eastern boundary is defined by either the western boundary of the Paleozoic Extended Crust (PEZ) and RR wide or narrow geometries (see Sections 7.3.4 and 7.3.5, respectively). The southern boundary west of the RR is defined by the northern boundary of the Extended Continental Crust–Gulf Coast (ECC-GC) and OKA seismotectonic zones (Sections 7.3.9 and 7.3.11, respectively).

7.3.12.4 Basis for Zone Mmax

The Mmax distribution for the MidC source zone is based on the two approaches, Kijko (2004) and Bayesian, as outlined in Section 5.2.

For the Kijko approach, the *P*-values for the four MidC alternative geometries (MidC-A, MidC-B, MidC-C, and MidC-D) are all 0.03; therefore, in all cases this approach is weighted 0.24.

For the Bayesian approach, both the composite (COMP) prior and the non-Mesozoic and younger extension (NMESE) prior are used; the NMESE is selected based on the evidence for no Mesozoic or younger extension in the craton region of the Midcontinent. The priors are truncated and modified using the likelihood function based on the largest historical earthquakes recorded within the zone: the May 16, 1909, E[**M**] 5.72; November 15, 1877, E[**M**] 5.50; and March 28, 1964, E[**M**] 4.84 earthquakes. The location of the largest earthquake in this zone, the May 16, 1909, E[**M**] 5.72 earthquake at a latitude/longitude intersection in eastern Montana near the Canadian border suggests this earthquake is poorly constrained.

The weights for Kijko and Bayesian approaches for the RR zone also are discussed in Section 7.4.2, and the weighted composite posterior maximum-magnitude probability distribution for the RR zone is provided in Section 7.4.2. The derived Mmax distributions for the MidC seismotectonic zone are presented in Section 7.4.2.

7.3.12.5 Future Earthquake Characteristics

The MidC seismotectonic zone uses default characteristics for future rupture characteristics listed in Table 5.4-2. The MidC zone encompasses a large intracratonic region characterized by

deeply buried Precambrian structures for which independent interpretational constraints are limited. The available data for the CEUS on style of faulting, focal mechanisms, and depth of well-constrained earthquakes used to develop the "default" characteristics as outlined in Table 5.4-1 include information from the MidC region.

7.4 Maximum Magnitude Distributions for Seismotectonic Distributed Seismicity Sources

This section presents the maximum earthquake magnitude (Mmax) distributions for the seismotectonic distributed seismicity sources. The methodology used to develop these distributions is presented in Section 5.2.1. The steps involved in the process are identification of the maximum observed earthquake in each distributed seismicity source (described in Section 7.4.1) and then application of the quantitative approaches developed in Section 5.2.1 to produce the composite Mmax distributions (described in Section 7.4.2).

7.4.1 Maximum Observed Earthquake Magnitude

The maximum observed earthquake magnitude, $m_{\max-obs}$, represents the largest non-RLME earthquake observed to have occurred with each source. The value of this magnitude is used in developing the likelihood function for the Bayesian Mmax approach (Section 5.2.1.1) and is a parameter of the Kijko approach (Section 5.2.1.2). Two resources are used to assess $m_{\max-obs}$. One is the CEUS SSC Project catalog developed for this study (Chapter 3) and the other is identified paleoearthquakes that are not treated as RLMEs. The latter consist of the four non-RLME paleoearthquakes that have been identified in the IBEB seismotectonic zone and the potential liquefaction earthquake in the ECC_GZ zone. These earthquakes are discussed in Sections 7.3.5.4 and 7.3.9.5 for the IBEB and ECC_GC zones, respectively. The largest non-RLME historical earthquakes identified in the CEUS SSC Project catalog for each seismotectonic source zone are described in Section 7.3 in the subsection for each zone.

Uncertainty in $m_{\max-obs}$ was incorporated into the Mmax assessment using the procedure described in Section 5.2.1.1.6. The uncertainties in the magnitudes for the catalog of historical earthquakes or paleoearthquakes for each source were used to develop simulated catalogs of earthquake magnitudes. The largest values for each simulation were then used to develop a distribution for $m_{\max-obs}$. Figure 7.4.1-1 shows the resulting distributions for $m_{\max-obs}$. The blue curve on each plot shows the distribution developed for $m_{\max-obs}$, and the red vertical line indicates the nominal observed magnitude. The phrase "paleo" in a plot legend (see IBEB on Figure 7.4.1-1) indicates that the set of paleoearthquakes is the controlling set for determining $m_{\max-obs}$ and was the set used to develop the Mmax distributions. For a number of zones, alternative earthquake catalogs (as indicated in the plot legends) were used to address the uncertainty in assigning particular earthquakes to the zone.

7.4.2 Mmax Distributions

Mmax distributions were developed for each seismotectonic distributed seismicity source using the Bayesian and Kijko methods. For the Bayesian Mmax approach, the alternative priors described in Section 5.2.1.1 were used. Figures 7.4.2-1 through 7.4.2-17 show the resulting Mmax distributions obtained by each method. Indicated in the legend of each figure are the weights assigned to the individual Mmax methods following the weighting approach described in Section 5.2.1.1. The final weighted composite distributions are indicated by the thick red bars on each plot.

The weights assigned to the Kijko method are tabulated below. In general, the numbers of earthquakes in many of the seismotectonic source zones are too few to allow weight to be applied to the Kijko method.

Seismotectonic Source Zone	Weight Assigned to Kijko Method
AHEX	0
ECC_AM	0.05
ECC_GC	0
GHEX	0
GMH	0
IBEB	0
MidC-A	0.24
MidC-B	0.24
MidC-C	0.24
MidC-D	0.24
NAP	0
OKA	0
PEZ_N	0
PEZ_W	0.01
RR	0
RR_RCG	0.07
SLR	0.02

The continuous distributions shown on Figures 7.4.2-1 through 7.4.2-17 were used to construct five-point discrete approximations for use in hazard analyses. The resulting Mmax distributions are listed in Table 7.4.2-1.

7.5 Recurrence Parameters

The recurrence parameters (i.e., rate and *b*-values) for the seismotectonic zones were calculated using the methodology and parameters described in Section 5.3.2. Briefly, this methodology divides the source zone into cells of dimensions a quarter or half degree and then calculates the rate and *b*-value in each cell using the likelihood function of the data in that cell together with penalty functions that tend to smooth the cell-to-cell variation in the rate or the *b*-value, as discussed in Section 5.3.2.1. In addition, this procedure characterizes epistemic uncertainty in the recurrence parameters by generating eight alternative maps of the recurrence parameters.

7.5.1 Rate and b-Value Maps for Single Zone and Two Zones

Figures 7.5.1-1 through 7.5.1-12 show the mean recurrence maps for the four alternative configurations of the seismotectonic zones' distributed seismicity source zones and the three choices of magnitude weights (i.e., Cases A, B, and E presented in Section 5.3.2.2). Maps of the calculated uncertainties in recurrence parameters, as well as alternative recurrence maps that represent that uncertainty (eight alternative maps for each source-zone configuration), are shown in Appendix J.

The SLR zone exhibits lower *b*-values than other zones. This zone was fit using somewhat different smoothing parameters, as described in Section 5.3.2.

7.5.2 Comparison of Recurrence Parameters to Catalog

Figures 7.5.2-1 through 7.5.2-51 compare the expected counts from the recurrence maps for each source zone to the observed earthquake counts within the zone. The error bars on the data represent the 16–84 percent range of statistical uncertainty in the counts and are calculated using the approach by Weichert (1980). Each of the eight curves represents expected counts (i.e., rate times equivalent period of completeness) for one of the eight equally weighted alternative maps, taking Mmax into account.

These comparisons indicate a good agreement between predicted and observed rates. For some zones, such as ECC_AM, the recurrence model over- or underestimates the observed rates for a magnitude bin, but these discrepancies are not unexpected in bins with low earthquake counts.

These comparisons also illustrate the effect of earthquake counts on rate uncertainty at the source-zone scale. The eight alternative curves are nearly identical for MidC-A (Figures 7.5.2-19 through 7.5.2-21), which has hundreds of earthquakes in the low-magnitude range. In contrast, the eight curves differ by a factor of 2 to 5 for OKA (Figures 7.5.2-35 and 7.5.2-36), which has earthquake counts more than one order of magnitude lower. The results for OKA also illustrate the effect of the magnitude weights on the uncertainty in rates. The behavior of the uncertainty in rate at smaller scales is similar to that observed in these figures and is shown more clearly in the maps showing uncertainty (see Appendix J).

Table 7.1-1
Data Summary and Data Evaluation Tables for Seismotectonic Zones in Appendices C and D

Section	Source (with Acronym)	Data Table
7.3.1	St. Lawrence Rift (SLR)	C-7.3.1, D-7.3.1
7.3.2	Great Meteor Hotspot (GMH)	C-7.3.2, D-7.3.2
7.3.3	Northern Appalachian (NAP)	C-7.3.3, D-7.3.3
7.3.4	Paleozoic Extended Crust (PEZ)	C-7.3.4, D-7.3.4
7.3.5	Illinois Basin Extended Basement (IBEB)	C-7.3.5, D-6.1.9
7.3.6	Reelfoot Rift Zone (RR)	C-7.3.6, D-6.1.5
7.3.7	Extended Continental Crust–Atlantic Margin (ECC-AM)	C-7.3.7, D-7.3.7
7.3.8	Atlantic Highly Extended Crust (AHEX)	C-7.3.7, D-7.3.7
7.3.9	Extended Continental Crust–Gulf Coast (ECC-GC)	C-7.3.9, D-7.3.9
7.3.10	Gulf Coast Highly Extended Crust (GHEX)	C-7.3.9, D-7.3.9
7.3.11	Oklahoma Aulacogen (OKA; incl. Meers Fault)	C-6.1.4, D-6.1.4
7.3.12	Midcontinent-Craton (MidC)	C-7.3.12, D-7.3.12

Table 7.4.2-1
Maximum Magnitude Distributions for Seismotectonic Distributed Seismicity Sources

	Maximum Magnitude for:												
Weight	**AHEX**	**ECC_AM**	**ECC_GC**	**GHEX**	**GMH**	**IBEB**	**MidC-A, MidC-B, MidC-C, and MidC-D**	**NAP**	**OKA**	**PEZ_N and PEZ_W**	**RR**	**RR_RCG**	**SLR**
0.101	6.0	6.0	6.0	6.0	6.0	6.5	5.6	6.1	5.8	5.9	6.2	6.1	6.2
0.244	6.7	6.7	6.7	6.7	6.7	6.9	6.1	6.7	6.4	6.4	6.7	6.6	6.8
0.310	7.2	7.2	7.2	7.2	7.2	7.4	6.6	7.2	6.9	6.8	7.2	7.1	7.3
0.244	7.7	7.7	7.7	7.7	7.7	7.8	7.2	7.7	7.4	7.2	7.7	7.6	7.7
0.101	8.1	8.1	8.1	8.1	8.1	8.1	8.0	8.1	8.0	7.9	8.1	8.1	8.1

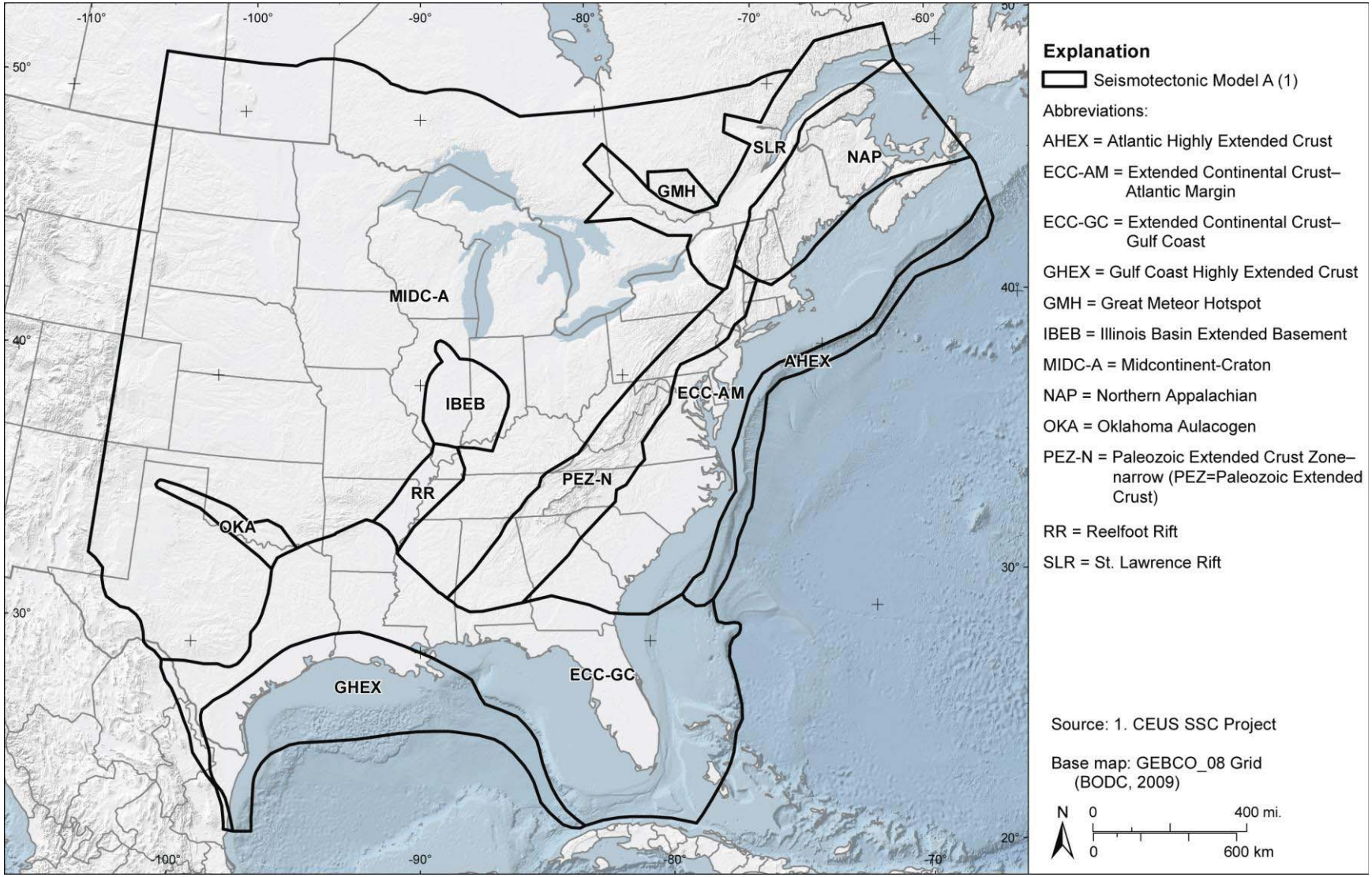

Figure 7.1-1
Seismotectonic zones shown in the case where the Rough Creek graben is not part of the Reelfoot rift (RR) and the Paleozoic Extended Crust is narrow (PEZ-N)

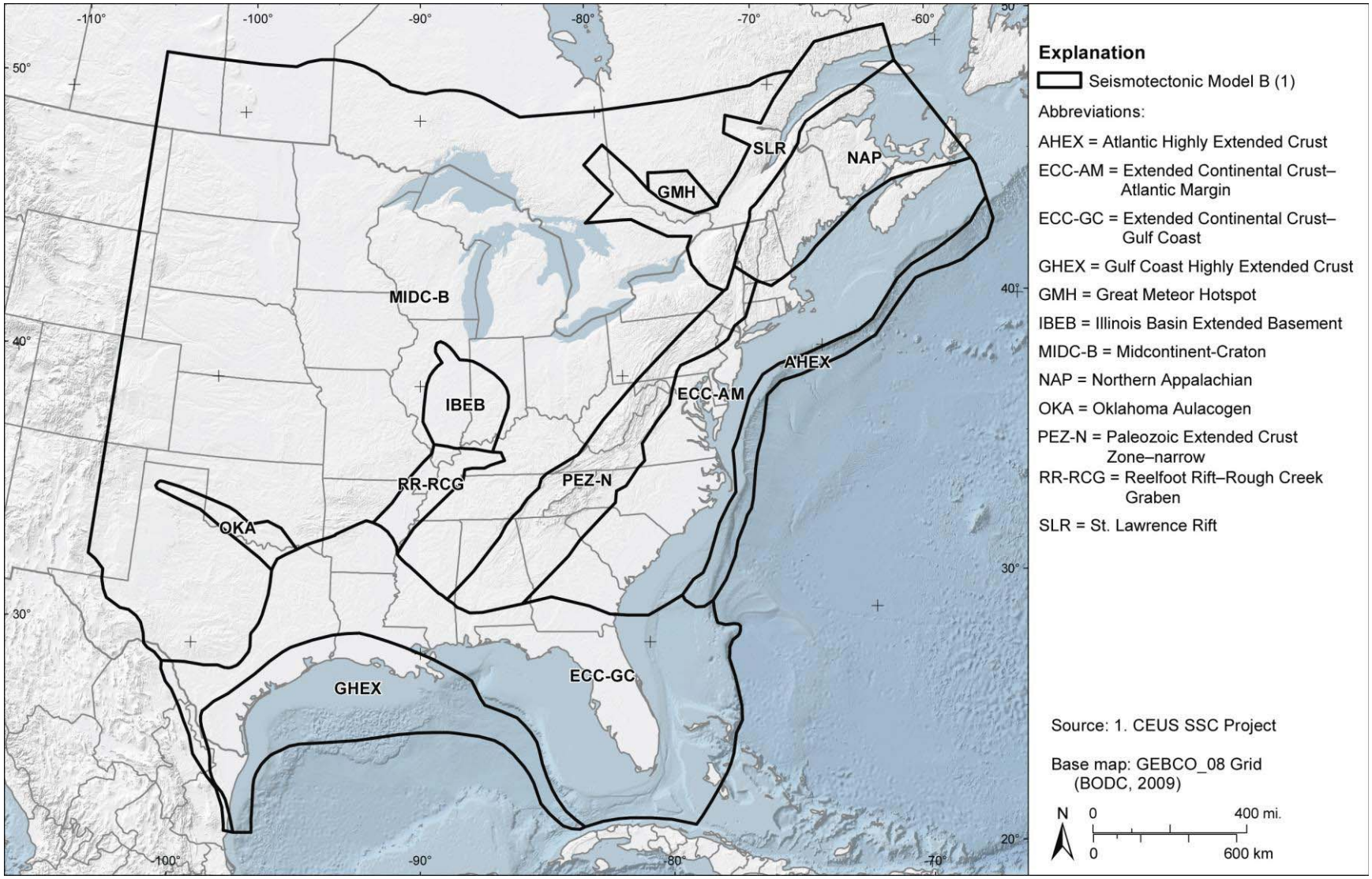

Figure 7.1-2
Seismotectonic zones shown in the case where the Rough Creek graben is part of the Reelfoot rift (RR_RCG) and the Paleozoic Extended Crust is narrow (PEZ-N)

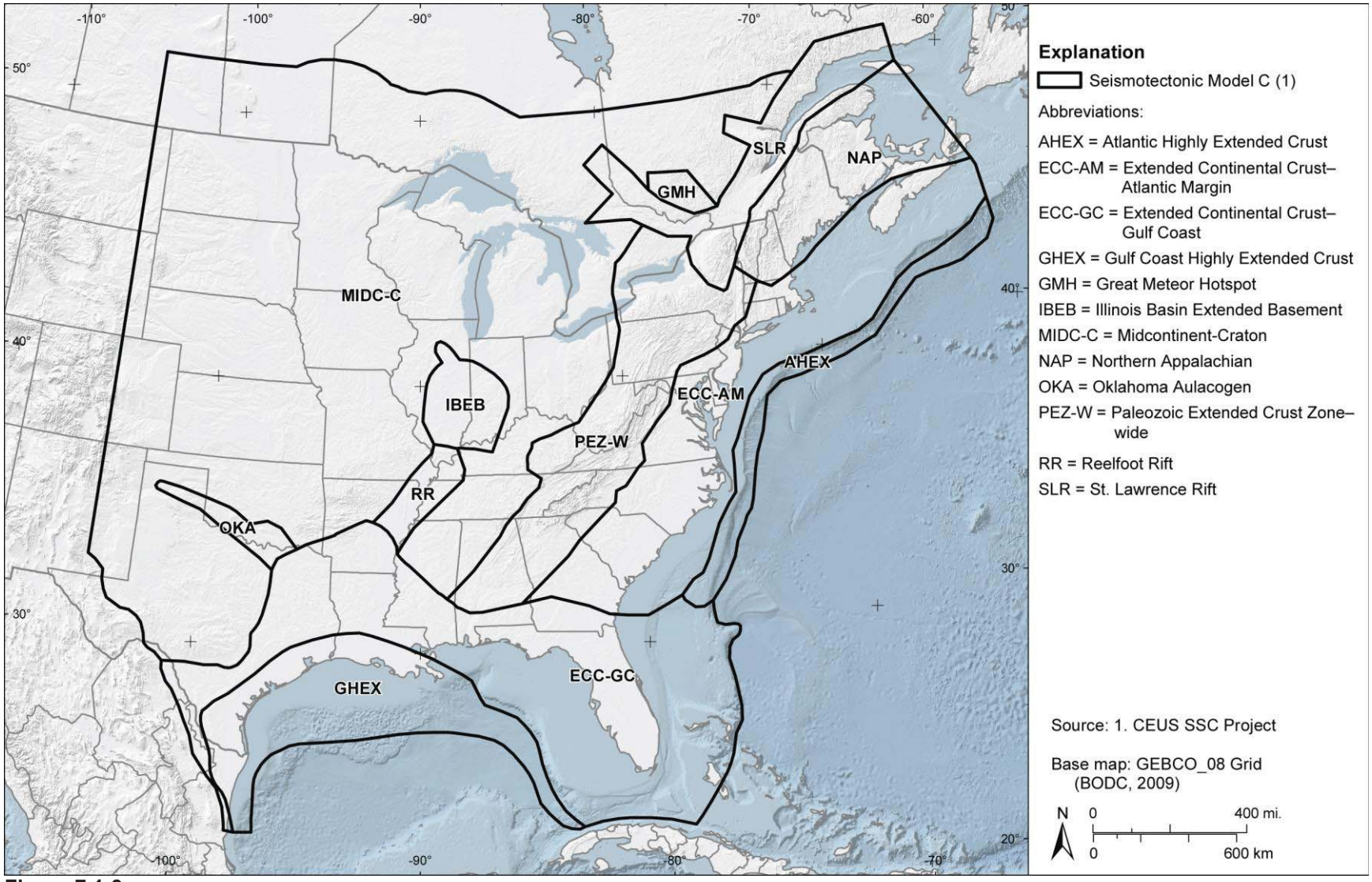

Figure 7.1-3
Seismotectonic zones shown in the case where the Rough Creek graben is not part of the Reelfoot rift (RR) and the Paleozoic Extended Crust is wide (PEZ-W)

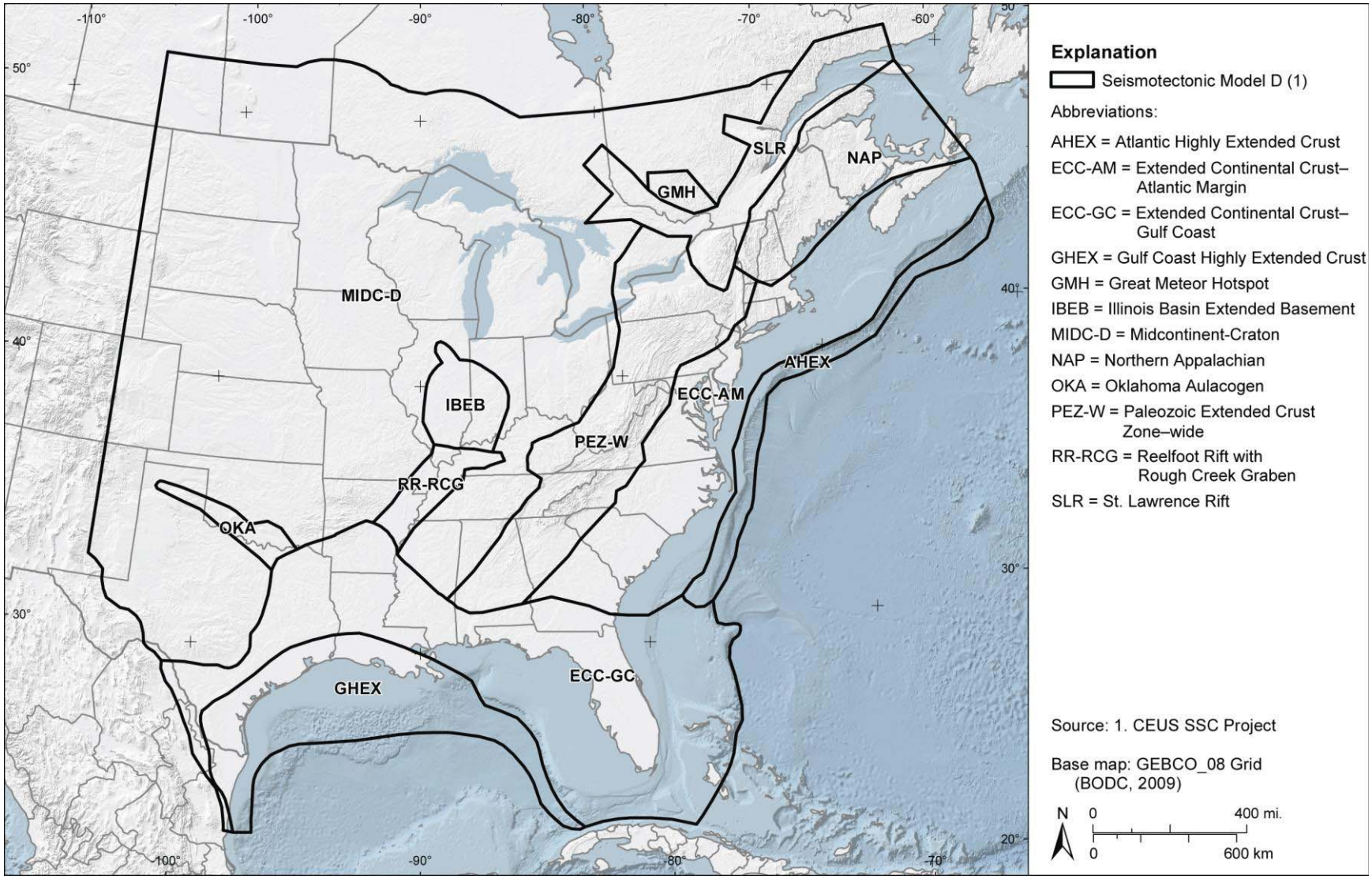

Figure 7.1-4
Seismotectonic zones shown in the case where the Rough Creek graben is part of the Reelfoot rift (RR_RCG) and the Paleozoic Extended Crust is wide (PEZ-W)

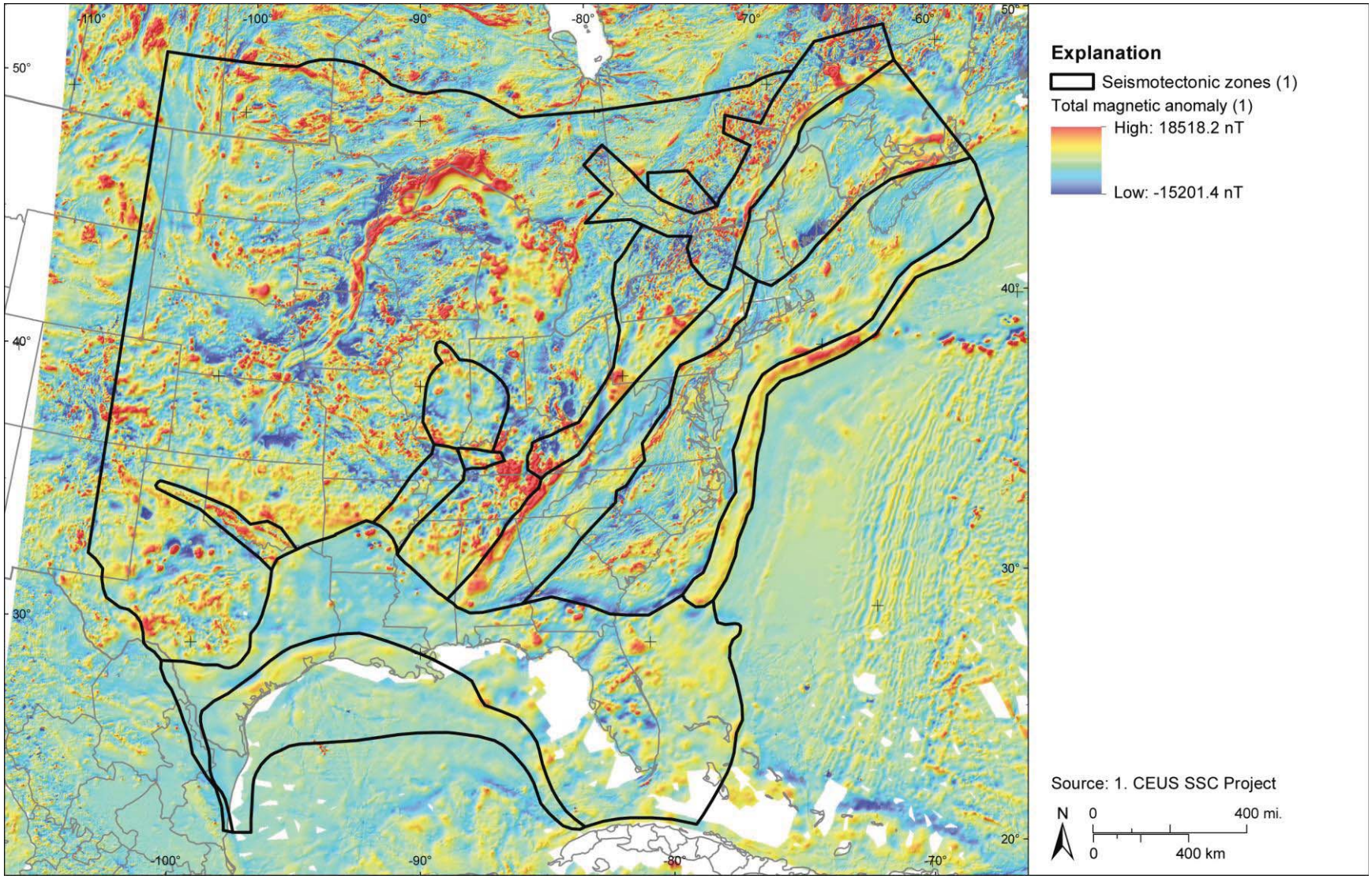

Figure 7.1-5
Example of comparing seismotectonic zones with magnetic map developed as part of the CEUS SSC Project

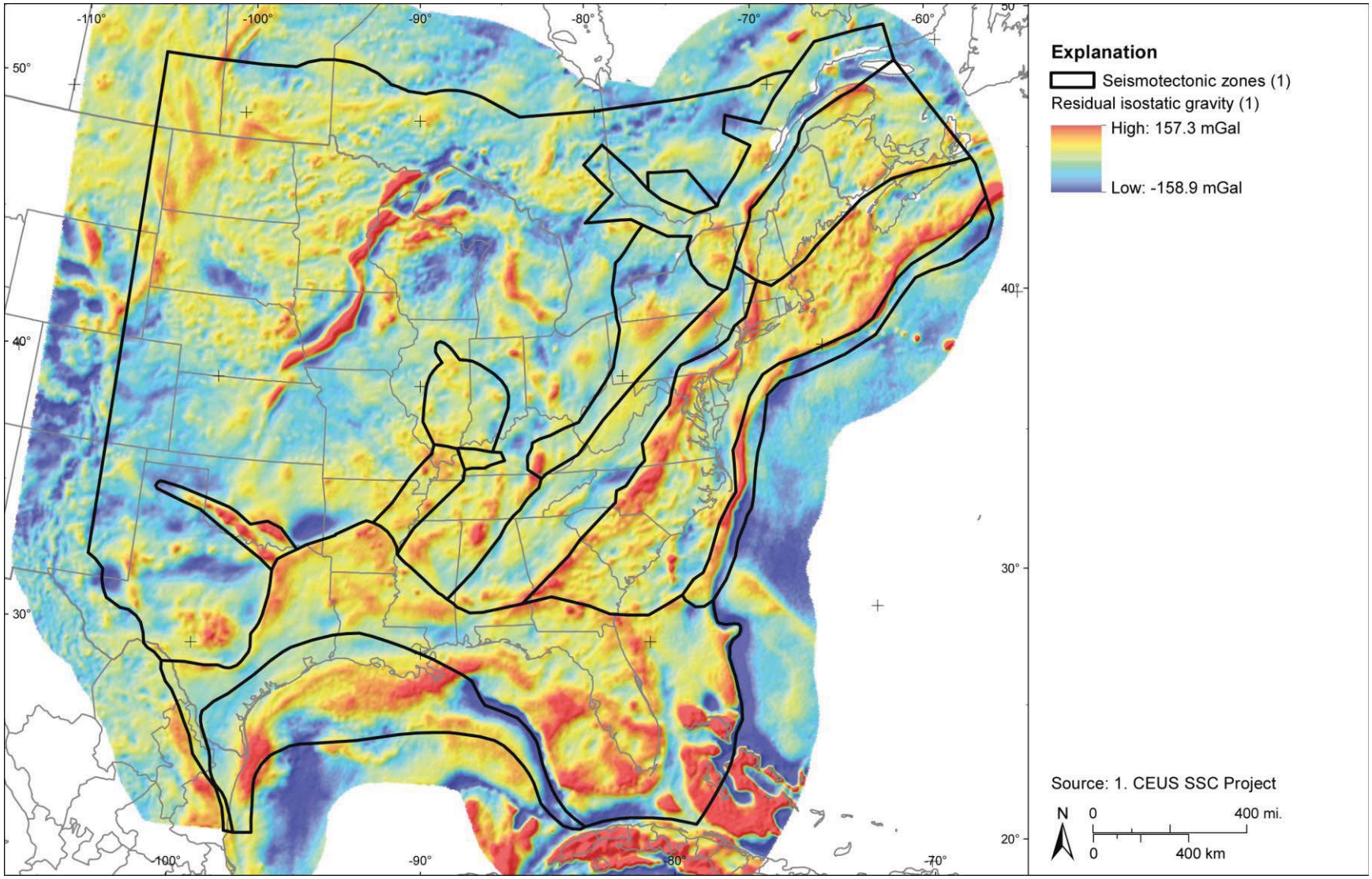

Figure 7.1-6
Example of comparing seismotectonic zones with isostatic gravity map developed as part of the CEUS SSC Project

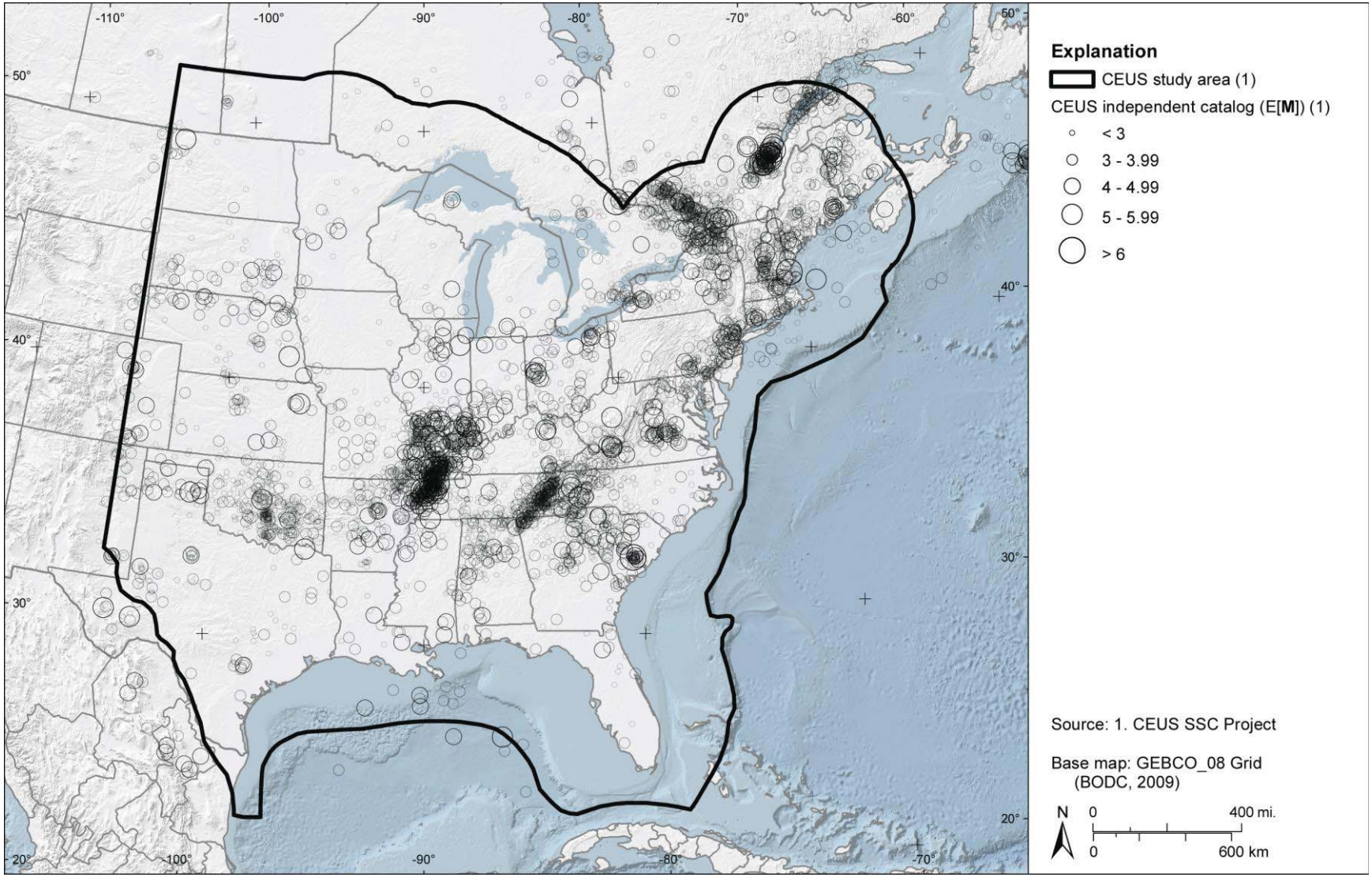

Figure 7.1-7
Map of seismicity based on the earthquake catalog developed for the CEUS SSC Project

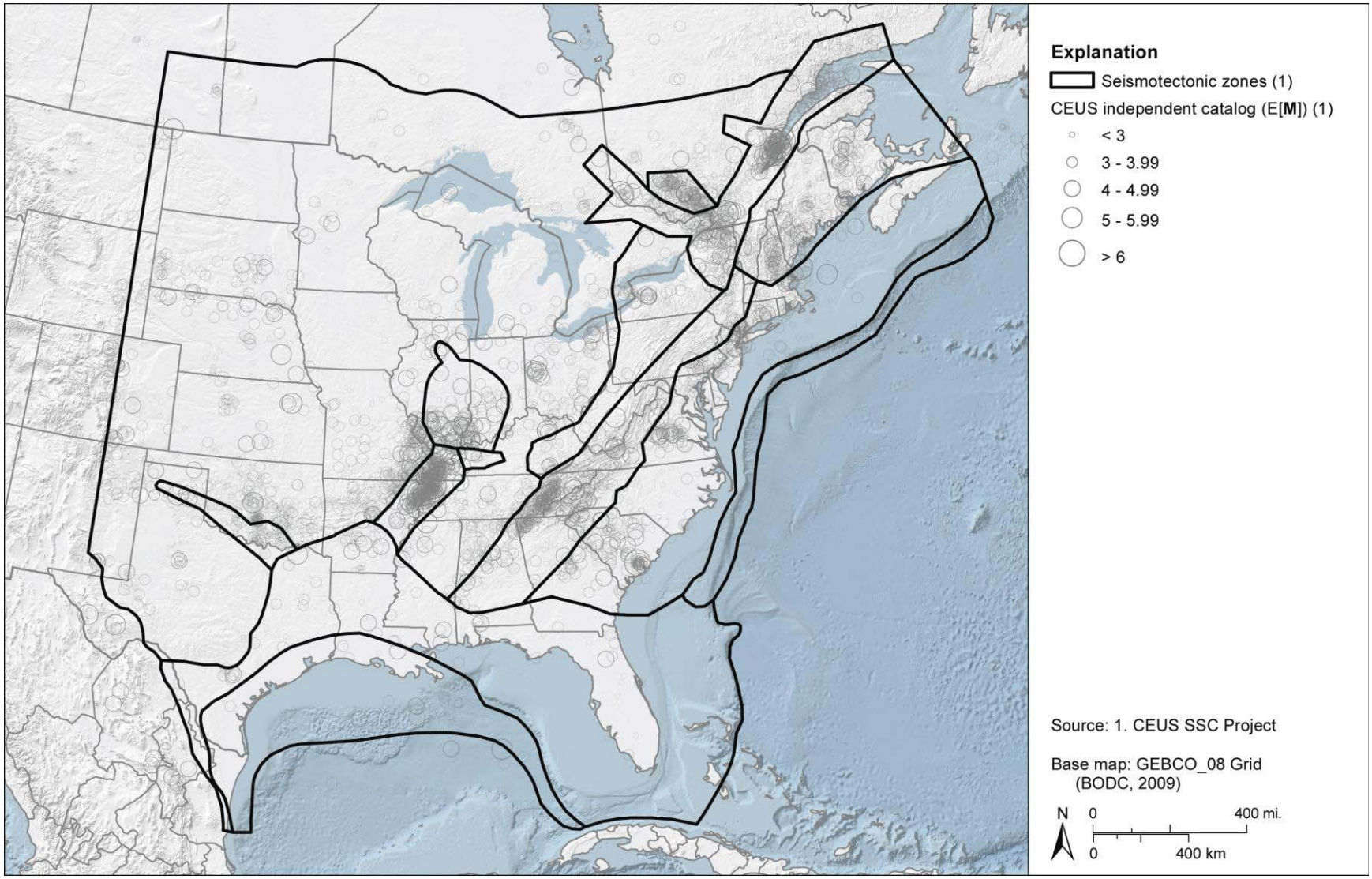

Figure 7.1-8
Map showing example comparison of seismotectonic zones with seismicity. Note the non-uniform spatial distribution of seismicity within the zones. Spatial smoothing of *a*- and *b*-values accounts for these spatial variations.

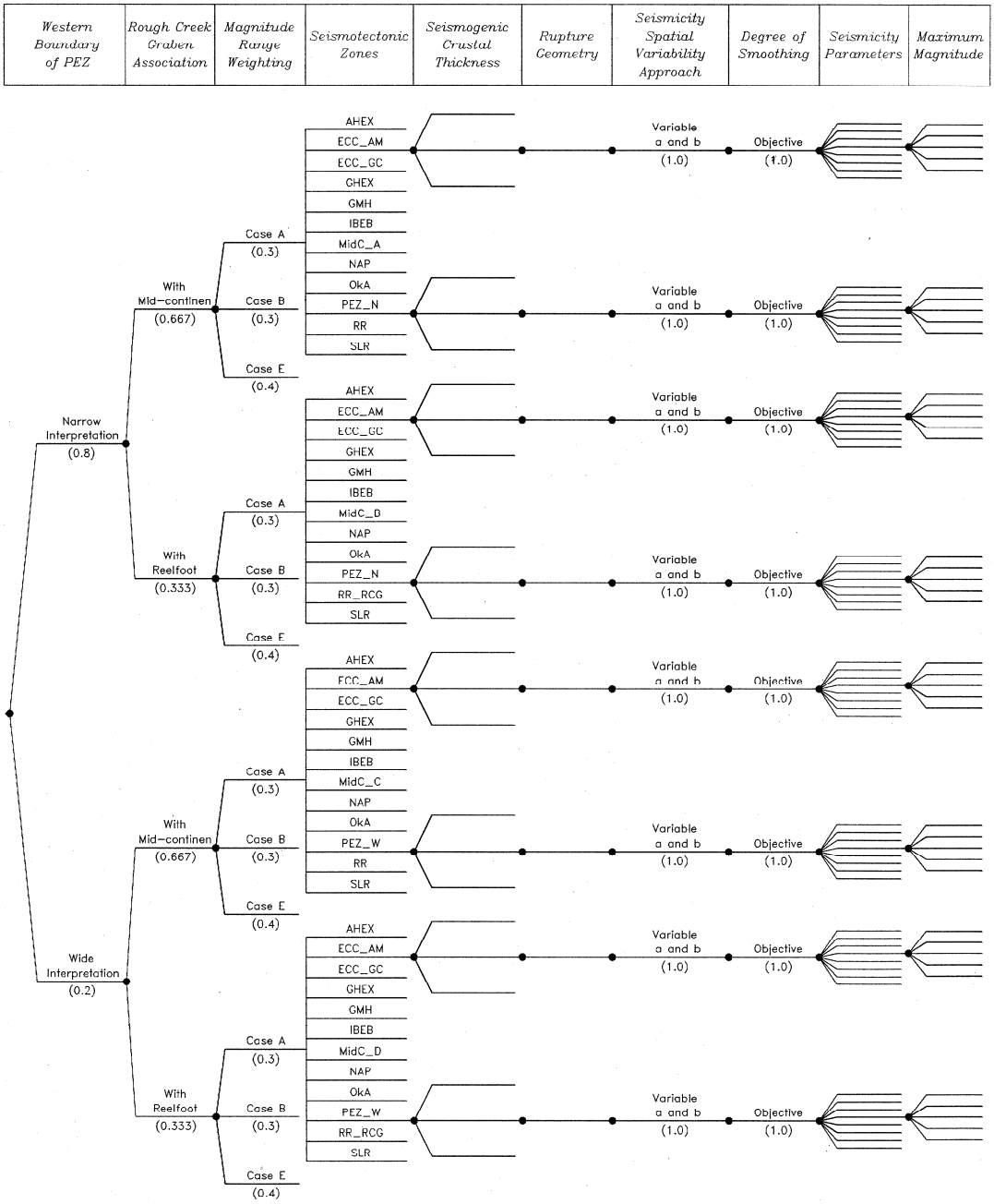

Figure 7.3-1
Logic tree for the seismotectonic zones branch of the master logic tree

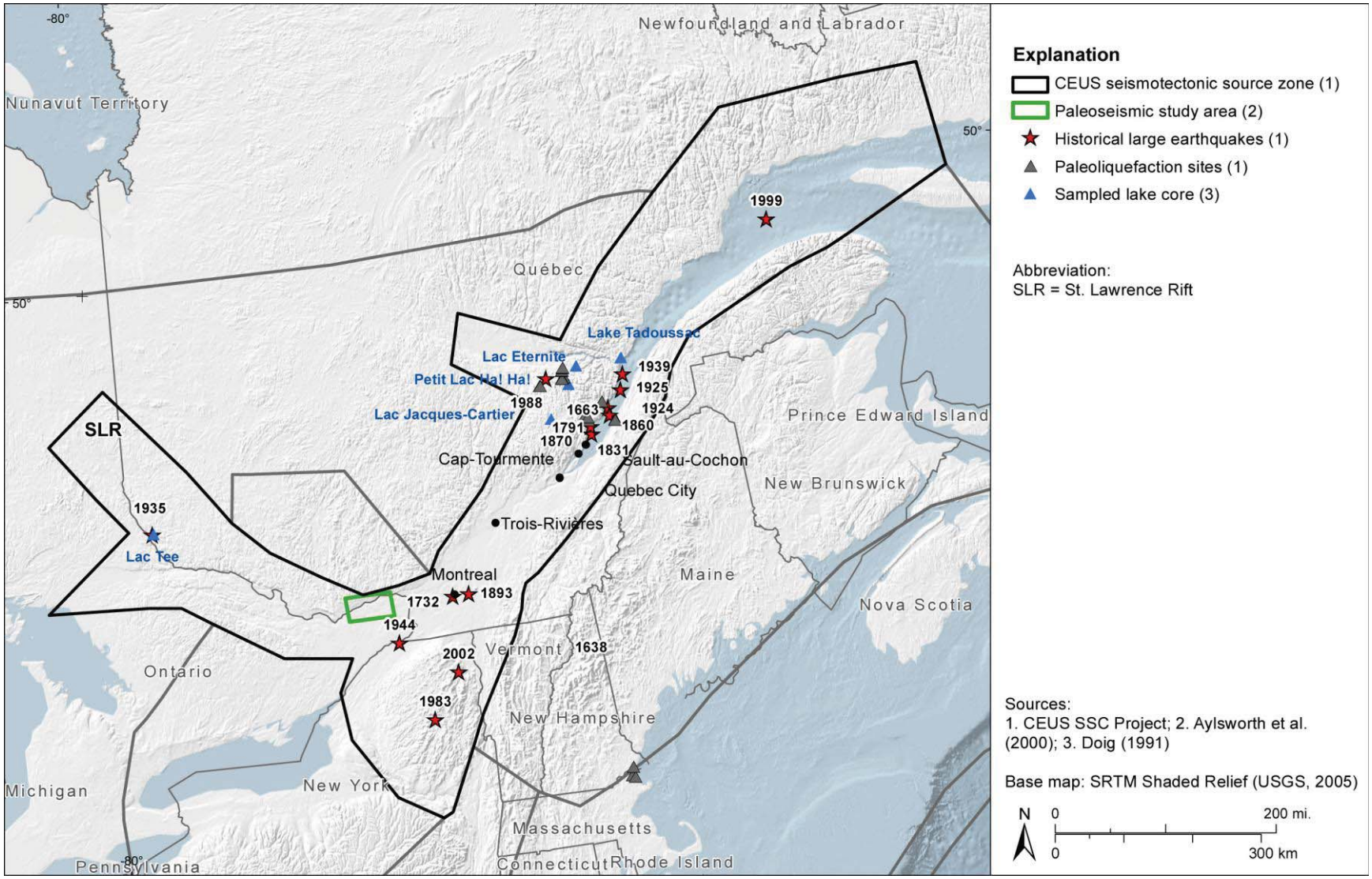

Figure 7.3.1-1
Significant earthquakes and paleoseismology of the SLR seismotectonic zone

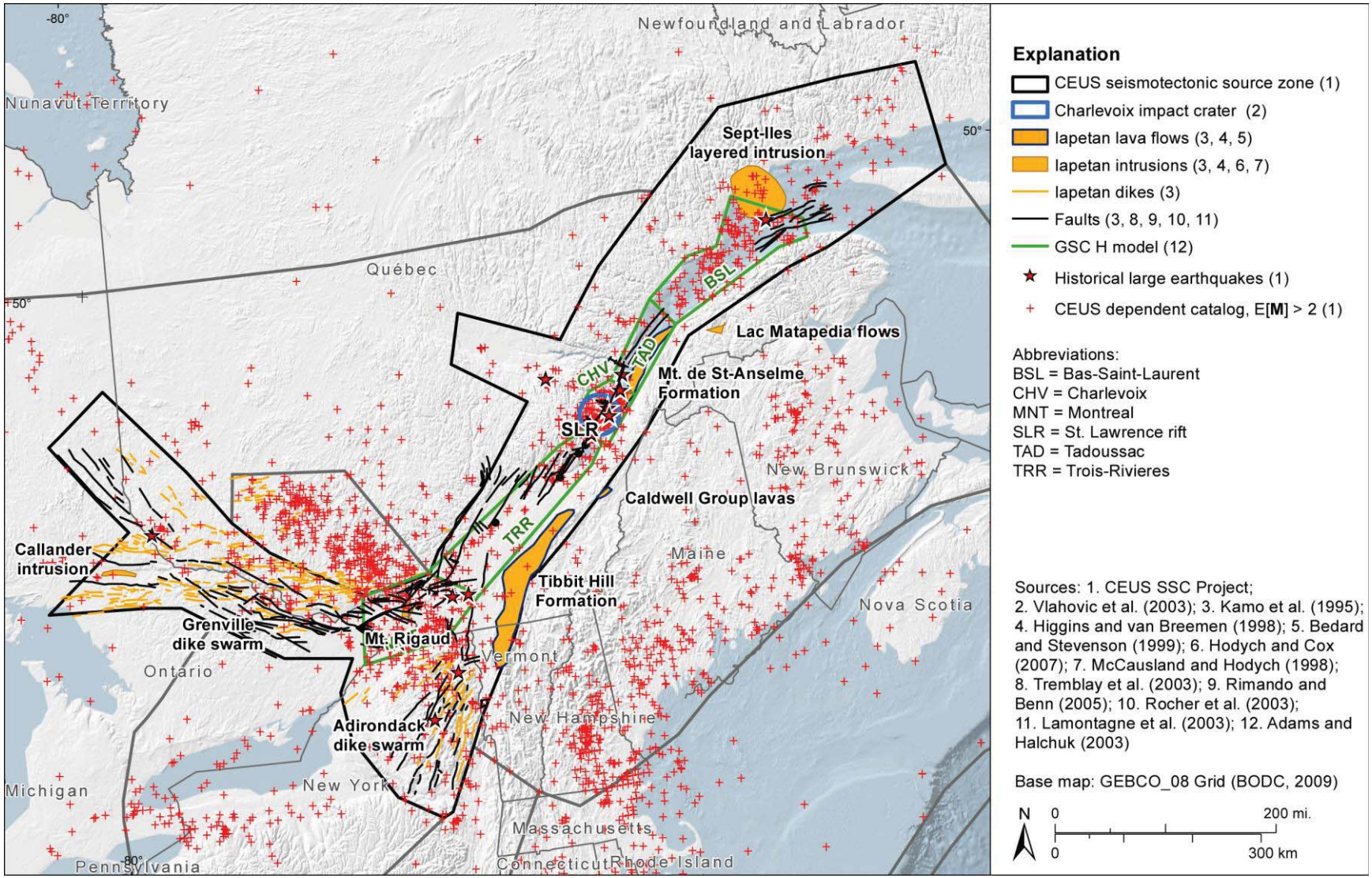

Figure 7.3.1-2
Tectonic features of the SLR seismotectonic zone

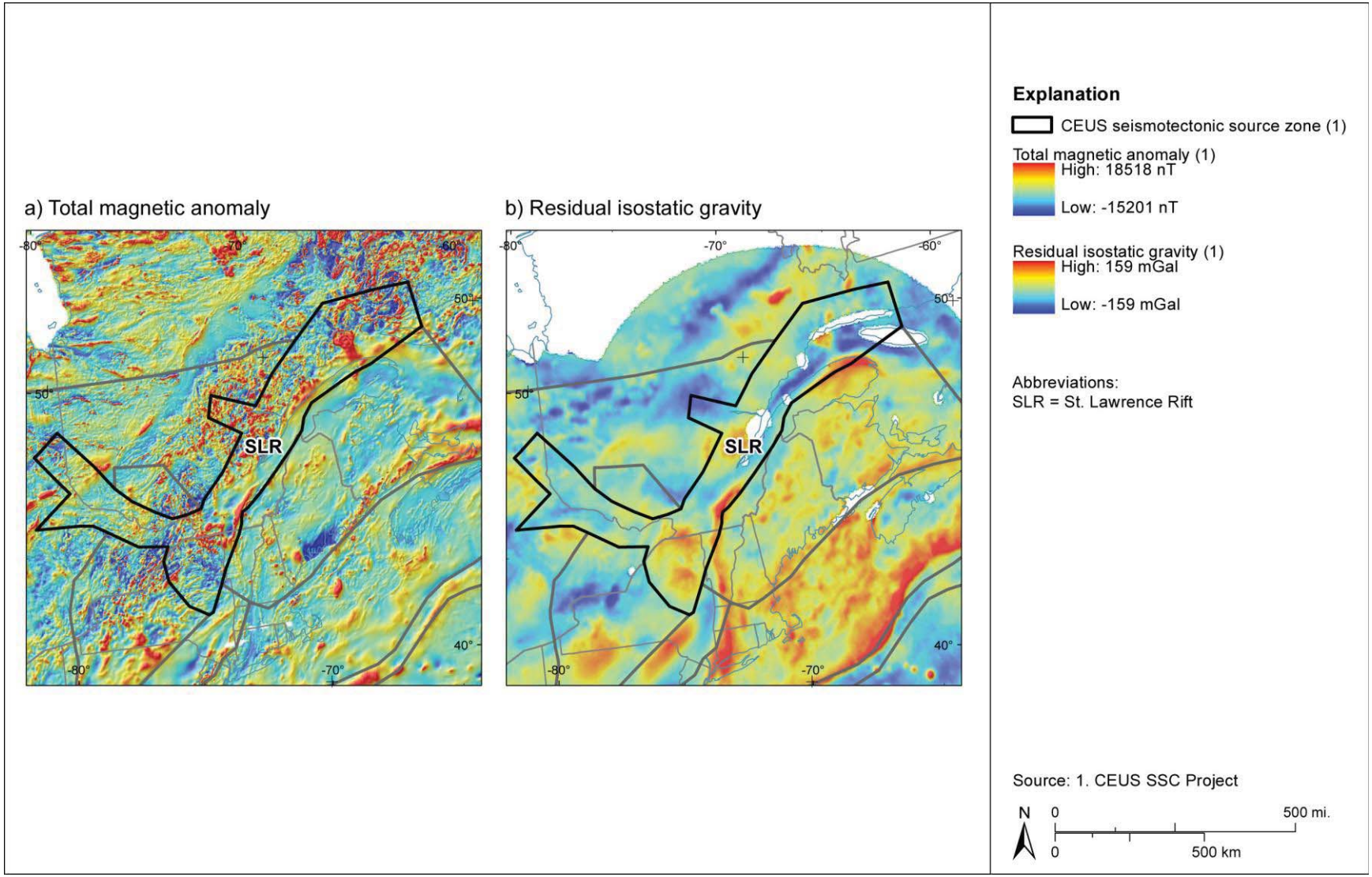

Figure 7.3.1-3
Magnetic and gravity anomaly maps of the SLR seismotectonic zone

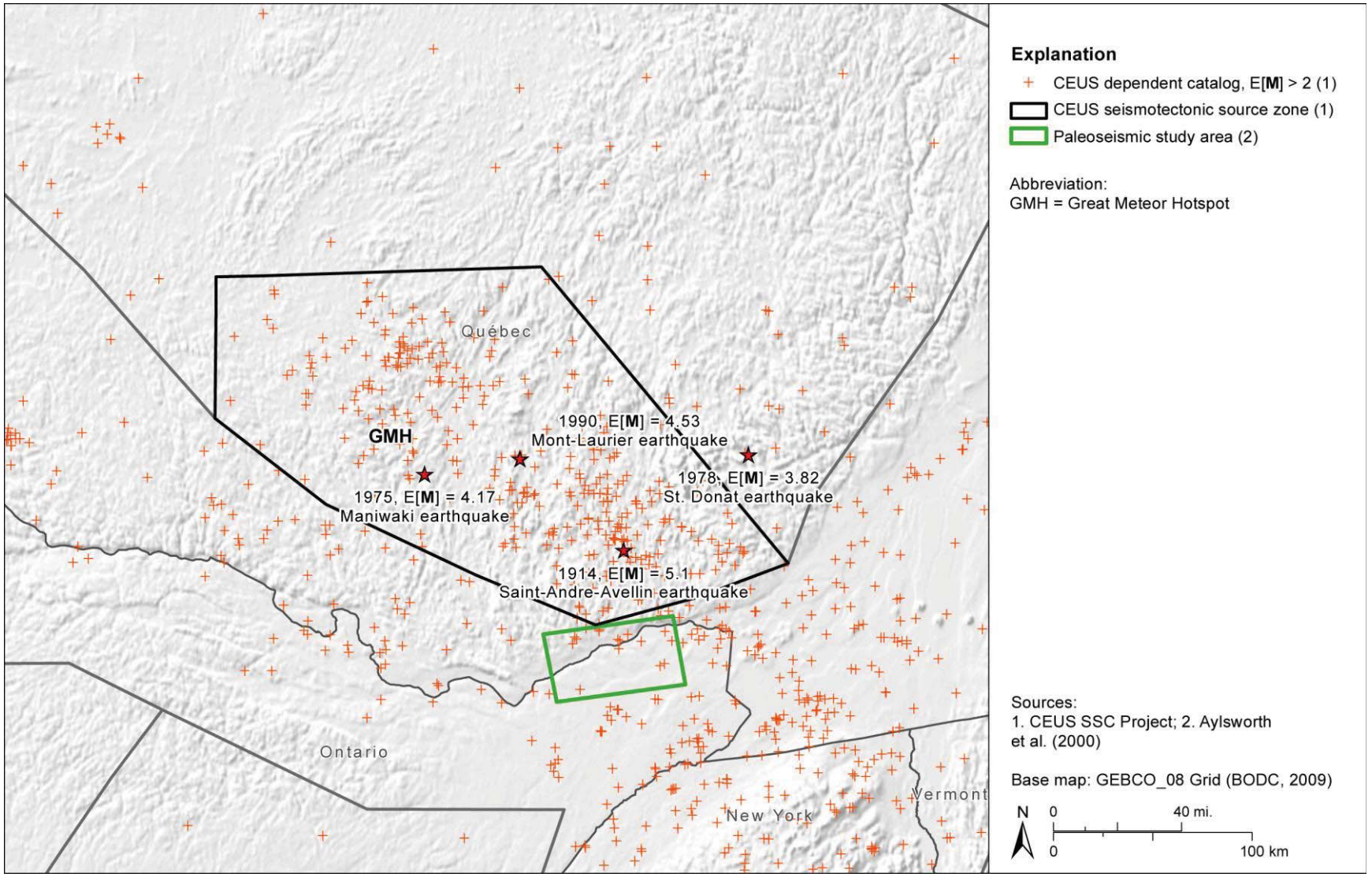

Figure 7.3.2-1
Significant earthquakes and paleoseismic study area in the region of the GMH seismotectonic zone

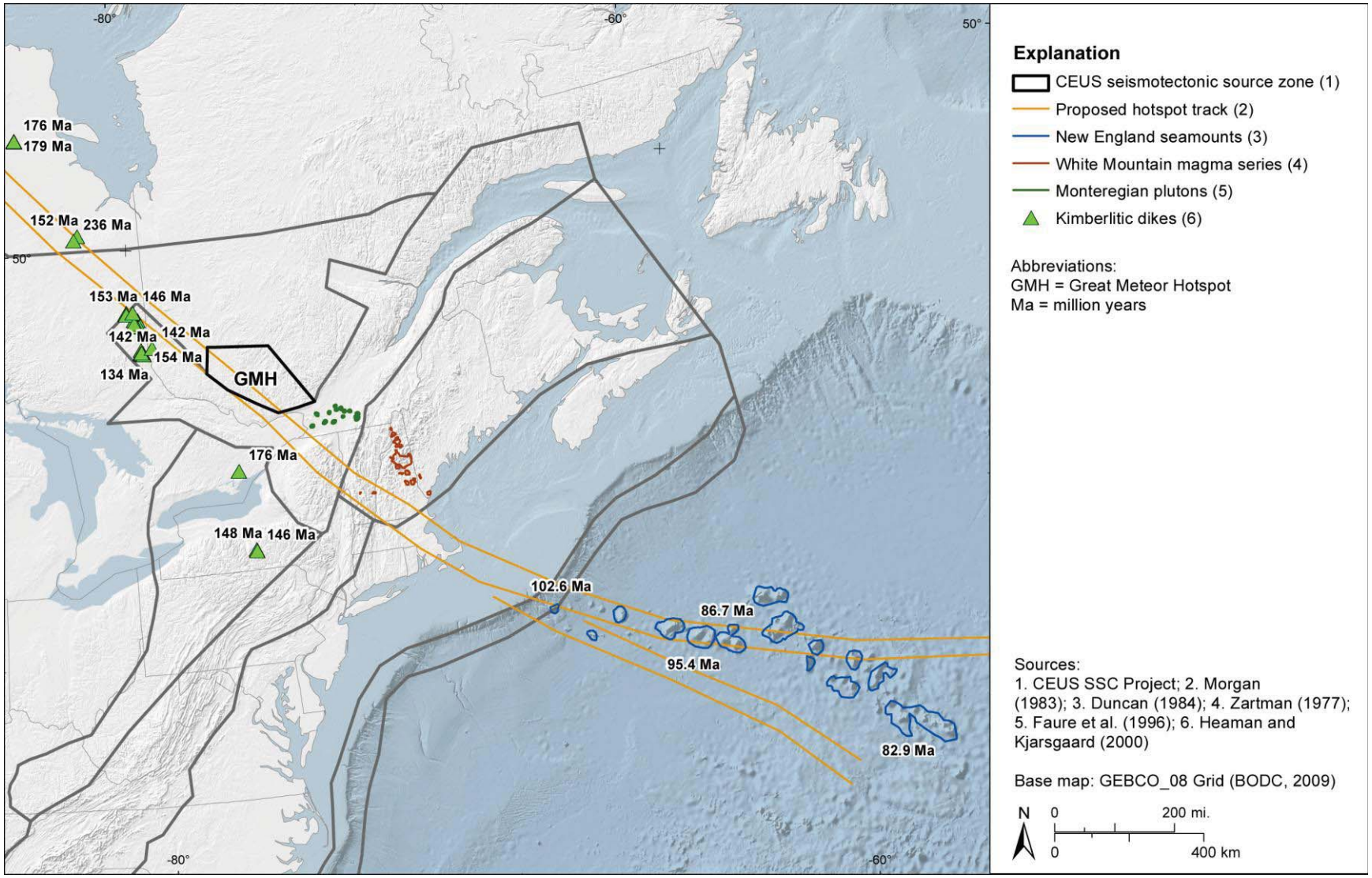

Figure 7.3.2-2
Igneous rocks attributed to the GMH seismotectonic zone

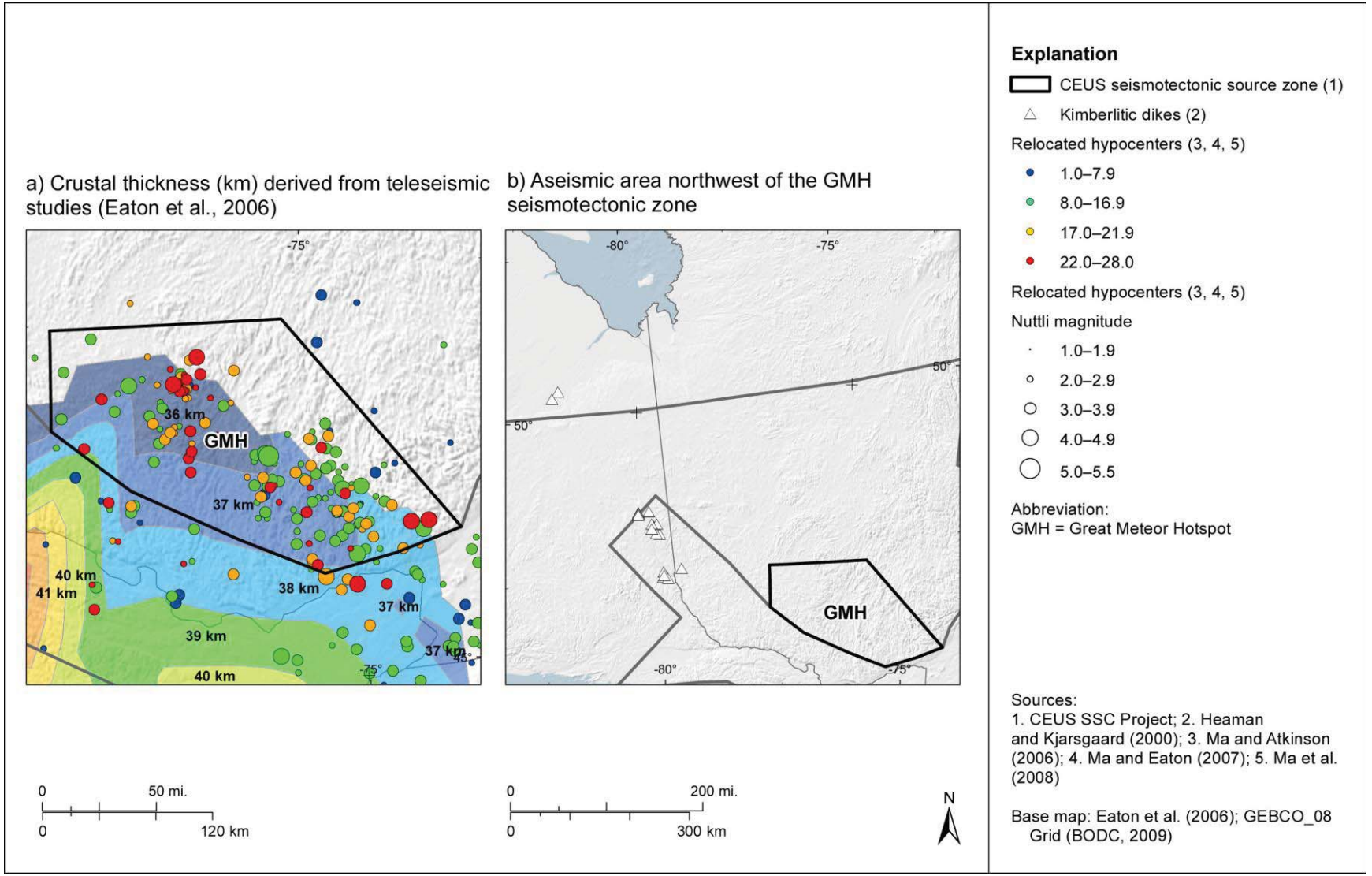

Figure 7.3.2-3
Relocated hypocentral depths and crustal depth of the GMH seismotectonic zone

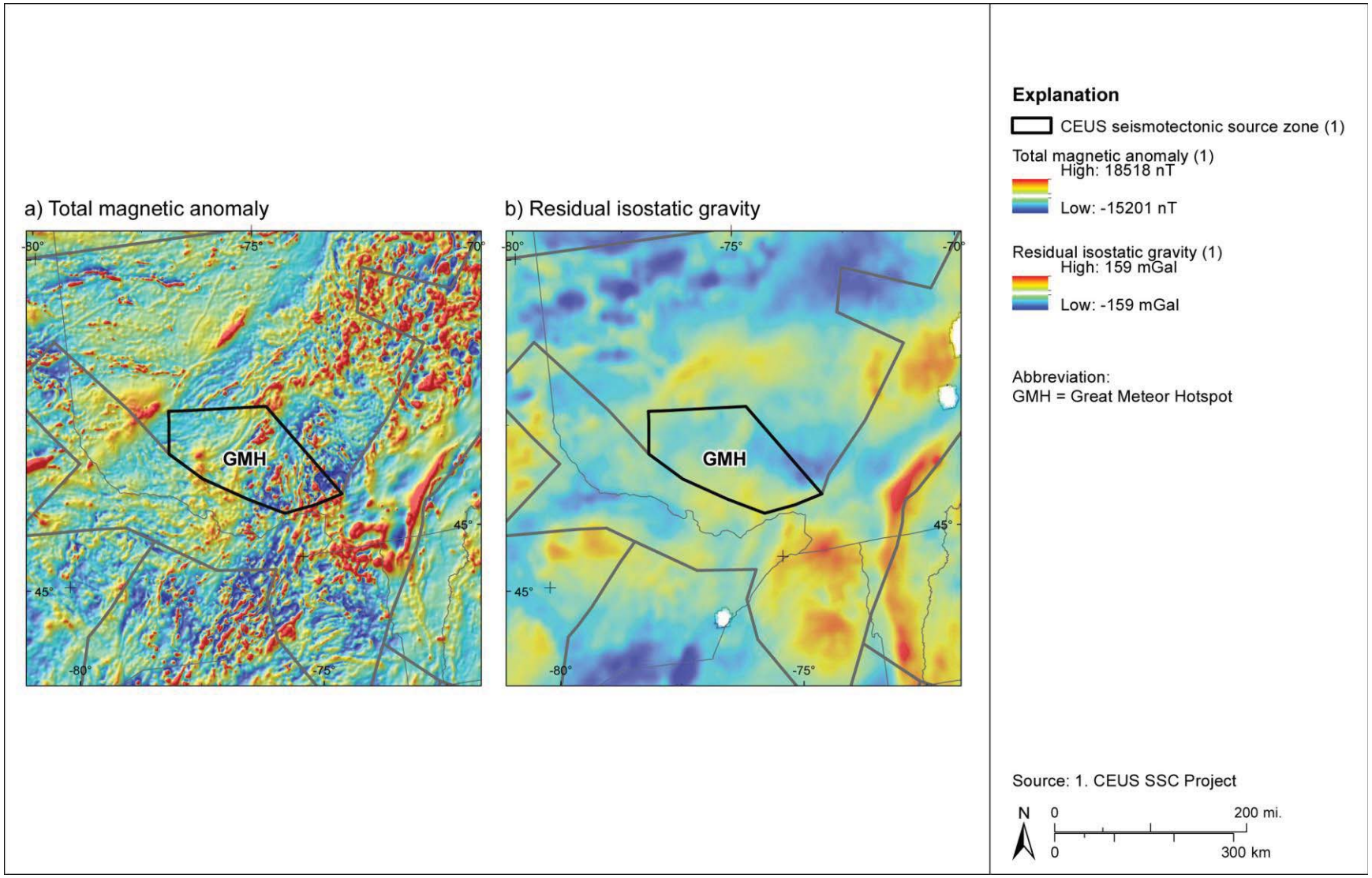

Figure 7.3.2-4
Magnetic and gravity anomaly maps of the GMH seismotectonic zone

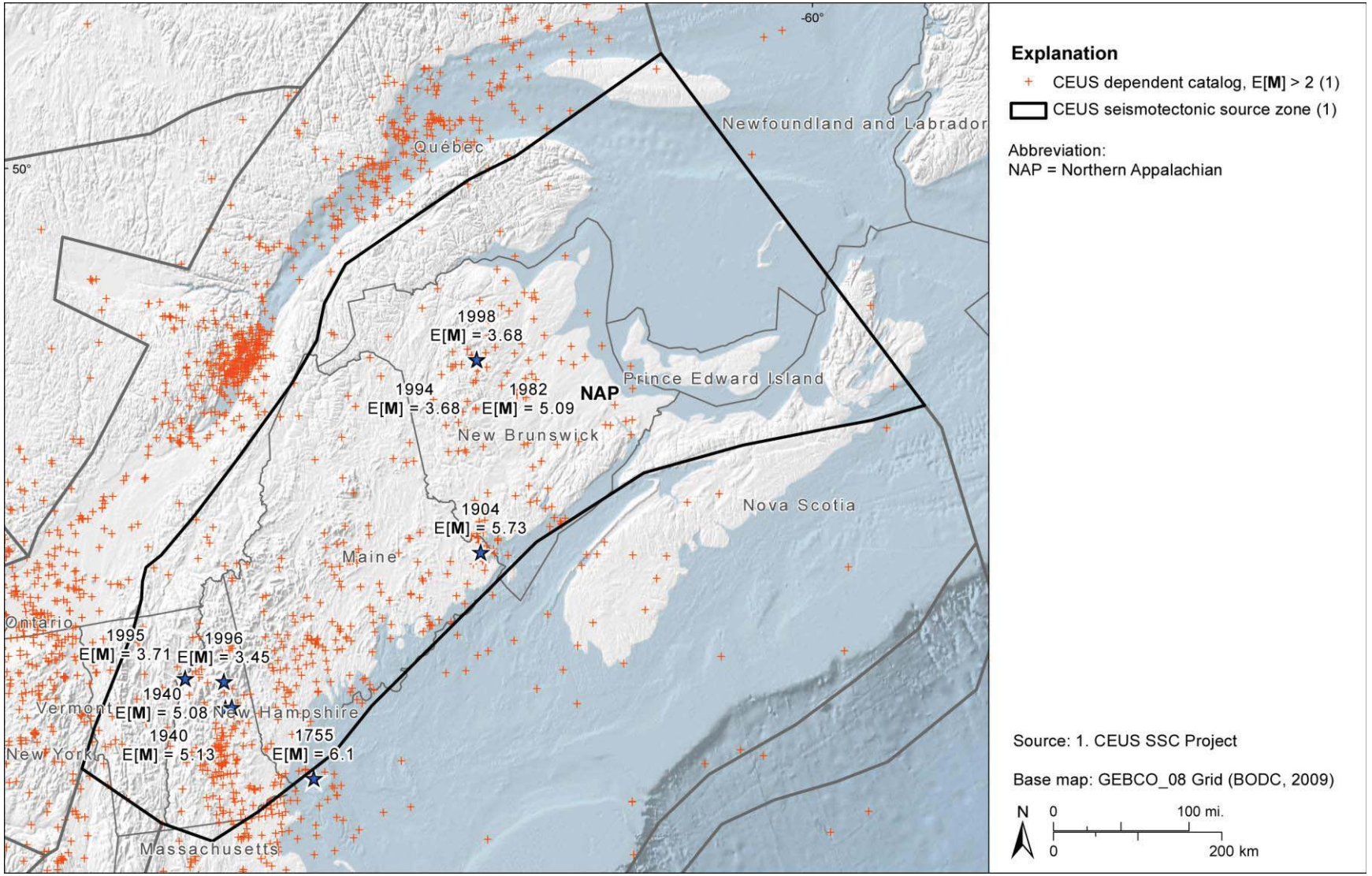

Figure 7.3.3-1
Seismicity of the NAP seismotectonic zone

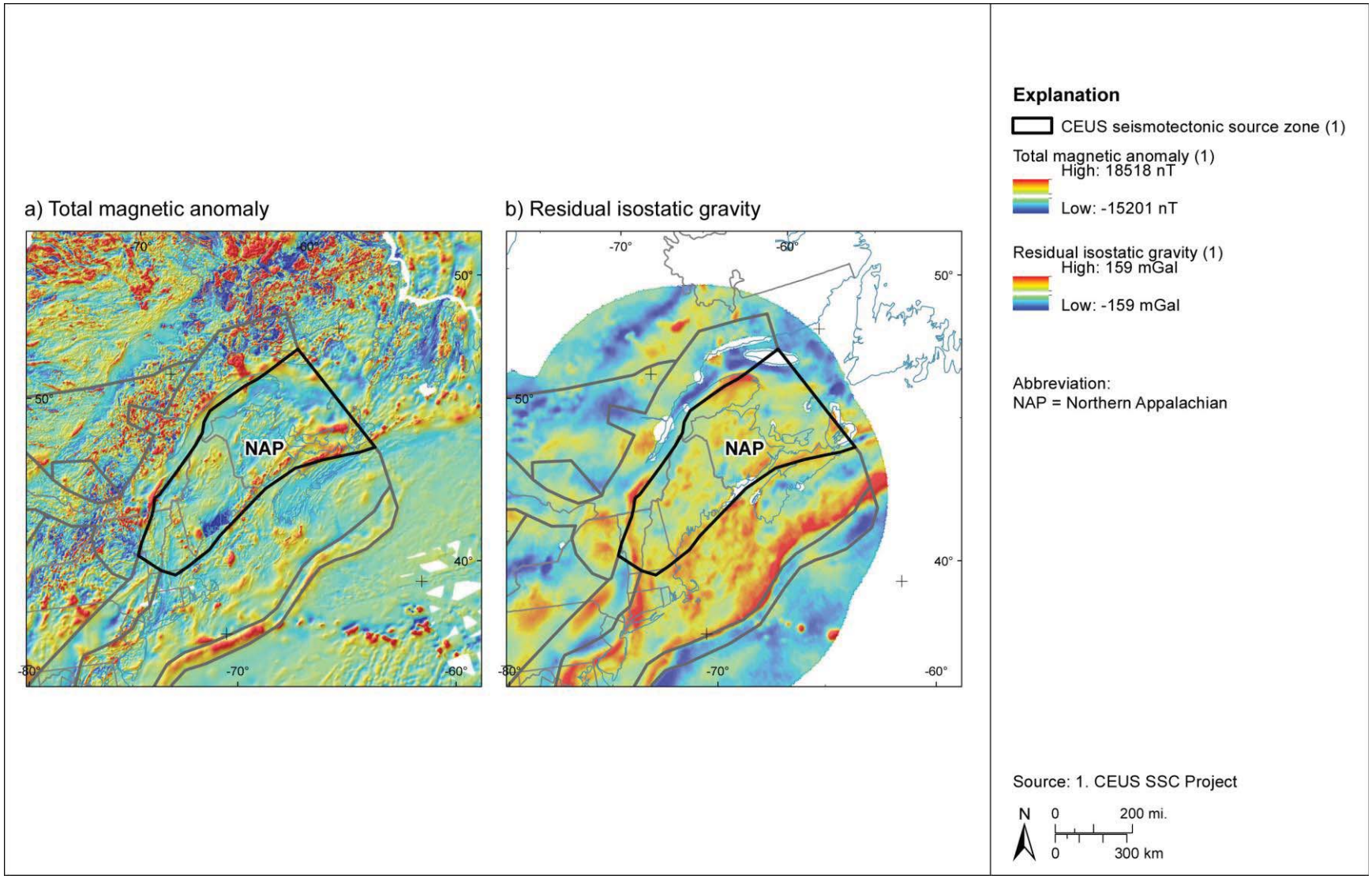

Figure 7.3.3-2
Magnetic and gravity anomaly maps of the NAP seismotectonic zone

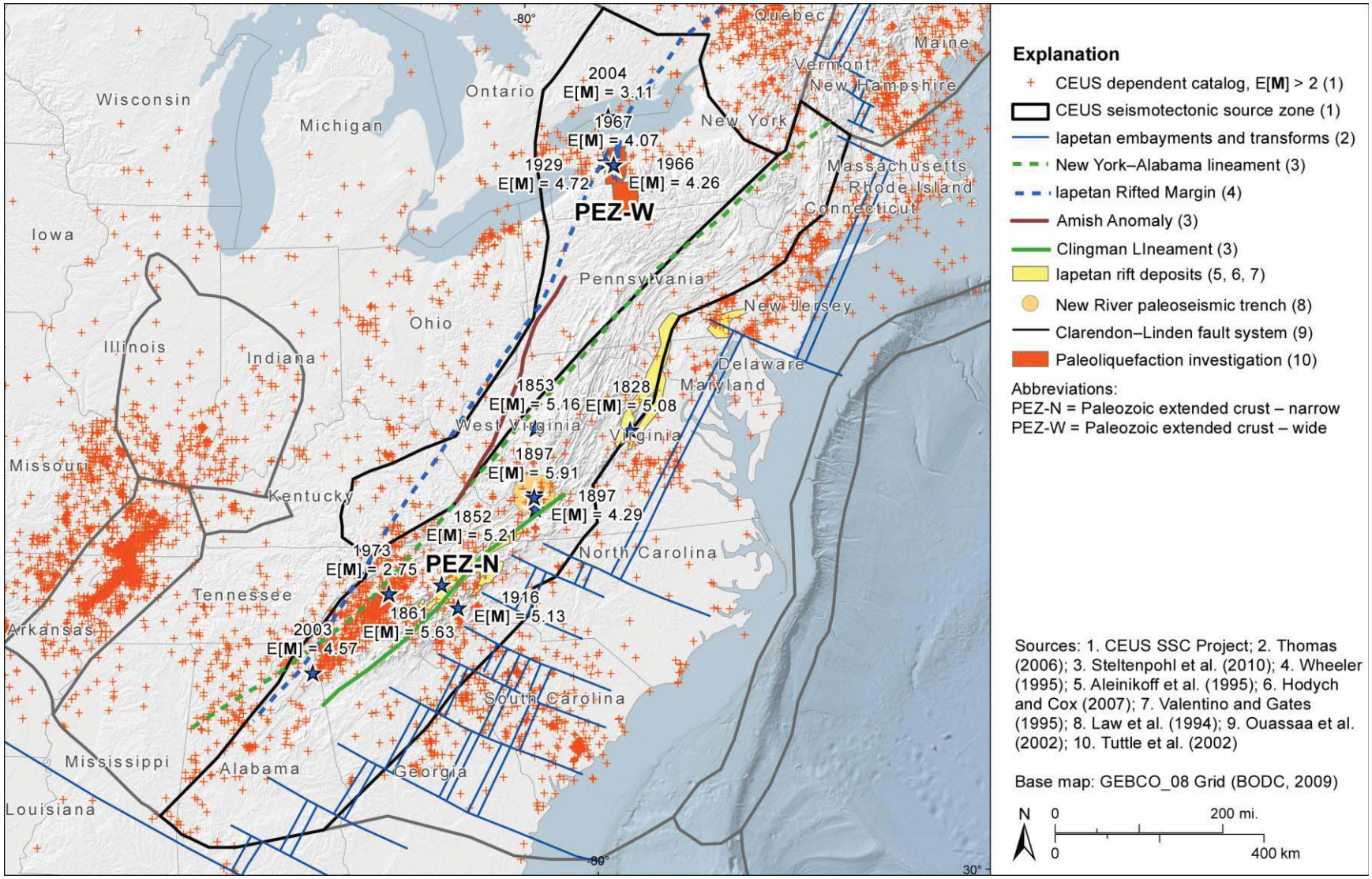

Figure 7.3.4-1
Seismicity and tectonic features of the PEZ seismotectonic zone

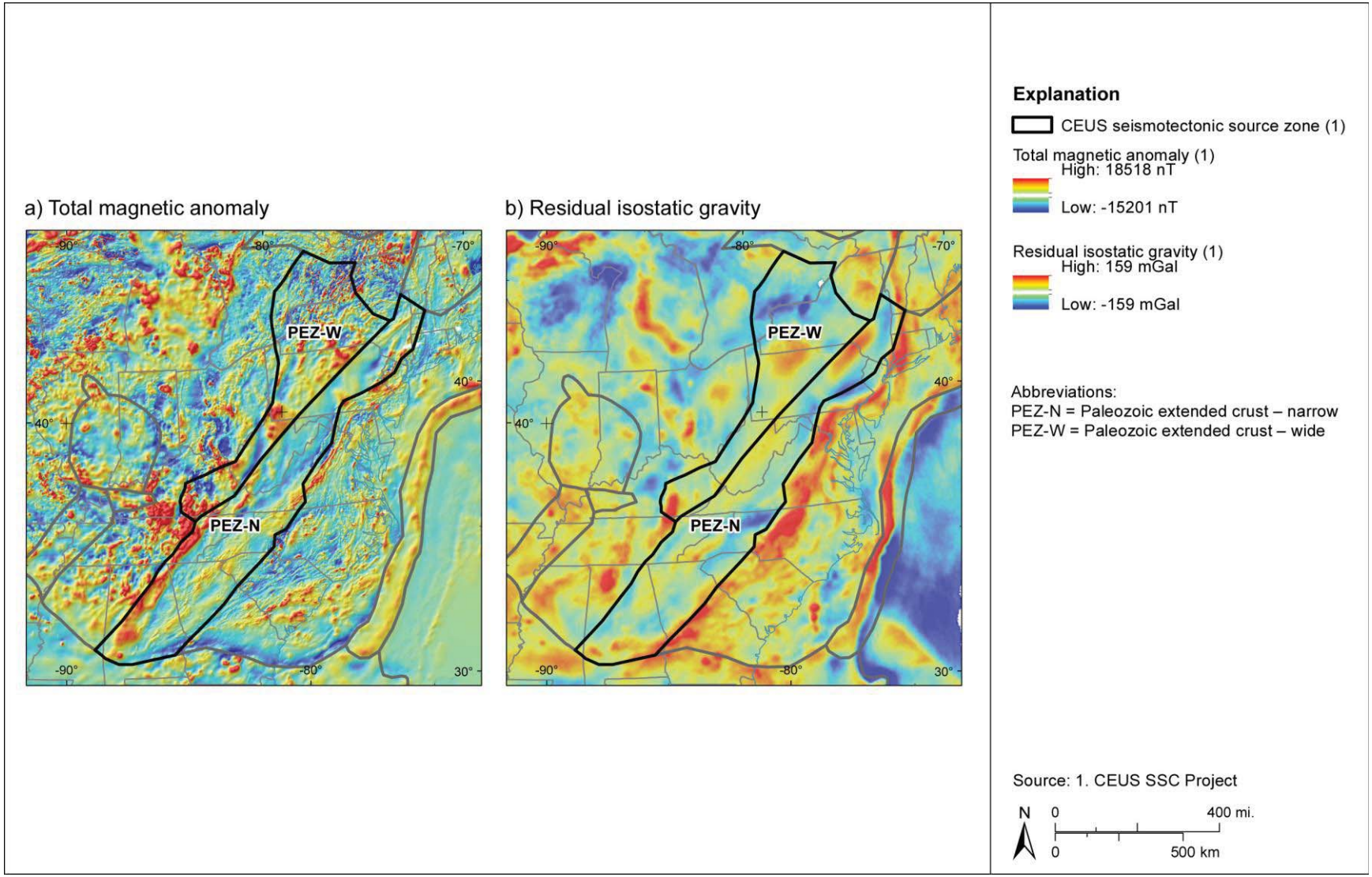

Figure 7.3.4-2
Magnetic and gravity anomaly maps of the PEZ seismotectonic zone

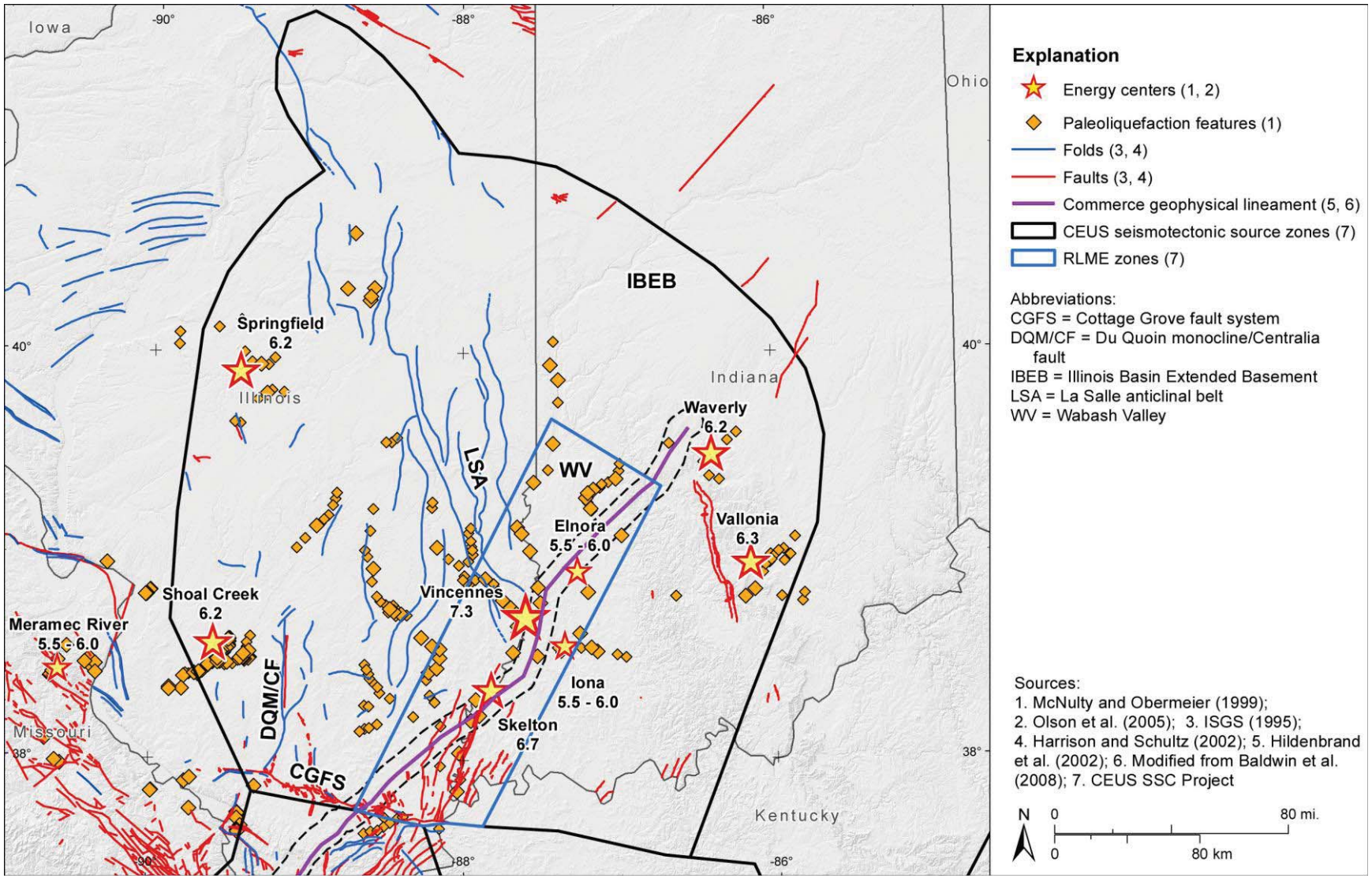

Figure 7.3.5-1
Map showing seismicity, subsurface Paleozoic and basement structures, and postulated energy centers for prehistoric earthquakes

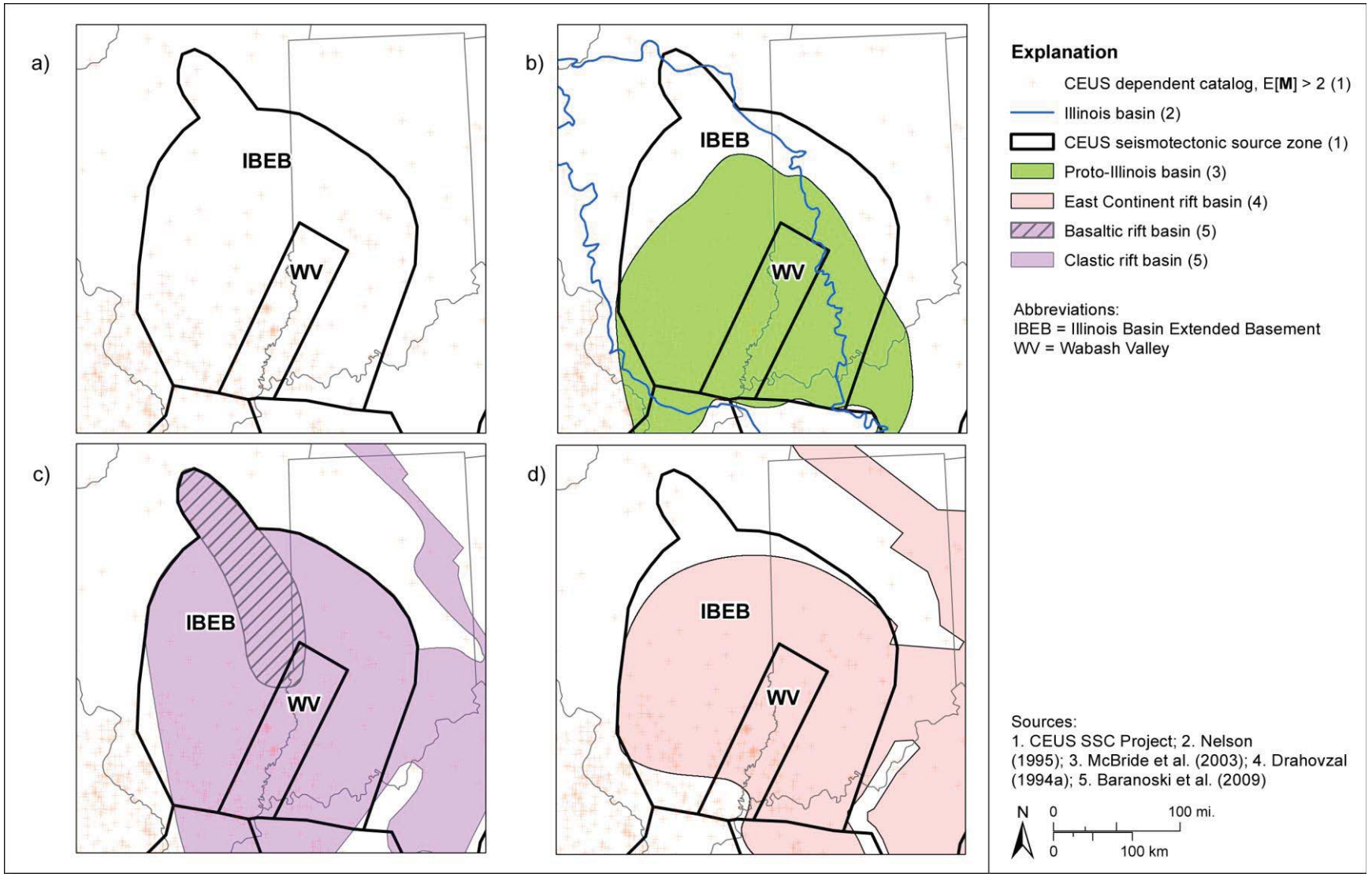

Figure 7.3.5-2
Map showing alternative boundaries for Precambrian (proto-Illinois basin) rift basins

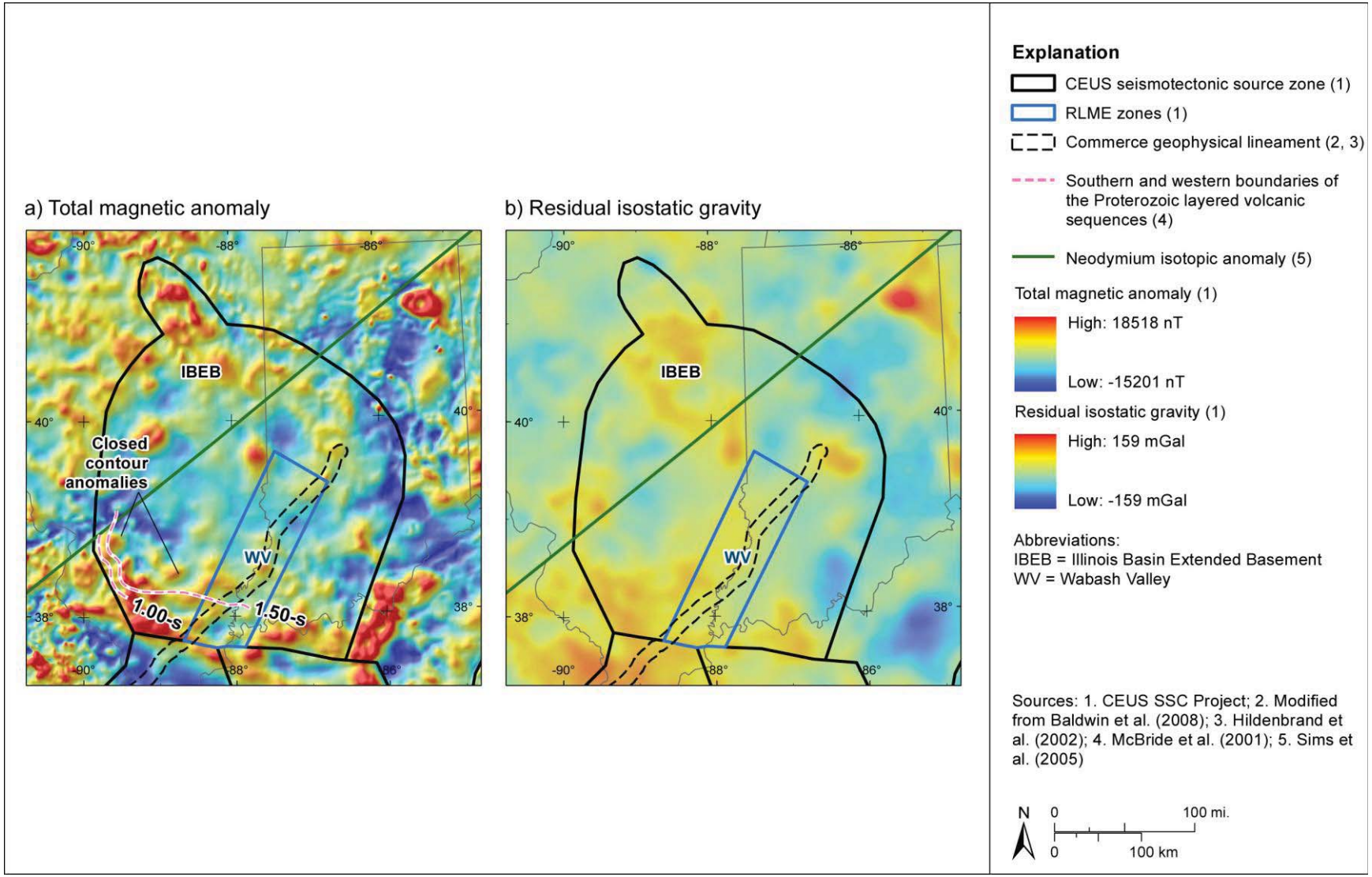

Figure 7.3.5-3
Maps showing the IBEB source zone boundaries, seismicity, and prehistoric earthquake centers relative to (a) regional magnetic anomalies and (b) regional gravity anomalies

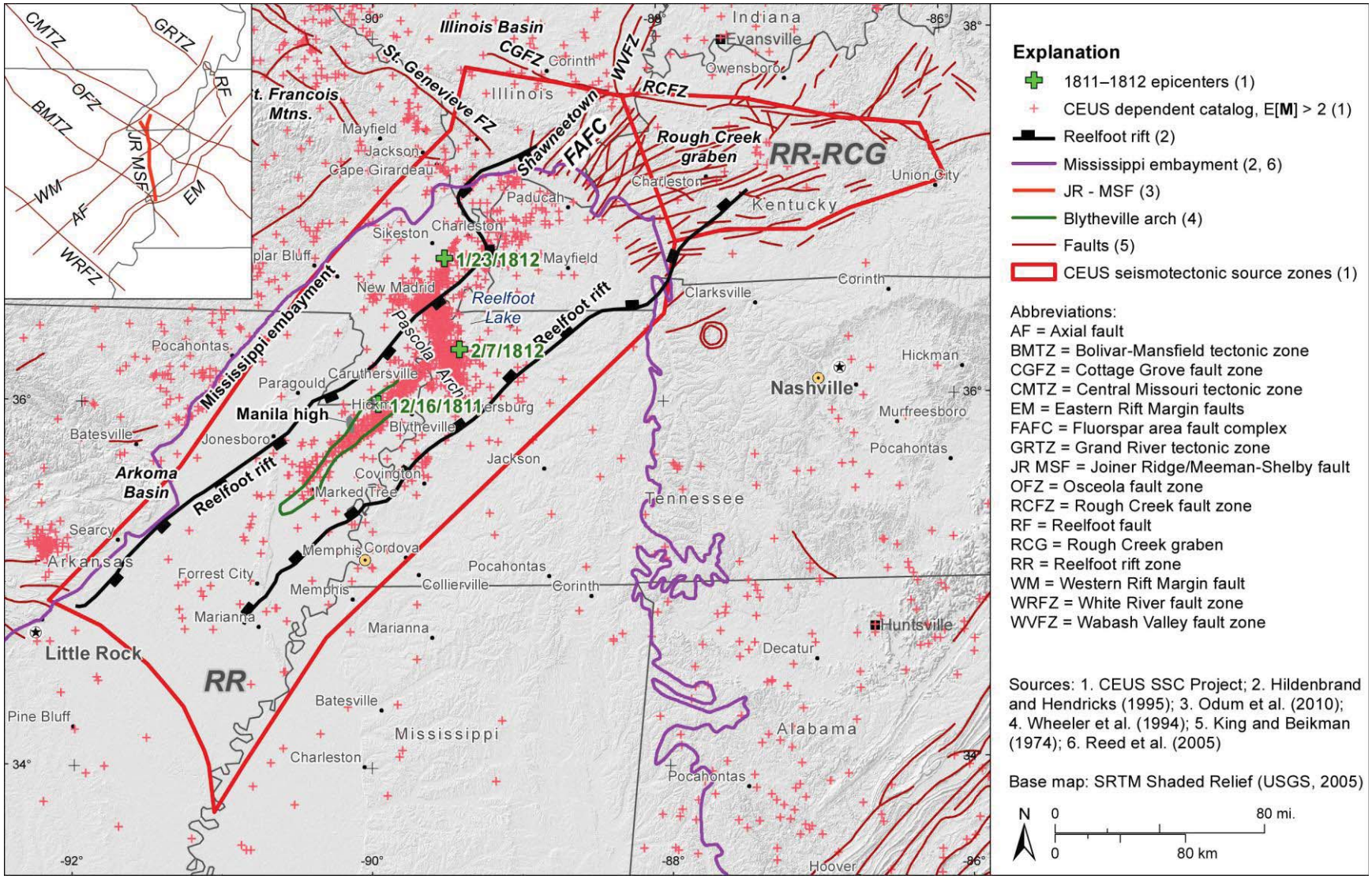

Figure 7.3.6-1
Map of seismicity and geomorphic features and faults showing evidence for Quaternary neotectonic deformation and reactivation. Inset map shows basement structures associated with the Reelfoot rift.

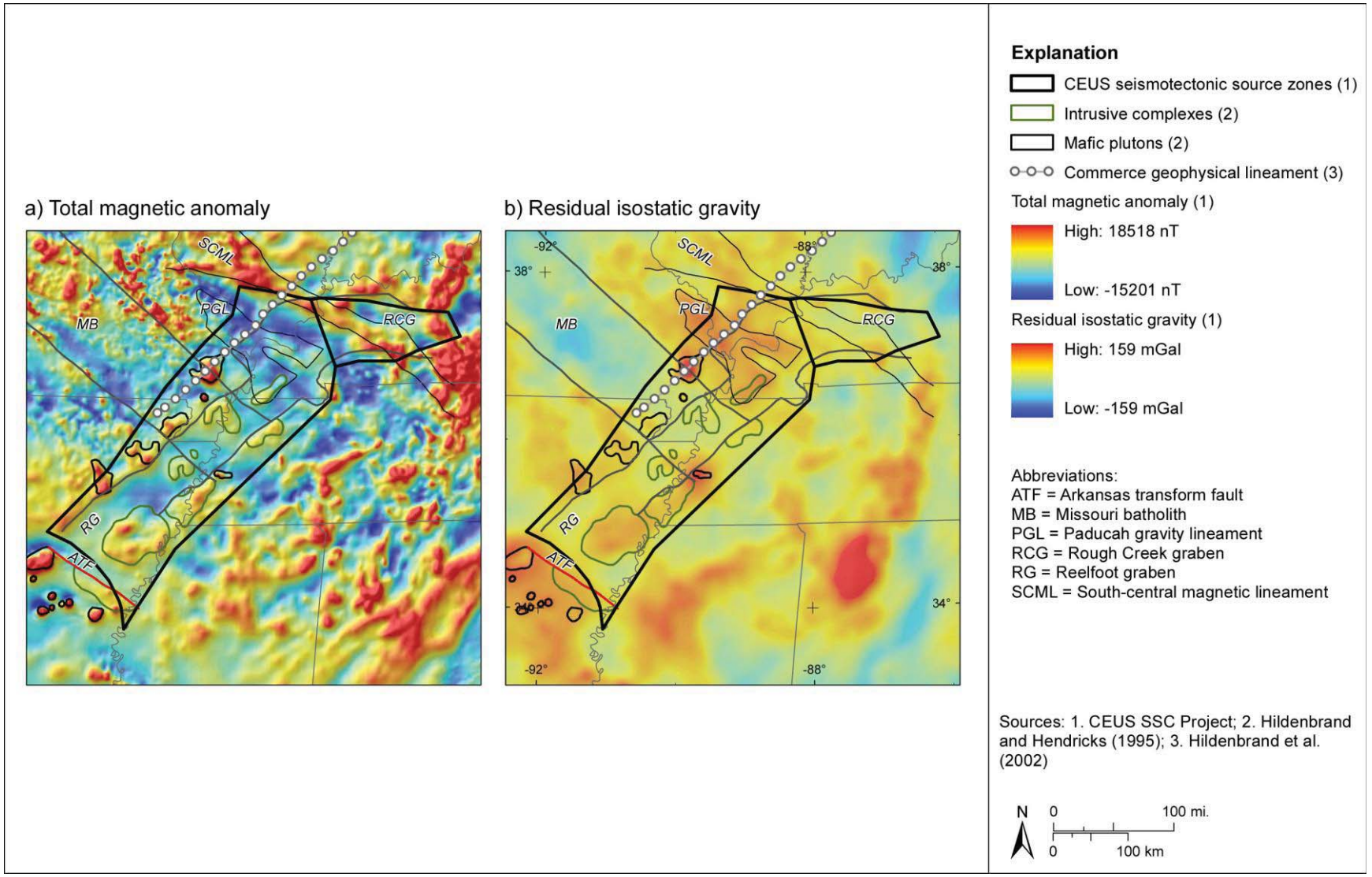

Figure 7.3.6-2
Maps showing geophysical anomalies in the Reelfoot rift region

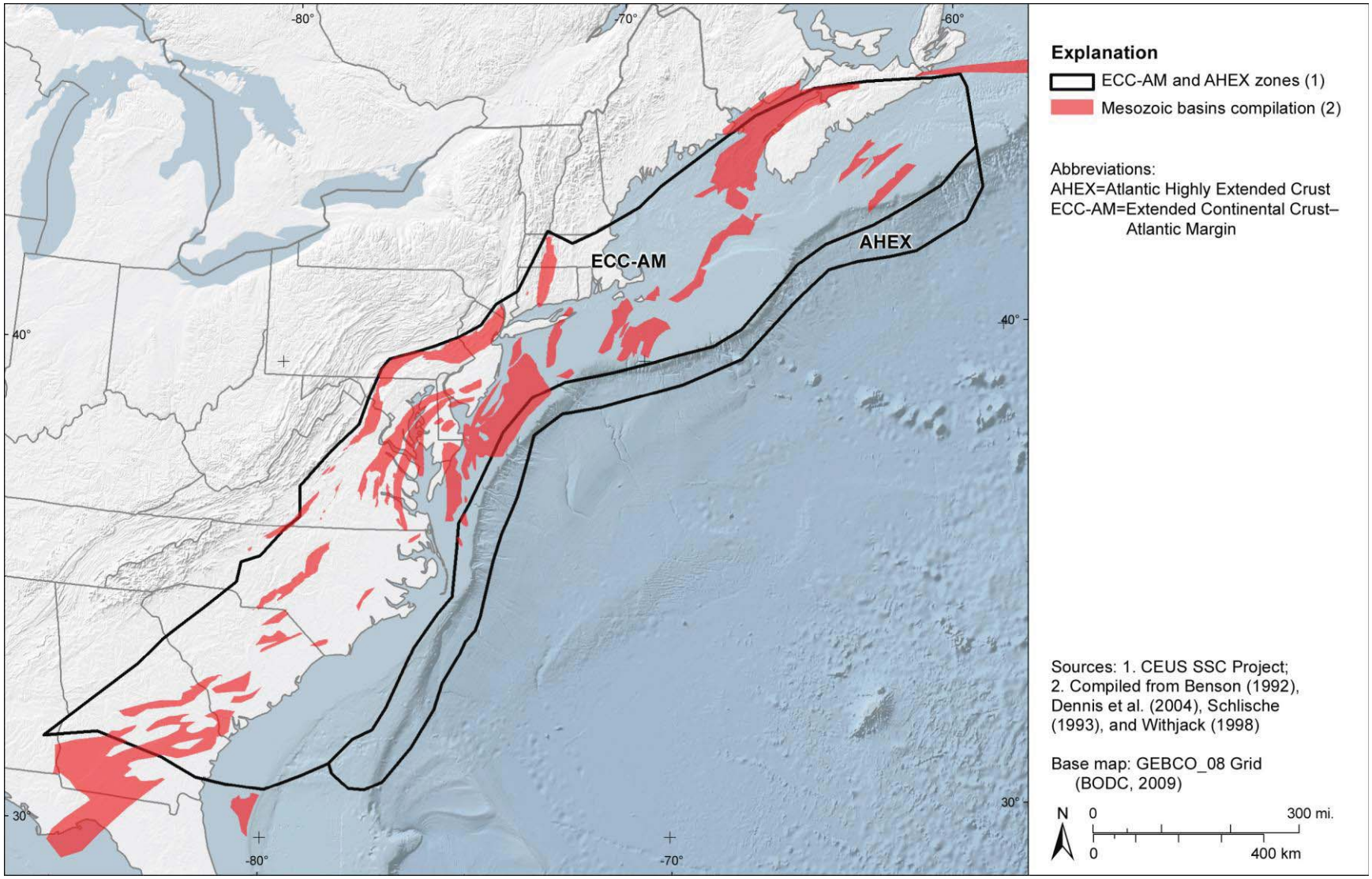

Figure 7.3.7-1
Mesozoic basins within the ECC-AM zone

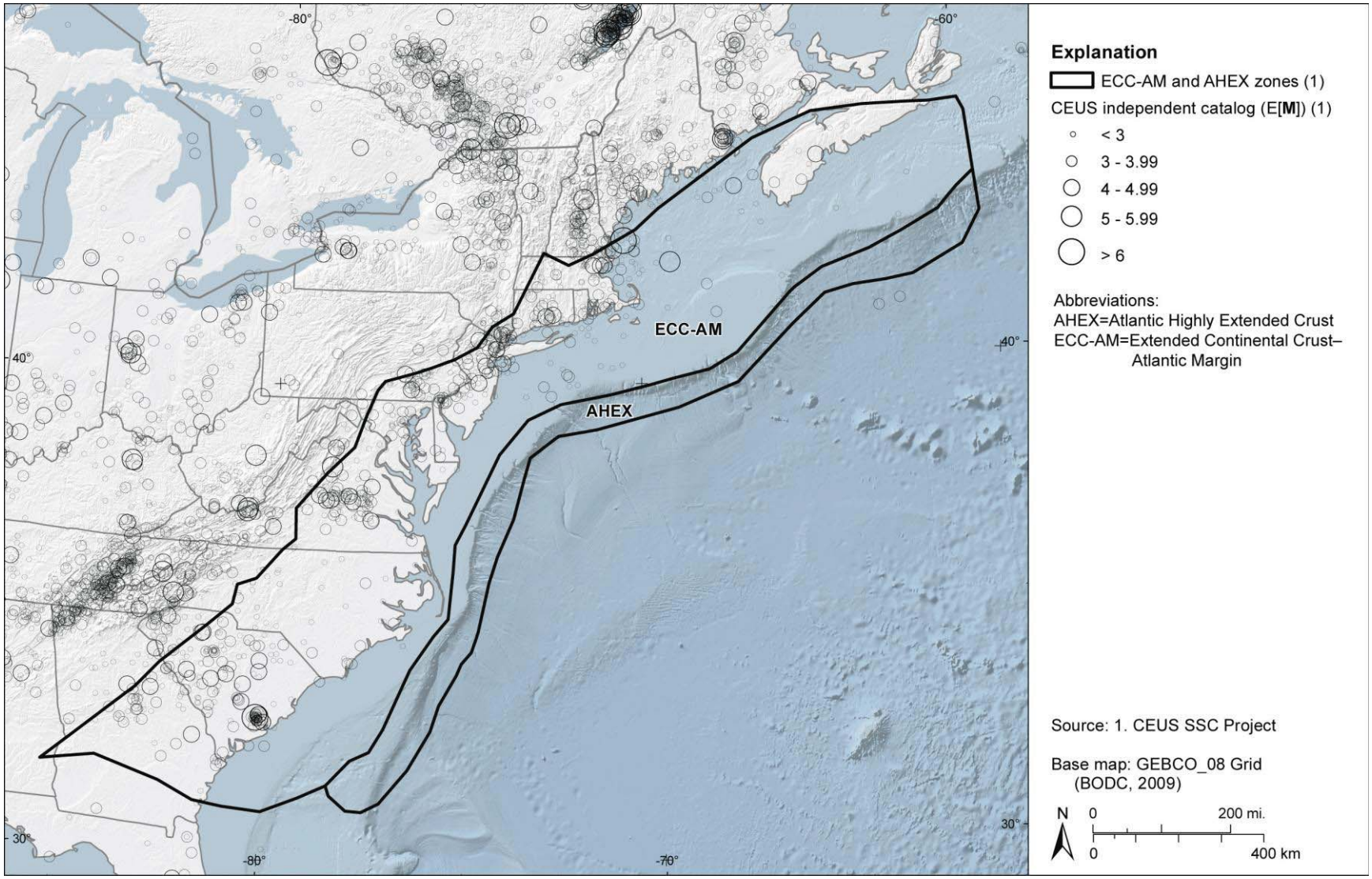

Figure 7.3.7-2
Seismicity within the ECC-AM and AHEX zones

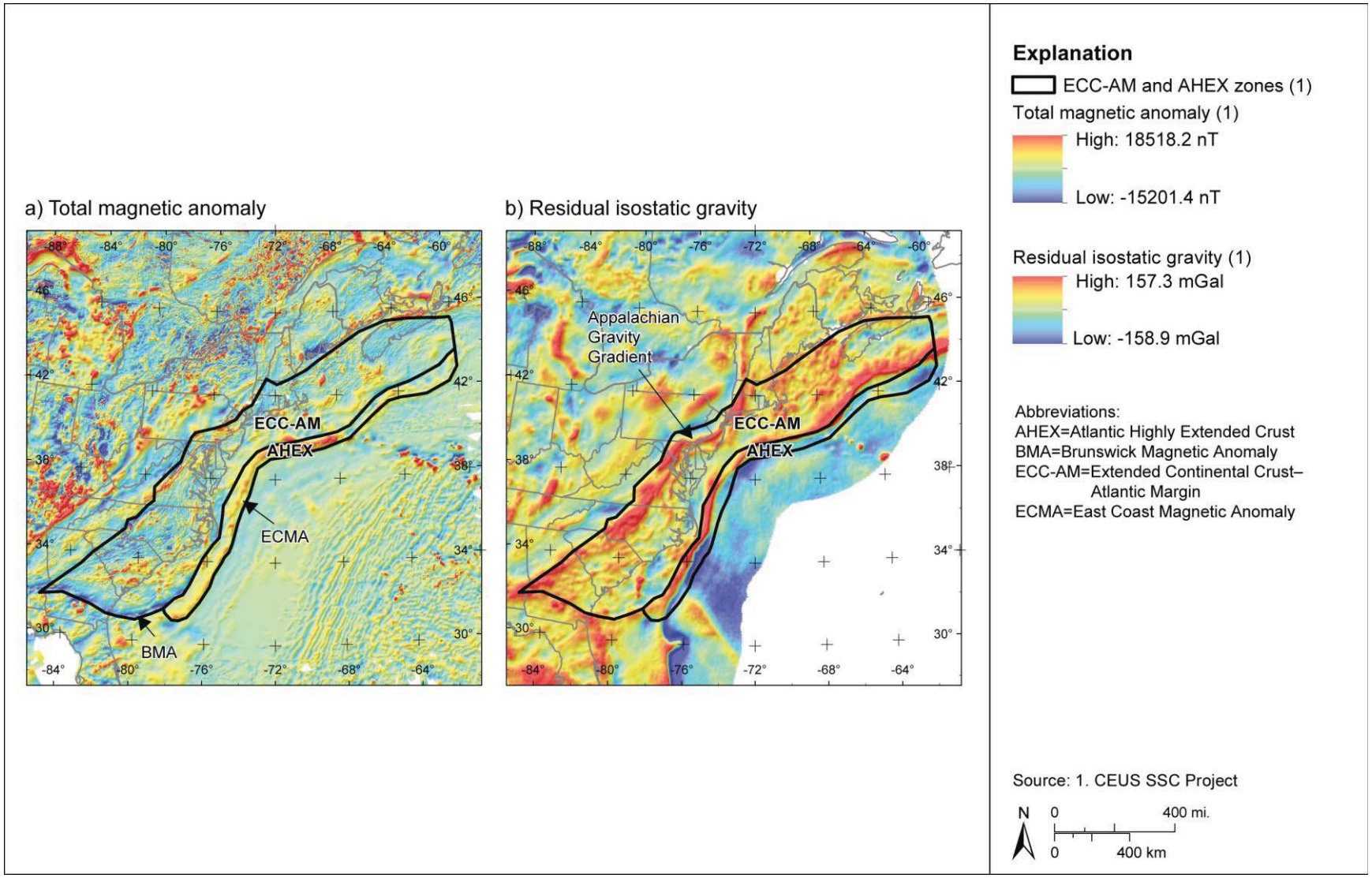

Figure 7.3.7-3
Magnetic and gravity data for ECC-AM and AHEX zones

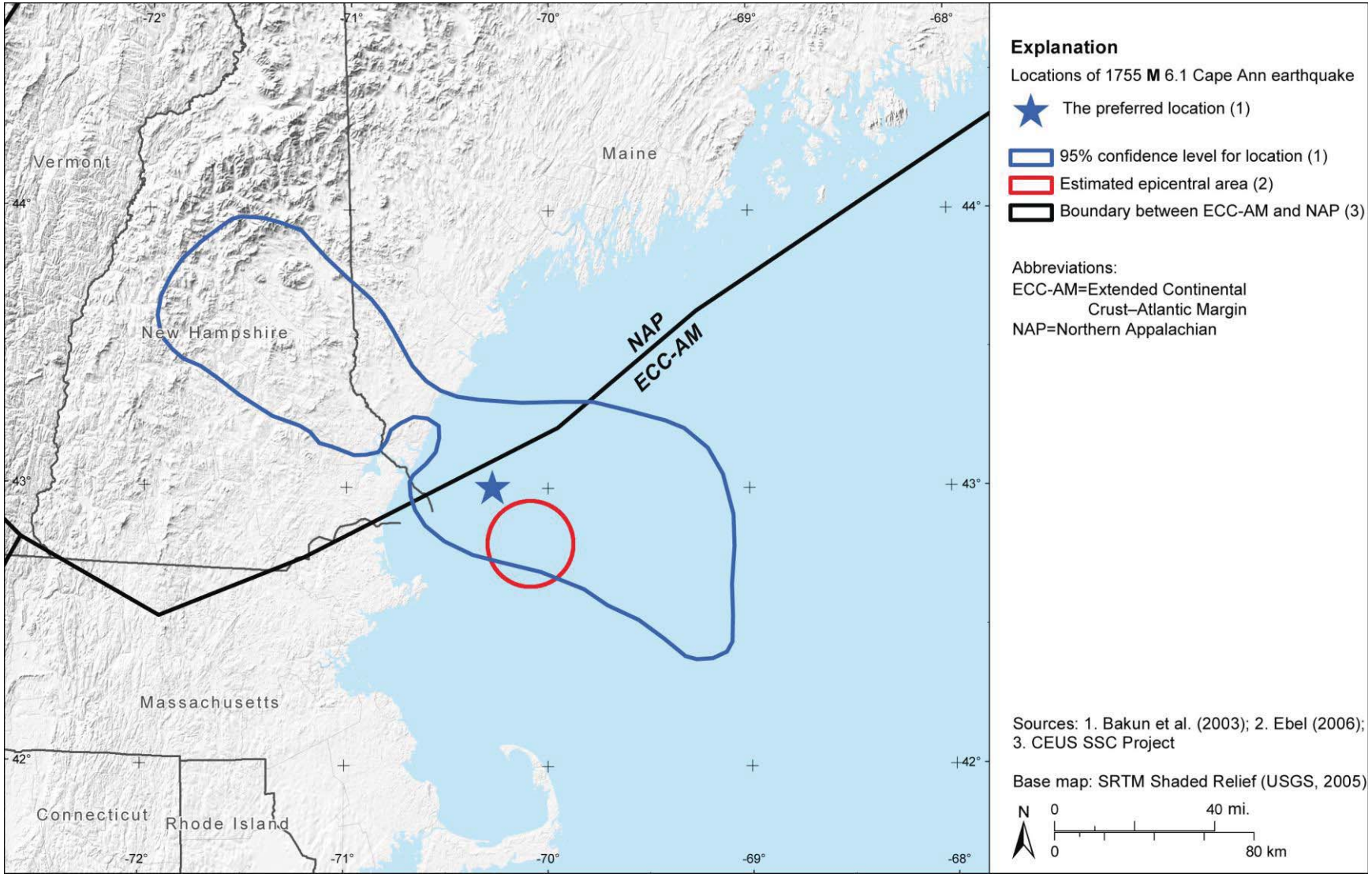

Figure 7.3.7-4
Estimated locations of the 1755 M 6.1 Cape Ann earthquake

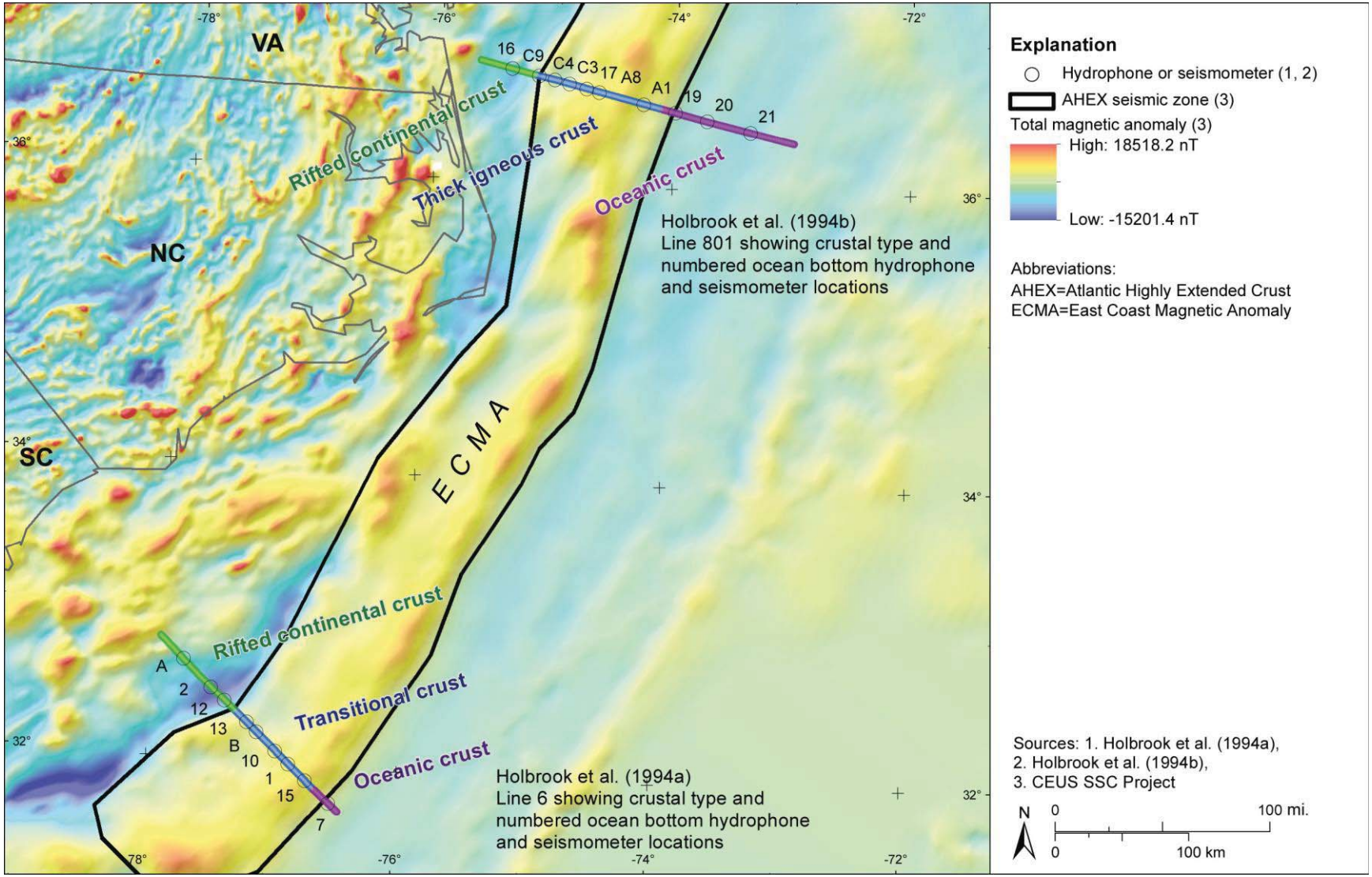

Figure 7.3.8-1
Correlation of interpreted transitional crust with the East Coast magnetic anomaly

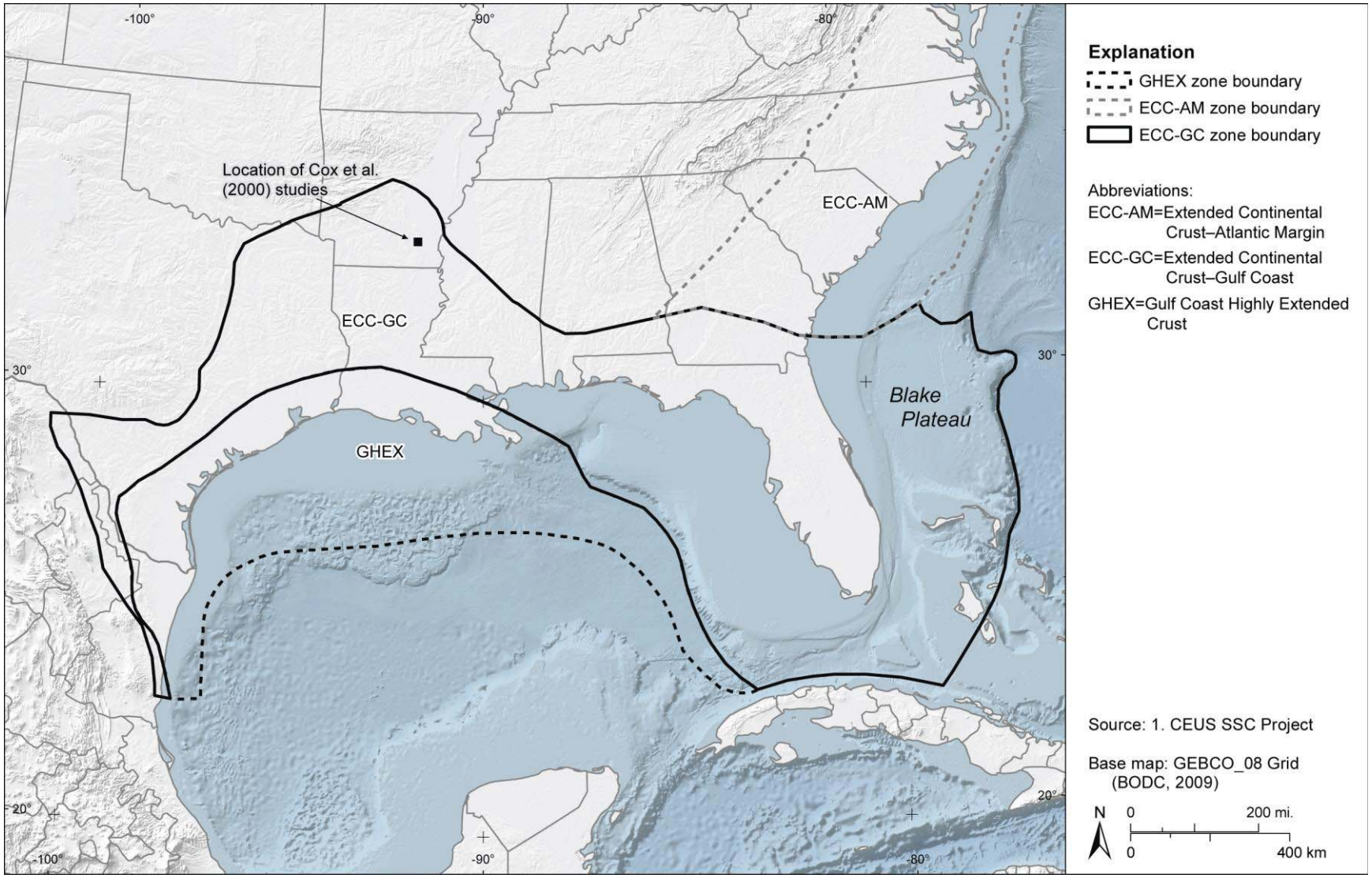

Figure 7.3.9-1
The ECC-GC seismotectonic zone

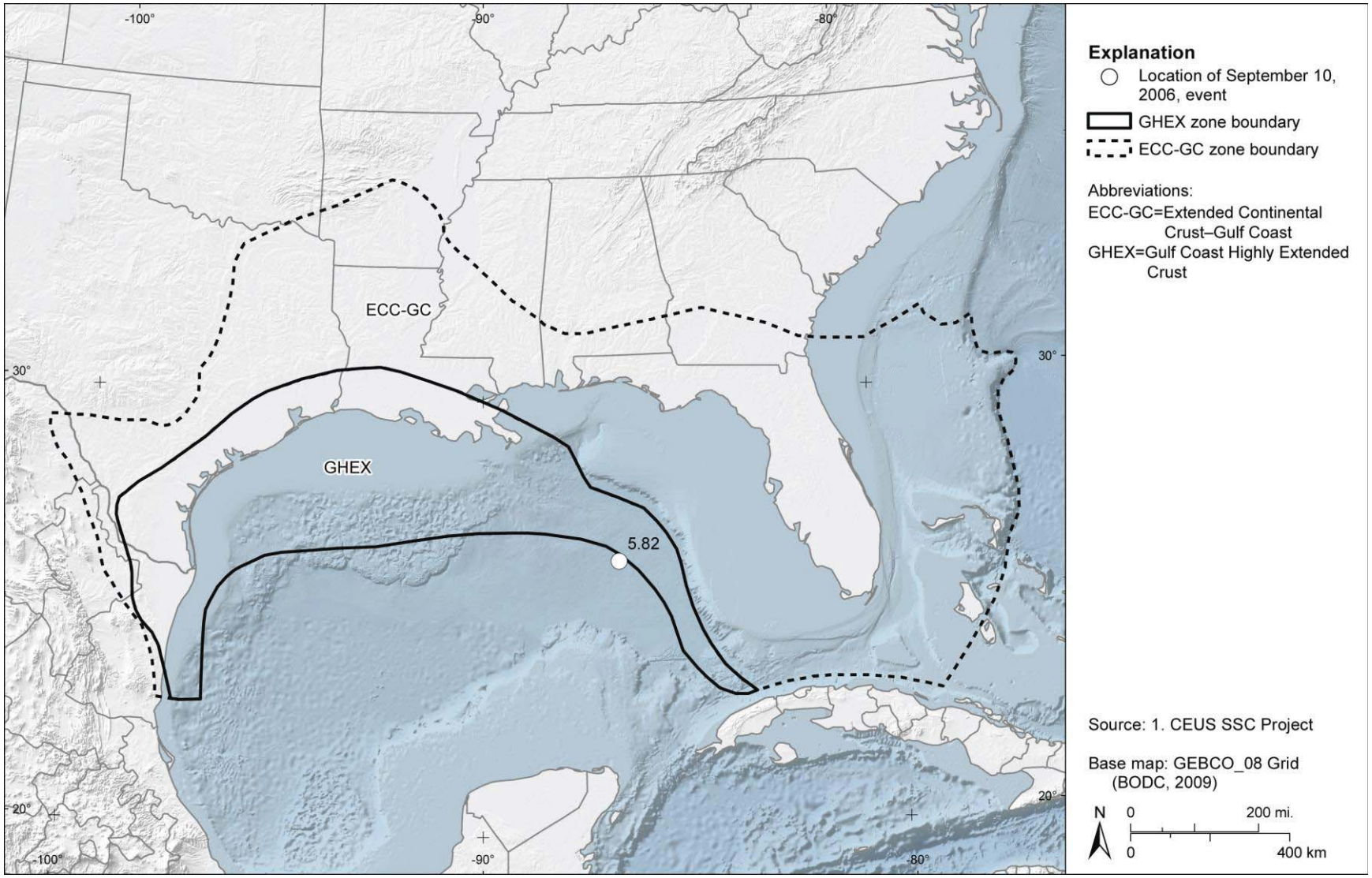

Figure 7.3.10-1
The GHEX seismotectonic zone

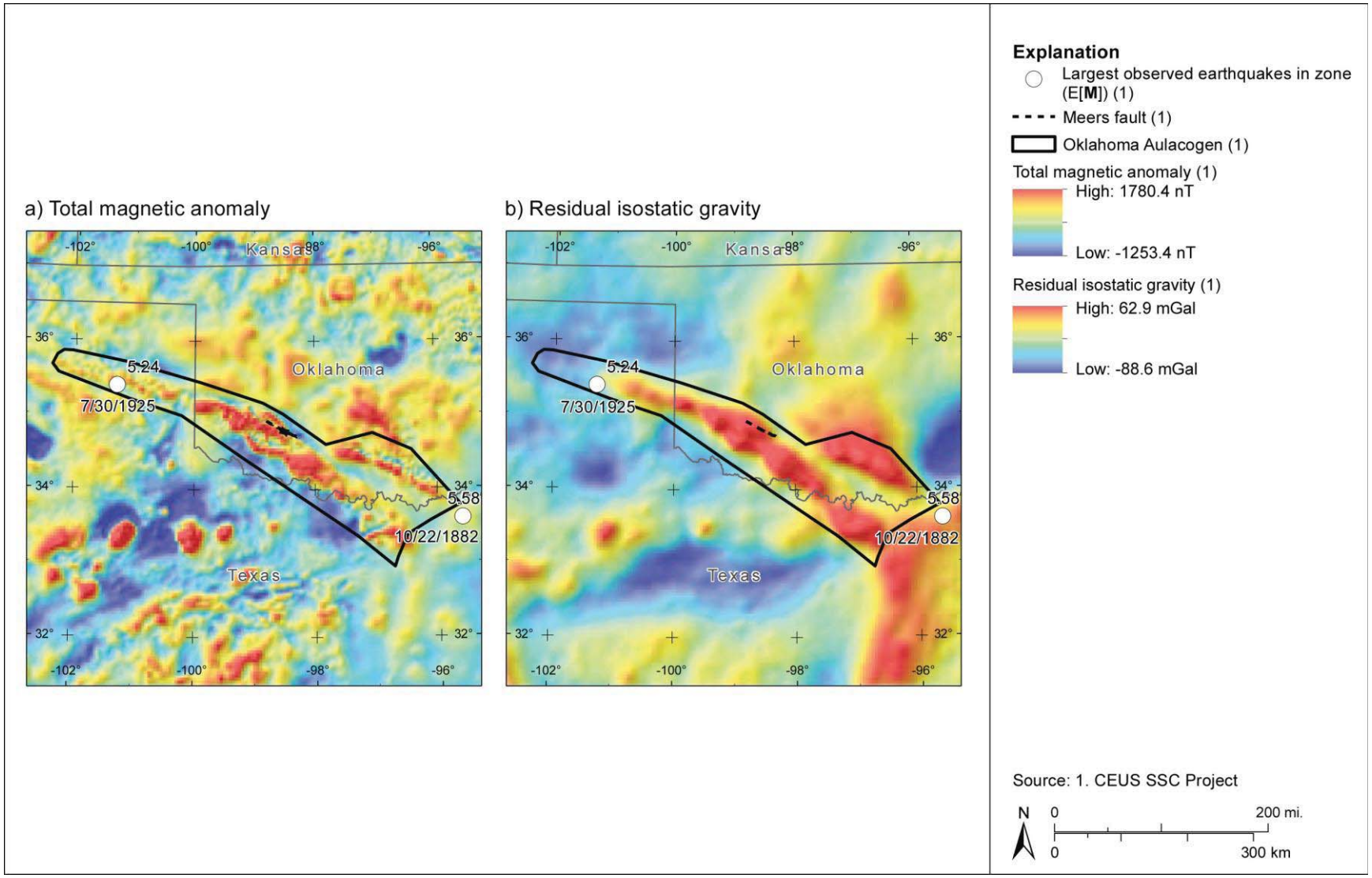

Figure 7.3.11-1
The OKA seismotectonic zone and regional gravity and magnetic data

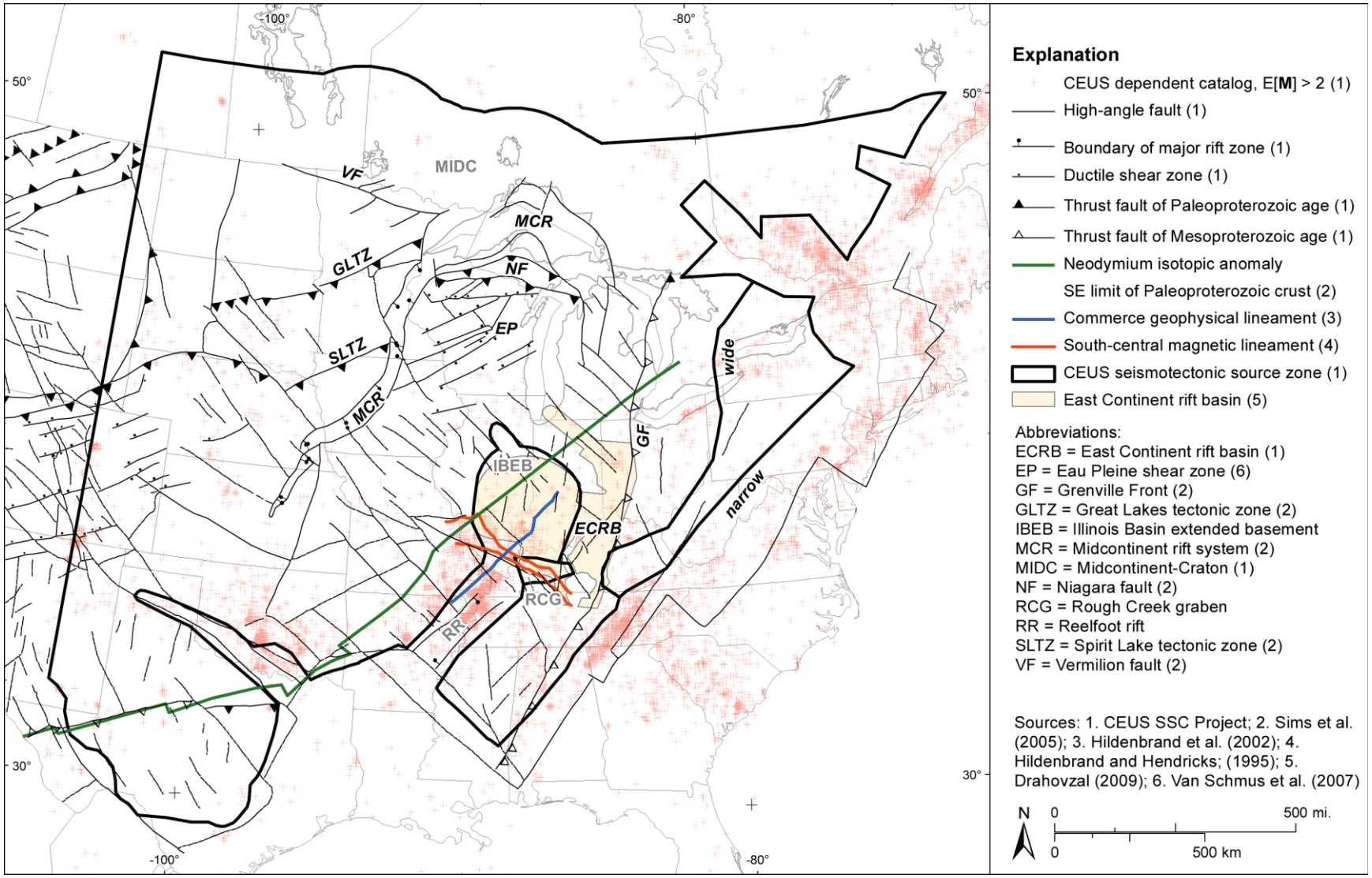

Figure 7.3.12-1
Simplified tectonic map showing the distribution of principal basement faults, rifts, and sutures in the Midcontinent

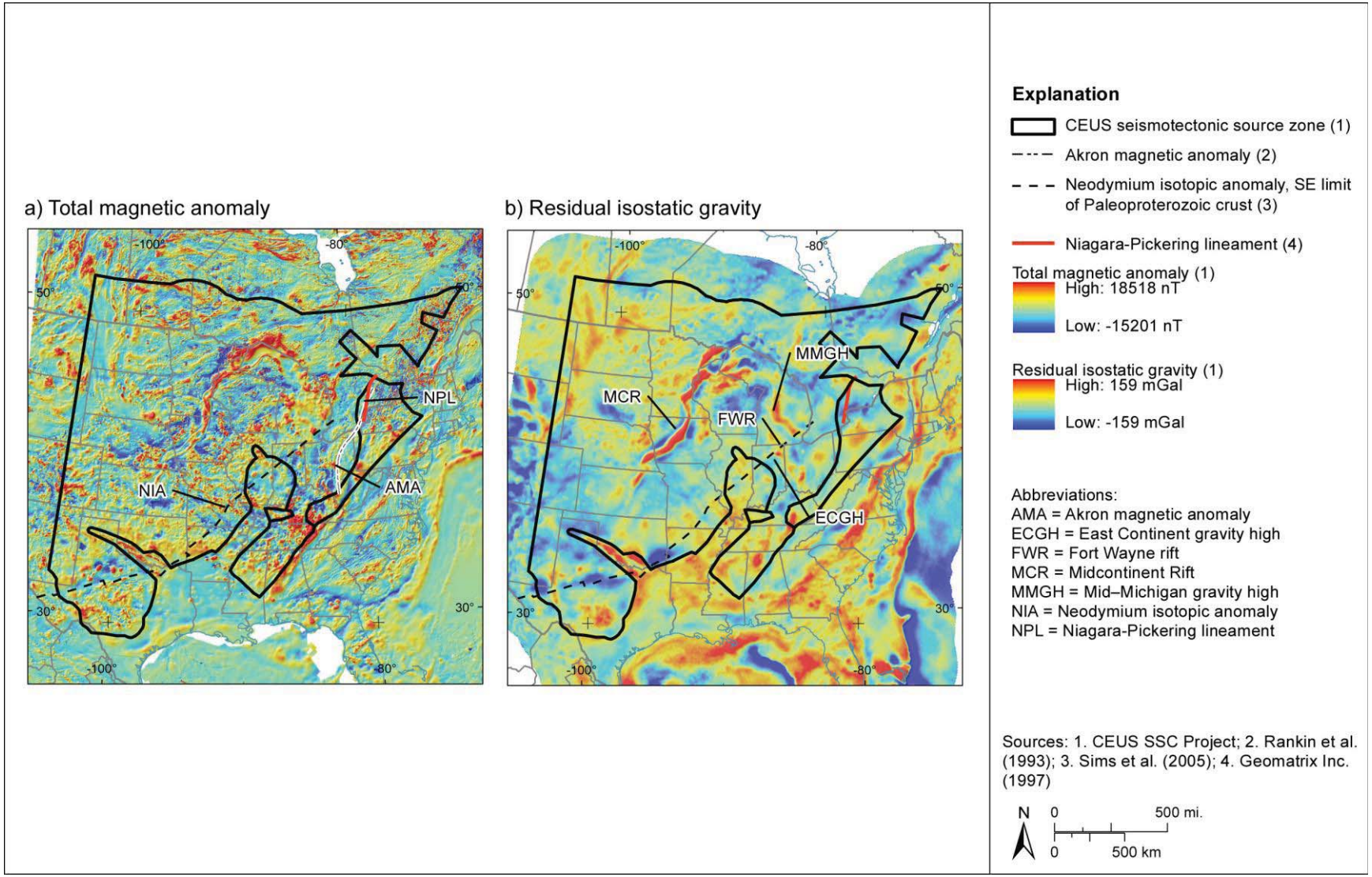

Figure 7.3.12-2
Maps showing major basement structural features relative to (a) regional magnetic anomalies and (b) regional gravity anomalies

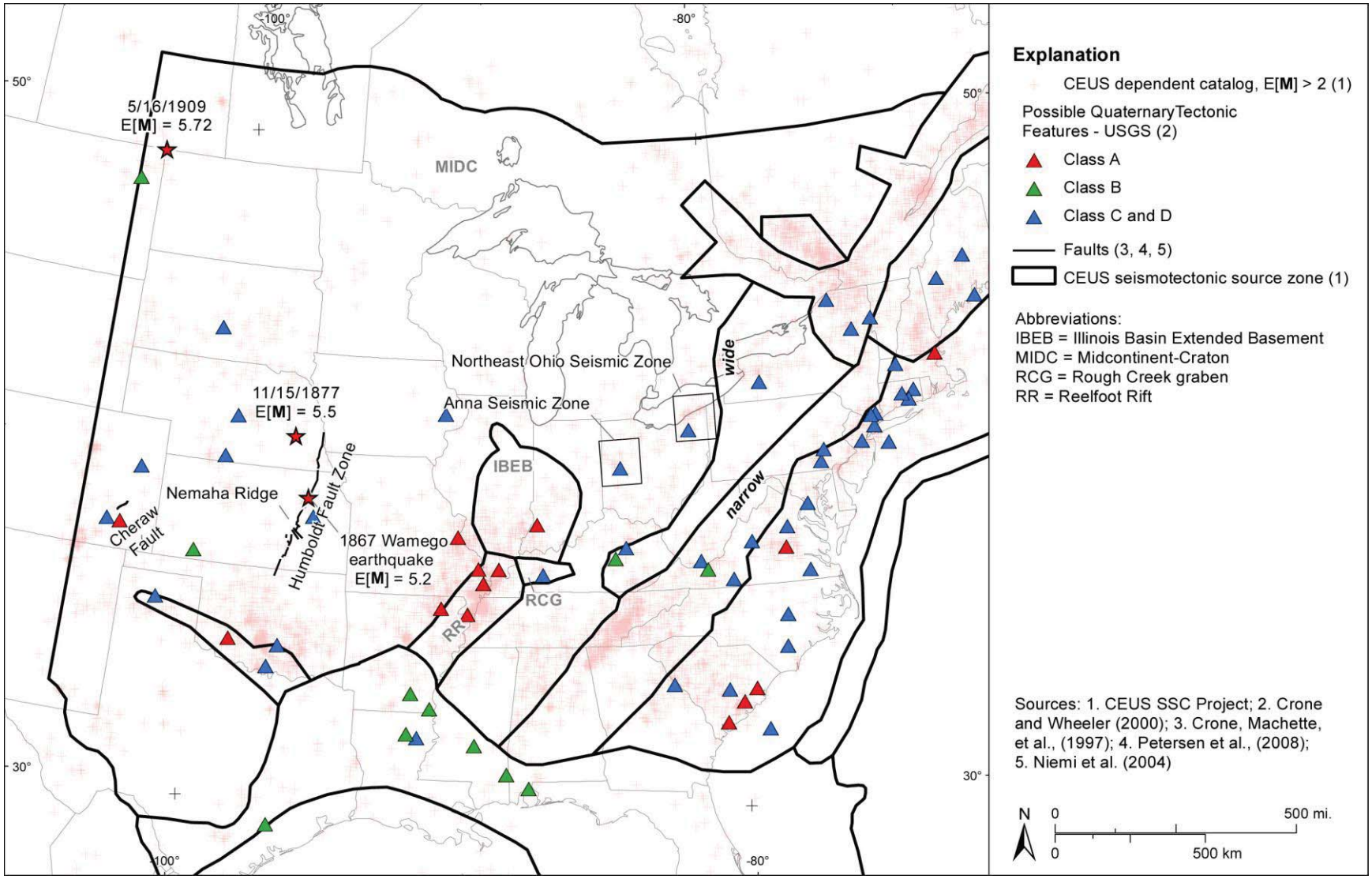

Figure 7.3.12-3
Seismic zones and maximum observed earthquakes in the MidC zone

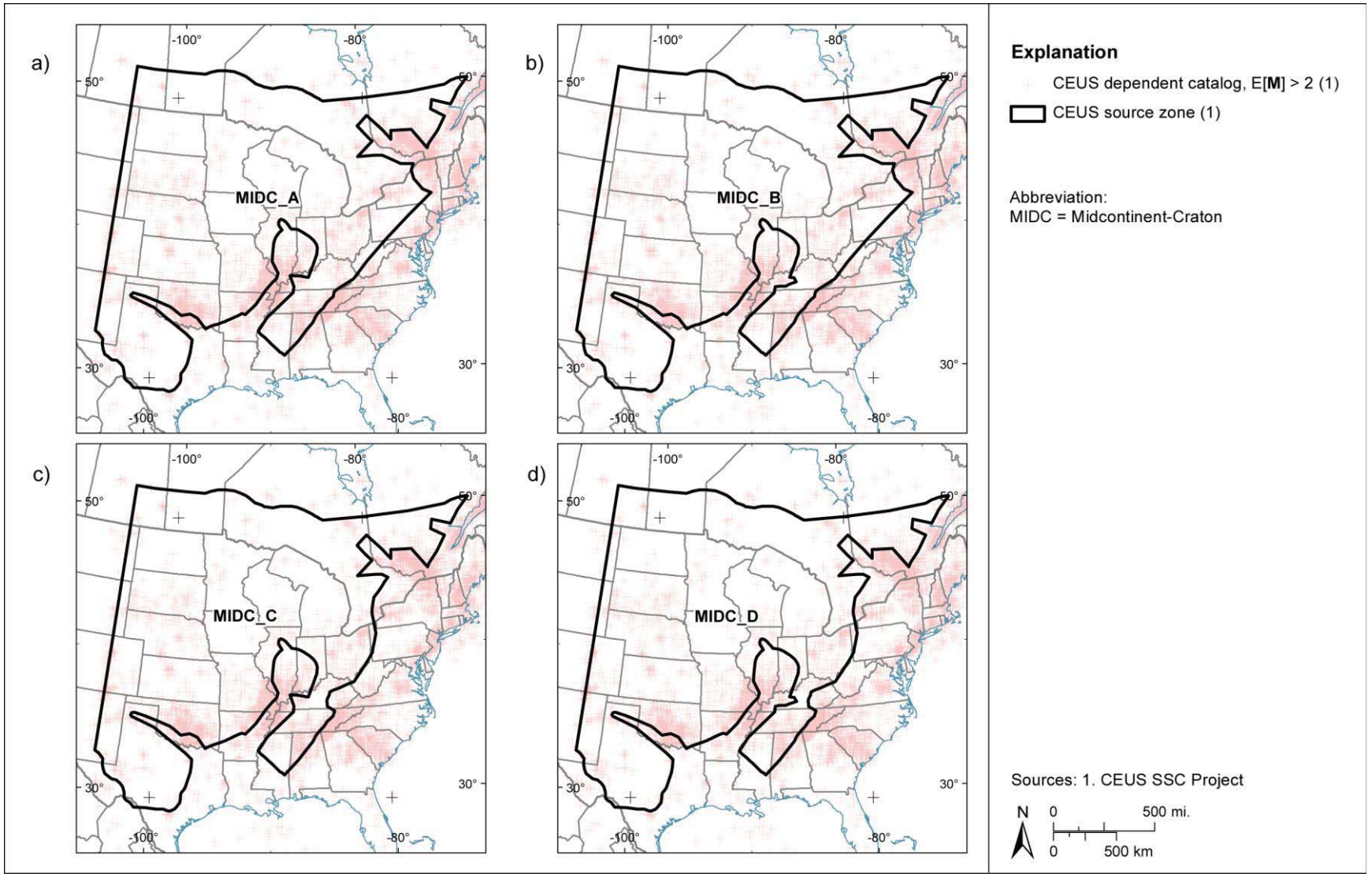

Figure 7.3.12-4
Alternative MidC source zone configurations

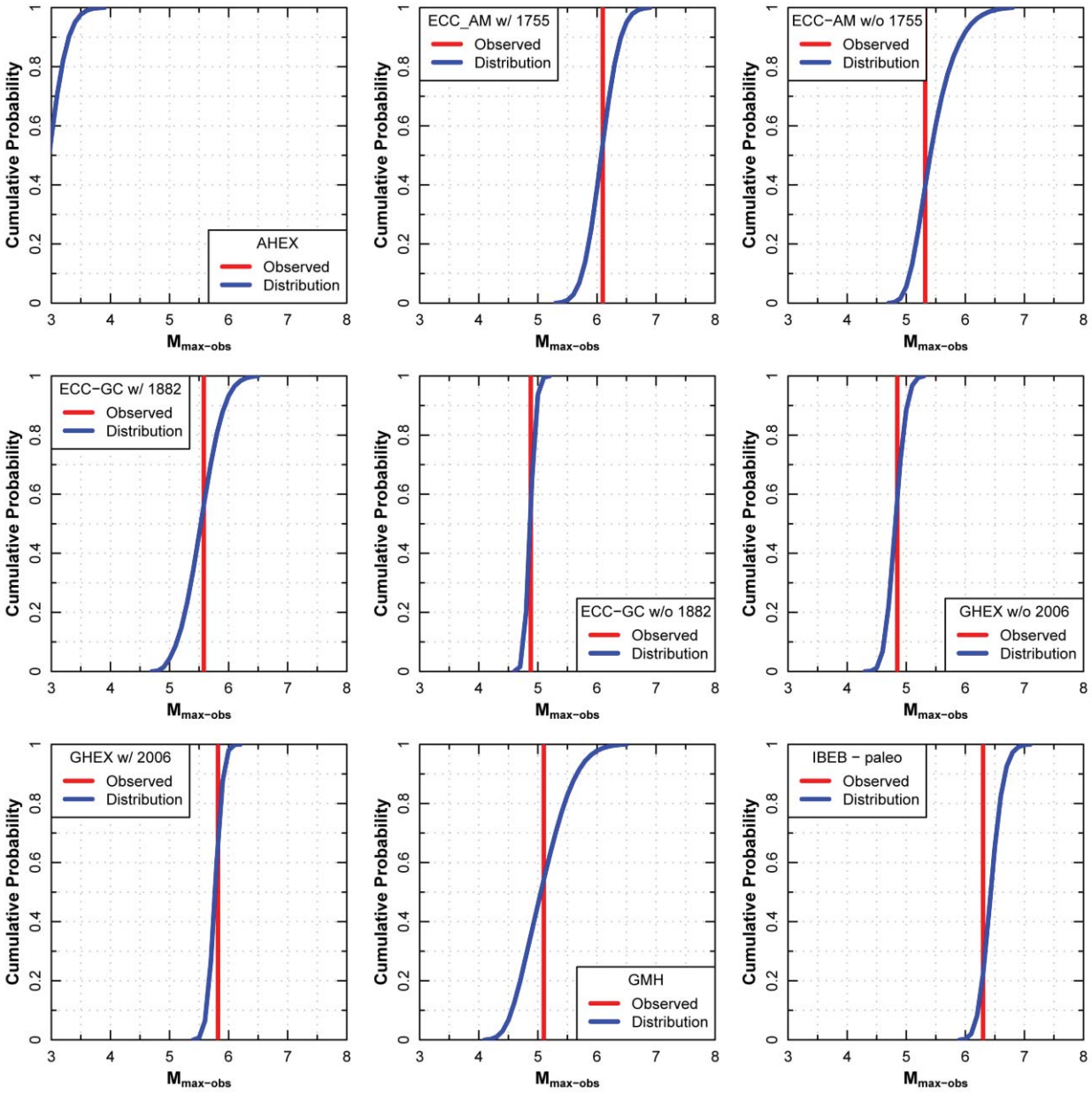

Figure 7.4.1-1 (1 of 3)
Distributions for $m_{\max-obs}$ for the seismotectonic distributed seismicity source zones

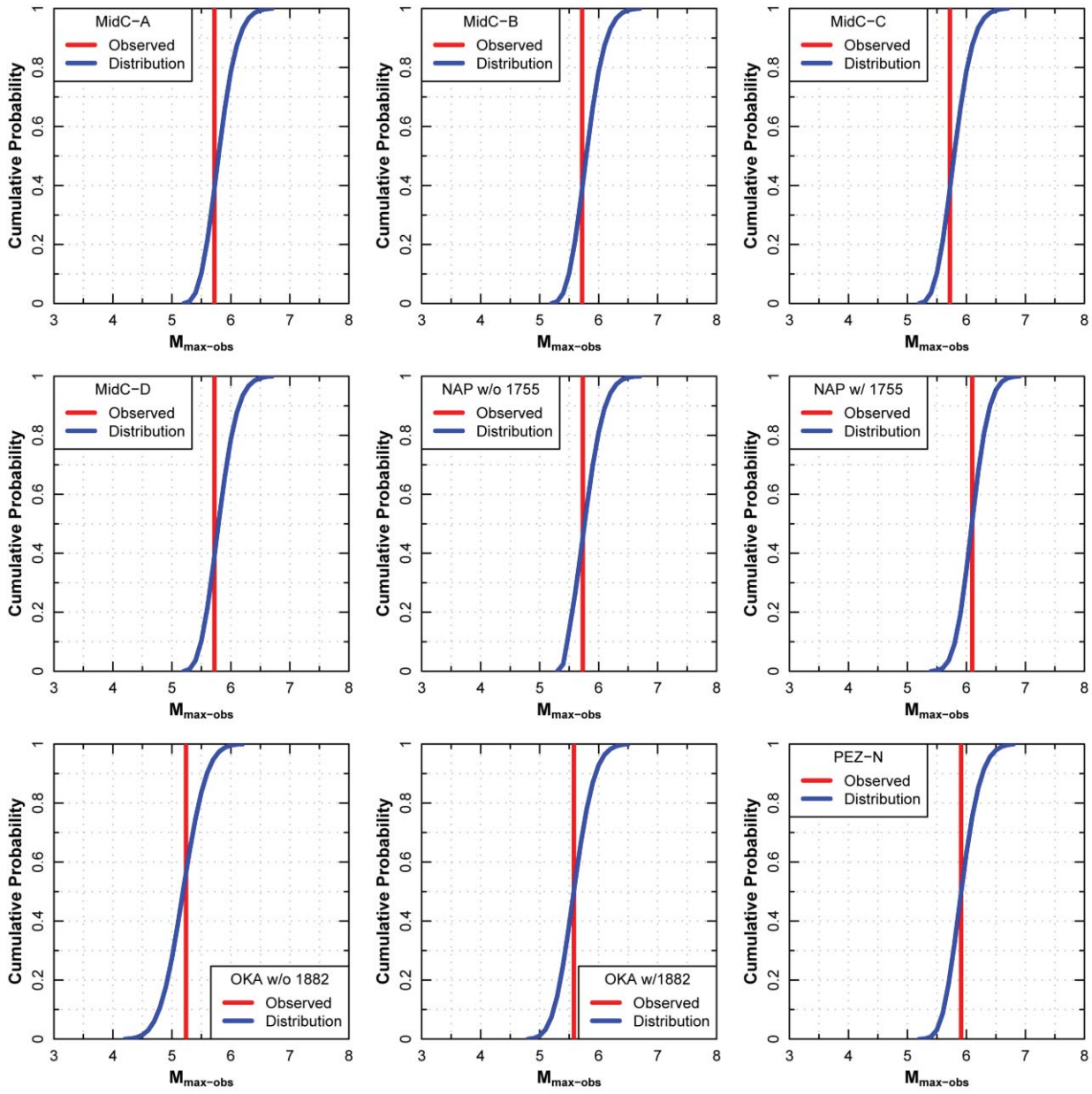

Figure 7.4.1-1 (2 of 3)
Distributions for $m_{\max-obs}$ for the seismotectonic distributed seismicity source zones

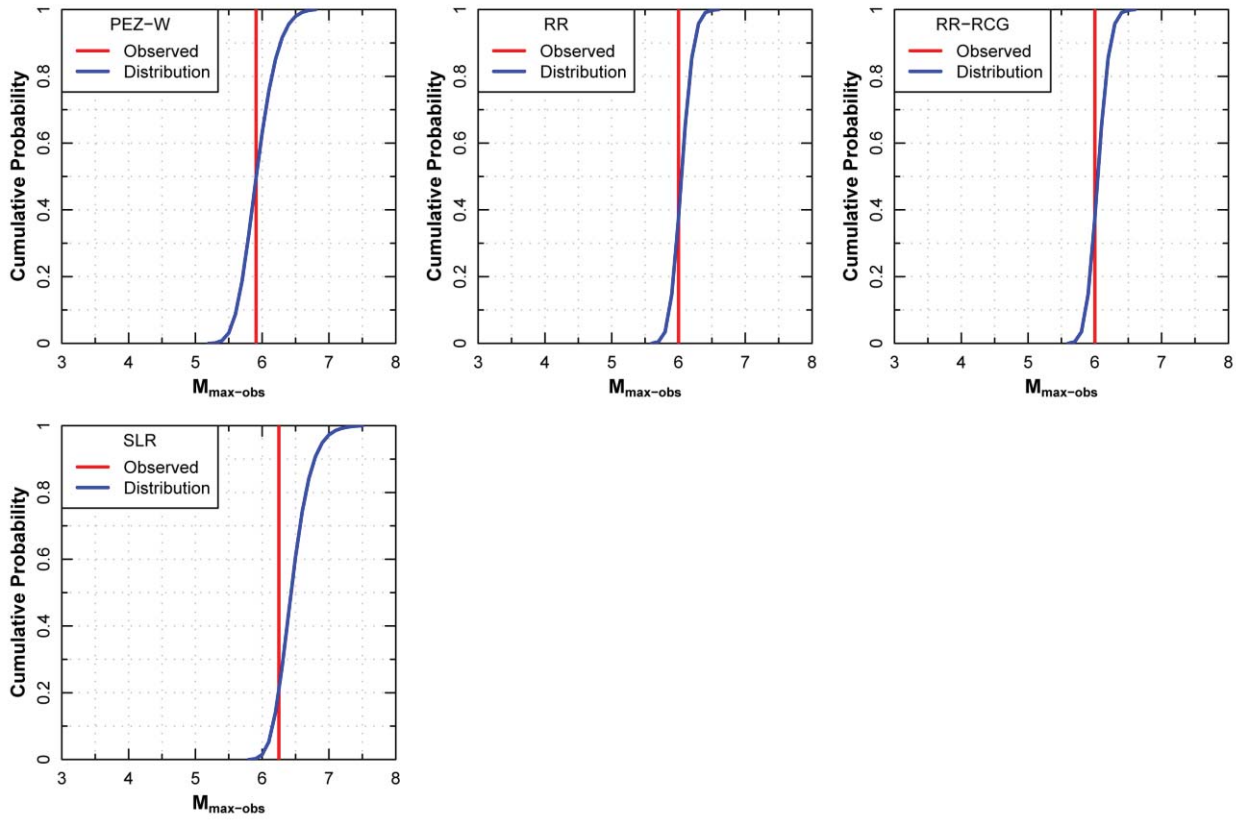

Figure 7.4.1-1 (3 of 3)
Distributions for $m_{\max-obs}$ for the seismotectonic distributed seismicity source zones

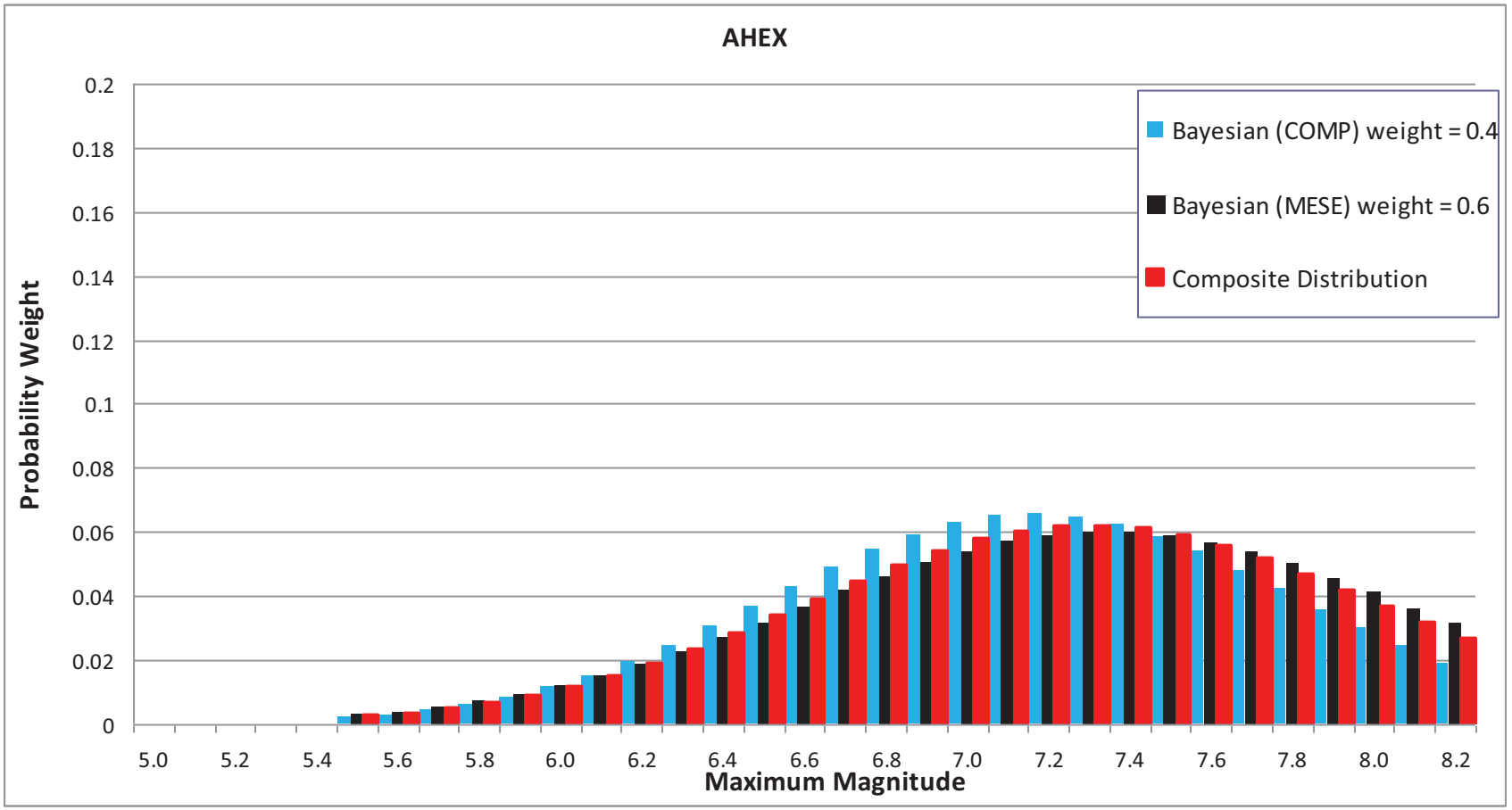

Figure 7.4.2-1
Mmax distributions for the AHEX seismotectonic zone

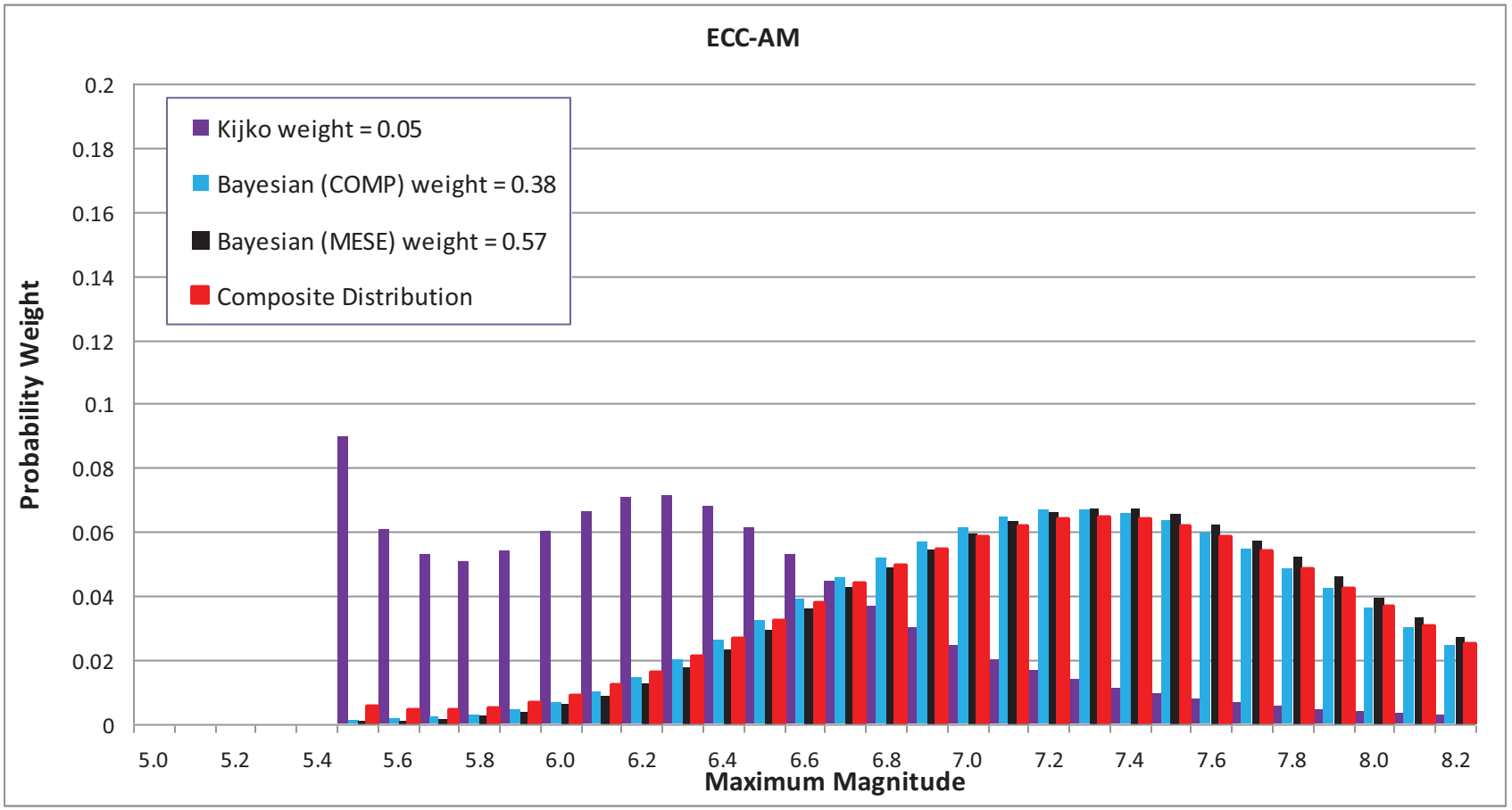

Figure 7.4.2-2
Mmax distributions for the ECC_AM seismotectonic zone

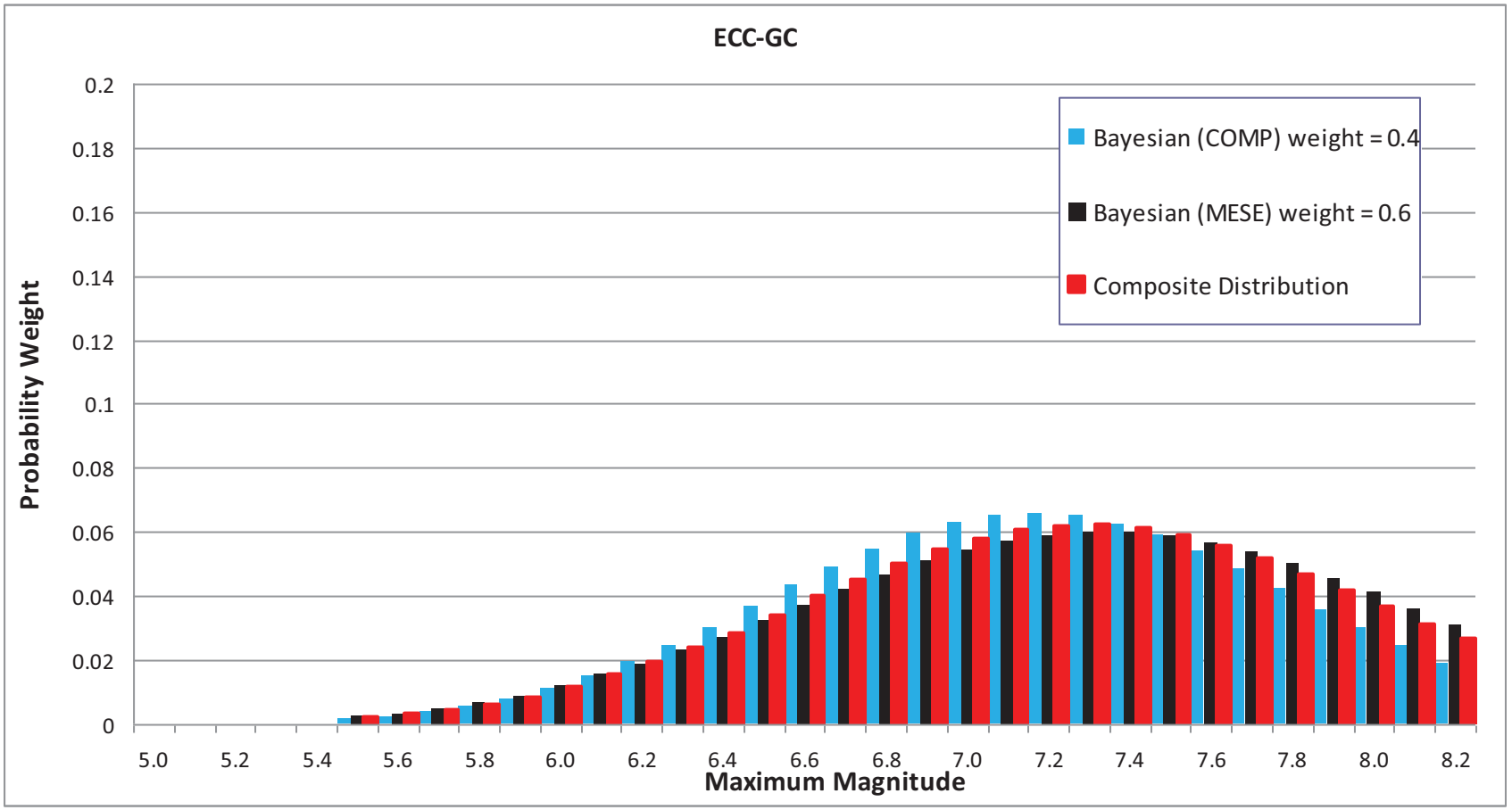

Figure 7.4.2-3
Mmax distributions for the ECC_GC seismotectonic zone

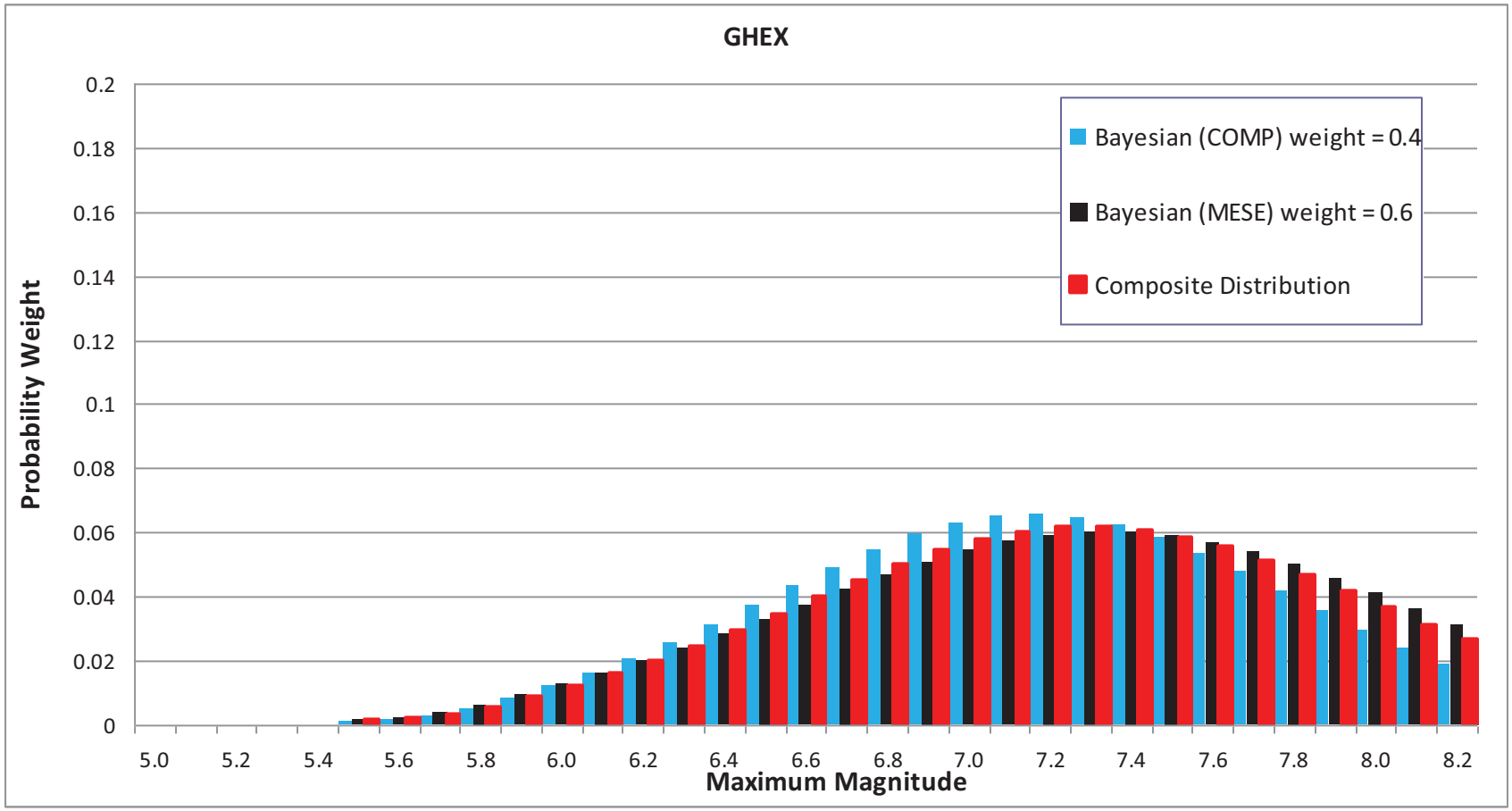

Figure 7.4.2-4
Mmax distributions for the GHEX seismotectonic zone

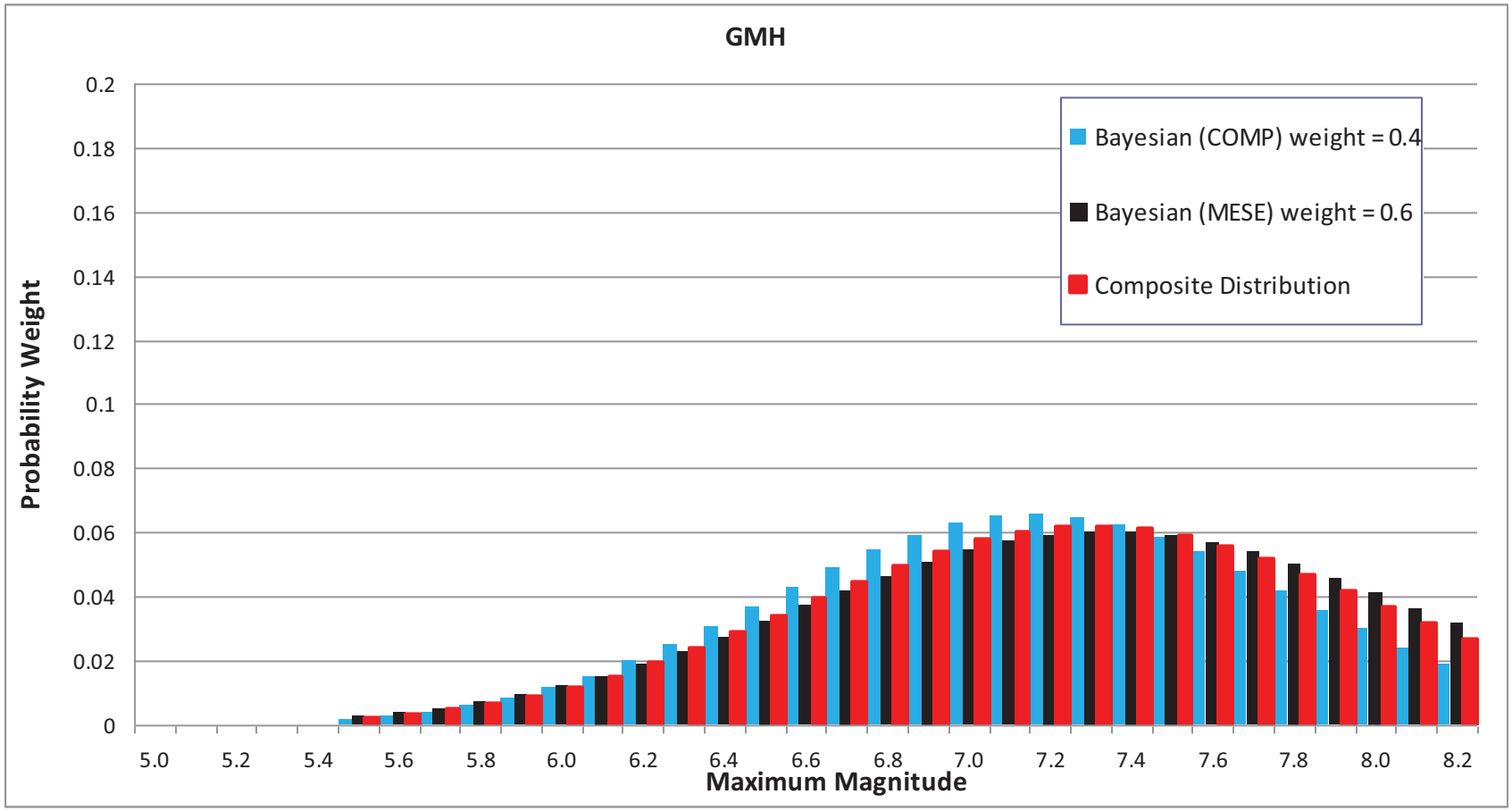

Figure 7.4.2-5
Mmax distributions for the GMH seismotectonic zone

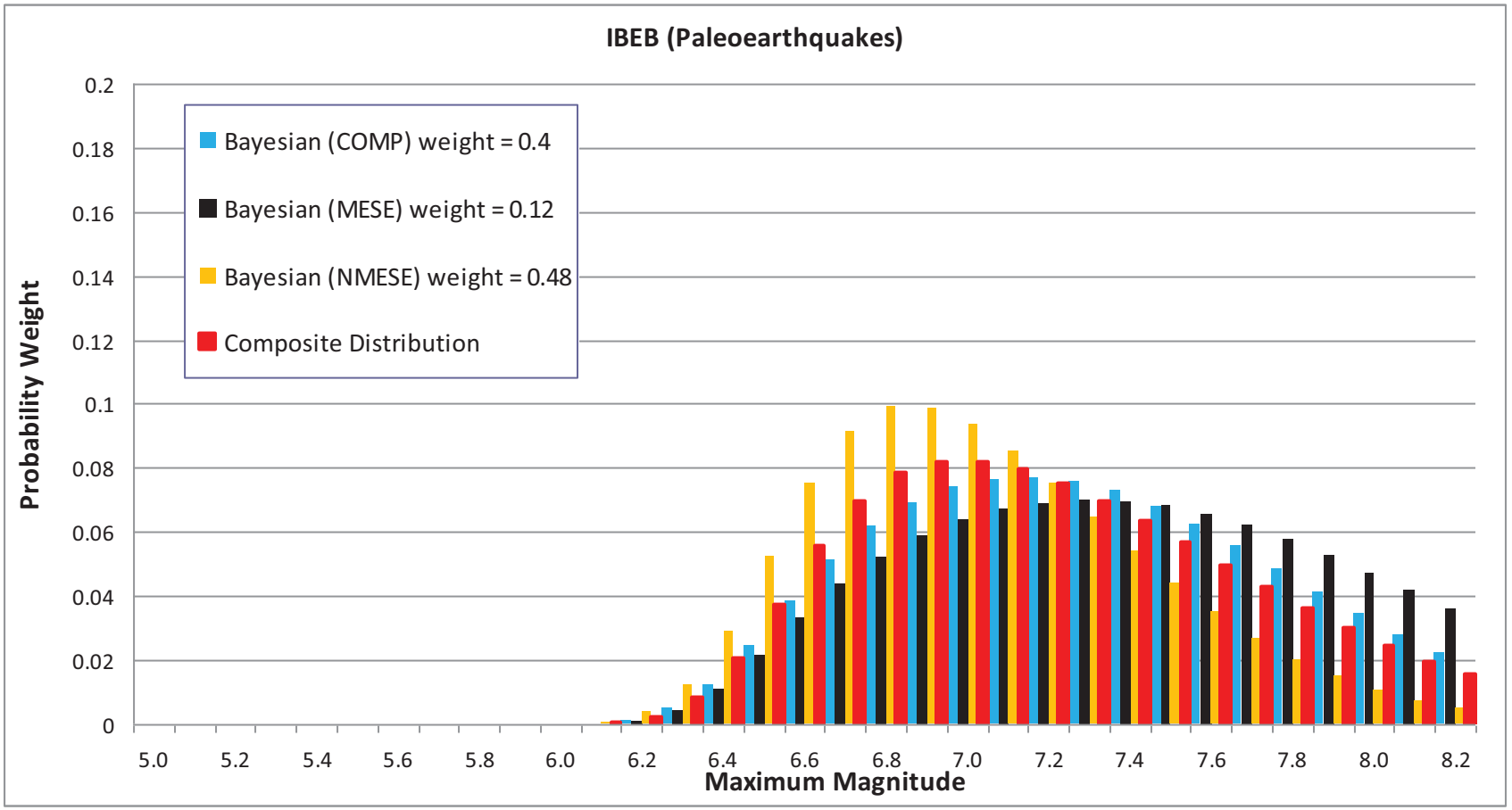

Figure 7.4.2-6
Mmax distributions for the IBEB seismotectonic zone

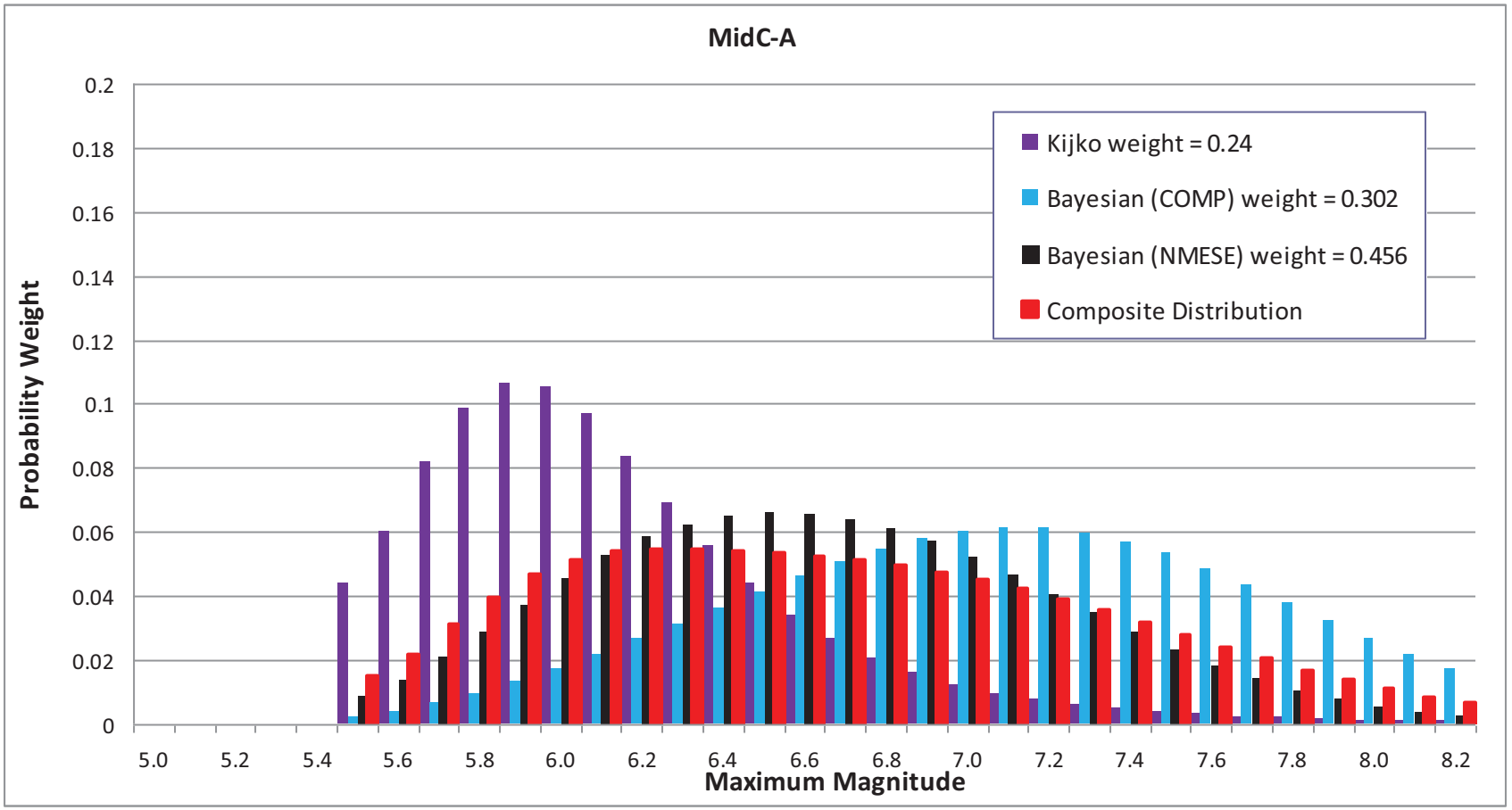

Figure 7.4.2-7
Mmax distributions for the MidC-A seismotectonic zone

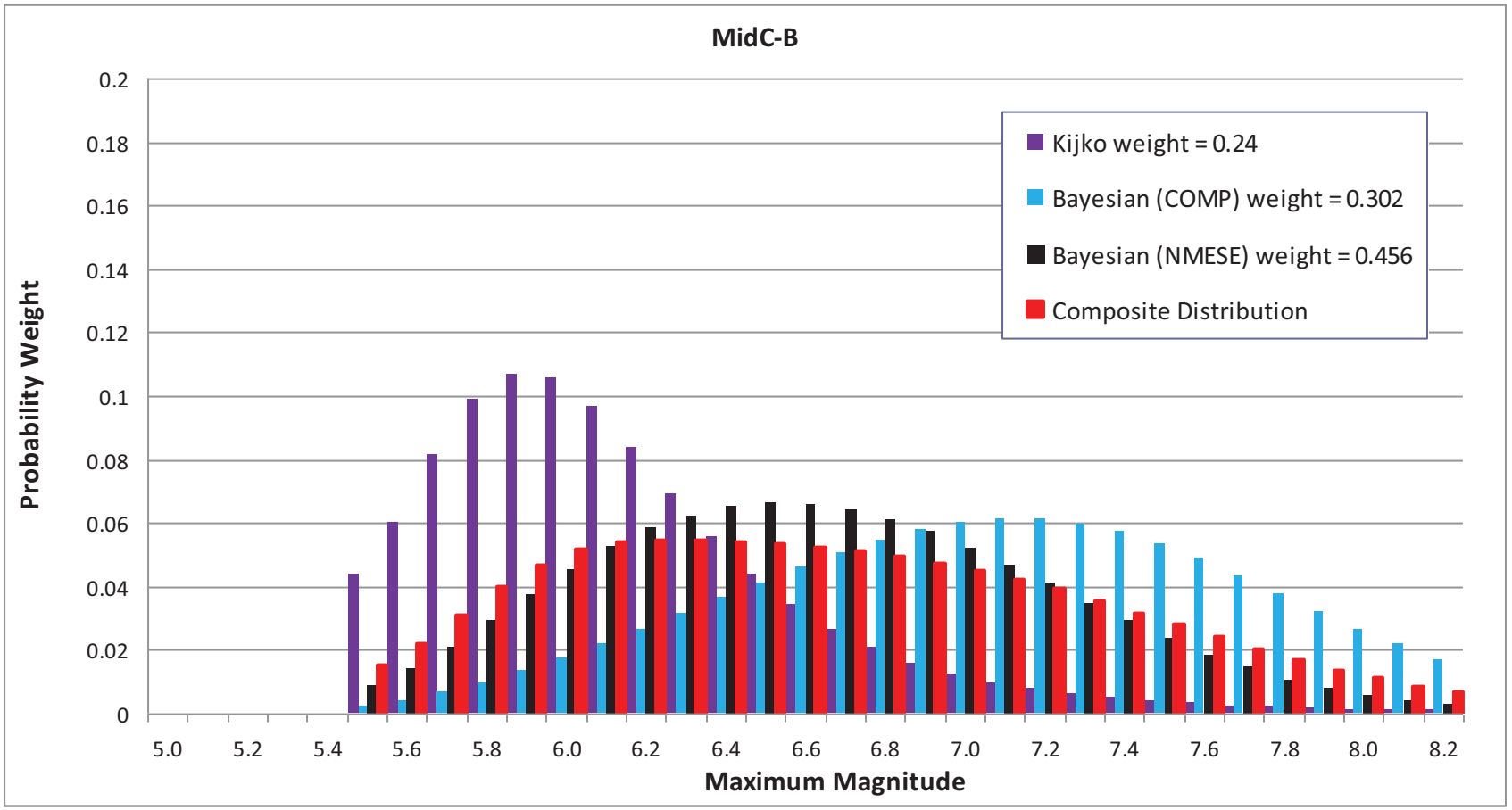

Figure 7.4.2-8
Mmax distributions for the MidC-B seismotectonic zone

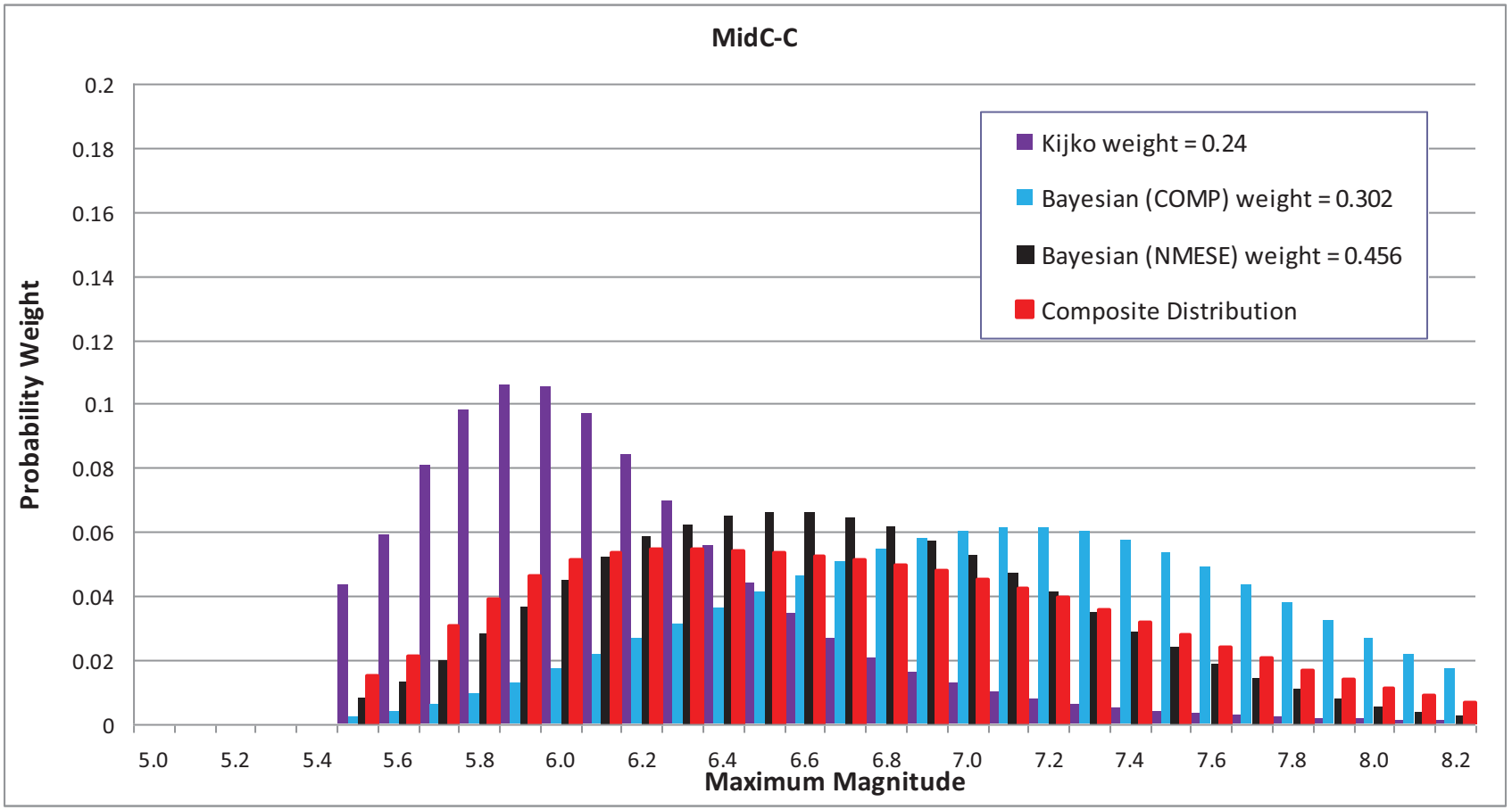

Figure 7.4.2-9
Mmax distributions for the MidC-C seismotectonic zone

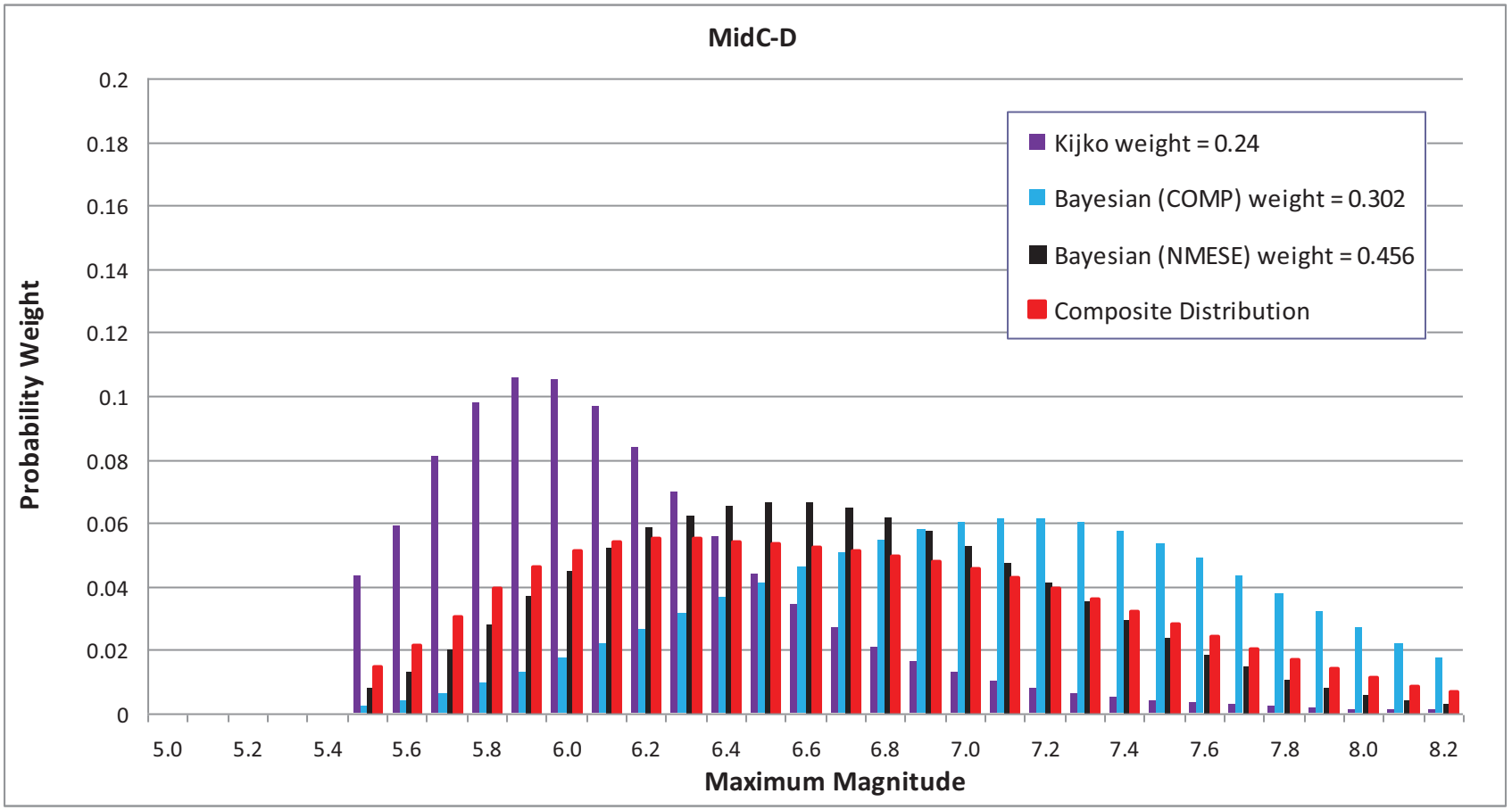

Figure 7.4.2-10
Mmax distributions for the MidC-D seismotectonic zone

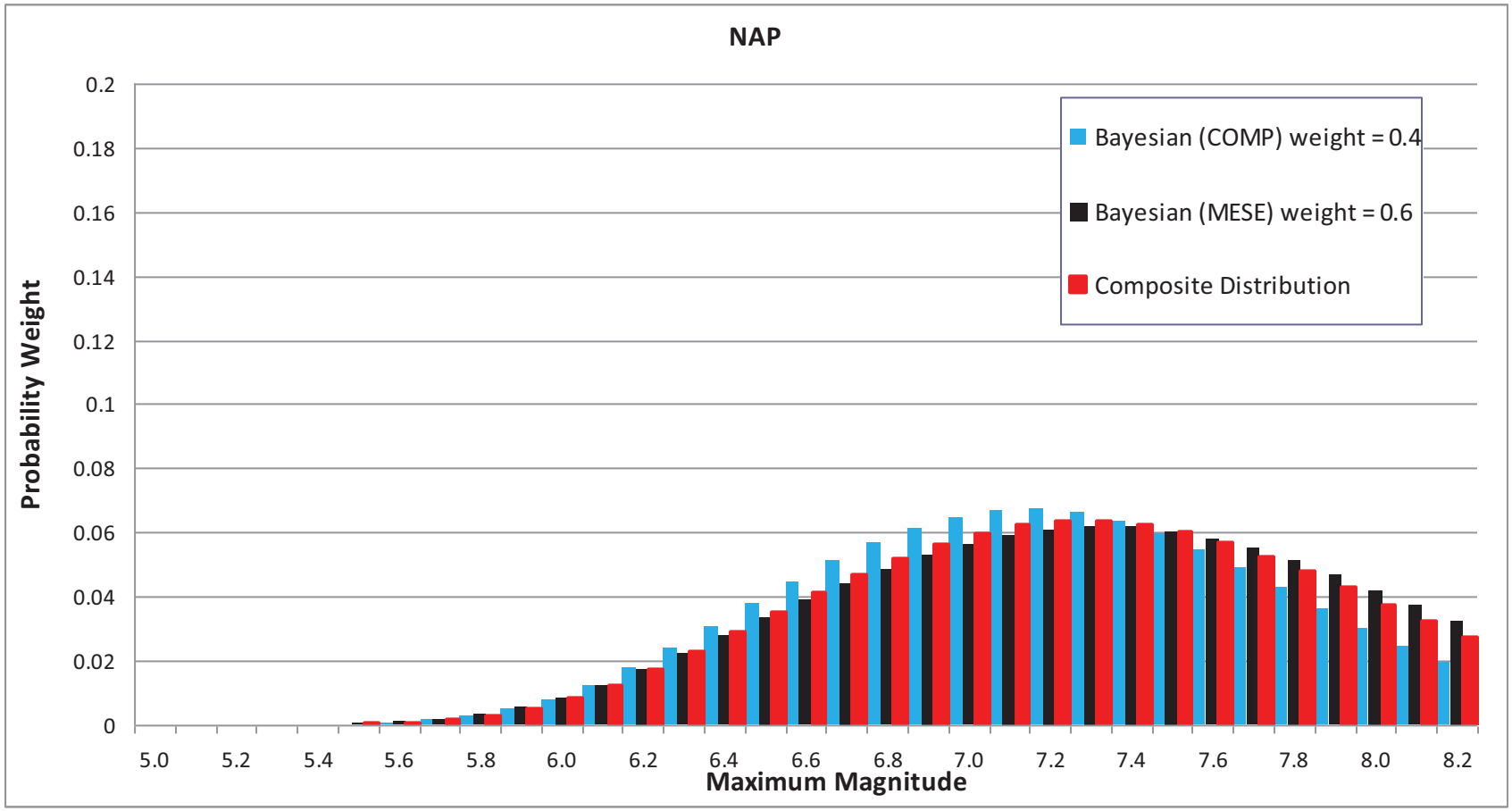

Figure 7.4.2-11
Mmax distributions for the NAP seismotectonic zone

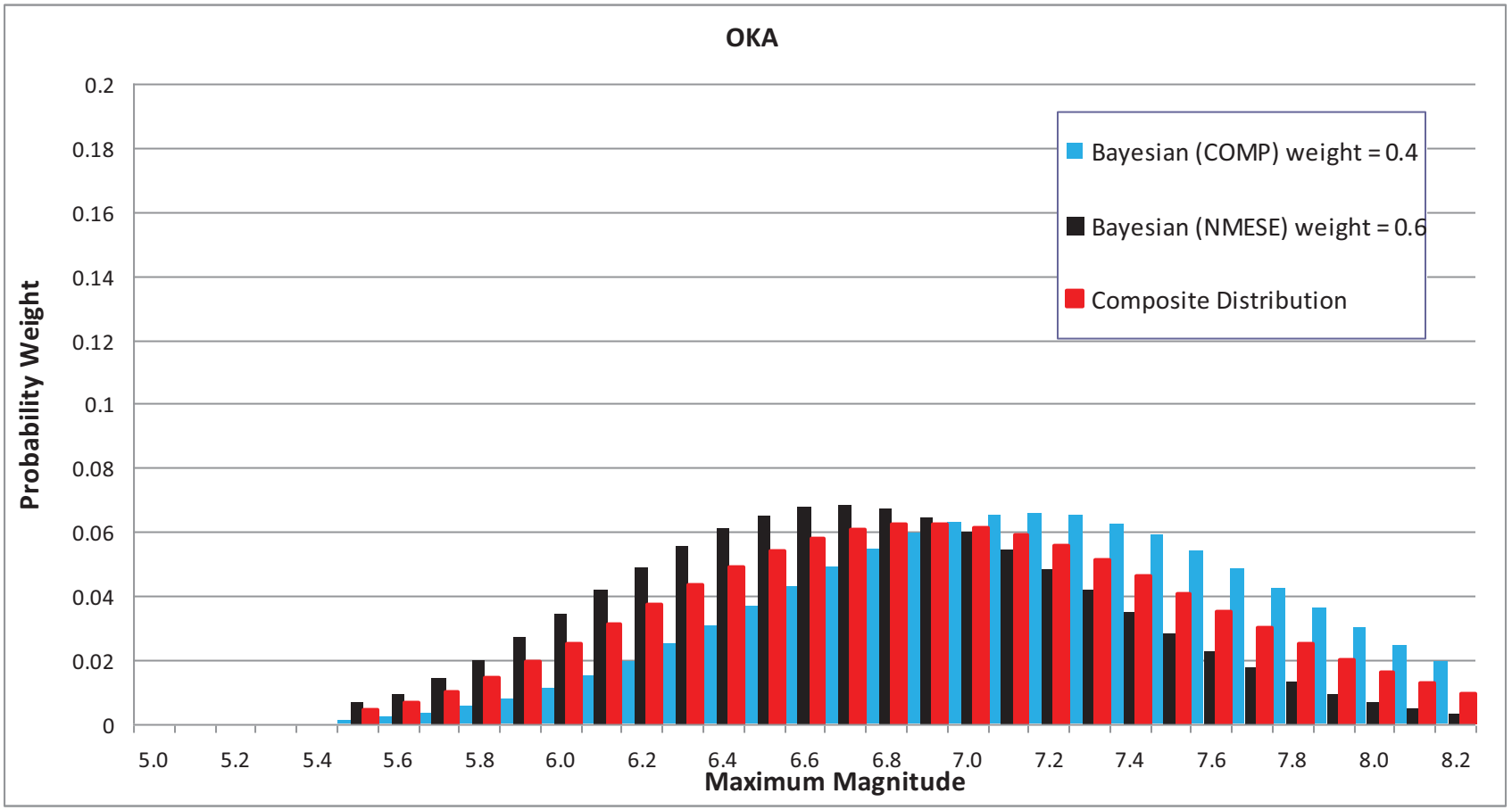

Figure 7.4.2-12
Mmax distributions for the OKA seismotectonic zone

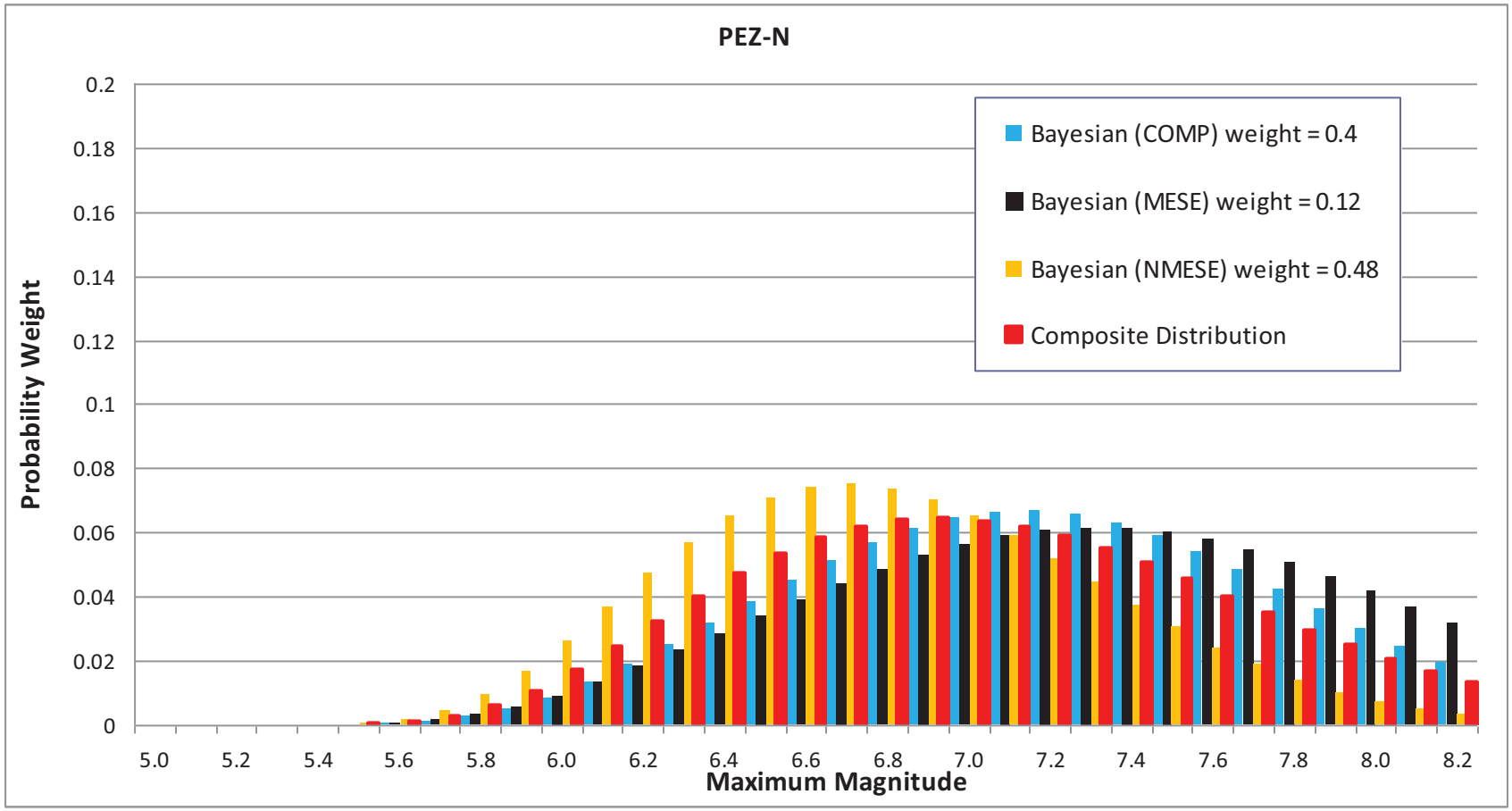

Figure 7.4.2-13
Mmax distributions for the PEZ_N seismotectonic zone

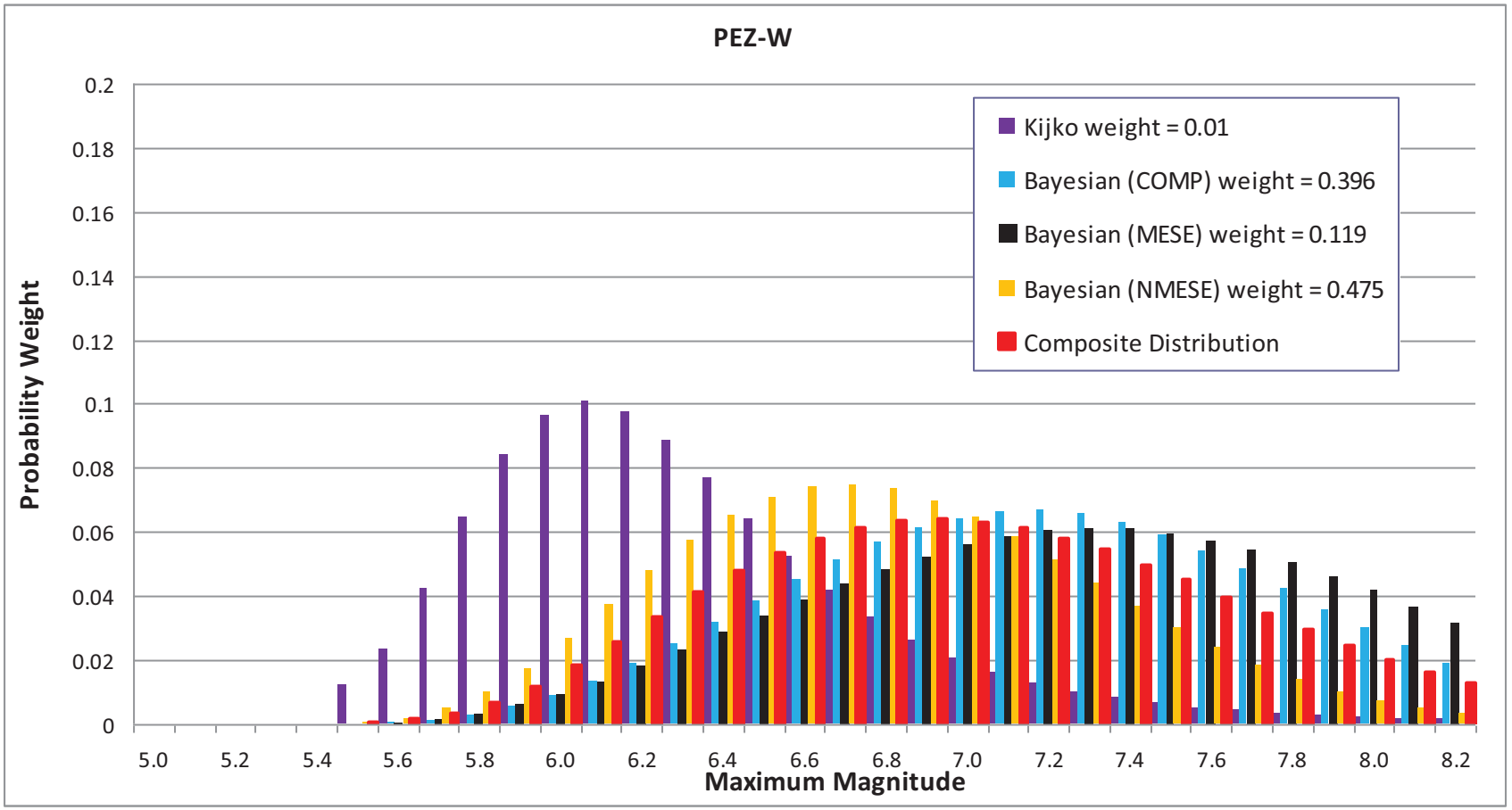

Figure 7.4.2-14
Mmax distributions for the PEZ_W seismotectonic zone

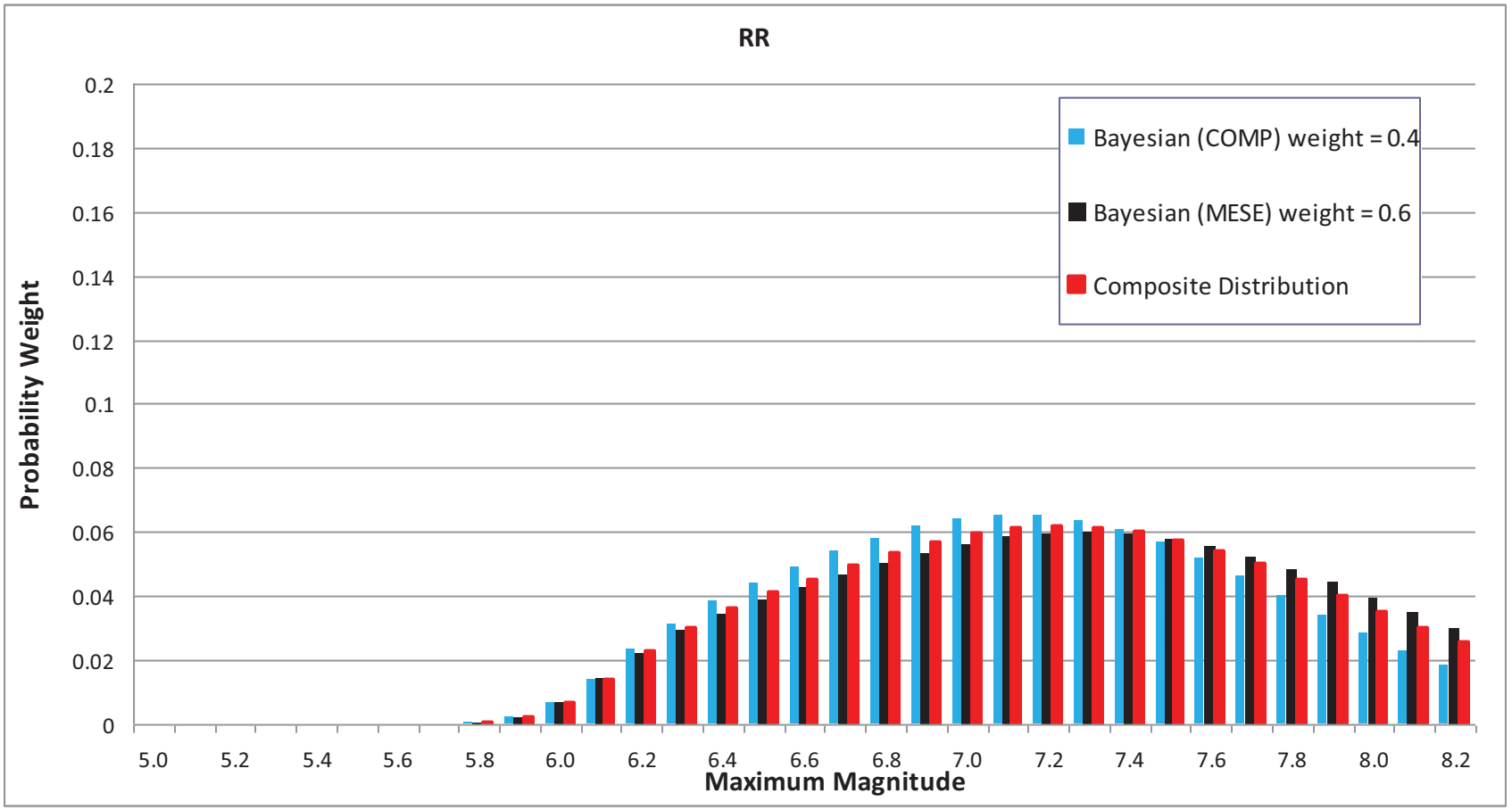

Figure 7.4.2-15
Mmax distributions for the RR seismotectonic zone

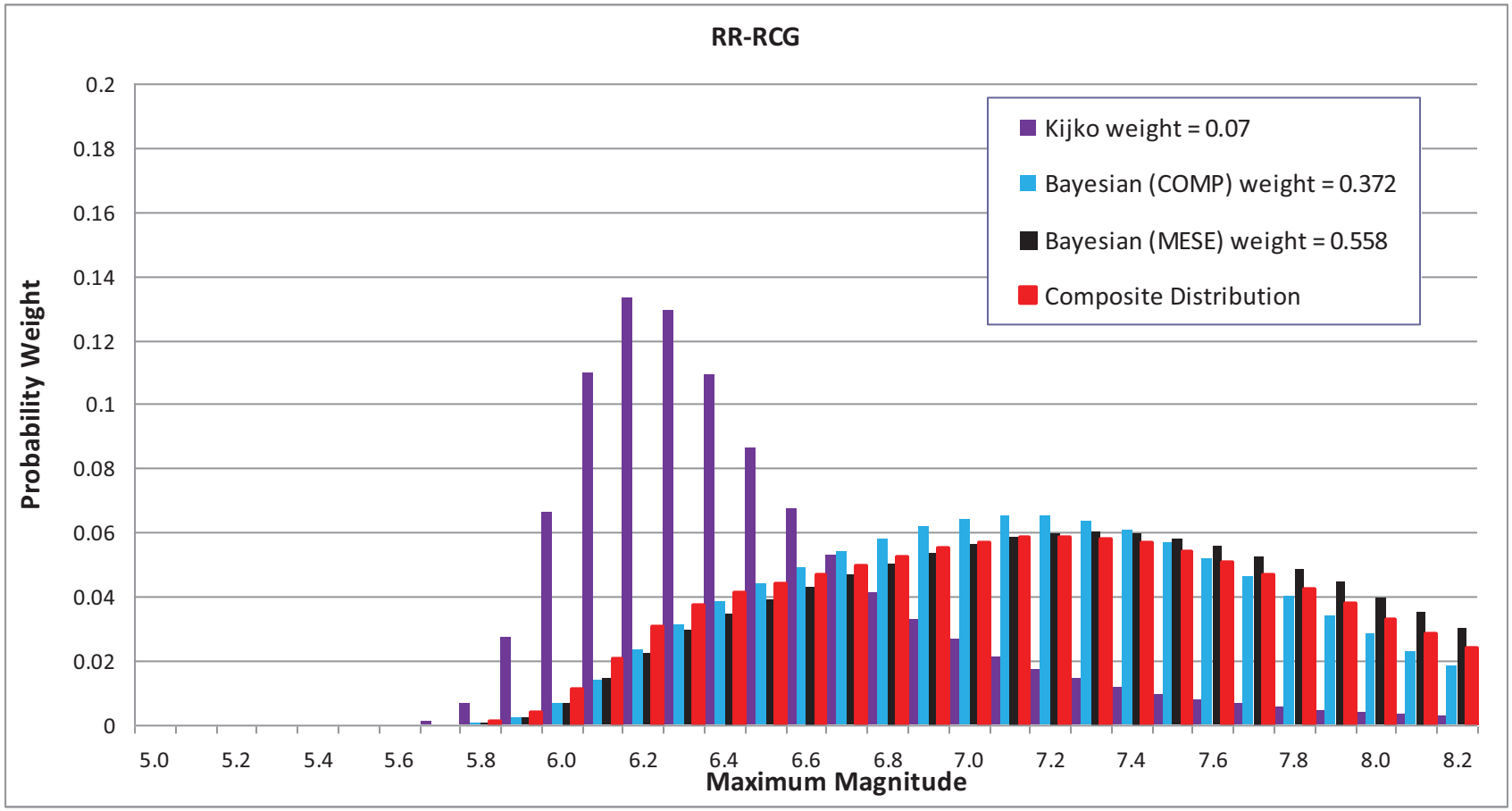

Figure 7.4.2-16
Mmax distributions for the RR_RCG seismotectonic zone

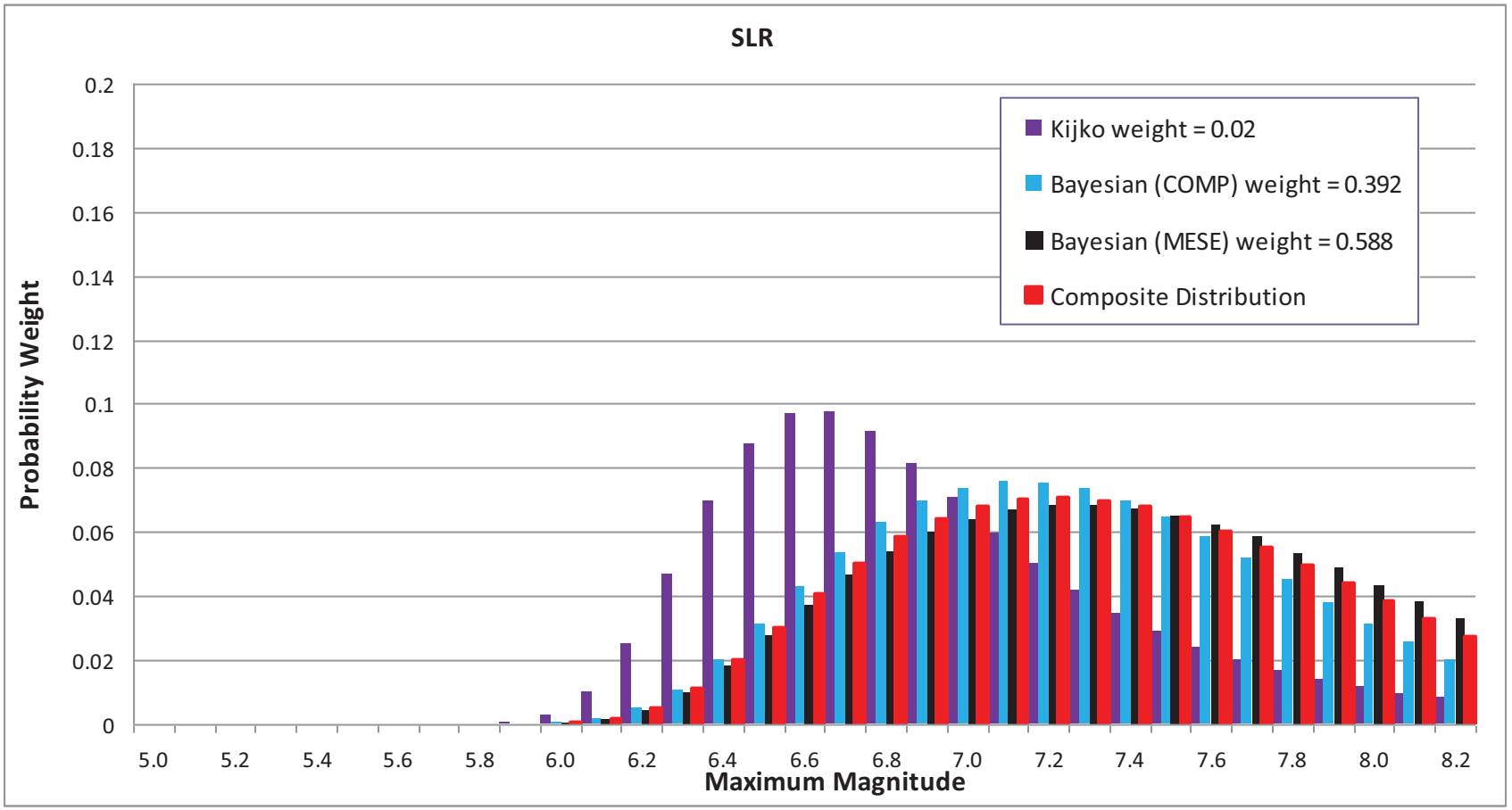

Figure 7.4.2-17
Mmax distributions for the SLR seismotectonic zone

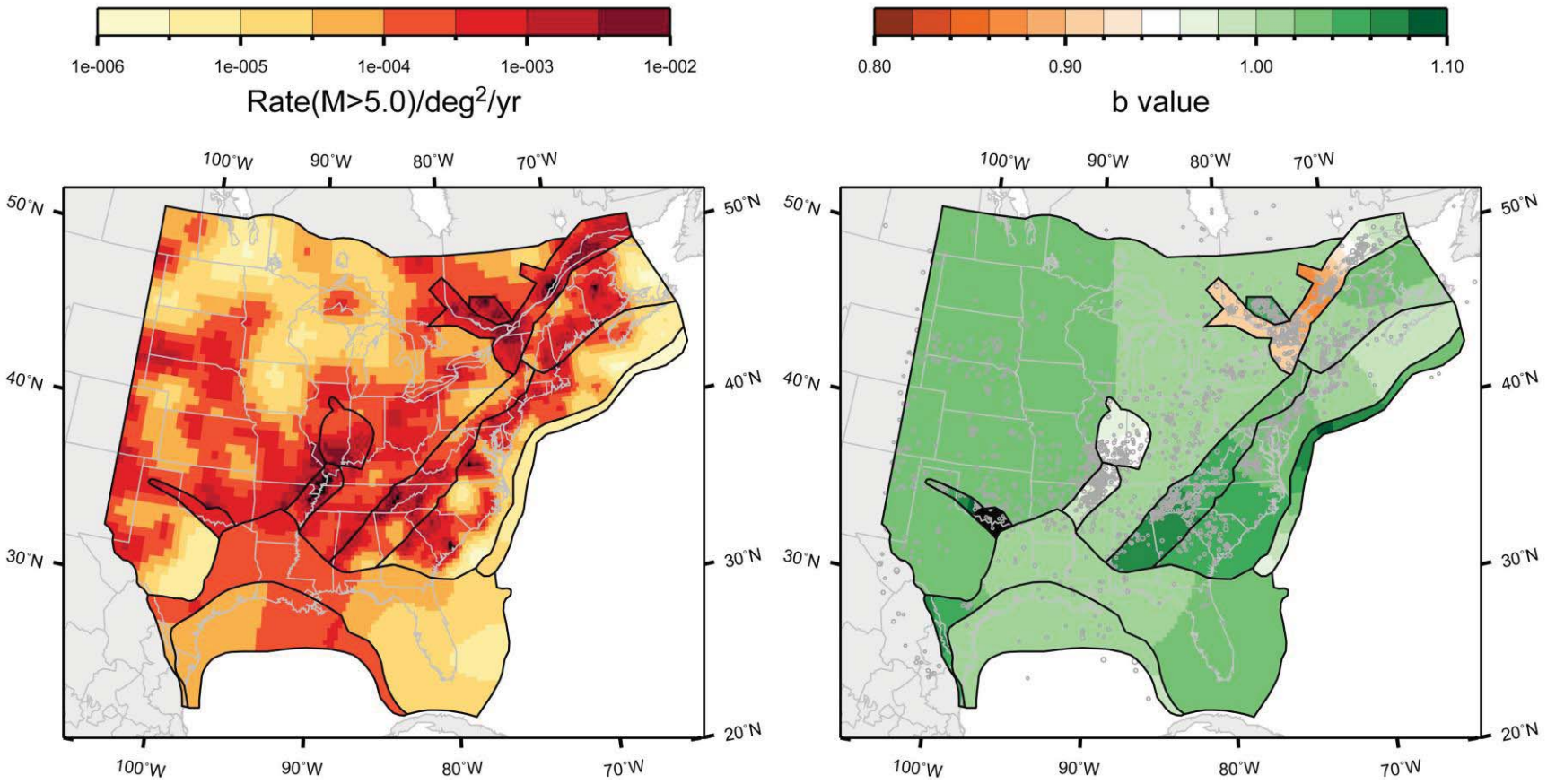

Figure 7.5.1-1
Mean map of rate and *b*-value for the study region under the source-zone configuration with narrow interpretation of PEZ, Rough Creek graben associated with Midcontinent; Case A magnitude weights

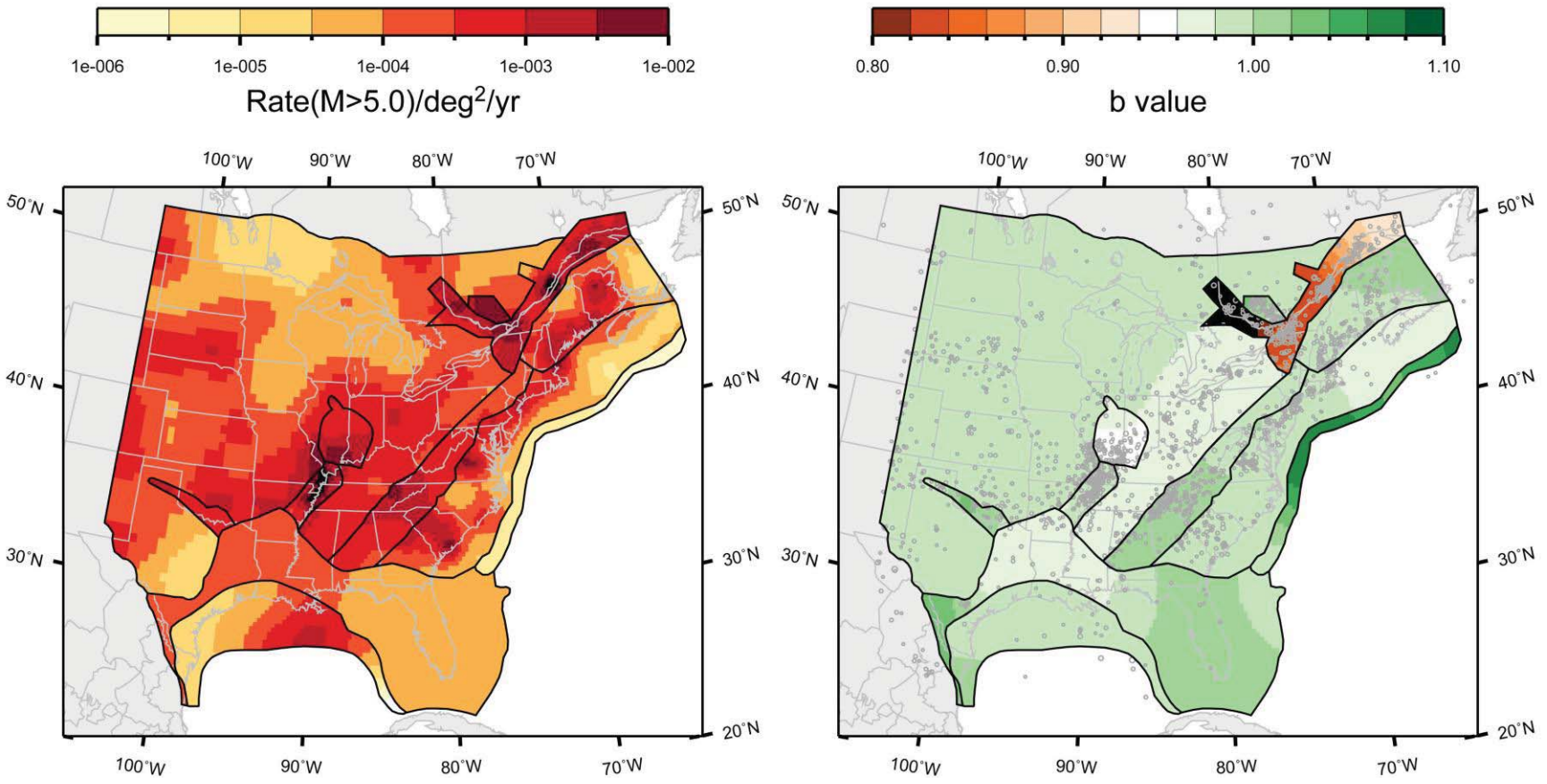

Figure 7.5.1-2
Mean map of rate and *b*-value for the study region under the source-zone configuration with narrow interpretation of PEZ, Rough Creek graben associated with Midcontinent; Case B magnitude weights

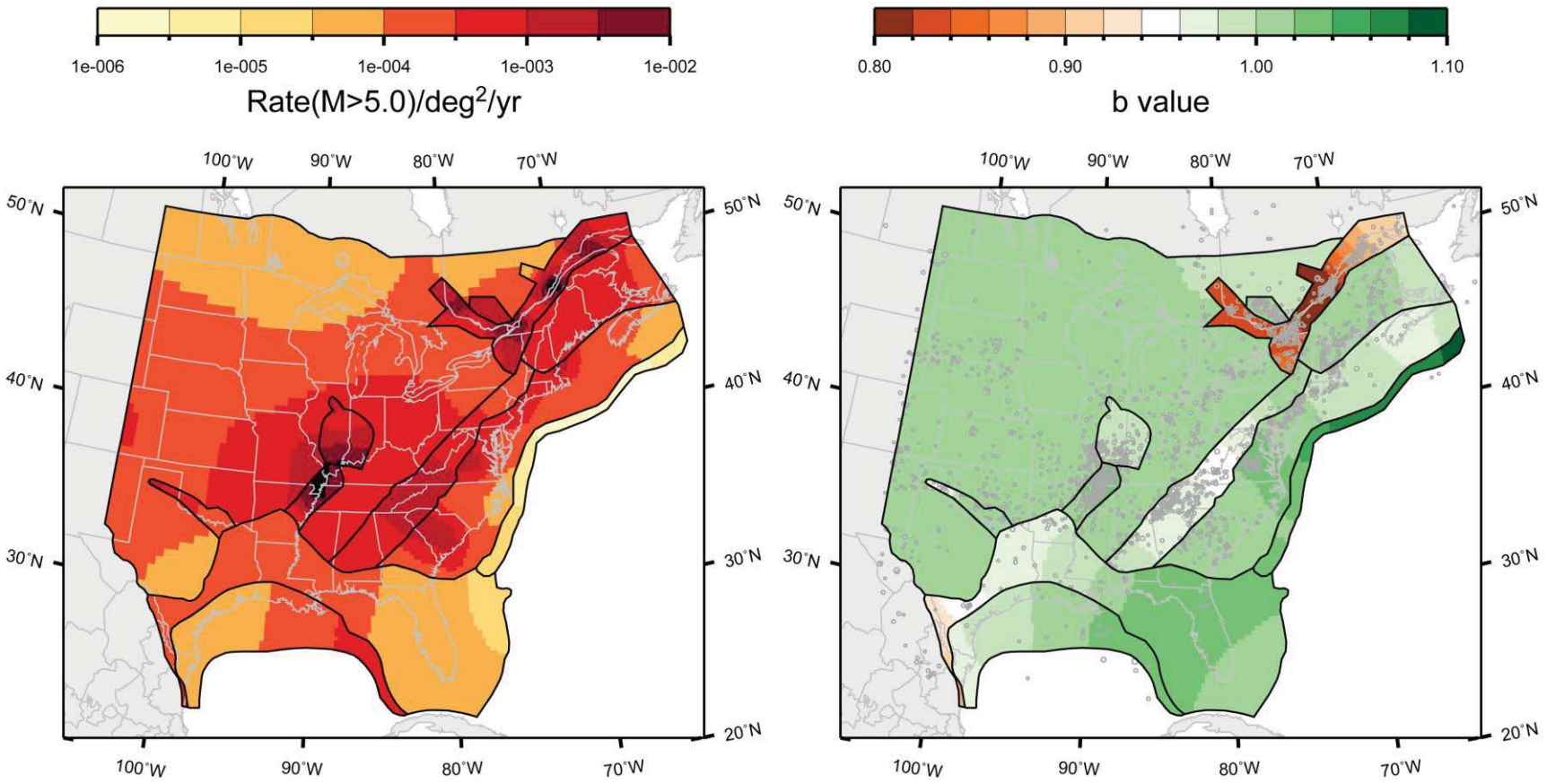

Figure 7.5.1-3
Mean map of rate and *b*-value for the study region under the source-zone configuration with narrow interpretation of PEZ, Rough Creek graben associated with Midcontinent; Case E magnitude weights

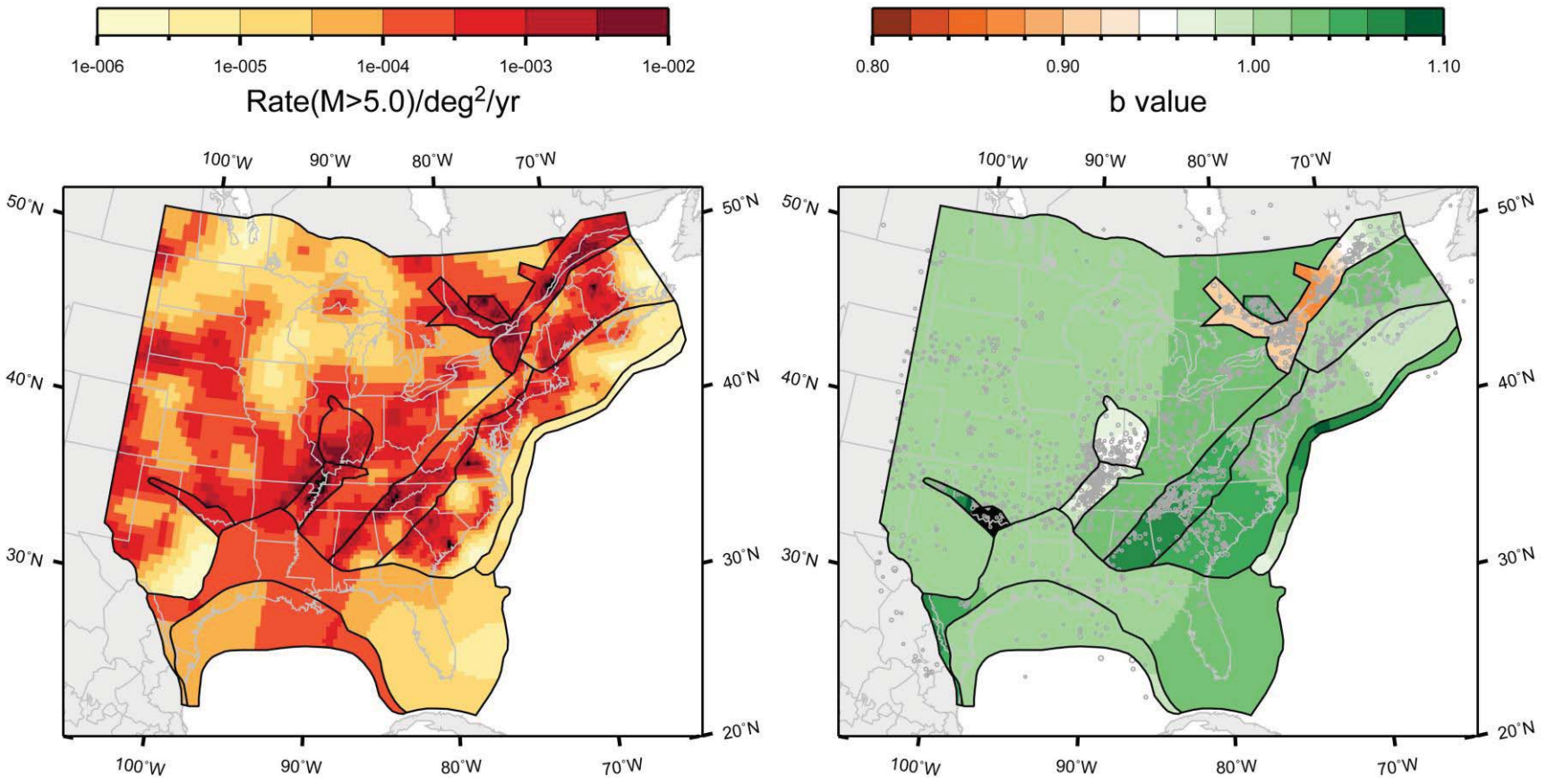

Figure 7.5.1-4
Mean map of rate and *b*-value for the study region under the source-zone configuration with narrow interpretation of PEZ, Rough Creek graben associated with Reelfoot rift; Case A magnitude weights

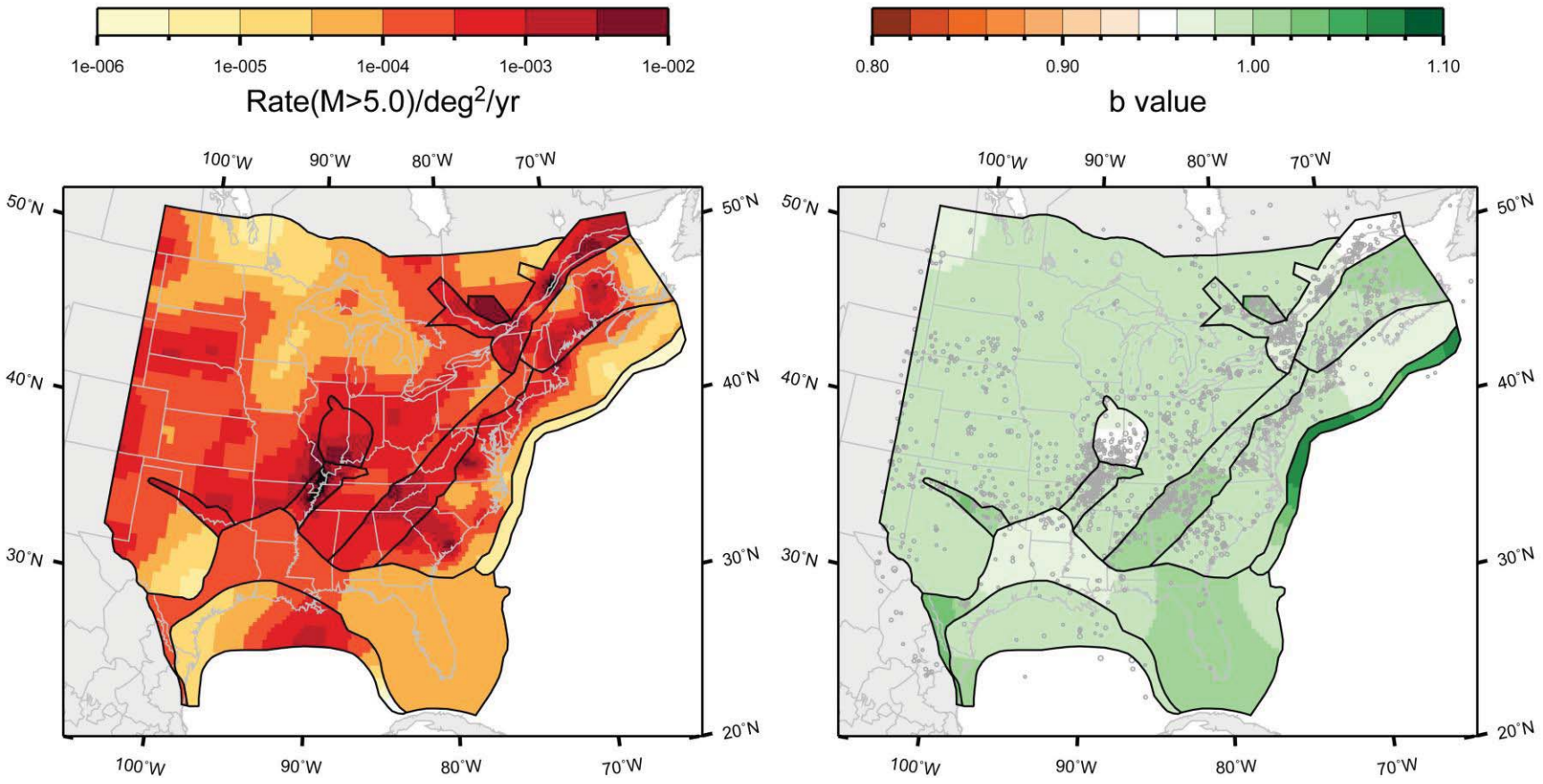

Figure 7.5.1-5
Mean map of rate and *b*-value for the study region under the source-zone configuration with narrow interpretation of PEZ, Rough Creek graben associated with Reelfoot rift; Case B magnitude weights

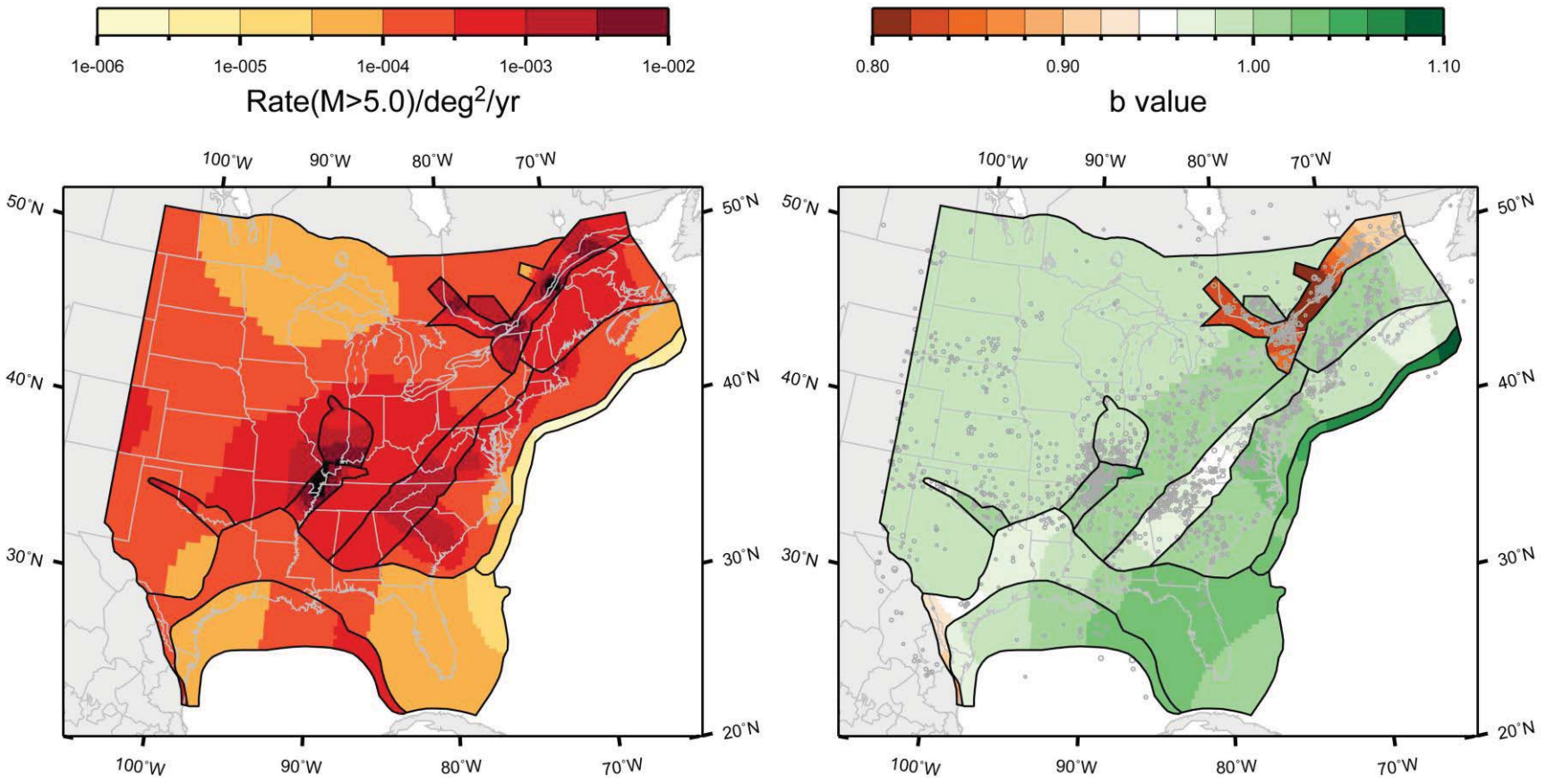

Figure 7.5.1-6
Mean map of rate and *b*-value for the study region under the source-zone configuration with narrow interpretation of PEZ, Rough Creek graben associated with Reelfoot rift; Case E magnitude weights

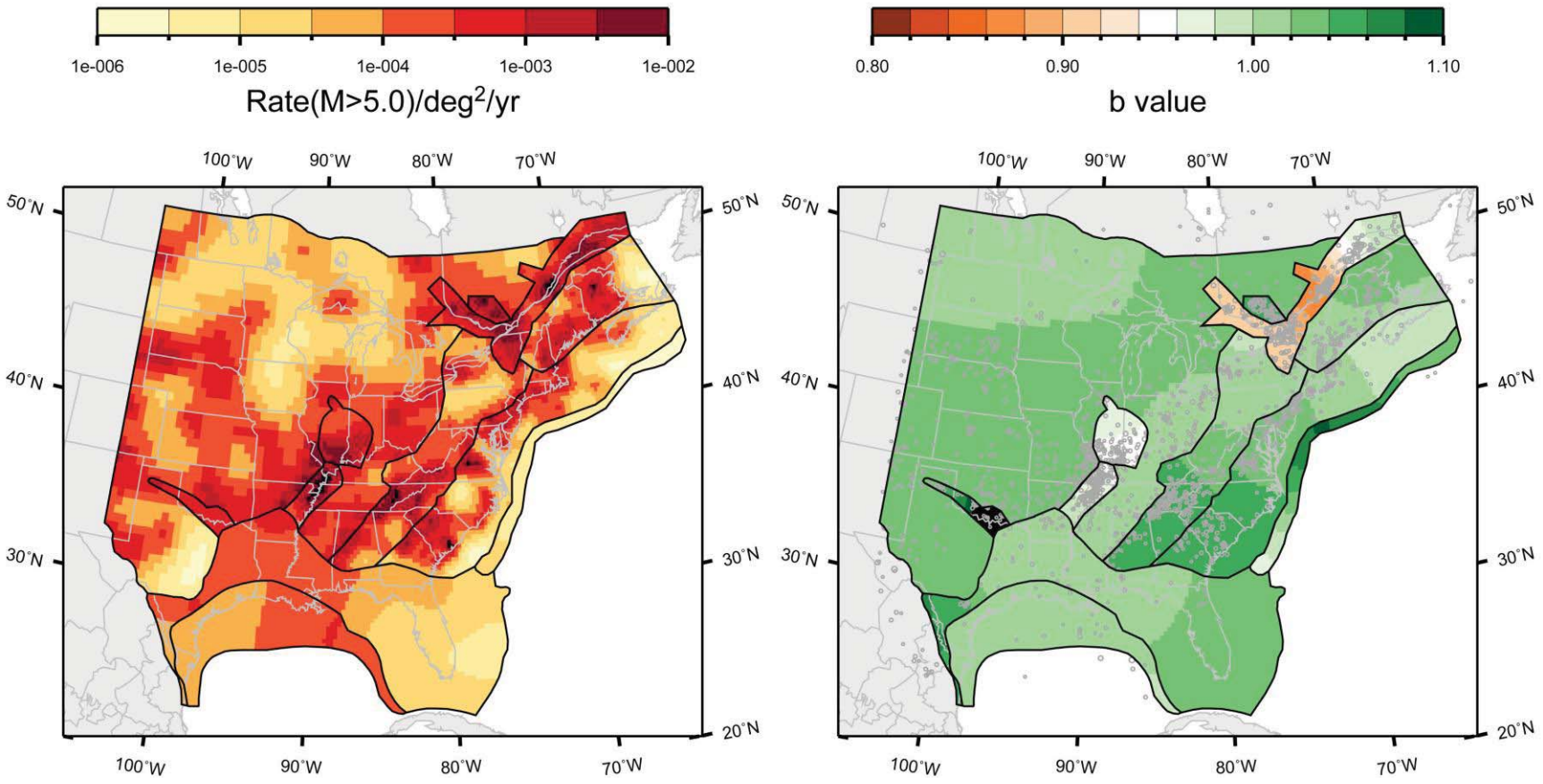

Figure 7.5.1-7
Mean map of rate and *b*-value for the study region under the source-zone configuration with wide interpretation of PEZ, Rough Creek graben associated with Midcontinent; Case A magnitude weights

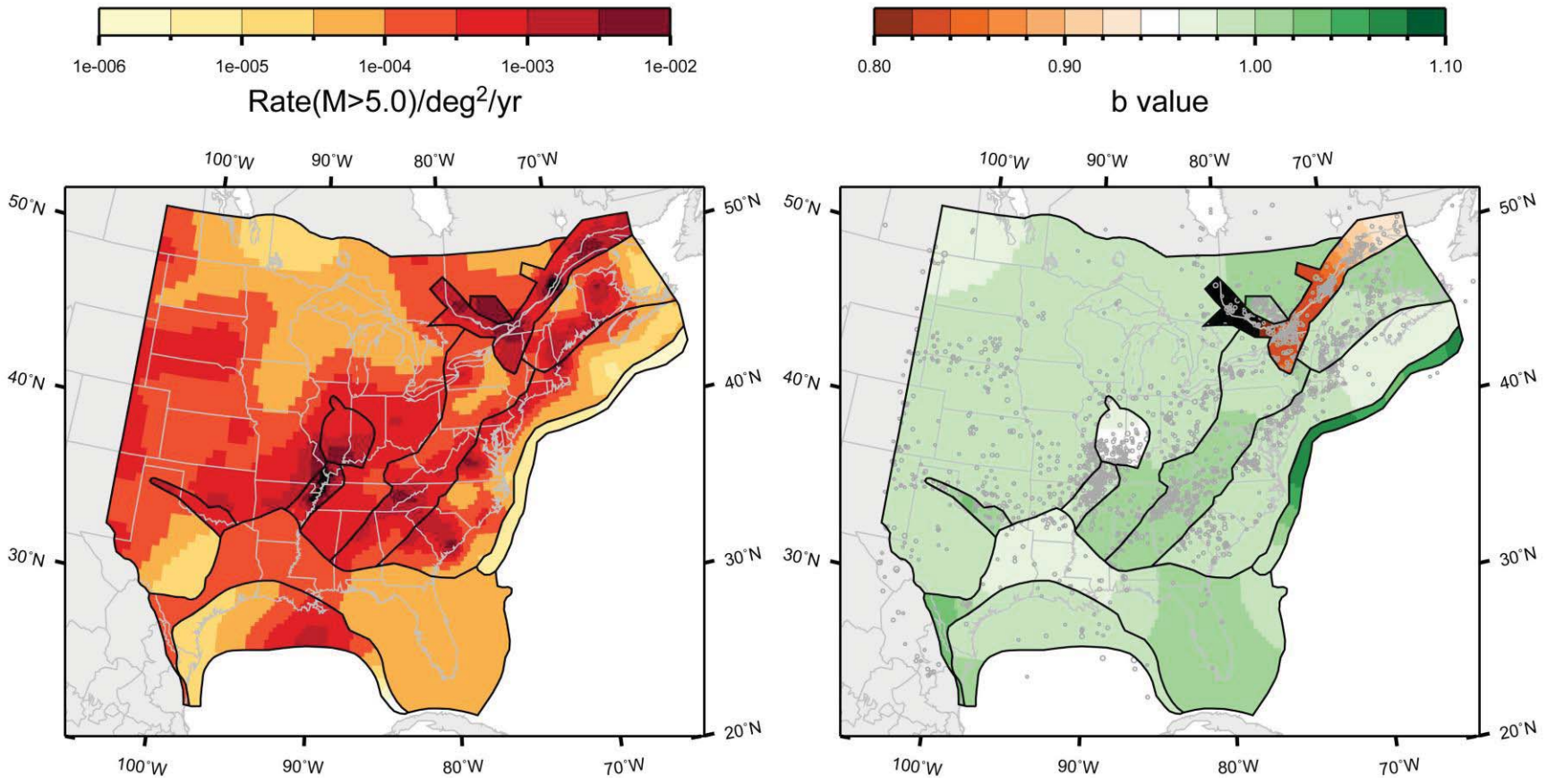

Figure 7.5.1-8
Mean map of rate and *b*-value for the study region under the source-zone configuration with wide interpretation of PEZ, Rough Creek graben associated with Midcontinent; Case B magnitude weights

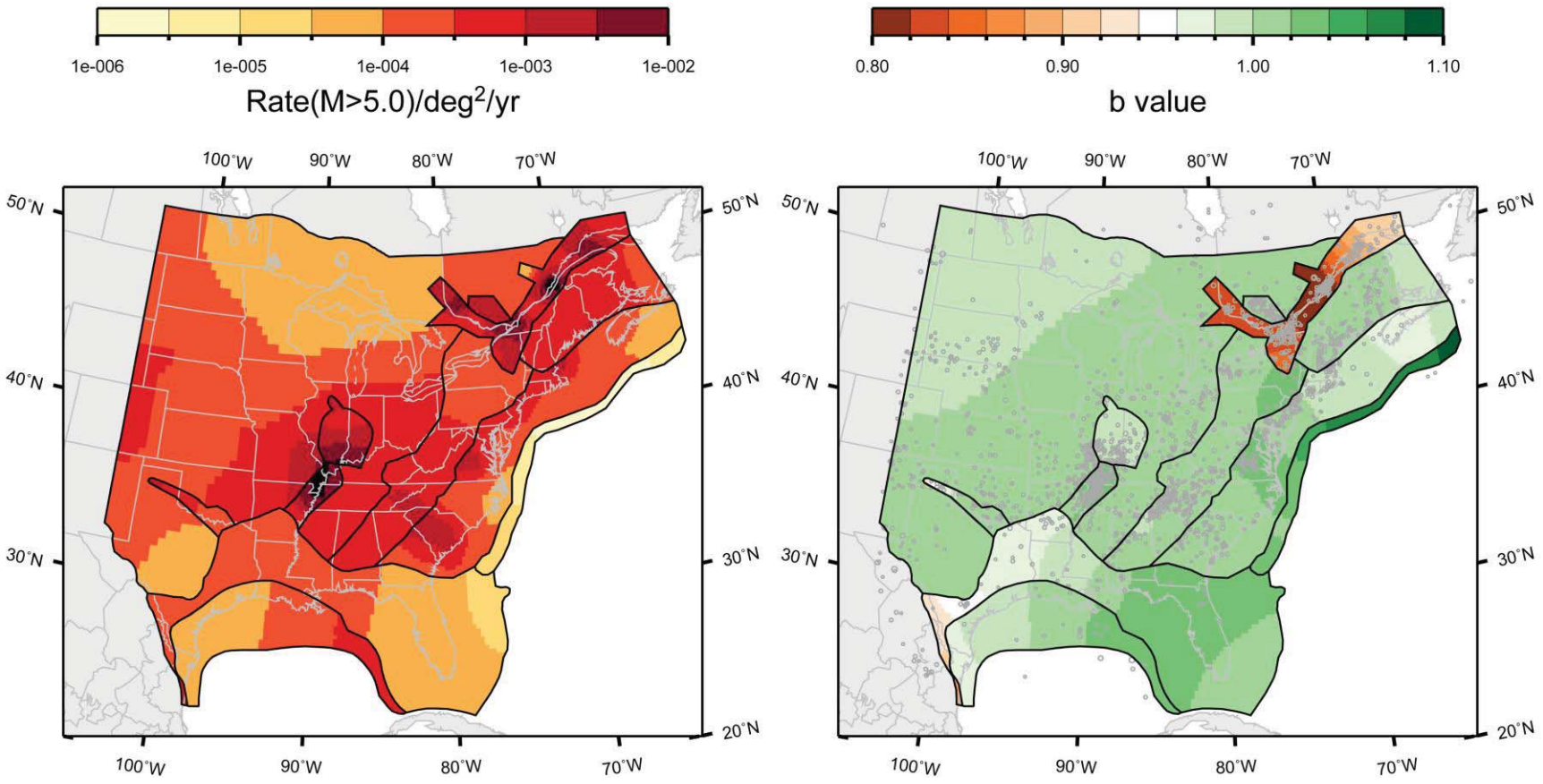

Figure 7.5.1-9
Mean map of rate and *b*-value for the study region under the source-zone configuration with wide interpretation of PEZ, Rough Creek graben associated with Midcontinent; Case E magnitude weights

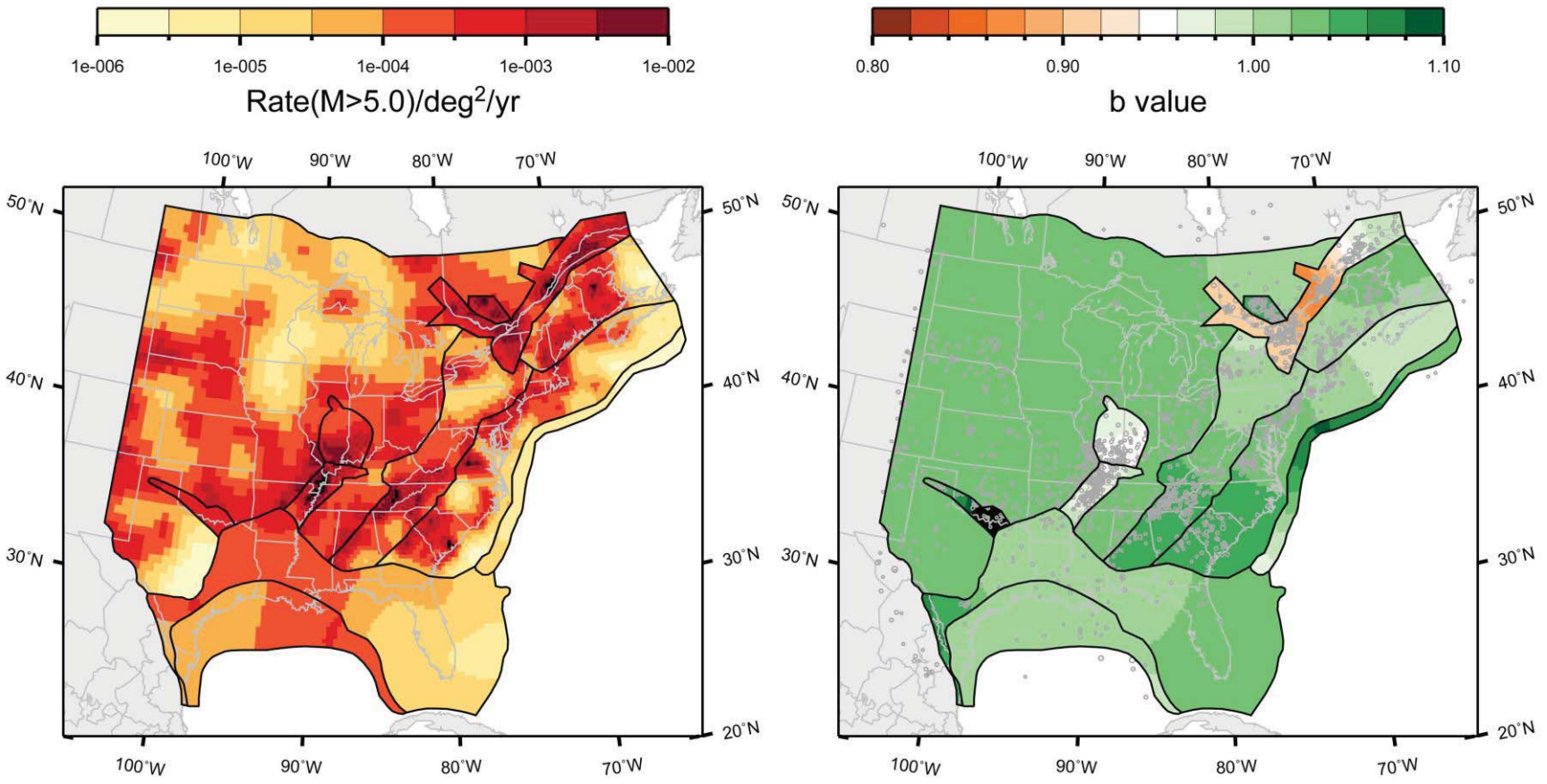

Figure 7.5.1-10
Mean map of rate and *b*-value for the study region under the source-zone configuration with wide interpretation of PEZ, Rough Creek graben associated with Reelfoot rift; Case A magnitude weights

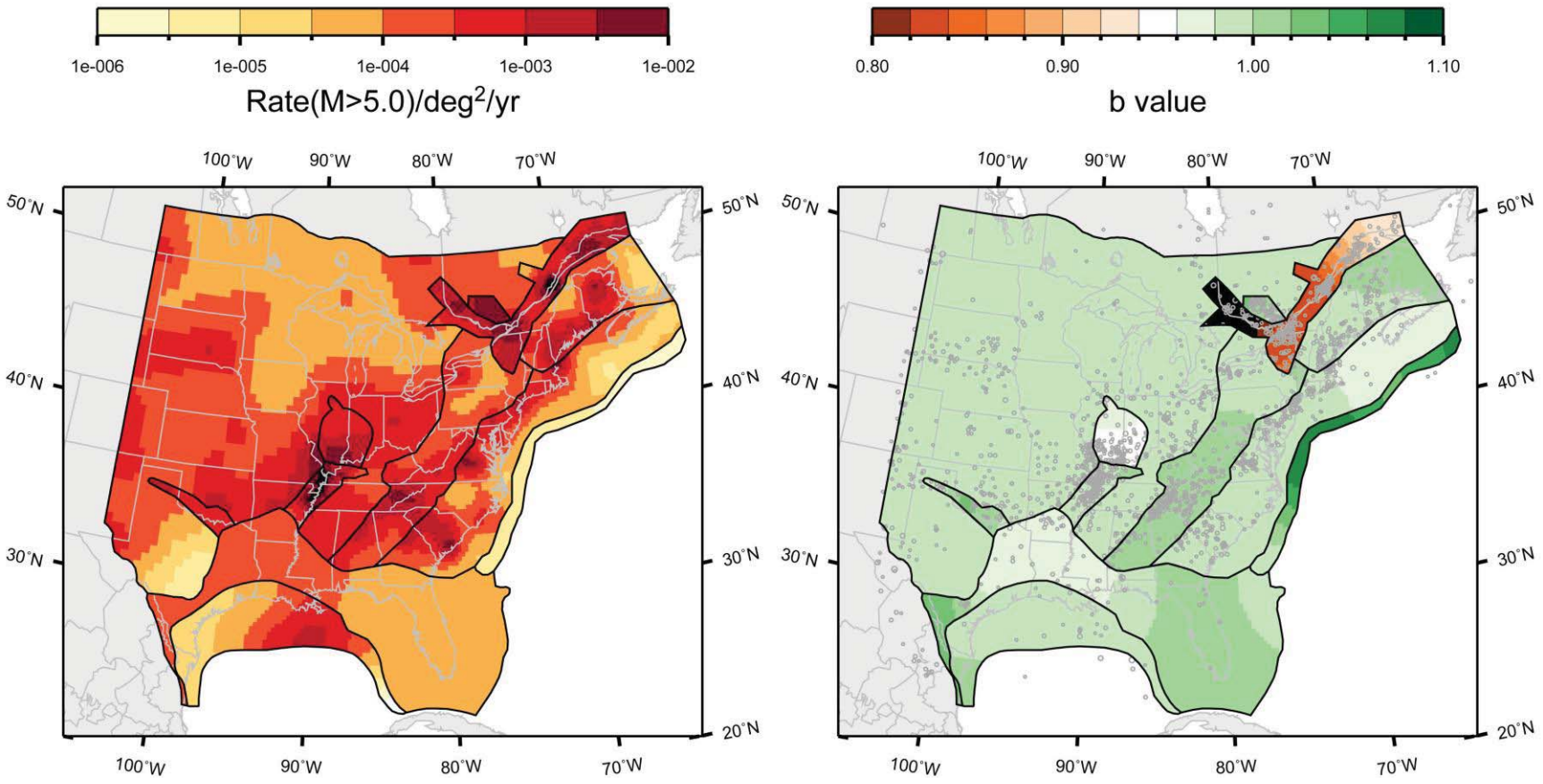

Figure 7.5.1-11
Mean map of rate and *b*-value for the study region under the source-zone configuration with wide interpretation of PEZ, Rough Creek graben associated with Reelfoot rift; Case B magnitude weights

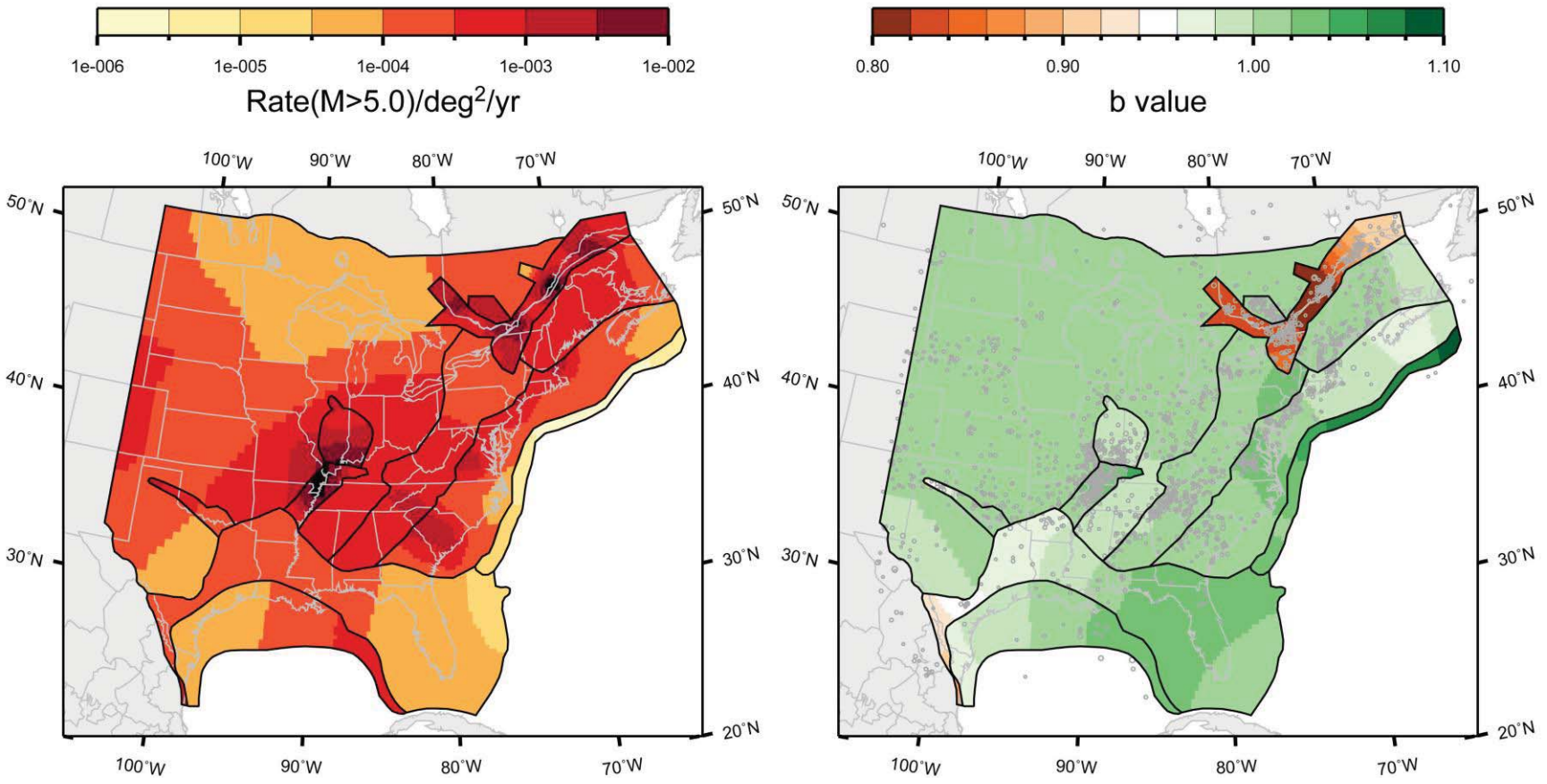

Figure 7.5.1-12
Mean map of rate and *b*-value for the study region under the source-zone configuration with wide interpretation of PEZ, Rough Creek graben associated with Reelfoot rift; Case E magnitude weights

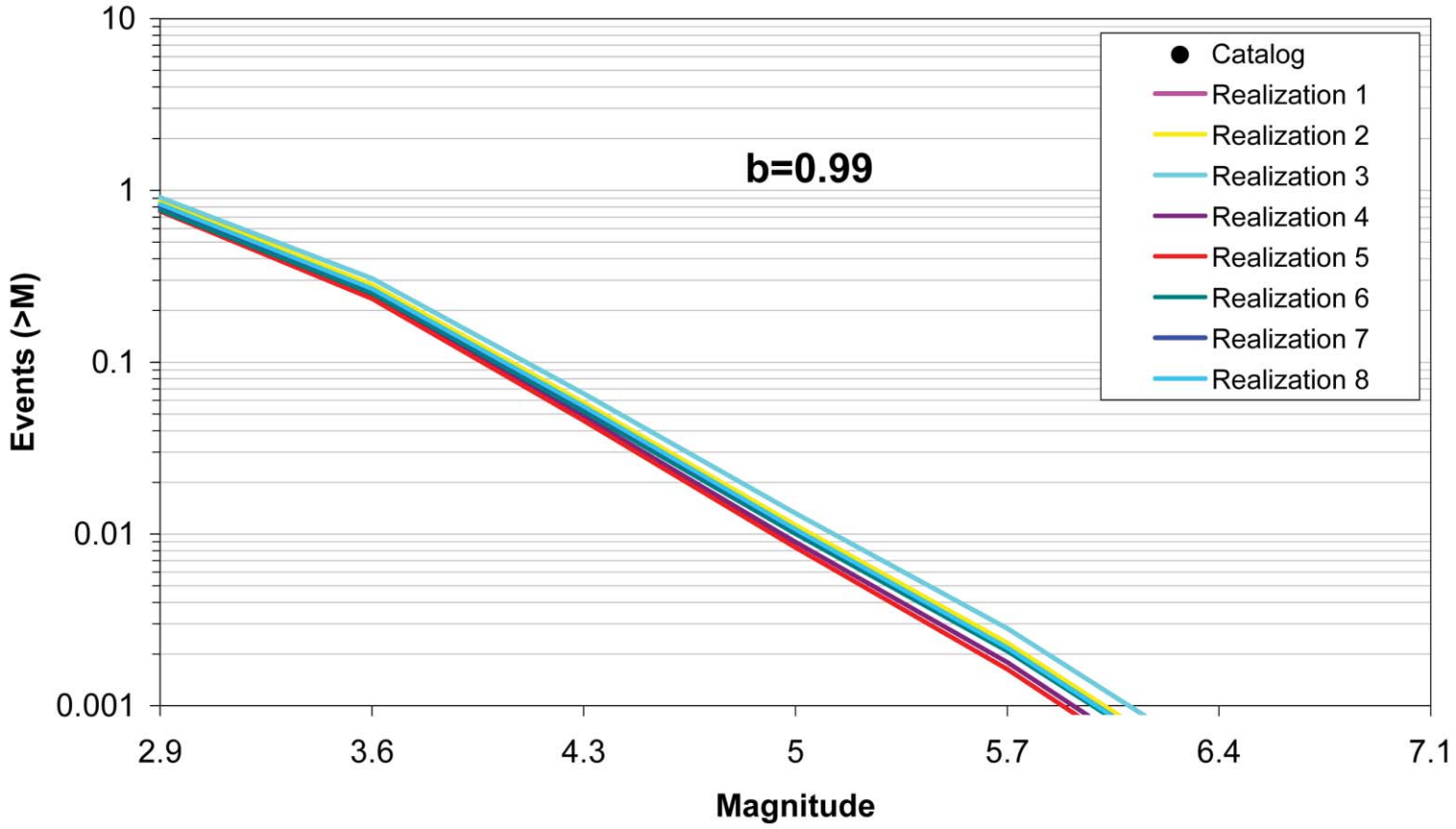

Figure 7.5.2-1
Comparison of model-predicted earthquake counts for AHEX using Case A magnitude weights. No earthquake counts are shown because this source zone contains no seismicity.

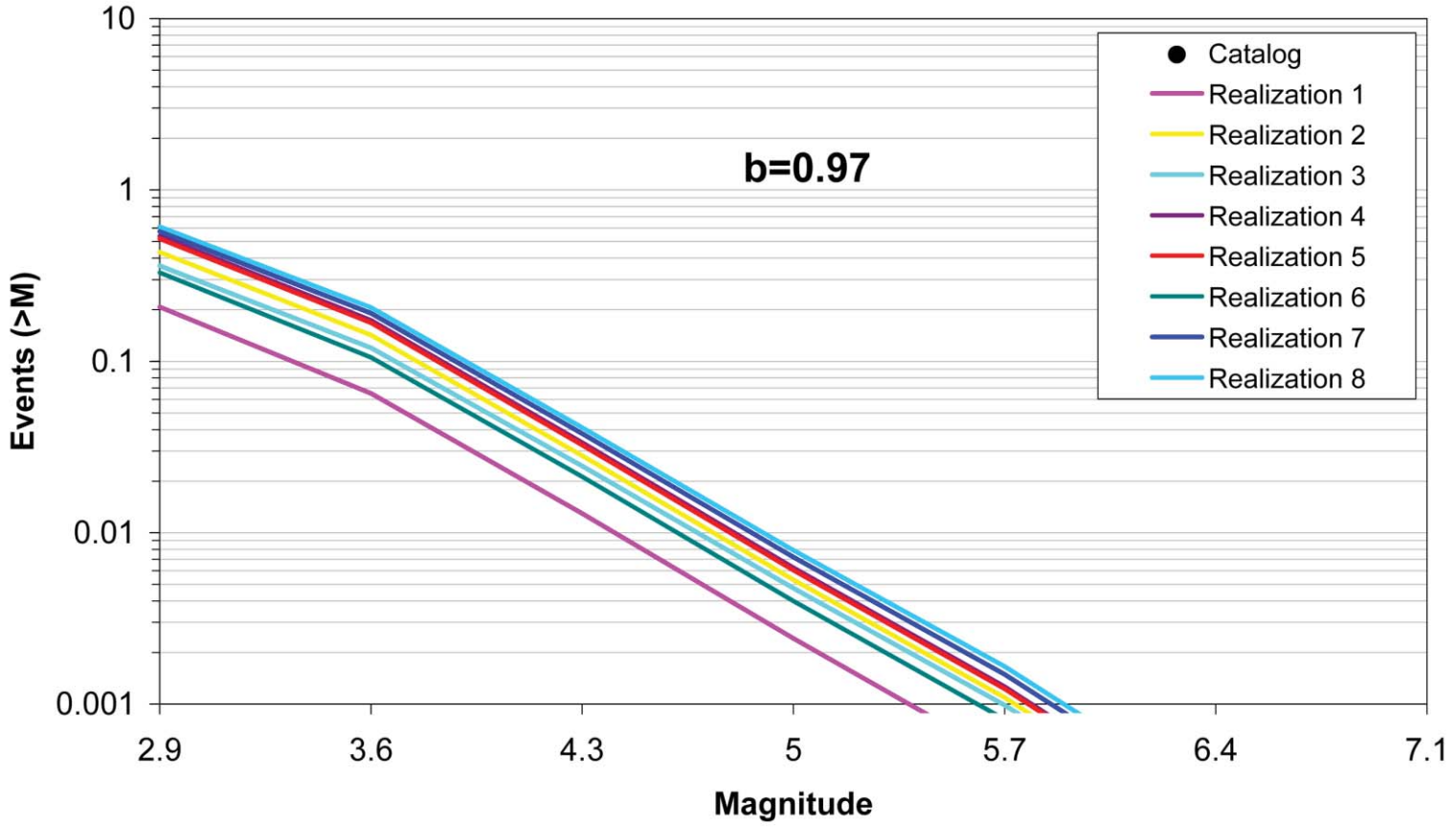

Figure 7.5.2-2
Comparison of model-predicted earthquake counts for AHEX using Case B magnitude weights. No earthquake counts are shown because this source zone contains no seismicity.

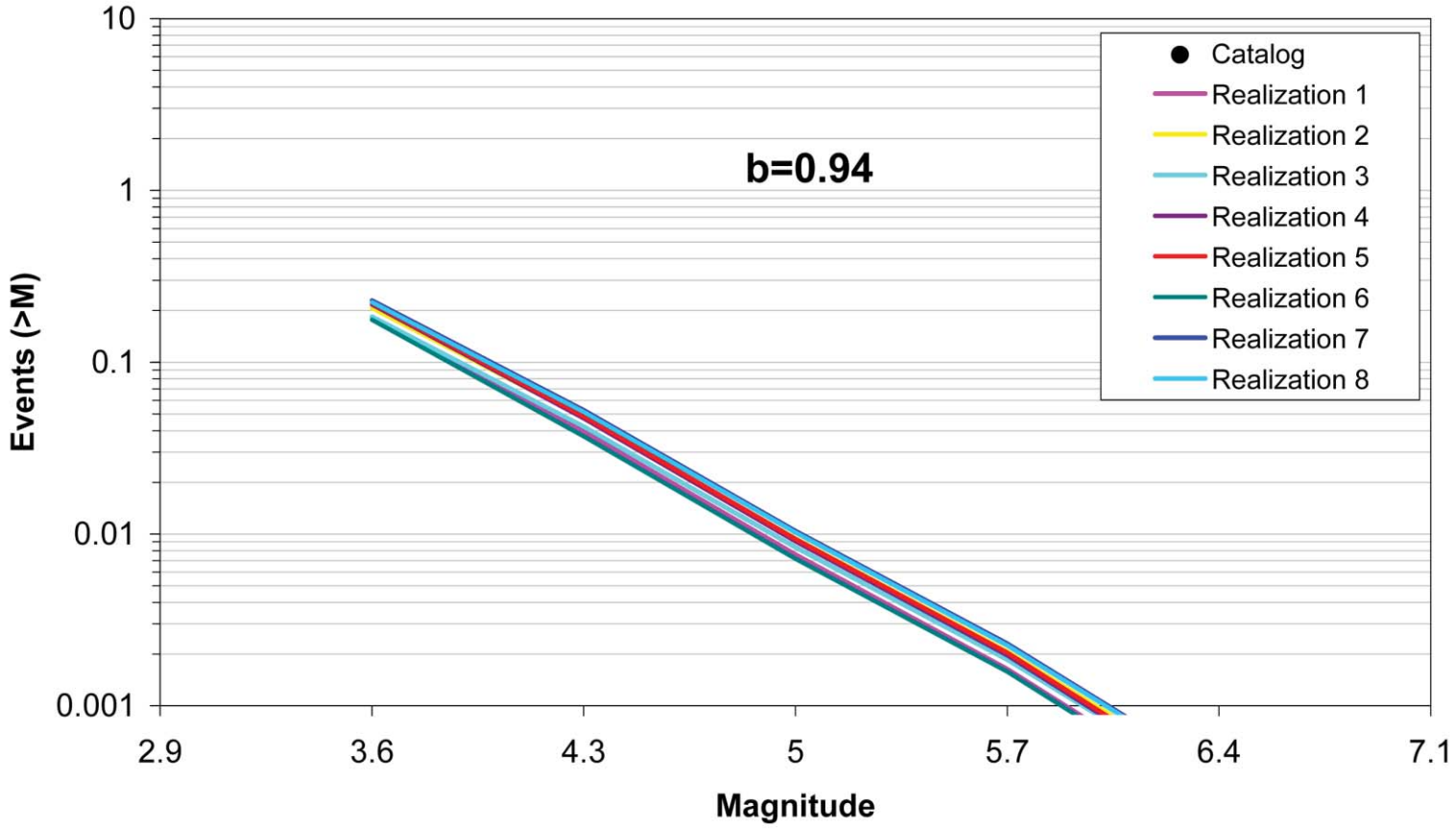

Figure 7.5.2-3
Comparison of model-predicted earthquake counts for AHEX using Case E magnitude weights. No earthquake counts are shown because this source zone contains no seismicity.

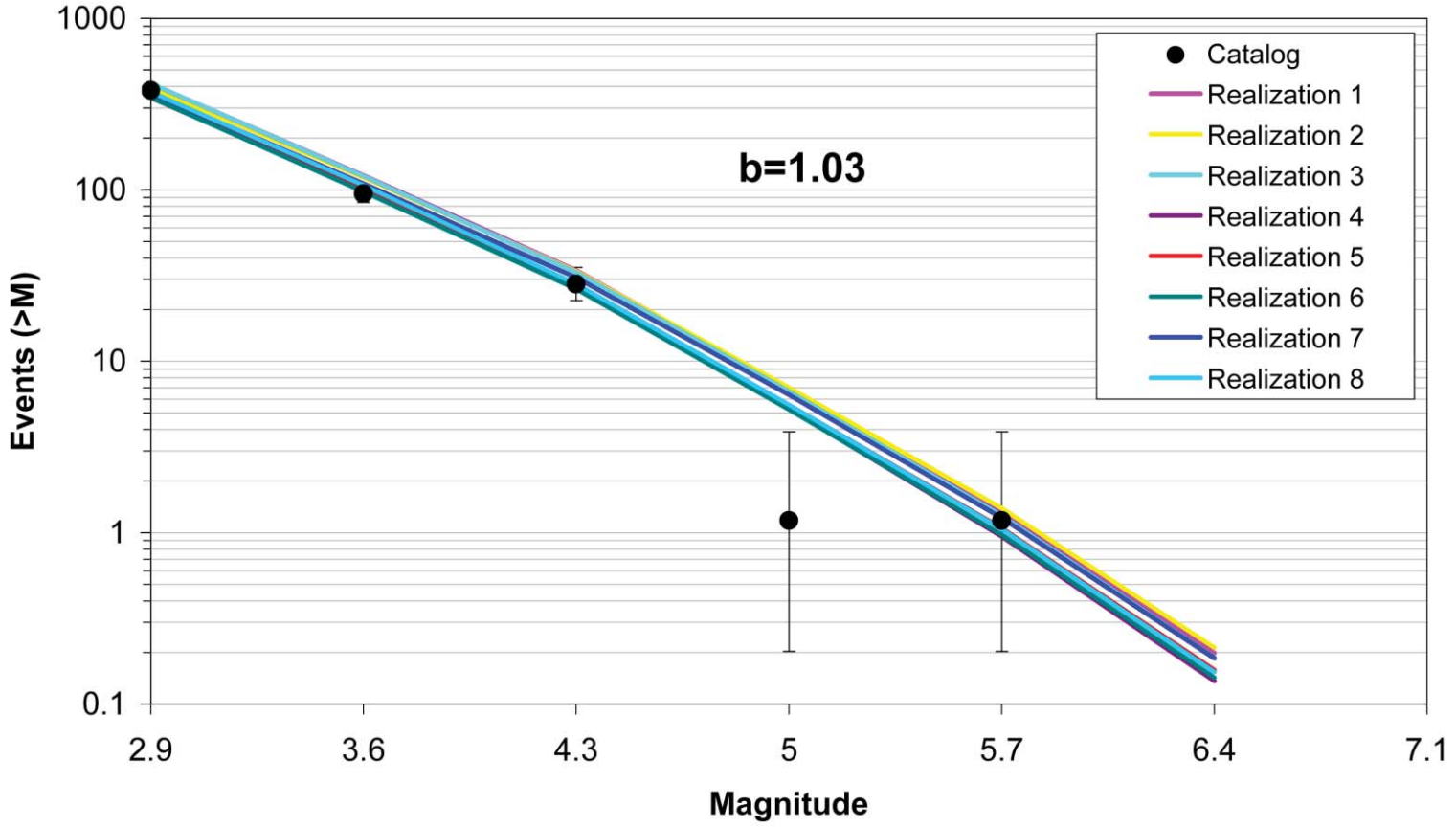

Figure 7.5.2-4
Comparison of model-predicted earthquake counts for ECC_AM using Case A magnitude weights. The error bars represent the 16%–84% uncertainty associated with the data, computed using the Weichert (1980) procedure.

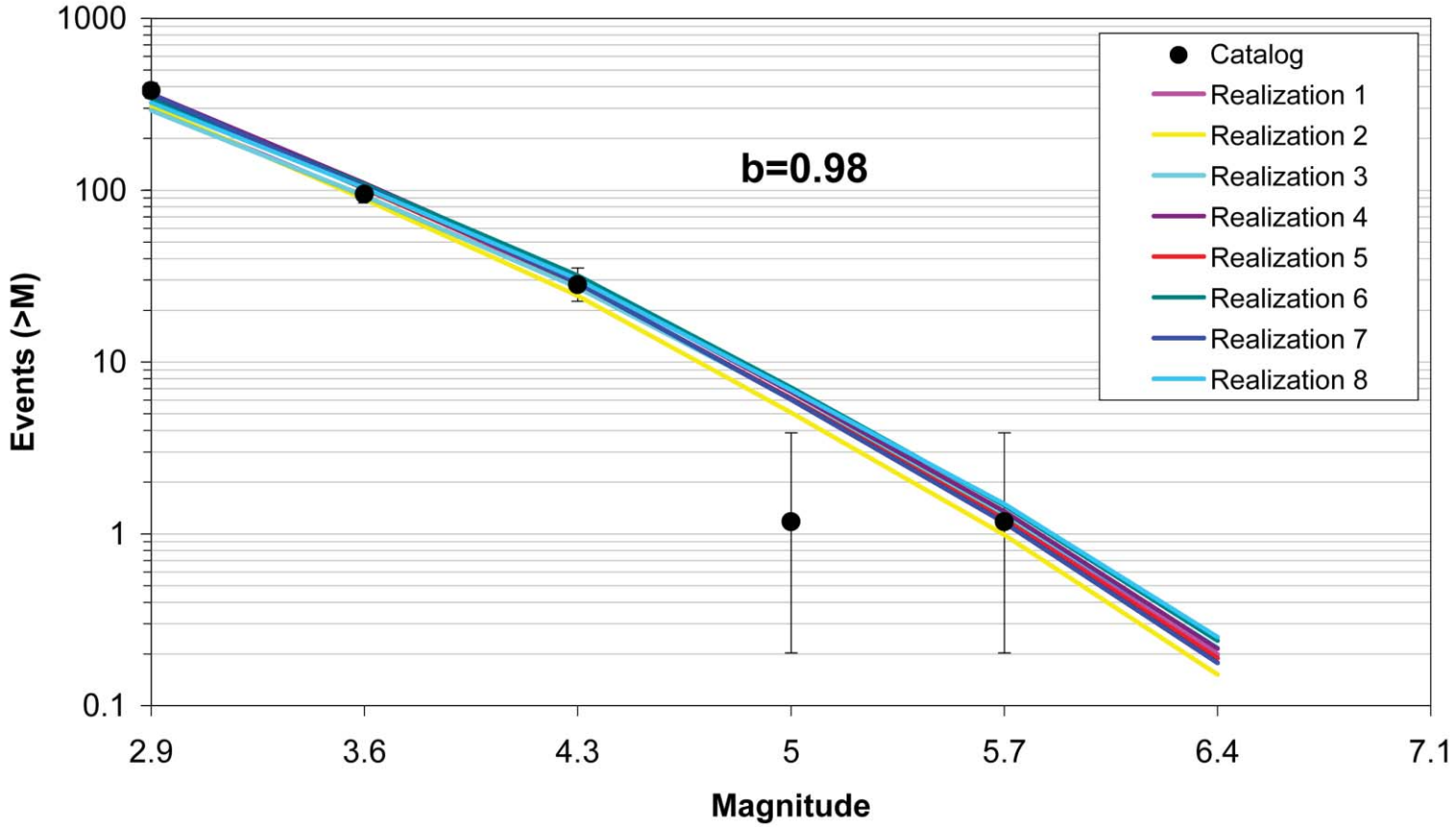

Figure 7.5.2-5
Comparison of model-predicted earthquake counts for ECC_AM using Case B magnitude weights. Error bars as in Figure 7.5.2-4.

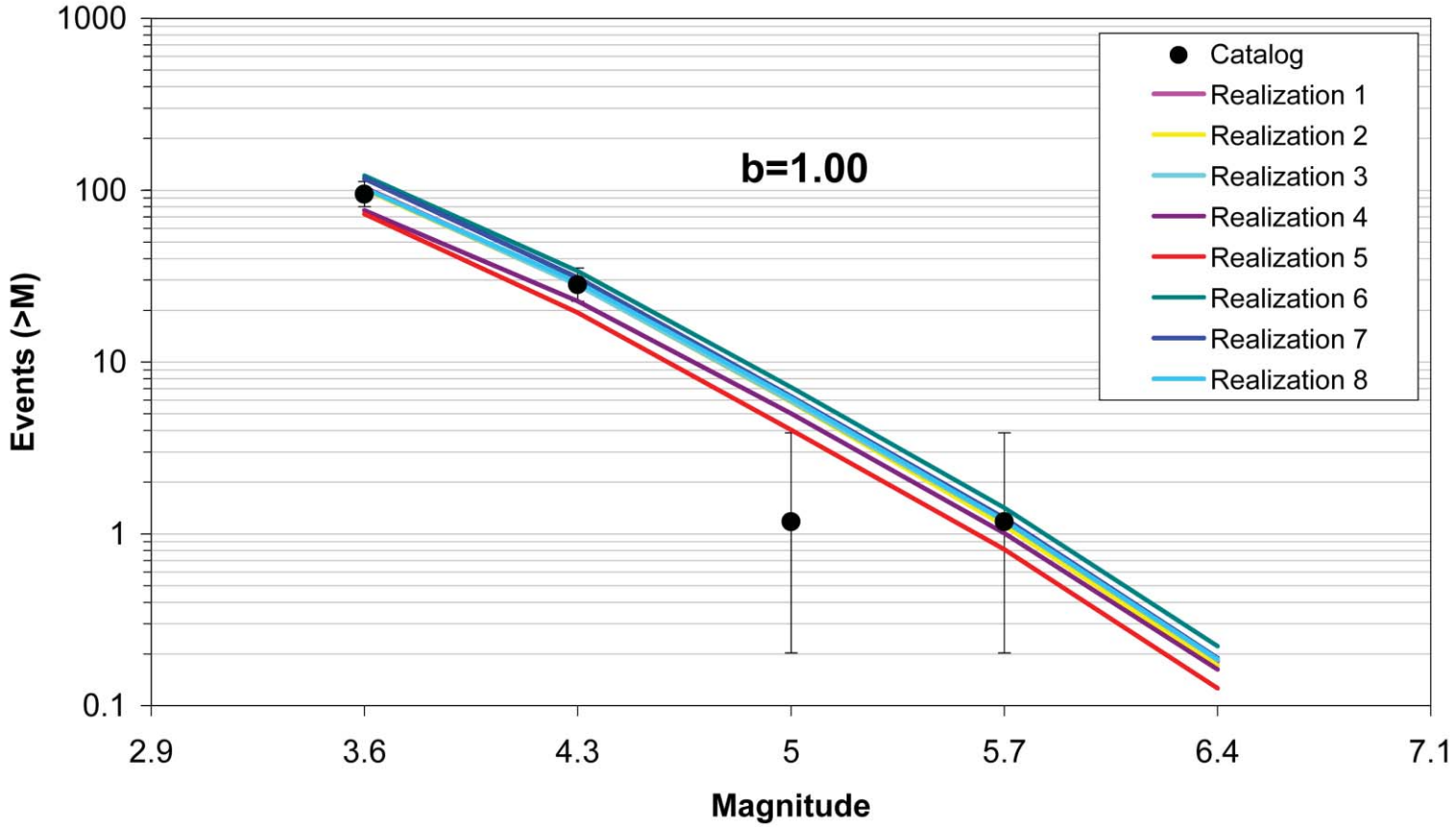

Figure 7.5.2-6
Comparison of model-predicted earthquake counts for ECC_AM using Case E magnitude weights. Error bars as in Figure 7.5.2-4.

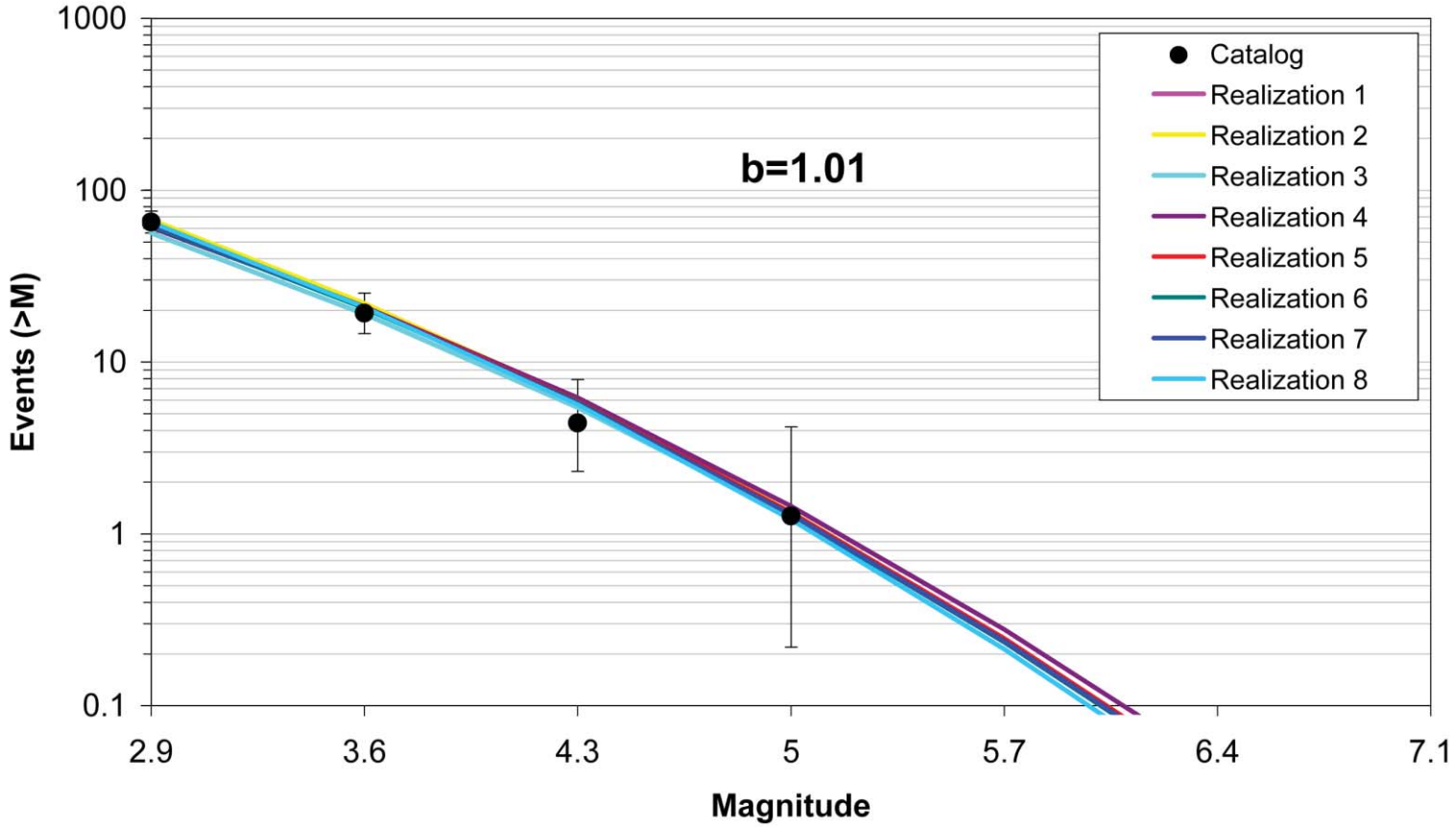

Figure 7.5.2-7
Comparison of model-predicted earthquake counts for ECC_GC using Case A magnitude weights. Error bars as in Figure 7.5.2-4.

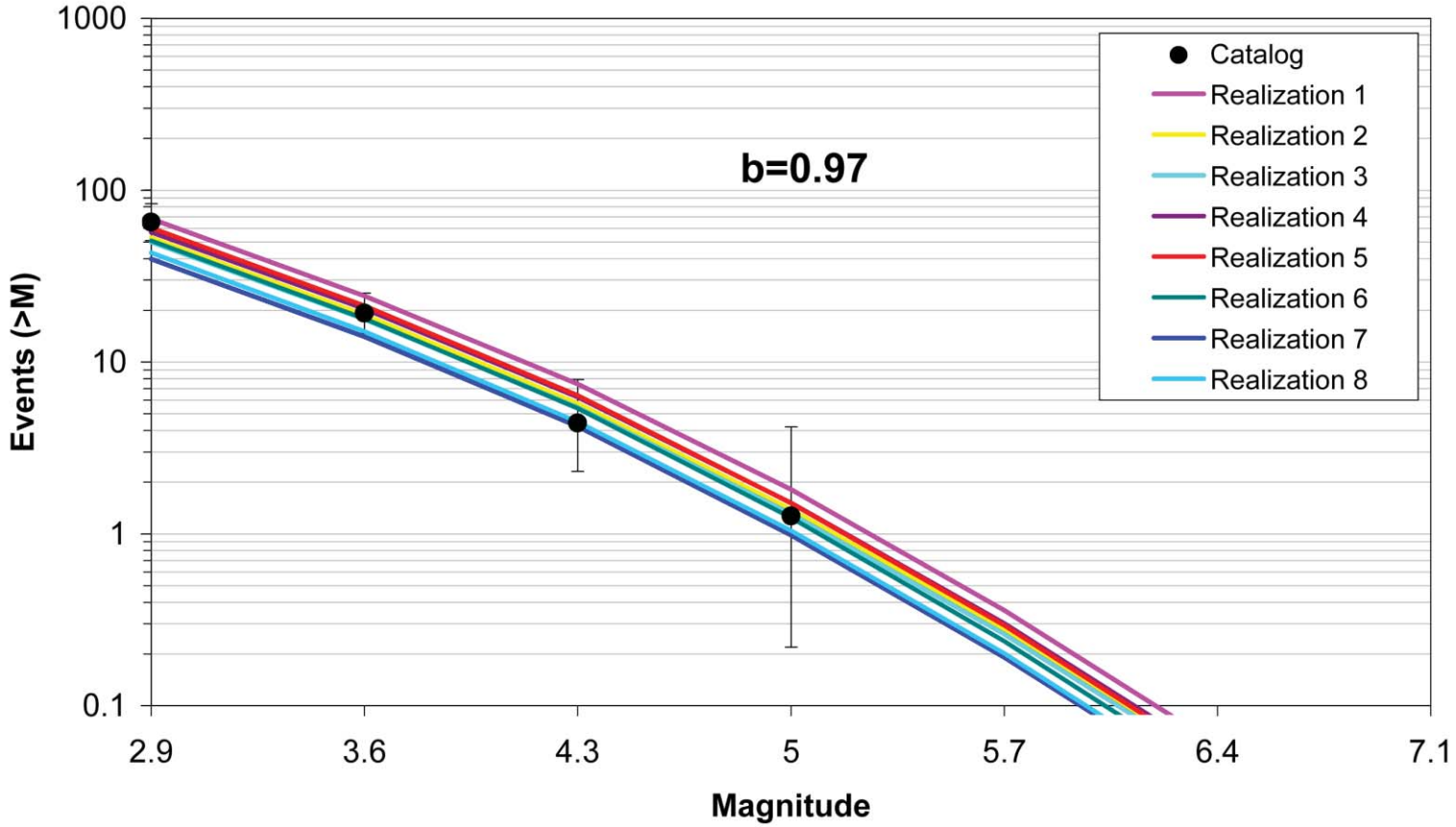

Figure 7.5.2-8
Comparison of model-predicted earthquake counts for ECC_GC using Case B magnitude weights. Error bars as in Figure 7.5.2-4.

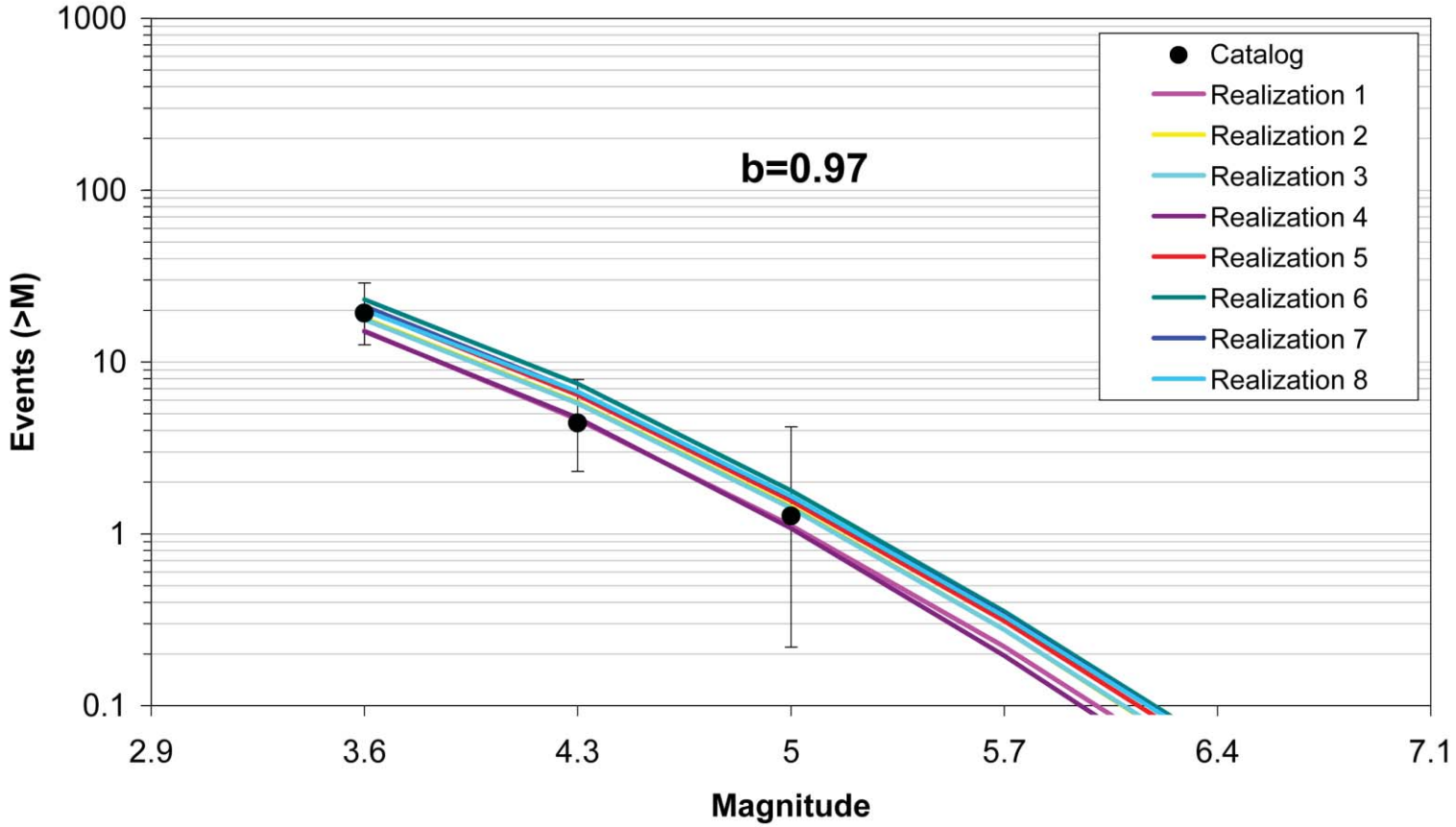

Figure 7.5.2-9
Comparison of model-predicted earthquake counts for ECC_GC using Case E magnitude weights. Error bars as in Figure 7.5.2-4.

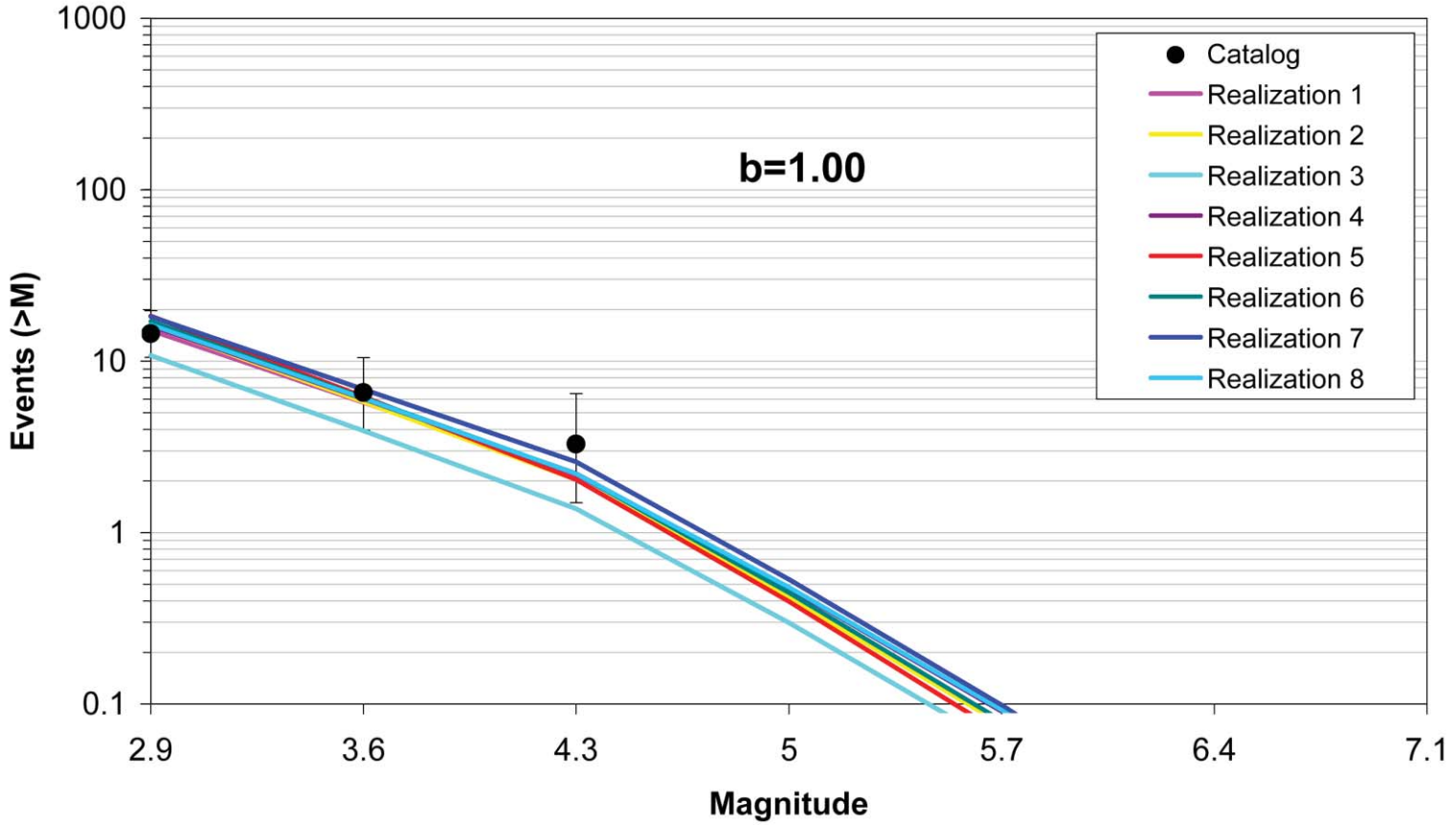

Figure 7.5.2-10
Comparison of model-predicted earthquake counts for GHEX using Case A magnitude weights. Error bars as in Figure 7.5.2-4.

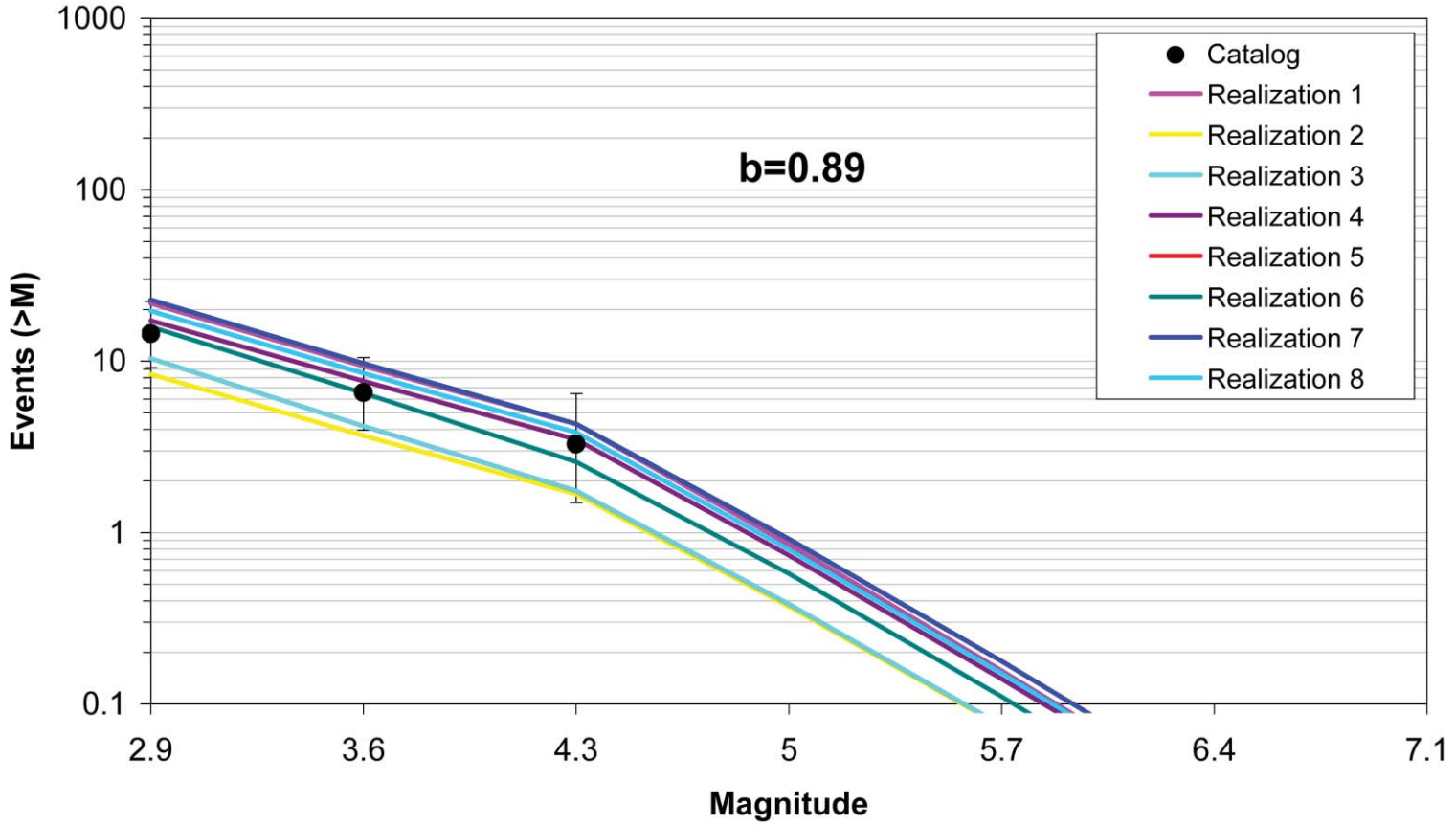

Figure 7.5.2-11
Comparison of model-predicted earthquake counts for GHEX using Case B magnitude weights. Error bars as in Figure 7.5.2-4.

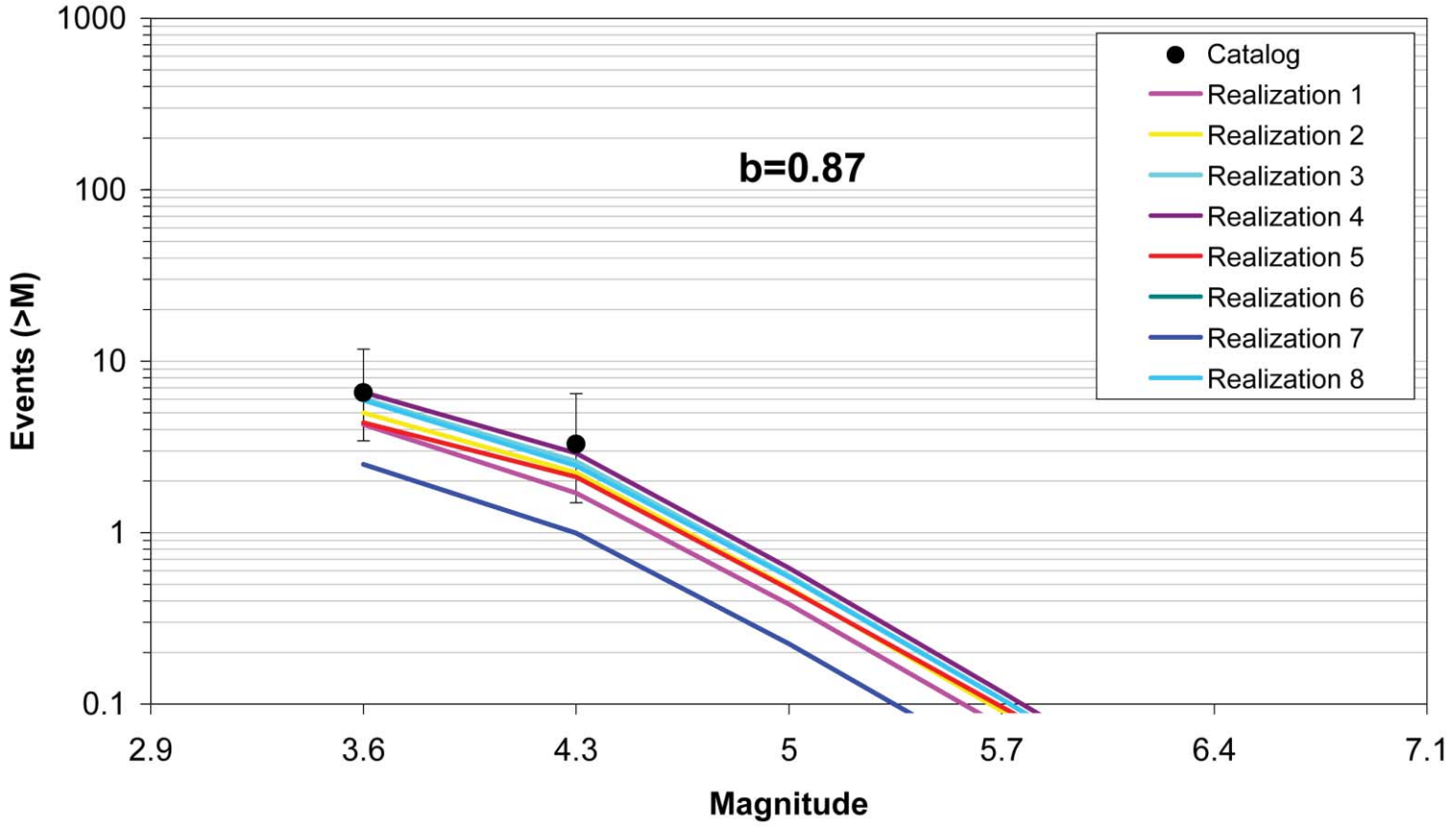

Figure 7.5.2-12
Comparison of model-predicted earthquake counts for GHEX using Case E magnitude weights. Error bars as in Figure 7.5.2-4.

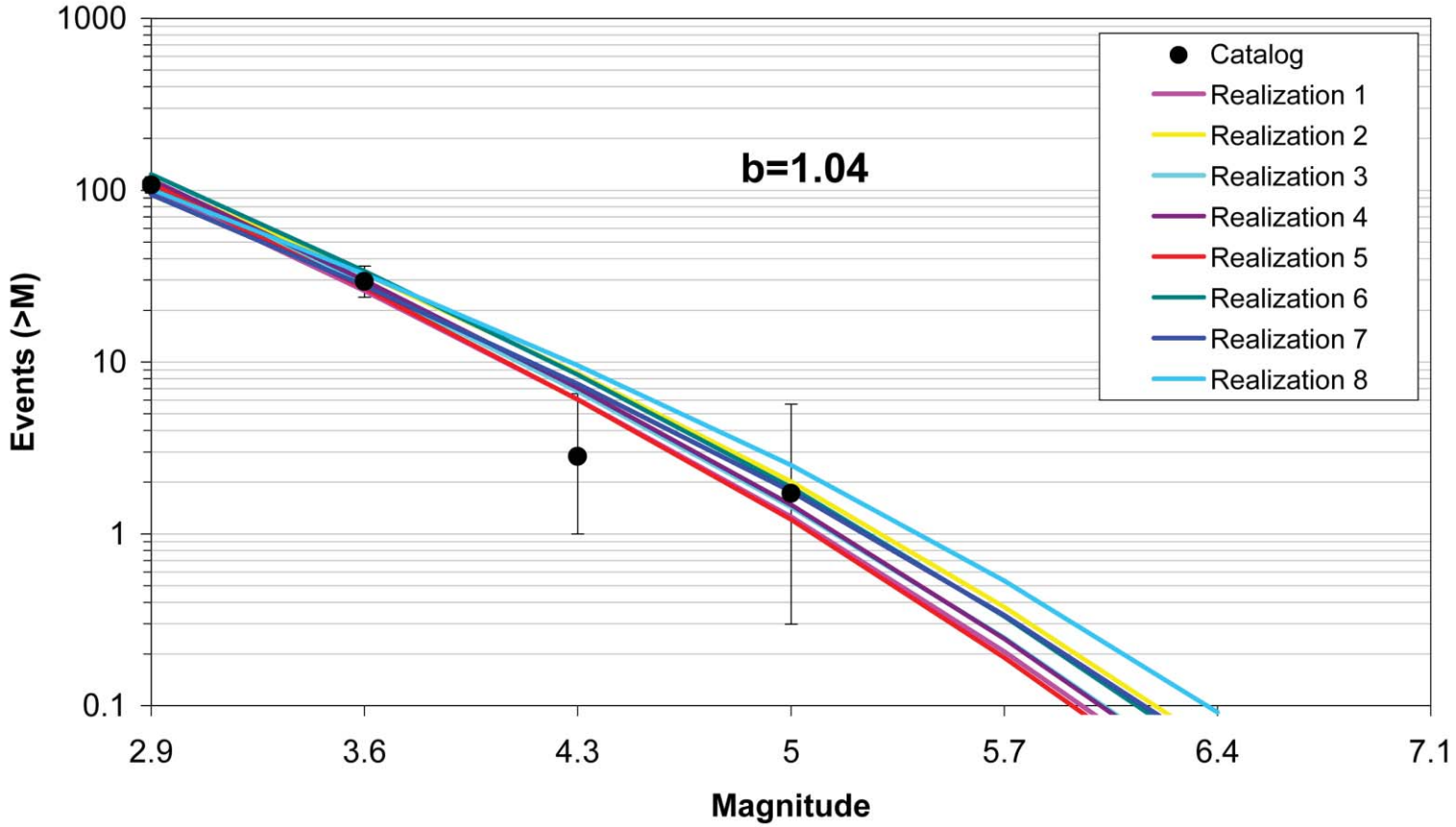

Figure 7.5.2-13
Comparison of model-predicted earthquake counts for GMH using Case A magnitude weights. Error bars as in Figure 7.5.2-4.

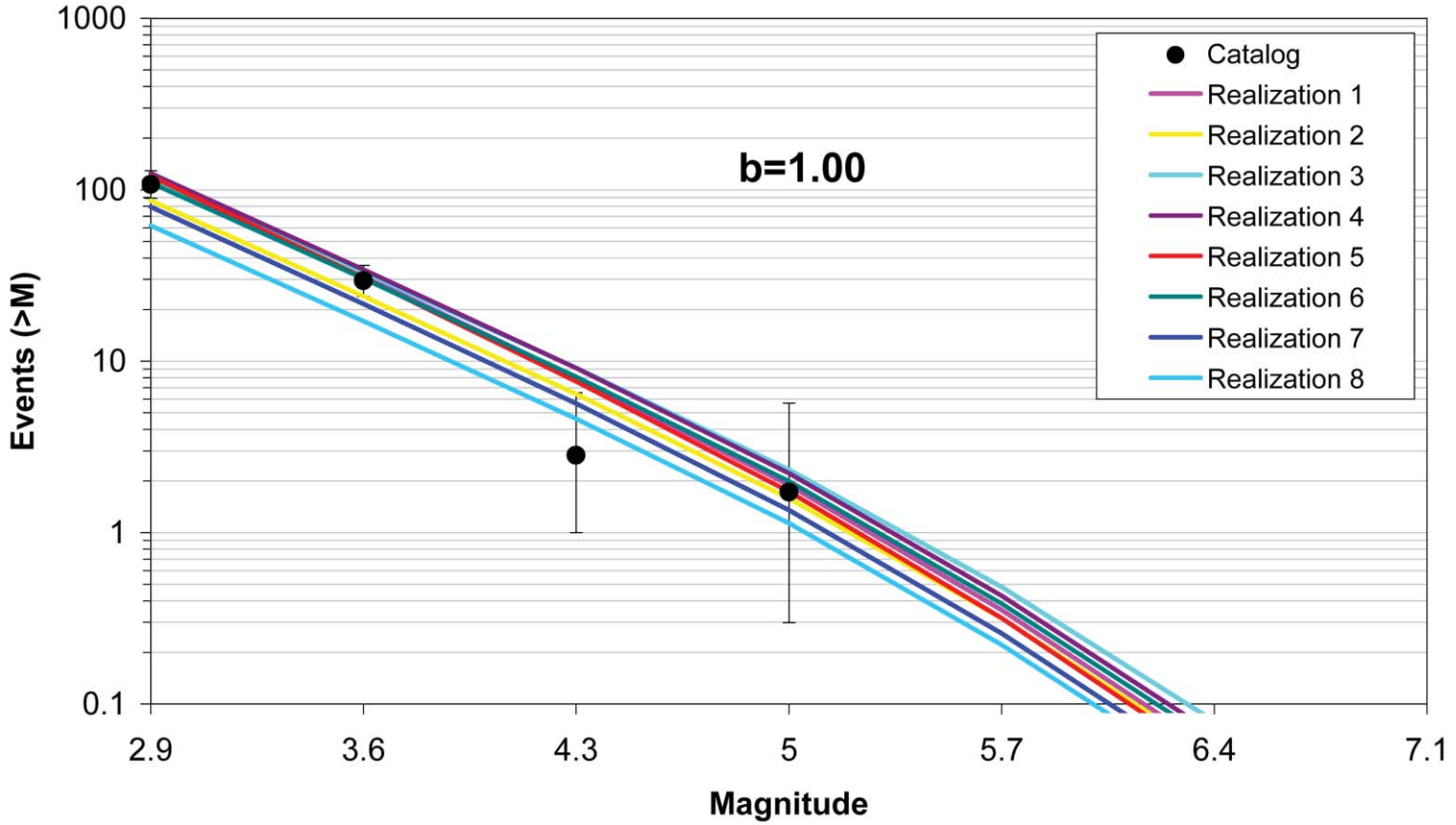

Figure 7.5.2-14
Comparison of model-predicted earthquake counts for GMH using Case B magnitude weights. Error bars as in Figure 7.5.2-4.

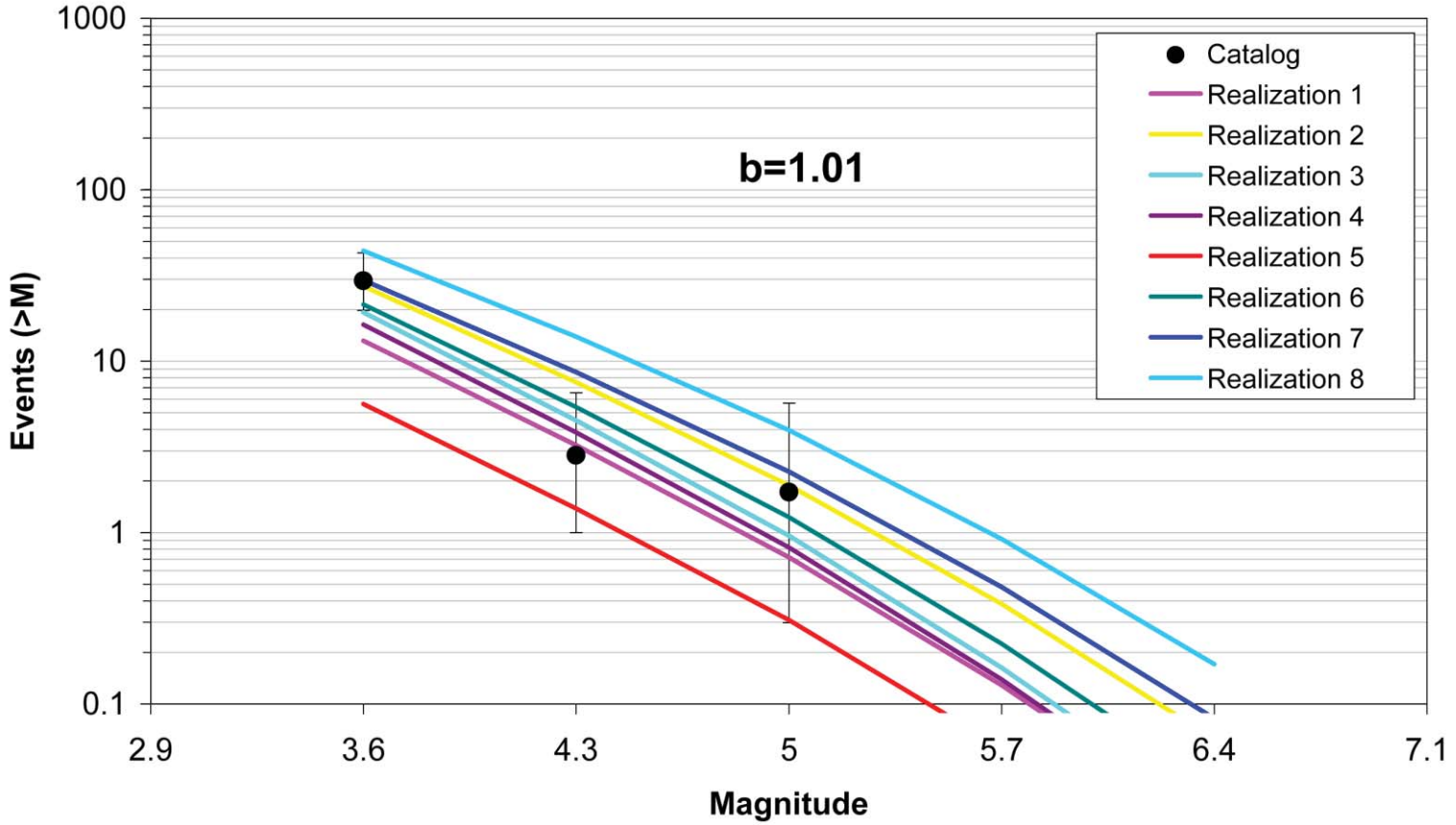

Figure 7.5.2-15
Comparison of model-predicted earthquake counts for GMH using Case E magnitude weights. Error bars as in Figure 7.5.2-4.

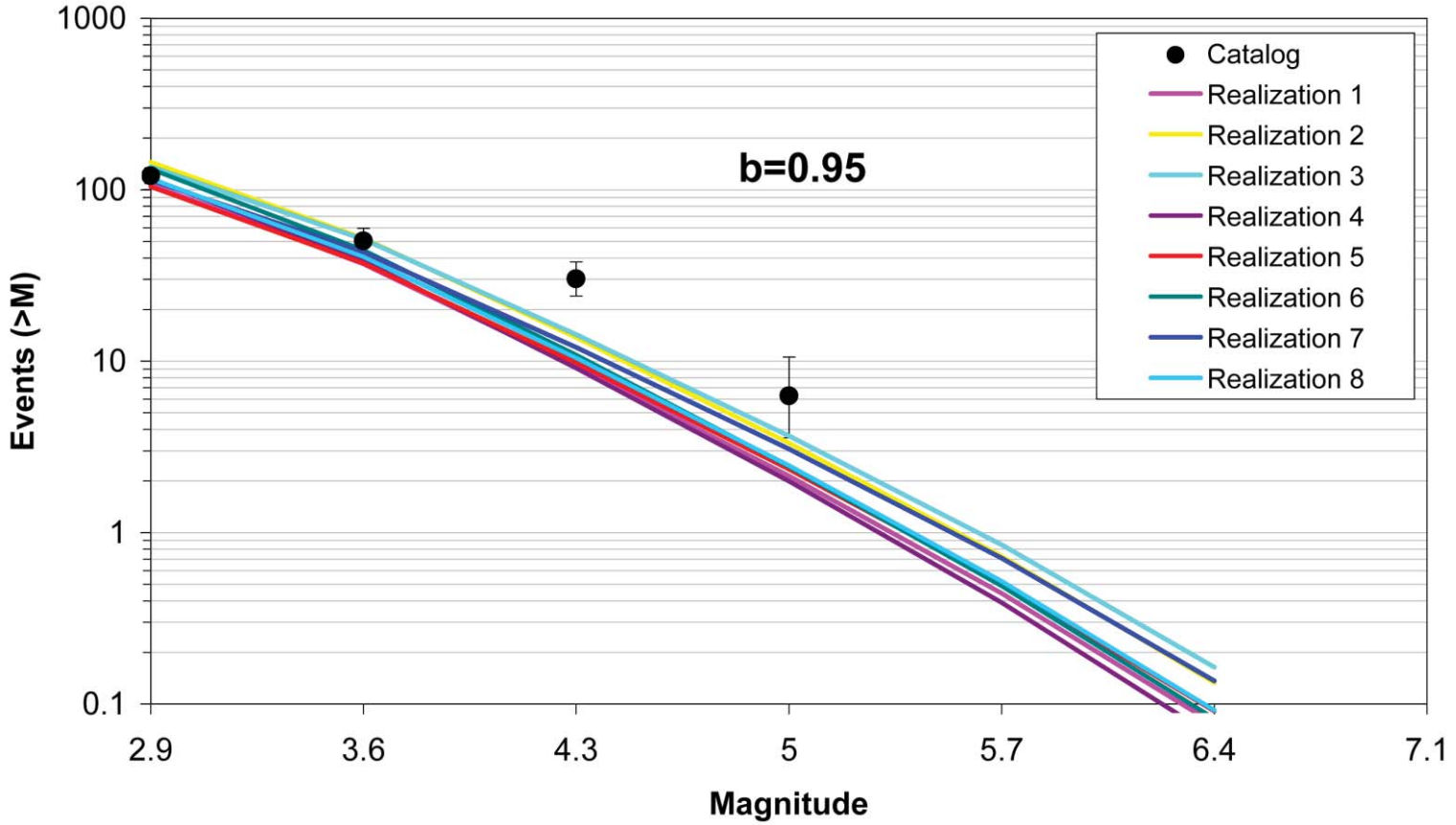

Figure 7.5.2-16
Comparison of model-predicted earthquake counts for IBEB using Case A magnitude weights. Error bars as in Figure 7.5.2-4.

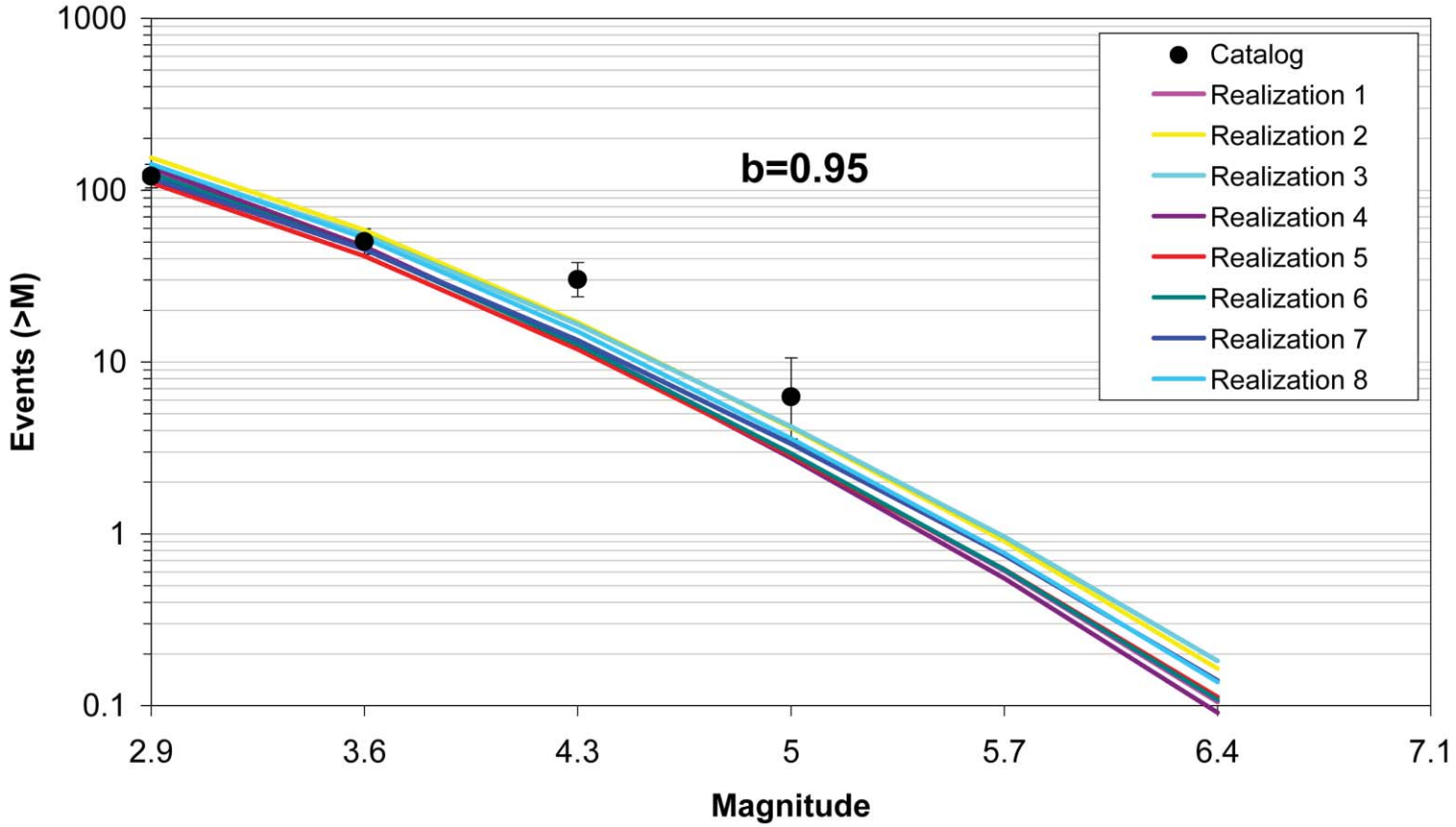

Figure 7.5.2-17
Comparison of model-predicted earthquake counts for IBEB using Case B magnitude weights. Error bars as in Figure 7.5.2-4.

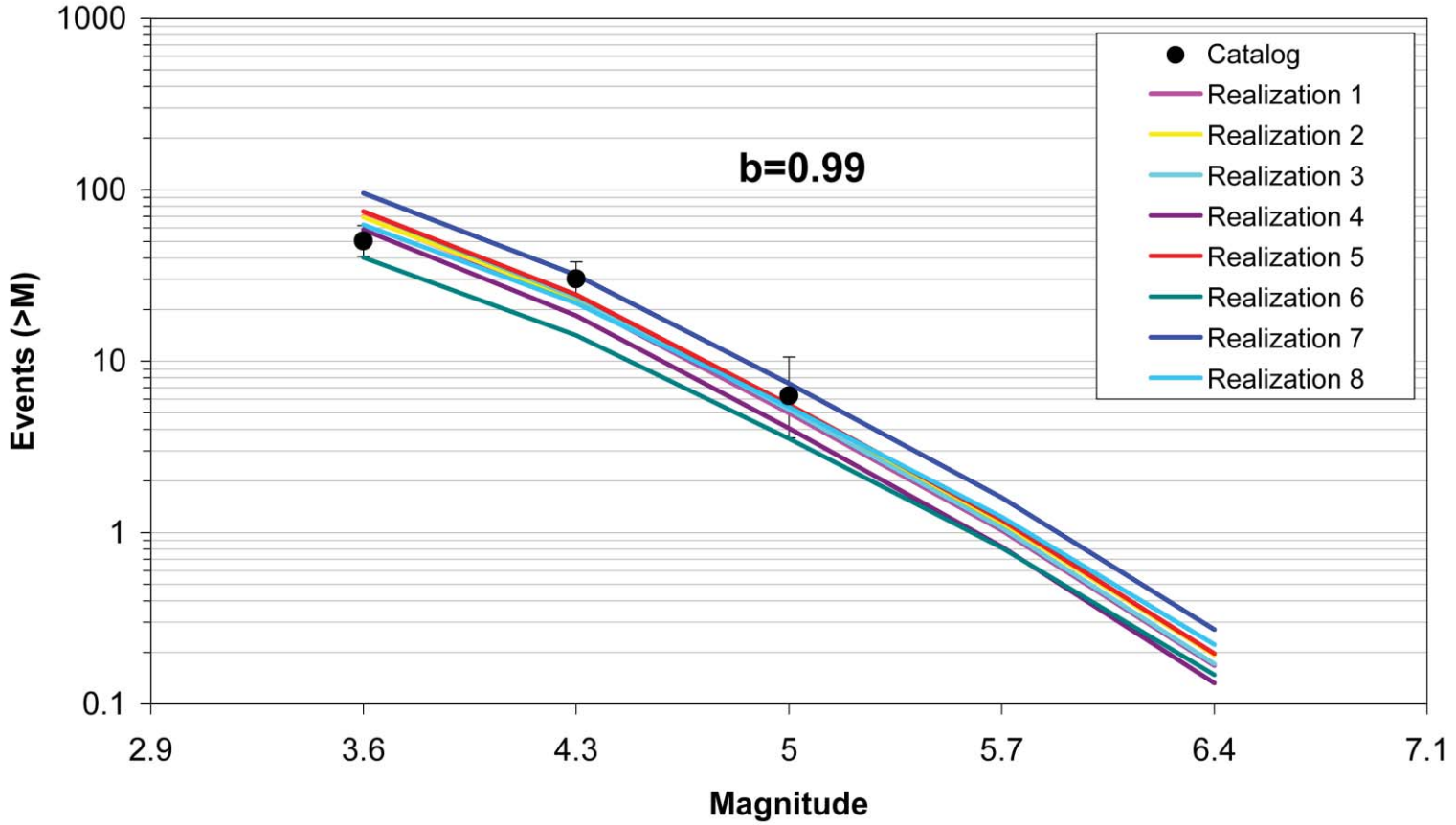

Figure 7.5.2-18
Comparison of model-predicted earthquake counts for IBEB using Case E magnitude weights. Error bars as in Figure 7.5.2-4.

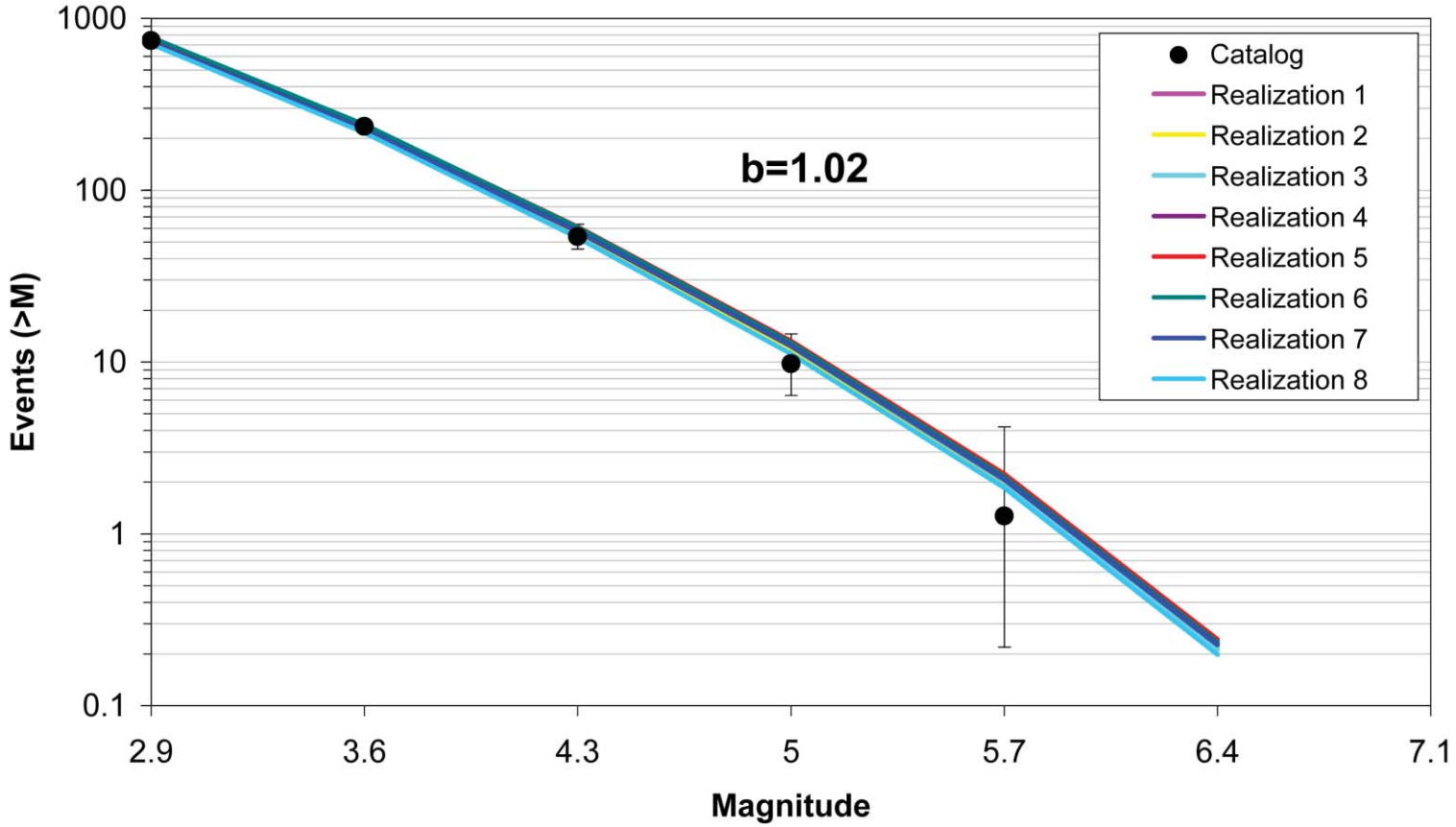

Figure 7.5.2-19
Comparison of model-predicted earthquake counts for MidC-A using Case A magnitude weights. Error bars as in Figure 7.5.2-4.

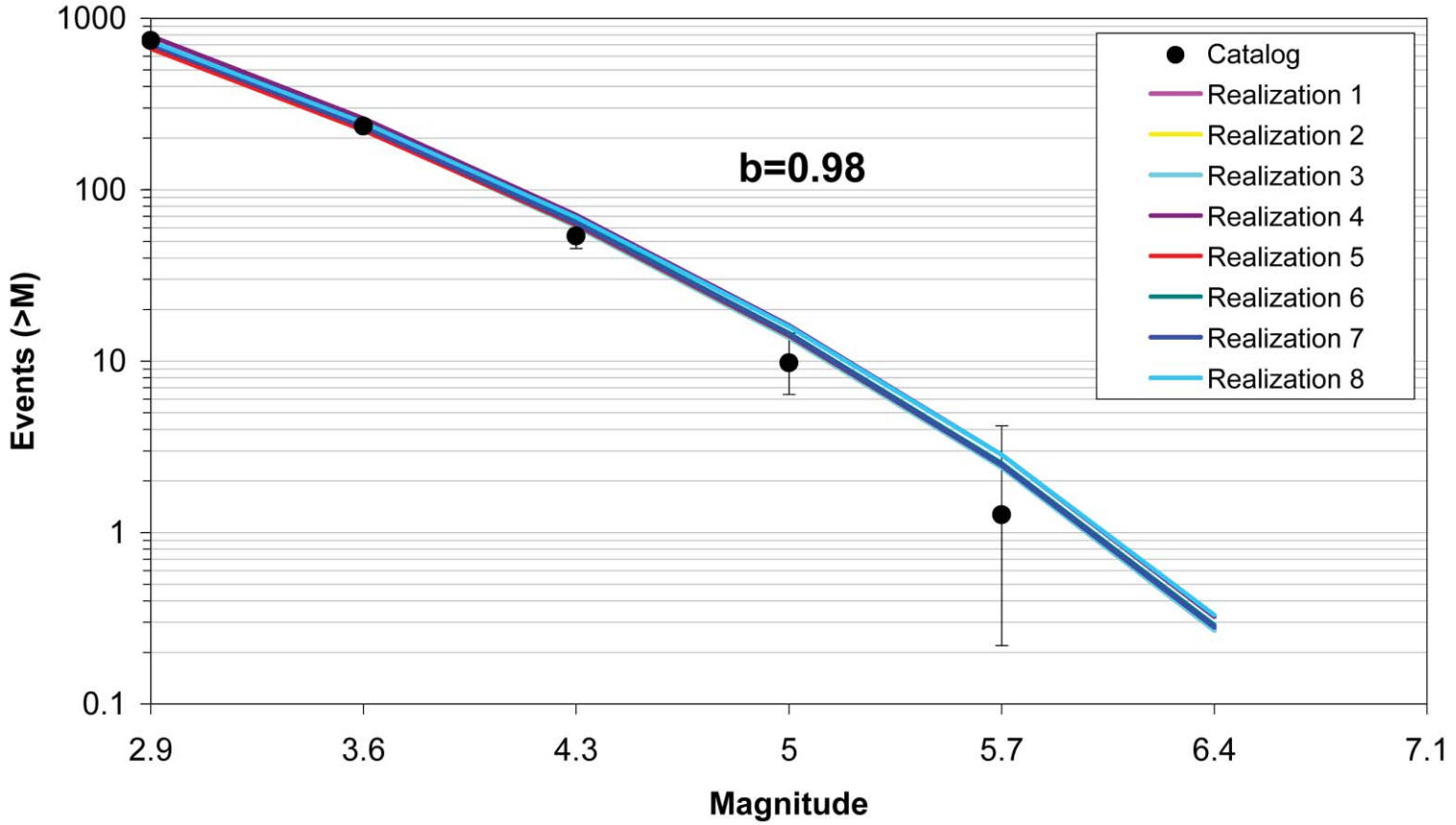

Figure 7.5.2-20
Comparison of model-predicted earthquake counts for MidC-A using Case B magnitude weights. Error bars as in Figure 7.5.2-4.

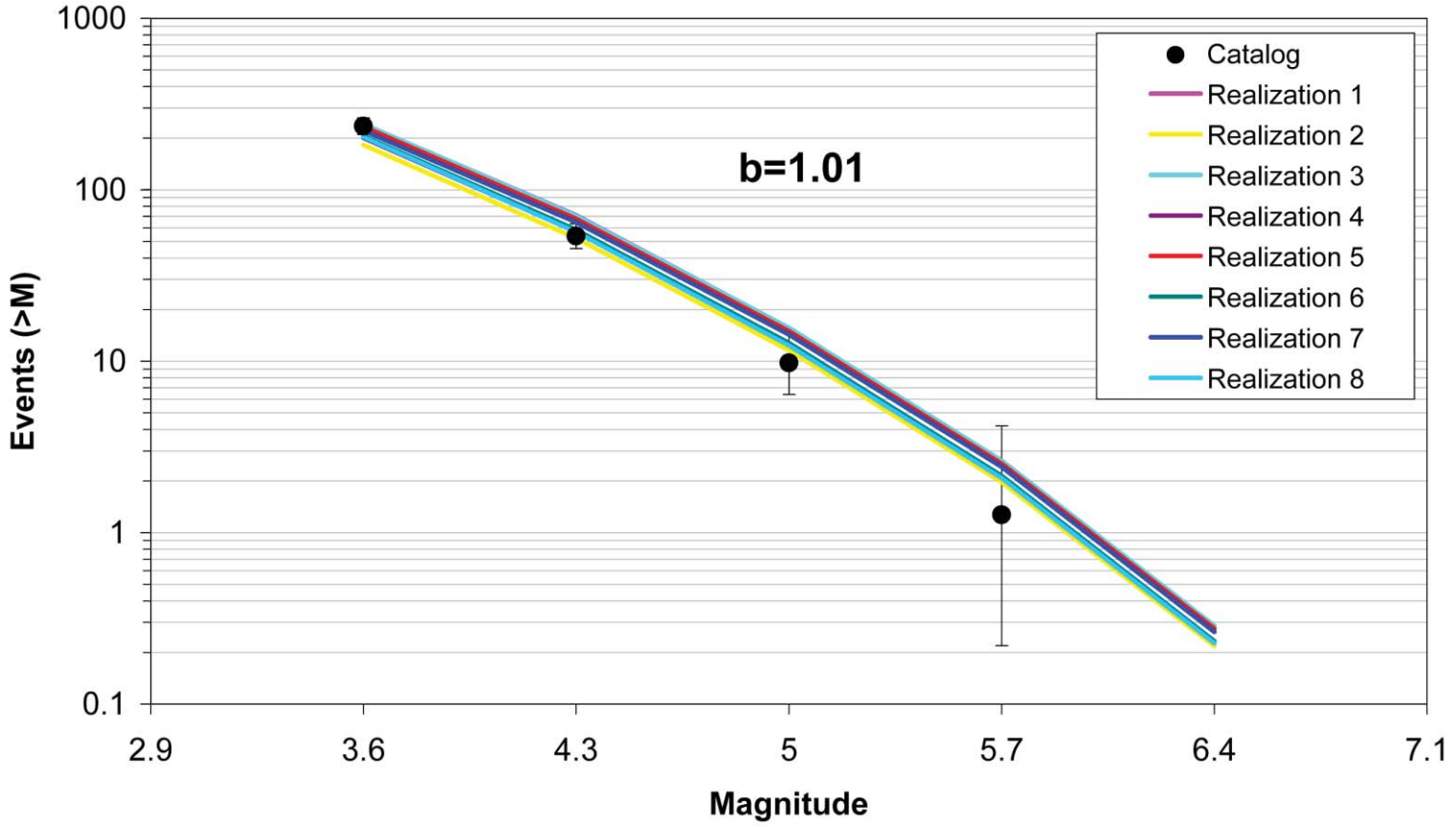

Figure 7.5.2-21
Comparison of model-predicted earthquake counts for MidC-A using Case E magnitude weights. Error bars as in Figure 7.5.2-4.

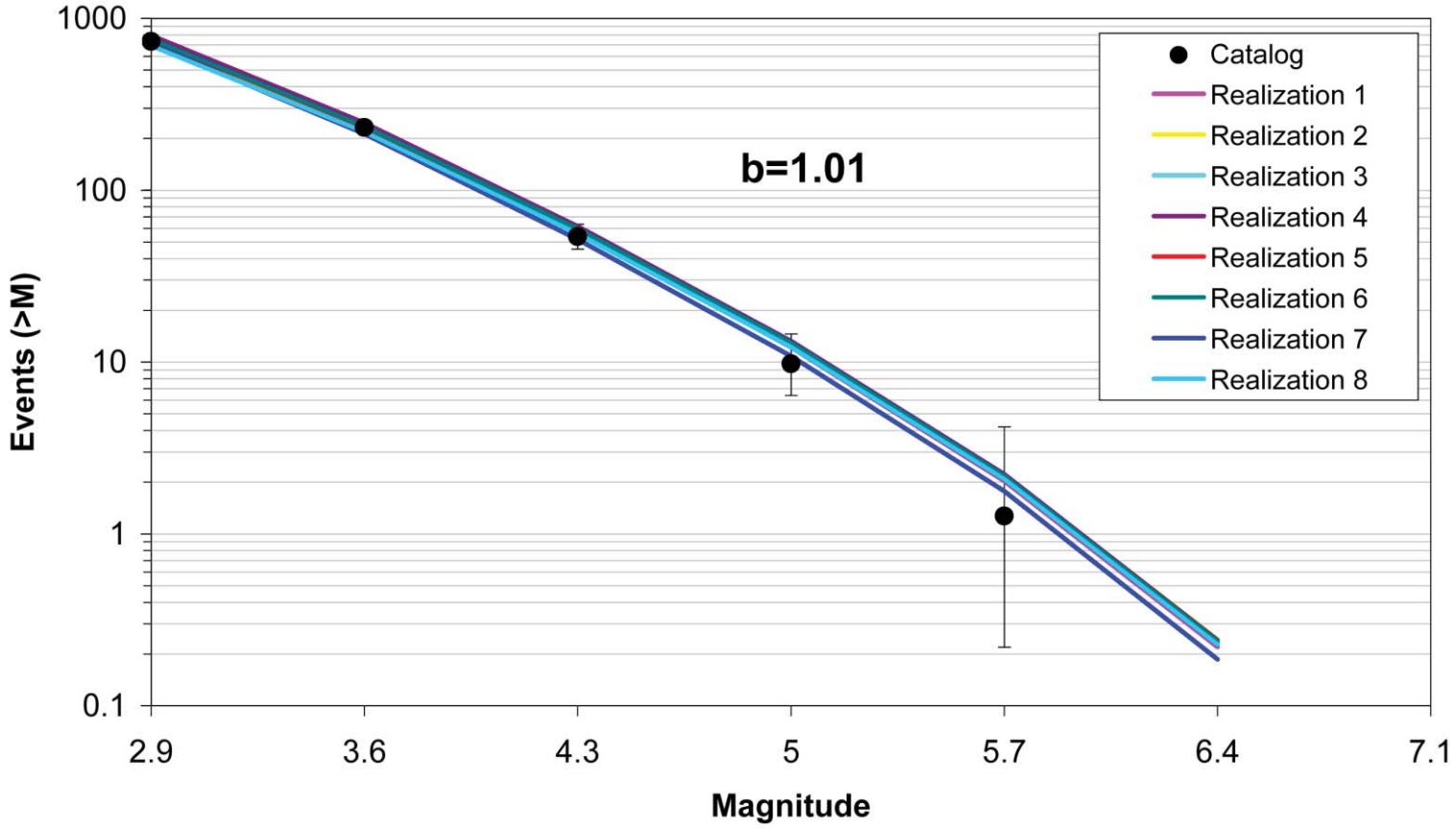

Figure 7.5.2-22
Comparison of model-predicted earthquake counts for MidC–B using Case A magnitude weights. Error bars as in Figure 7.5.2-4.

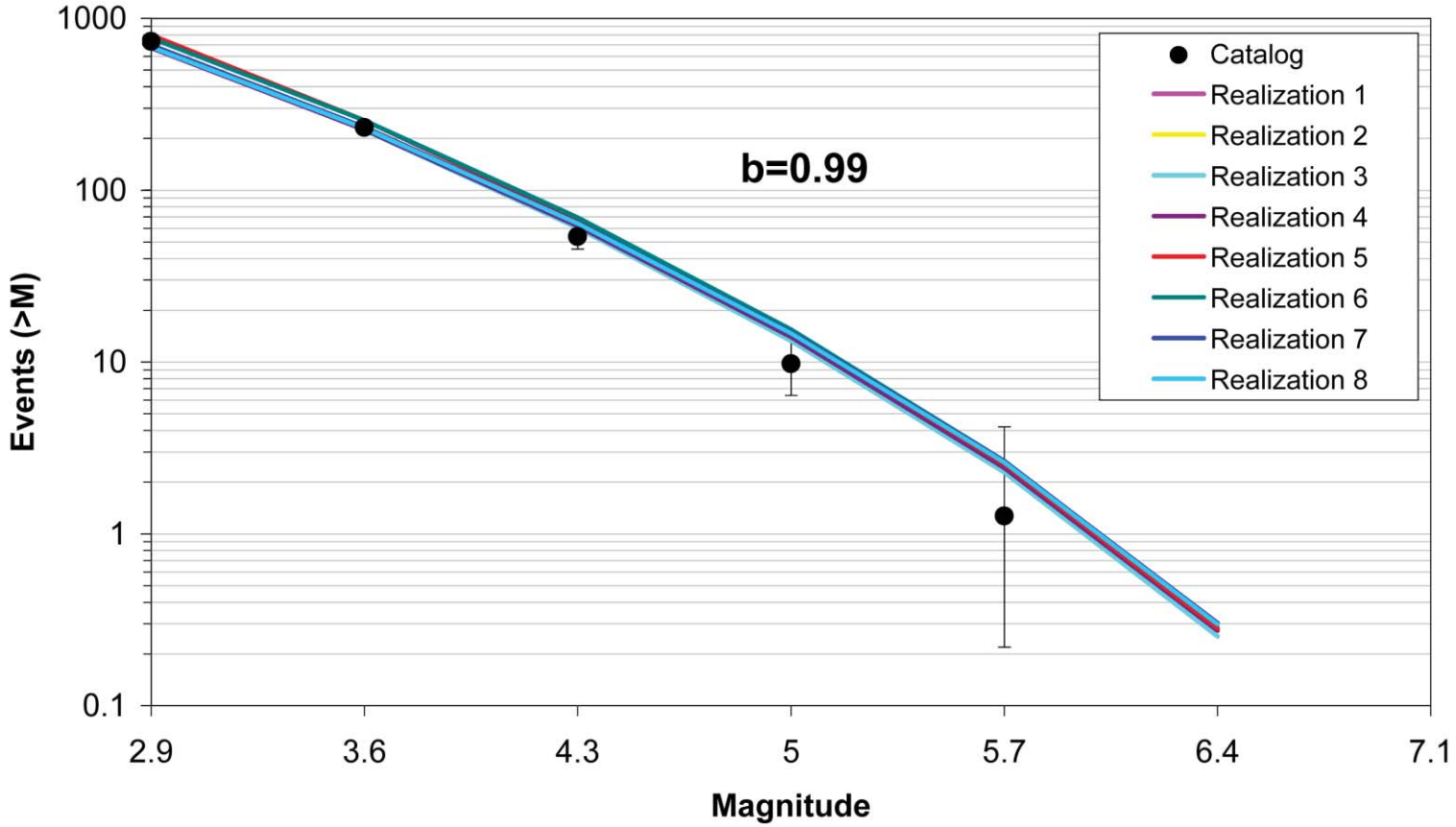

Figure 7.5.2-23
Comparison of model-predicted earthquake counts for MidC-B using Case B magnitude weights. Error bars as in Figure 7.5.2-4.

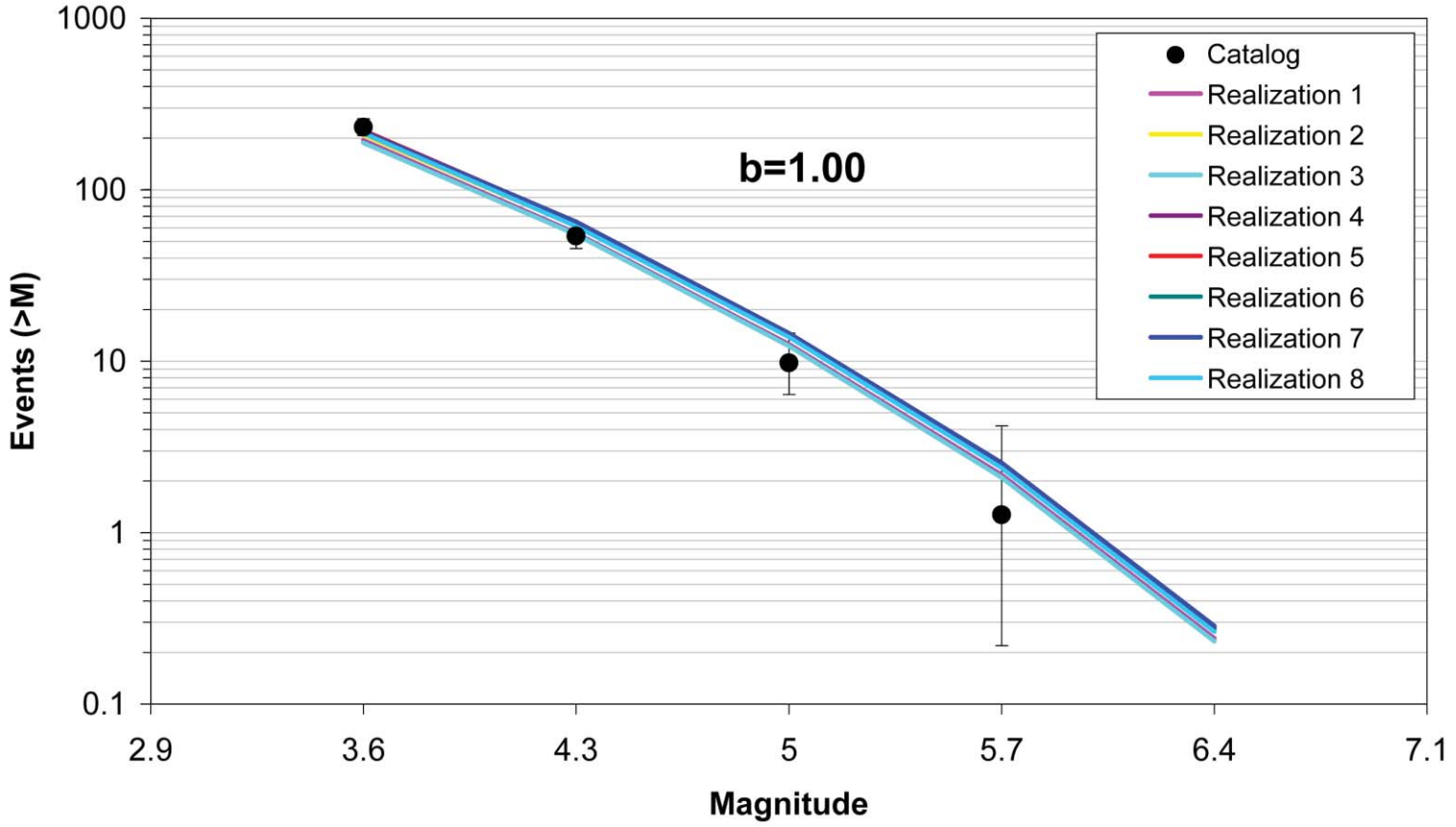

Figure 7.5.2-24
Comparison of model-predicted earthquake counts for MidC–B using Case E magnitude weights. Error bars as in Figure 7.5.2-4.

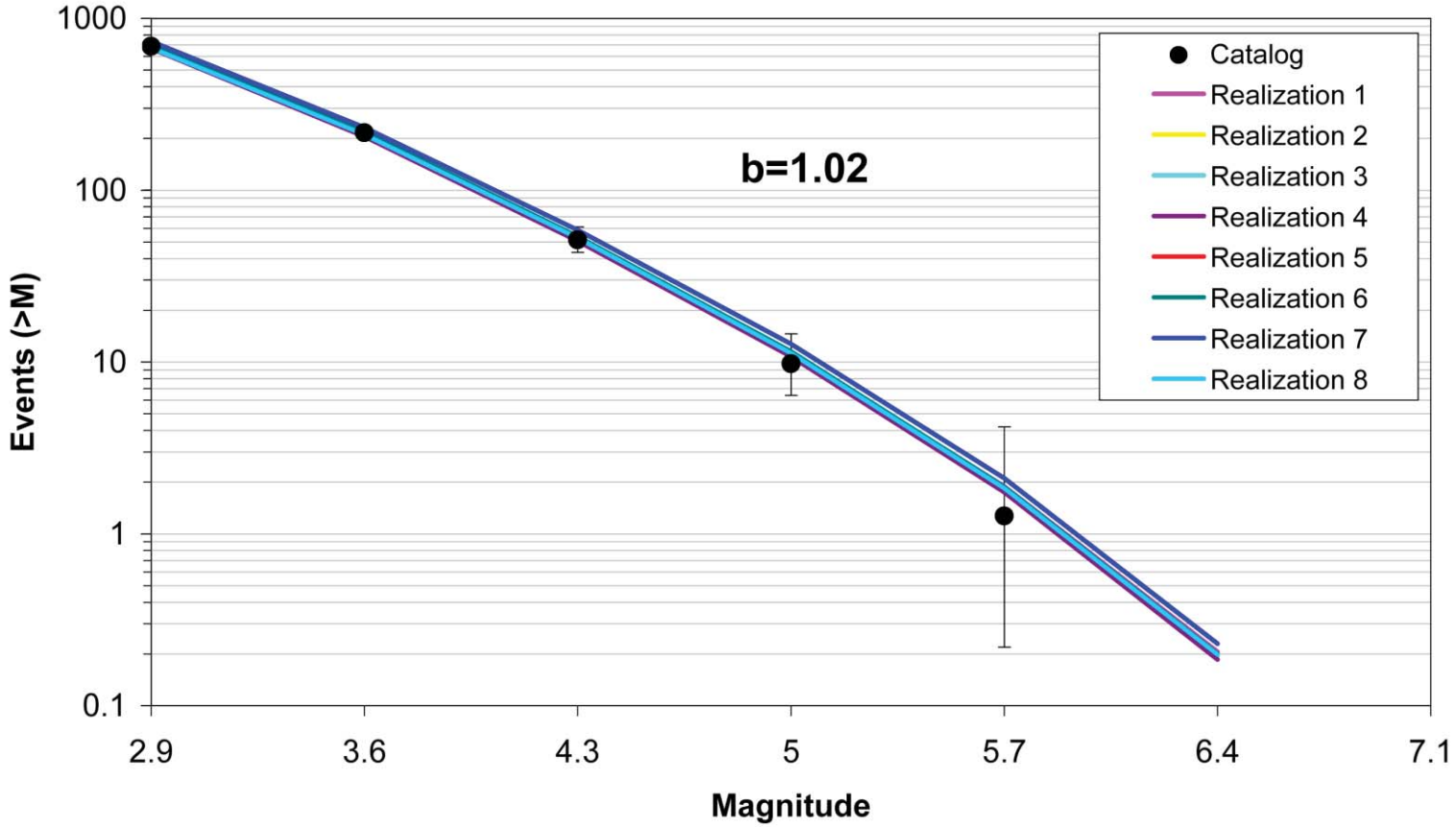

Figure 7.5.2-25
Comparison of model-predicted earthquake counts for MidC–C using Case A magnitude weights. Error bars as in Figure 7.5.2-4.

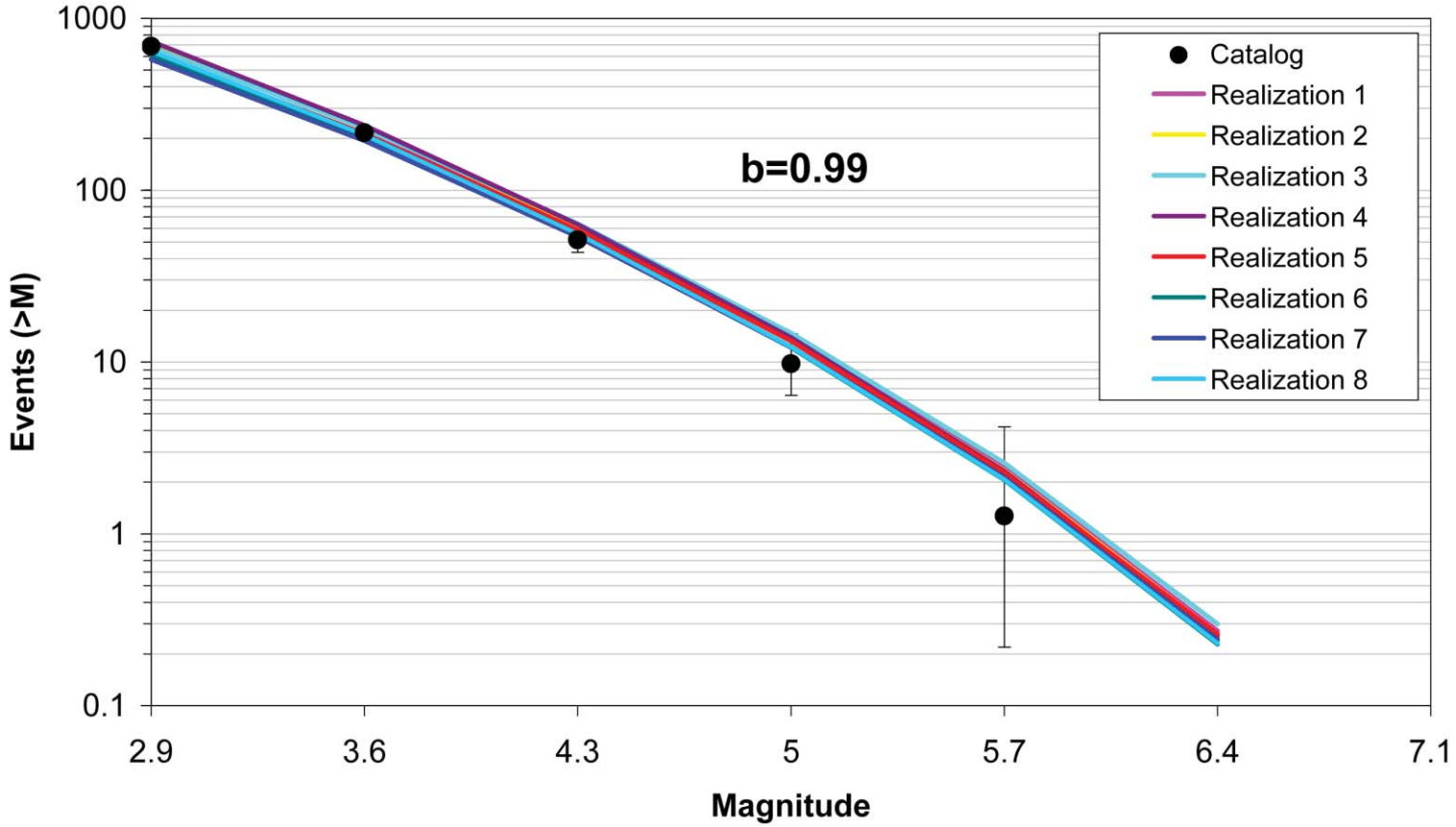

Figure 7.5.2-26
Comparison of model-predicted earthquake counts for MidC–C using Case B magnitude weights. Error bars as in Figure 7.5.2-4.

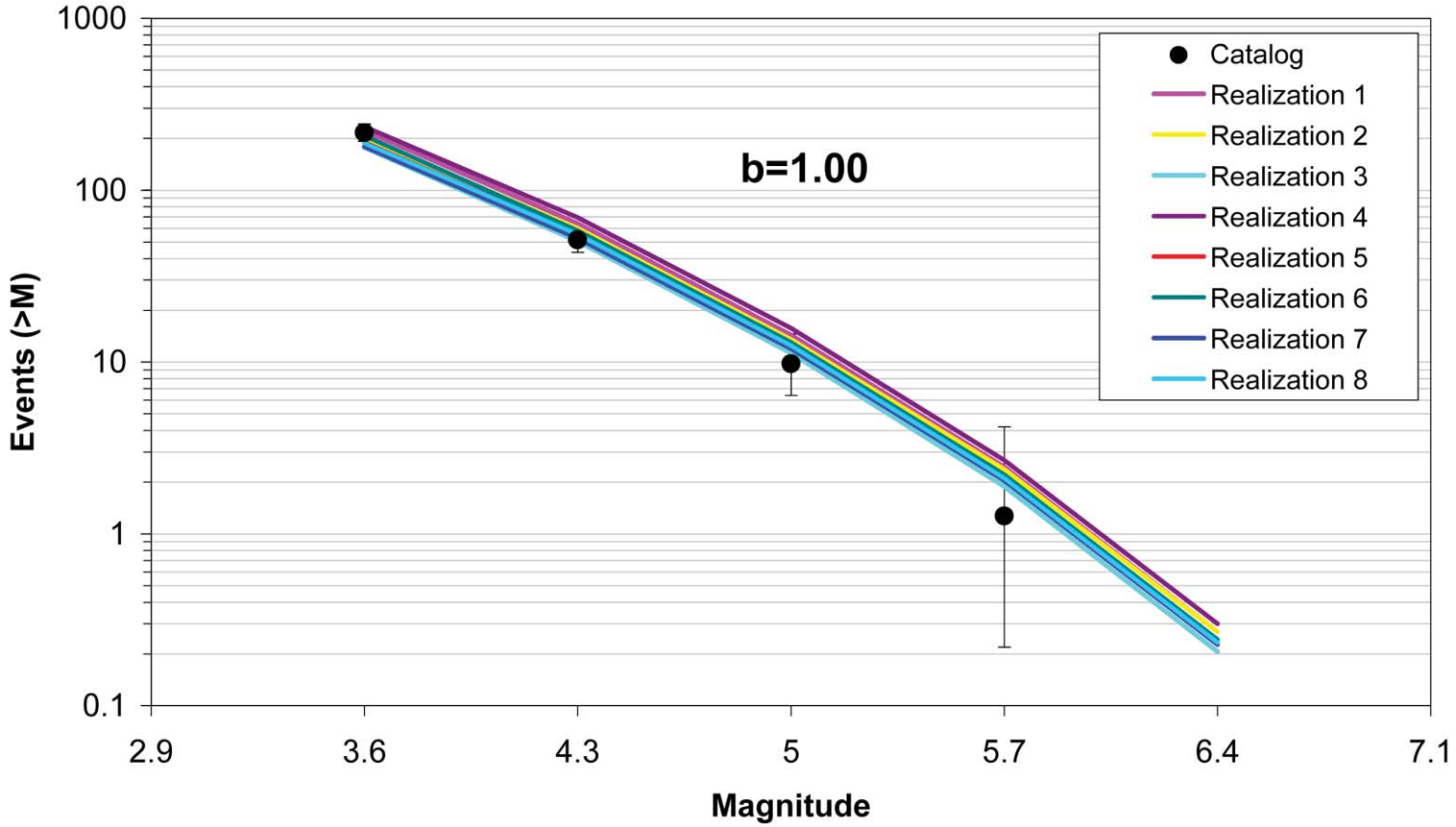

Figure 7.5.2-27
Comparison of model-predicted earthquake counts for MidC–C using Case E magnitude weights. Error bars as in Figure 7.5.2-4.

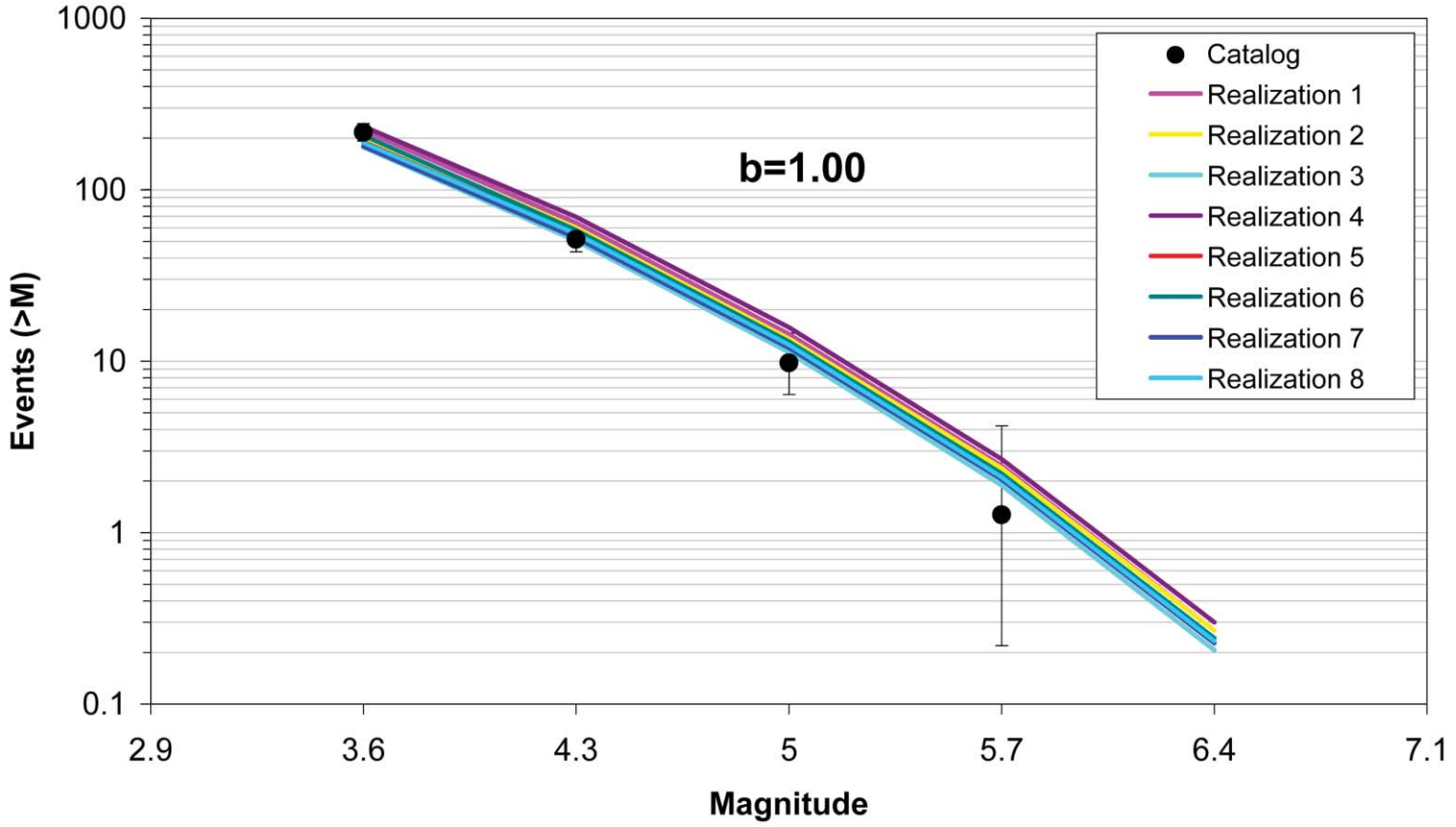

Figure 7.5.2-28
Comparison of model-predicted earthquake counts for MidC–D using Case A magnitude weights. Error bars as in Figure 7.5.2-4.

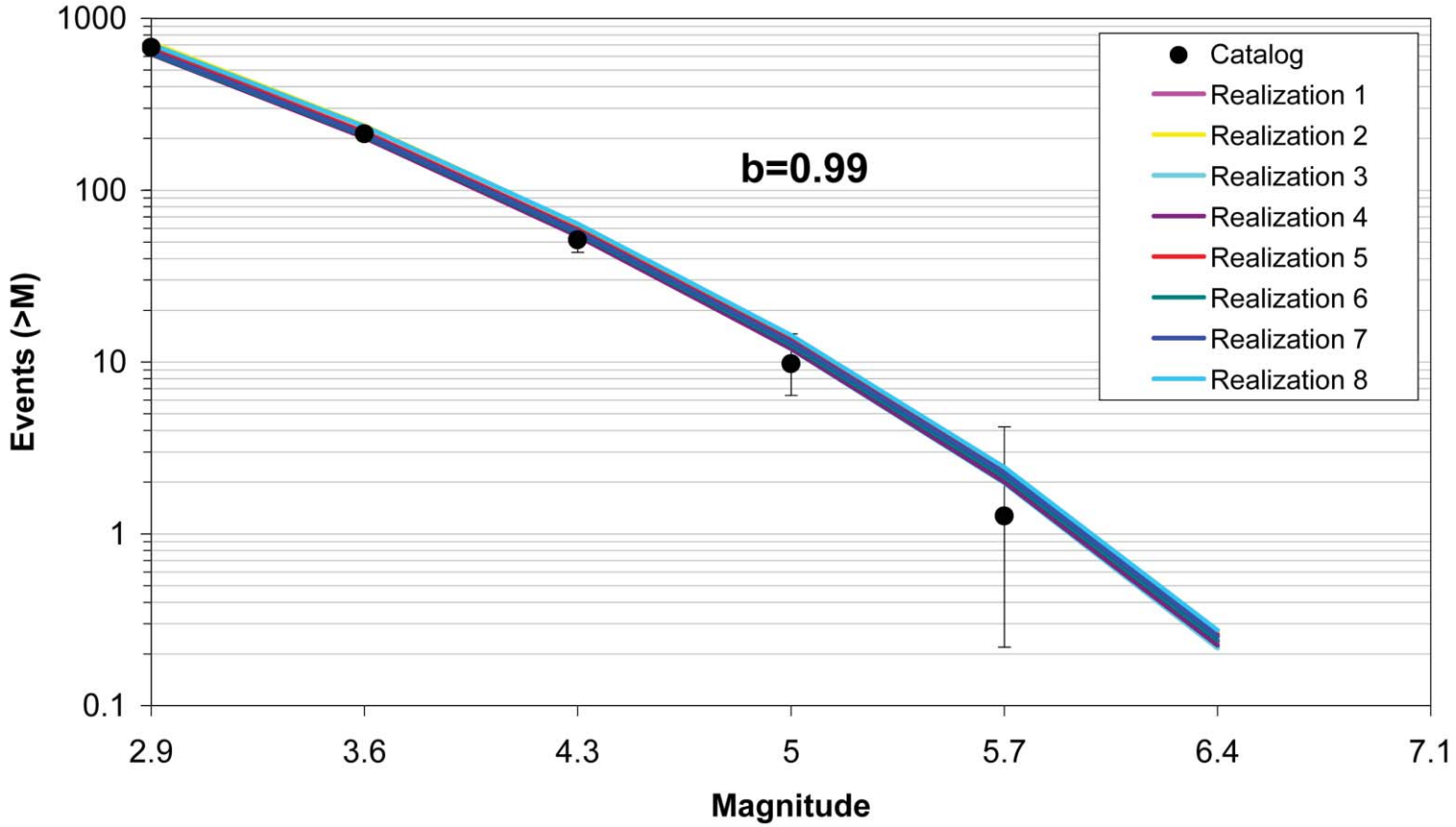

Figure 7.5.2-29
Comparison of model-predicted earthquake counts for MidC–D using Case B magnitude weights. Error bars as in Figure 7.5.2-4.

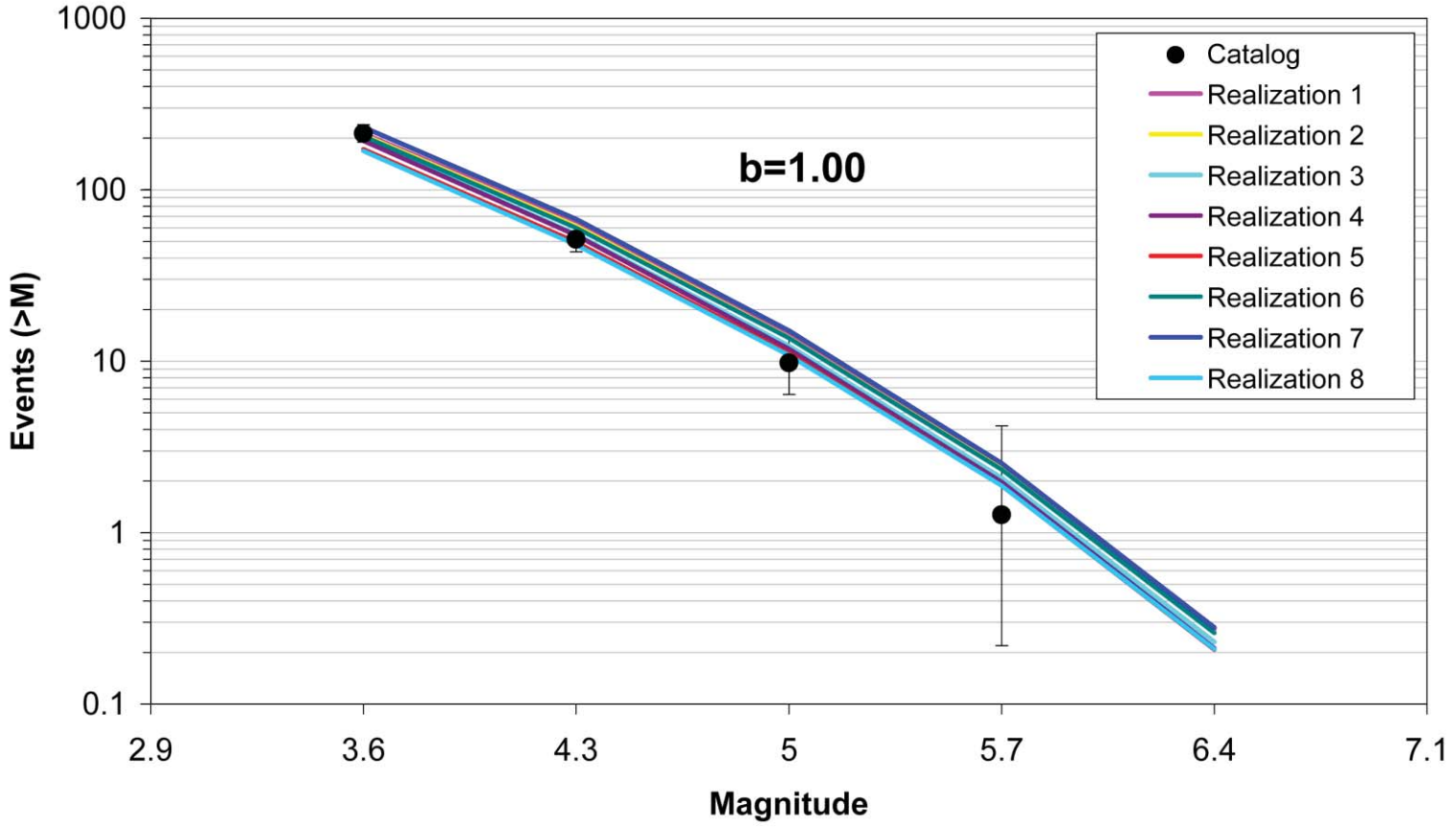

Figure 7.5.2-30
Comparison of model-predicted earthquake counts for MidC–D using Case E magnitude weights. Error bars as in Figure 7.5.2-4.

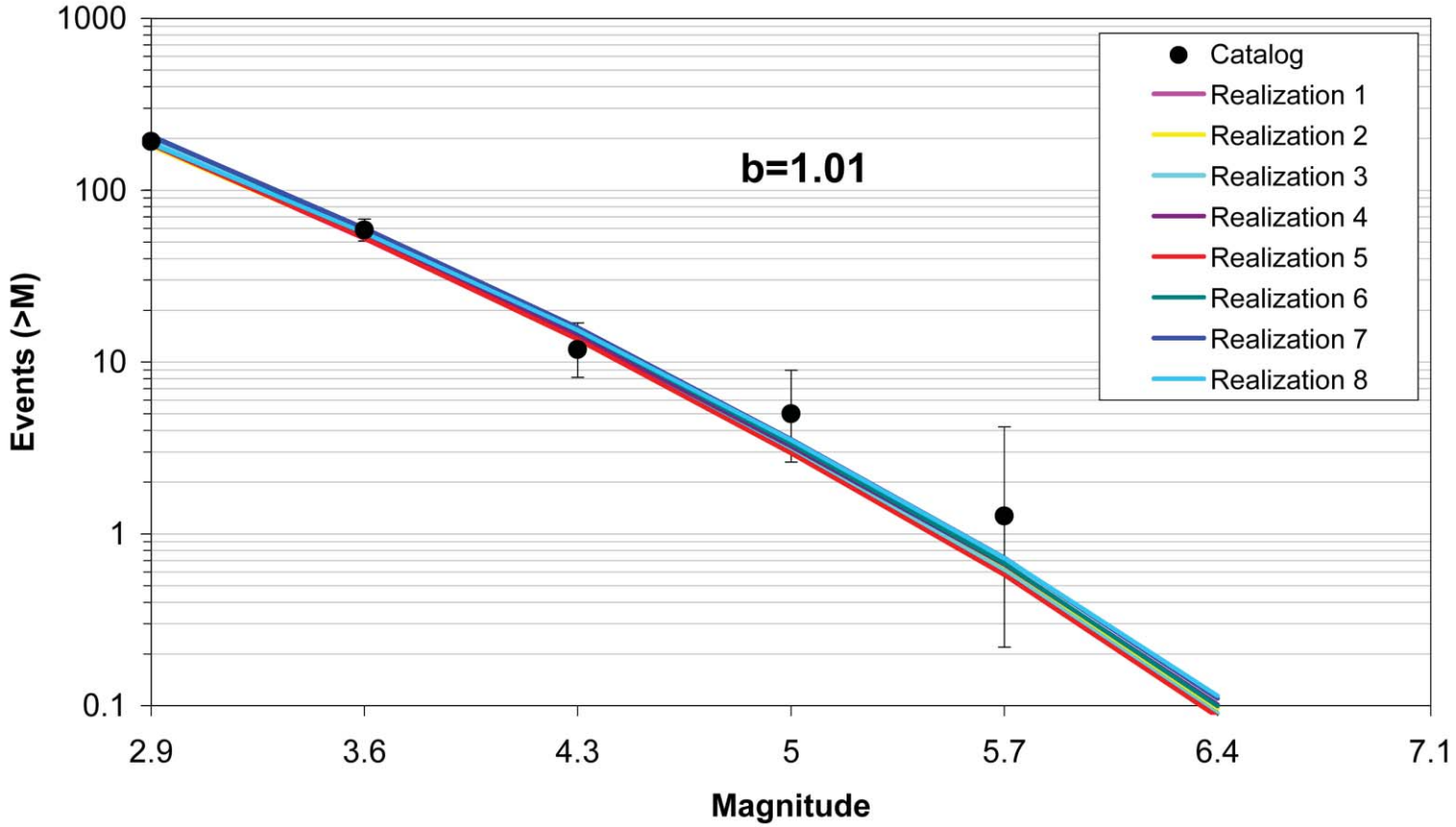

Figure 7.5.2-31
Comparison of model-predicted earthquake counts for NAP using Case A magnitude weights. Error bars as in Figure 7.5.2-4.

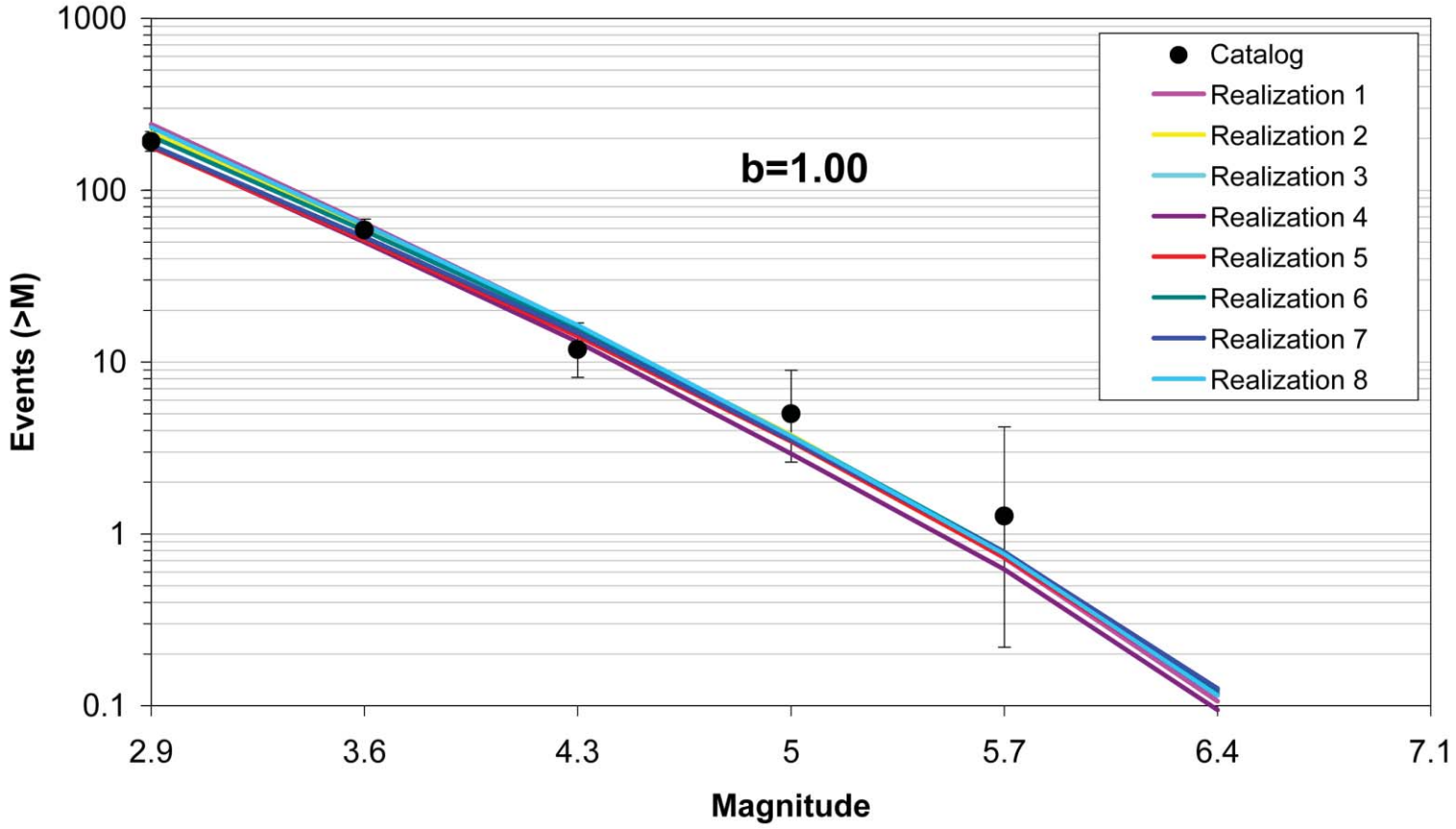

Figure 7.5.2-32
Comparison of model-predicted earthquake counts for NAP using Case B magnitude weights. Error bars as in Figure 7.5.2-4.

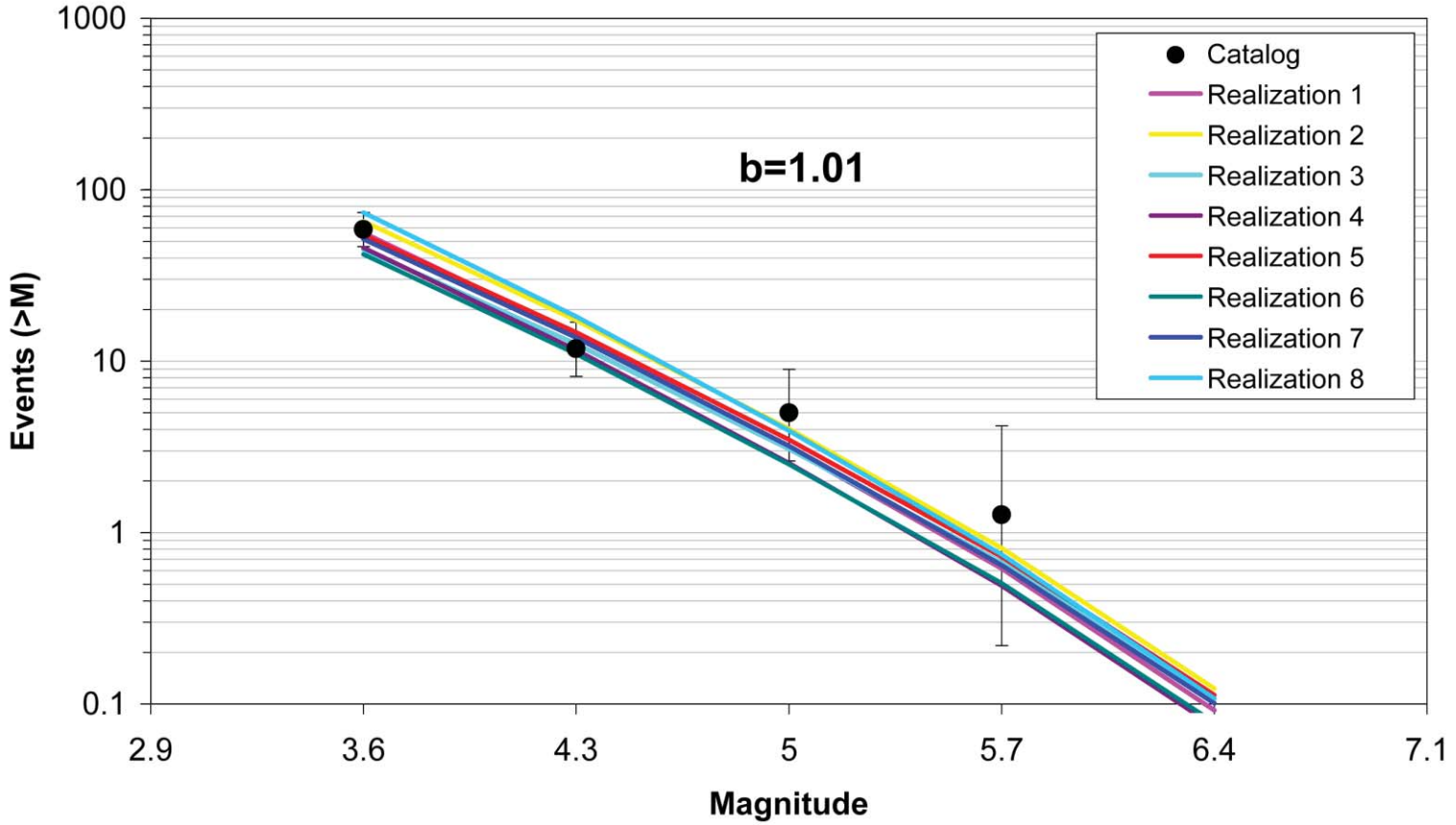

Figure 7.5.2-33
Comparison of model-predicted earthquake counts for NAP using Case E magnitude weights. Error bars as in Figure 7.5.2-4.

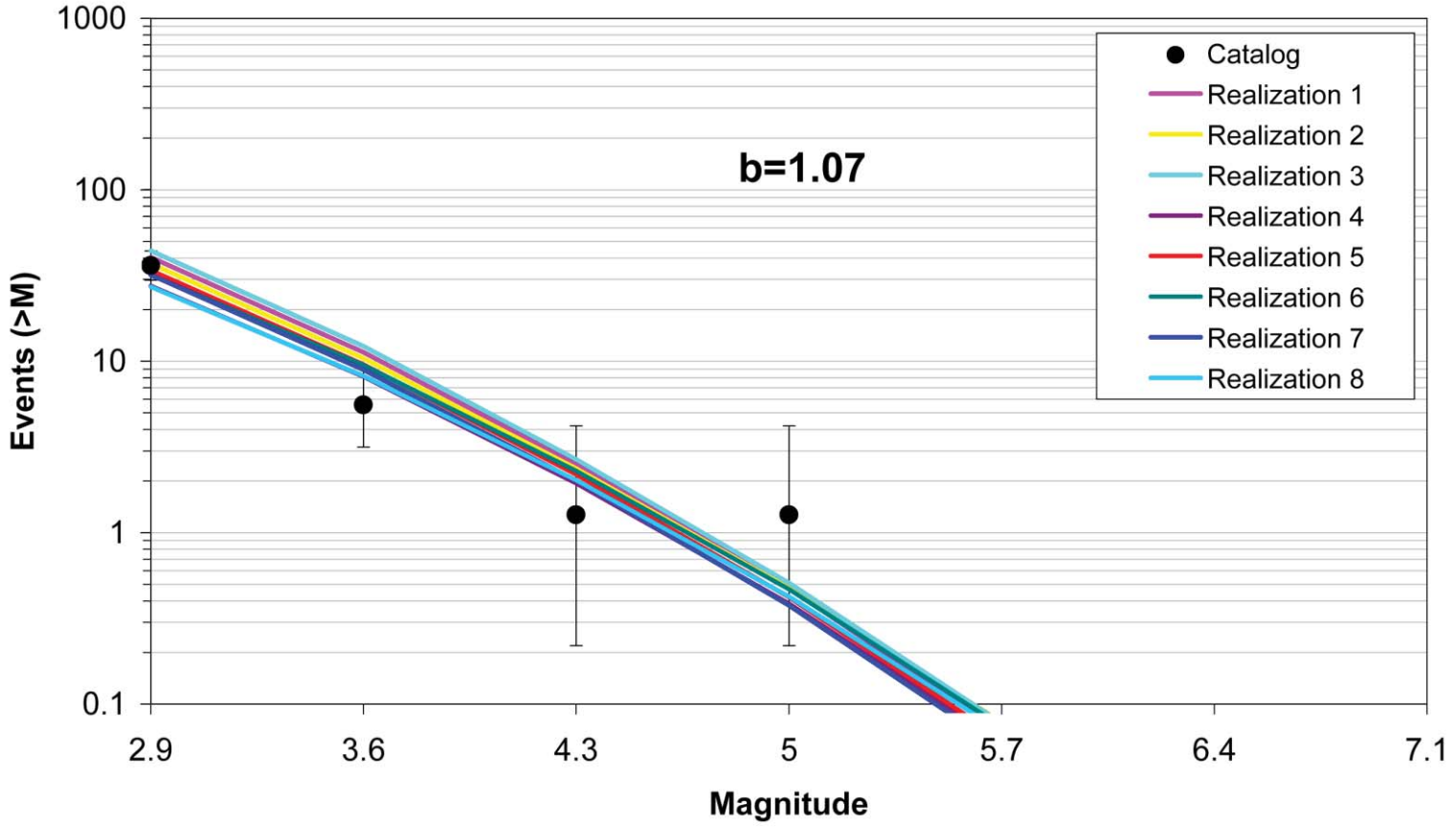

Figure 7.5.2-34
Comparison of model-predicted earthquake counts for OKA using Case A magnitude weights. Error bars as in Figure 7.5.2-4.

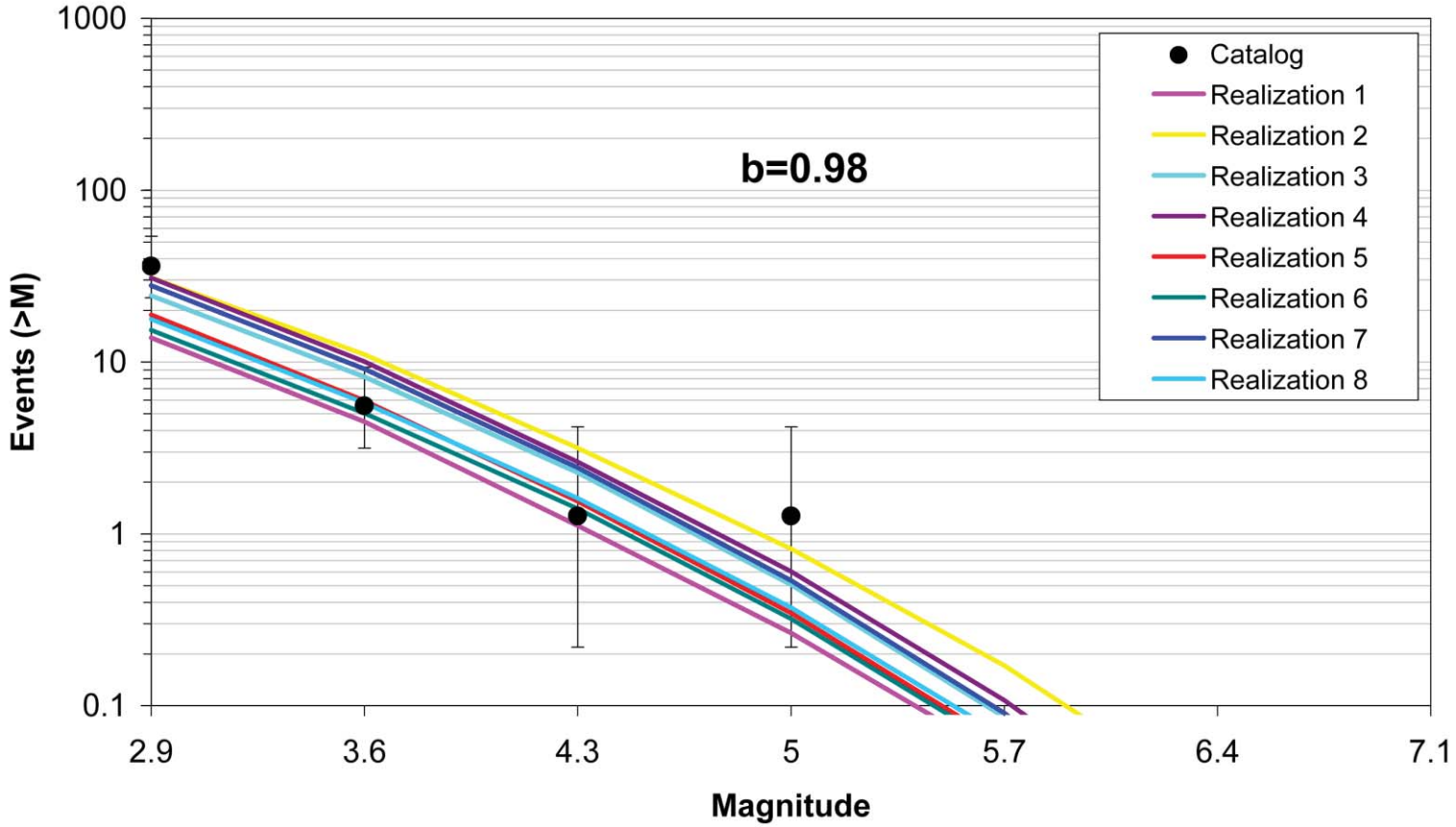

Figure 7.5.2-35
Comparison of model-predicted earthquake counts for OKA using Case B magnitude weights. Error bars as in Figure 7.5.2-4.

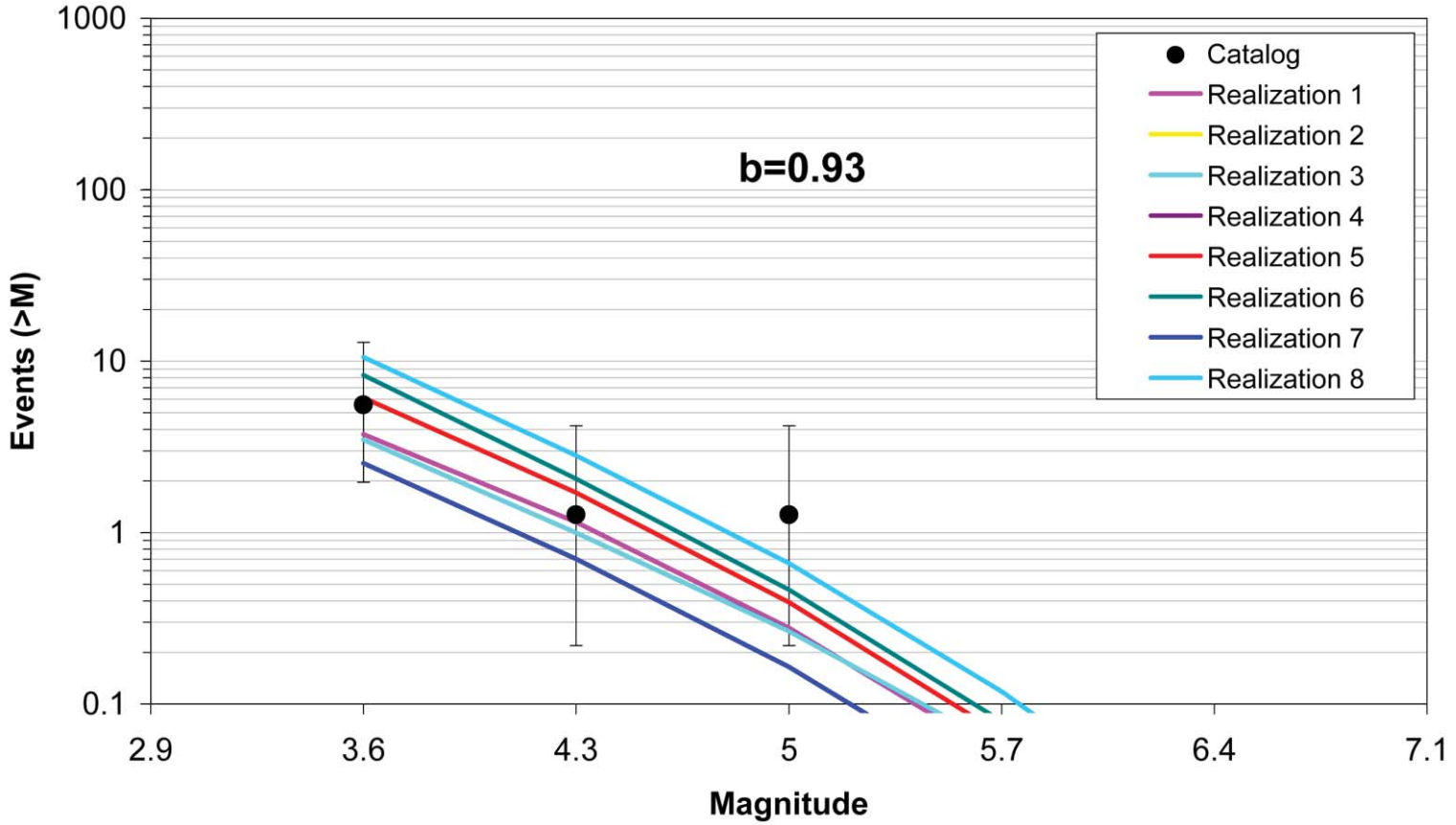

Figure 7.5.2-36
Comparison of model-predicted earthquake counts for OKA using Case E magnitude weights. Error bars as in Figure 7.5.2-4.

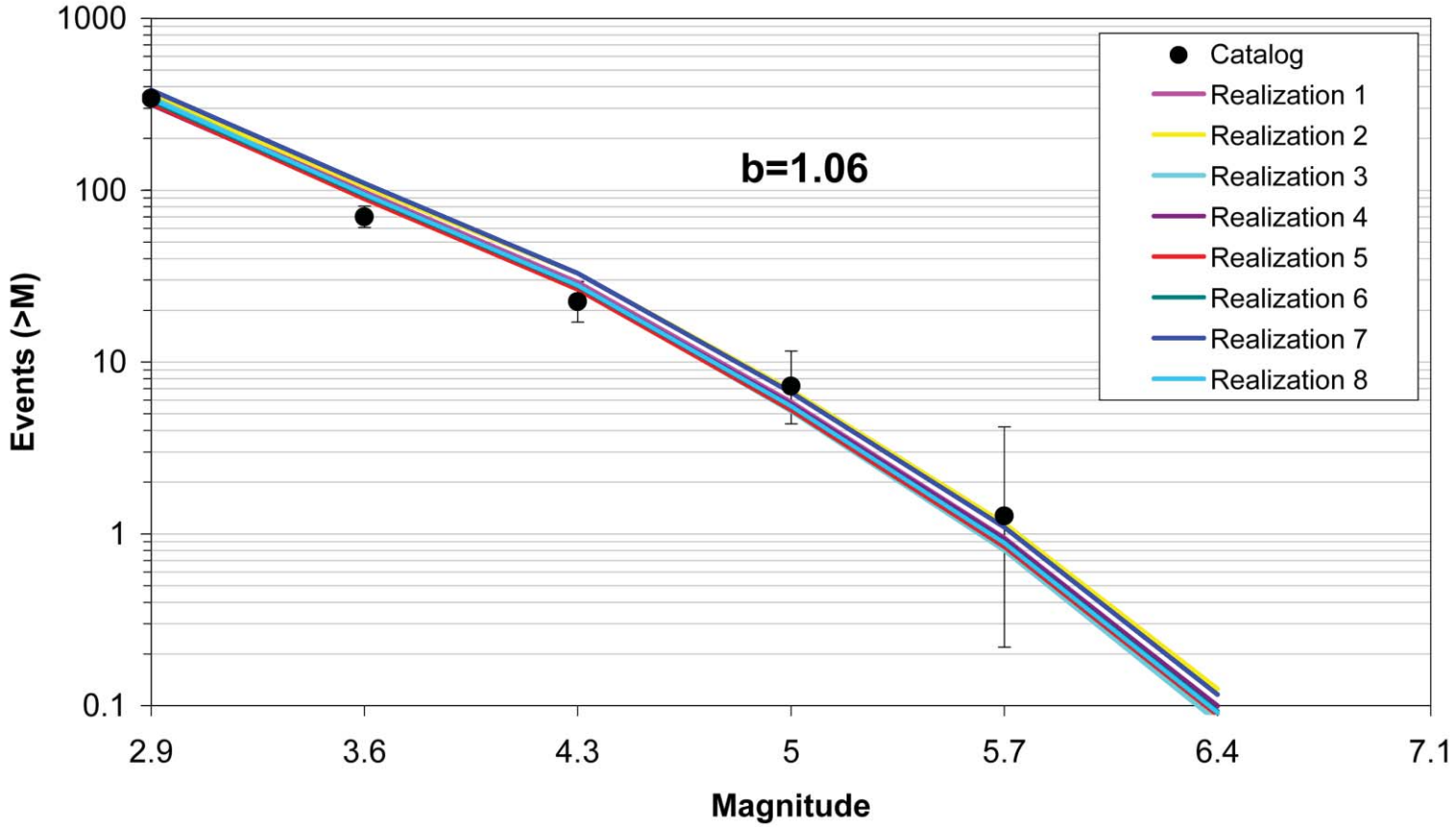

Figure 7.5.2-37
Comparison of model-predicted earthquake counts for PEZ_N using Case A magnitude weights. Error bars as in Figure 7.5.2-4.

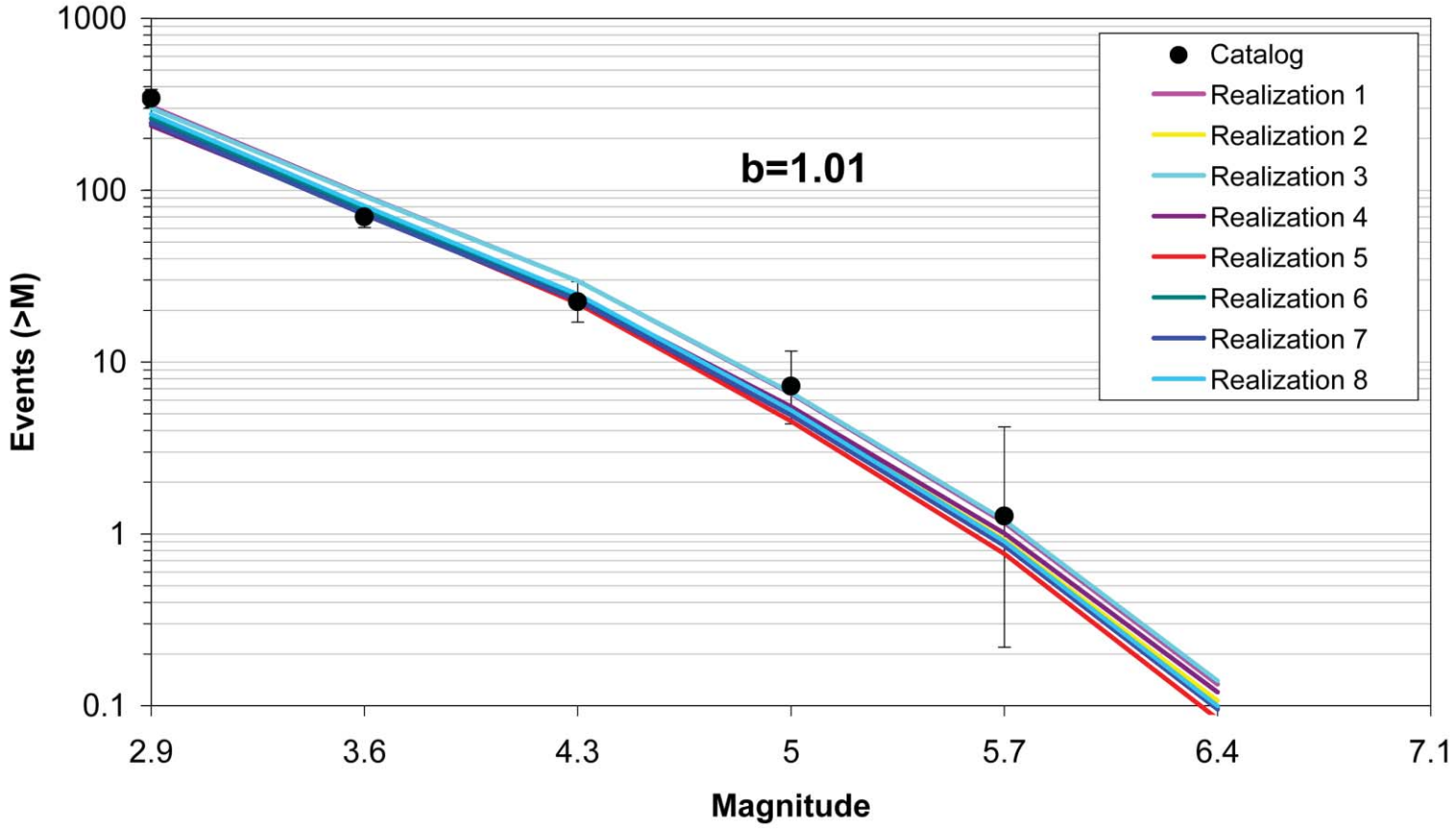

Figure 7.5.2-38
Comparison of model-predicted earthquake counts for PEZ_N using Case B magnitude weights. Error bars as in Figure 7.5.2-4.

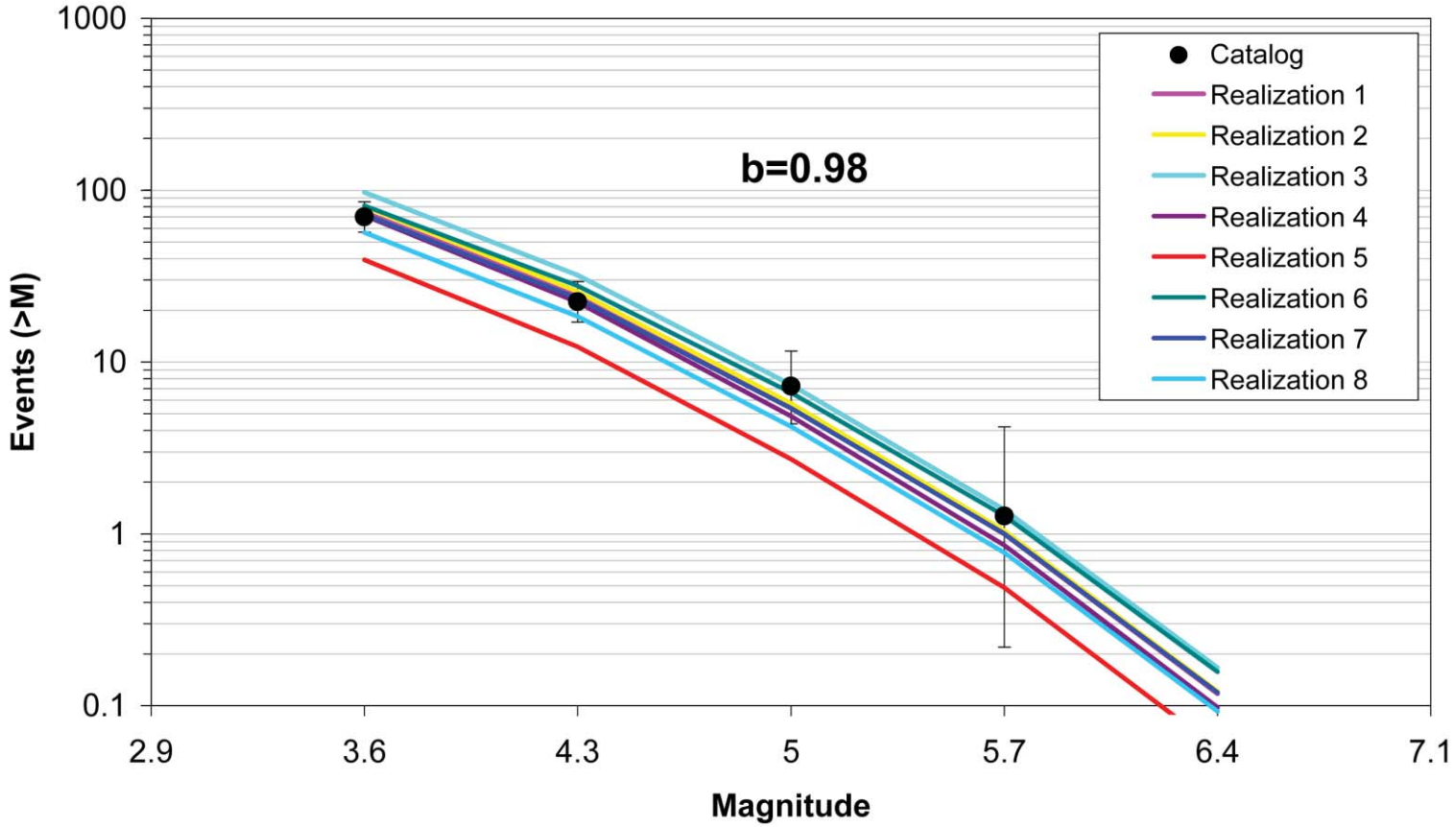

Figure 7.5.2-39
Comparison of model-predicted earthquake counts for PEZ_N using Case E magnitude weights. Error bars as in Figure 7.5.2-4.

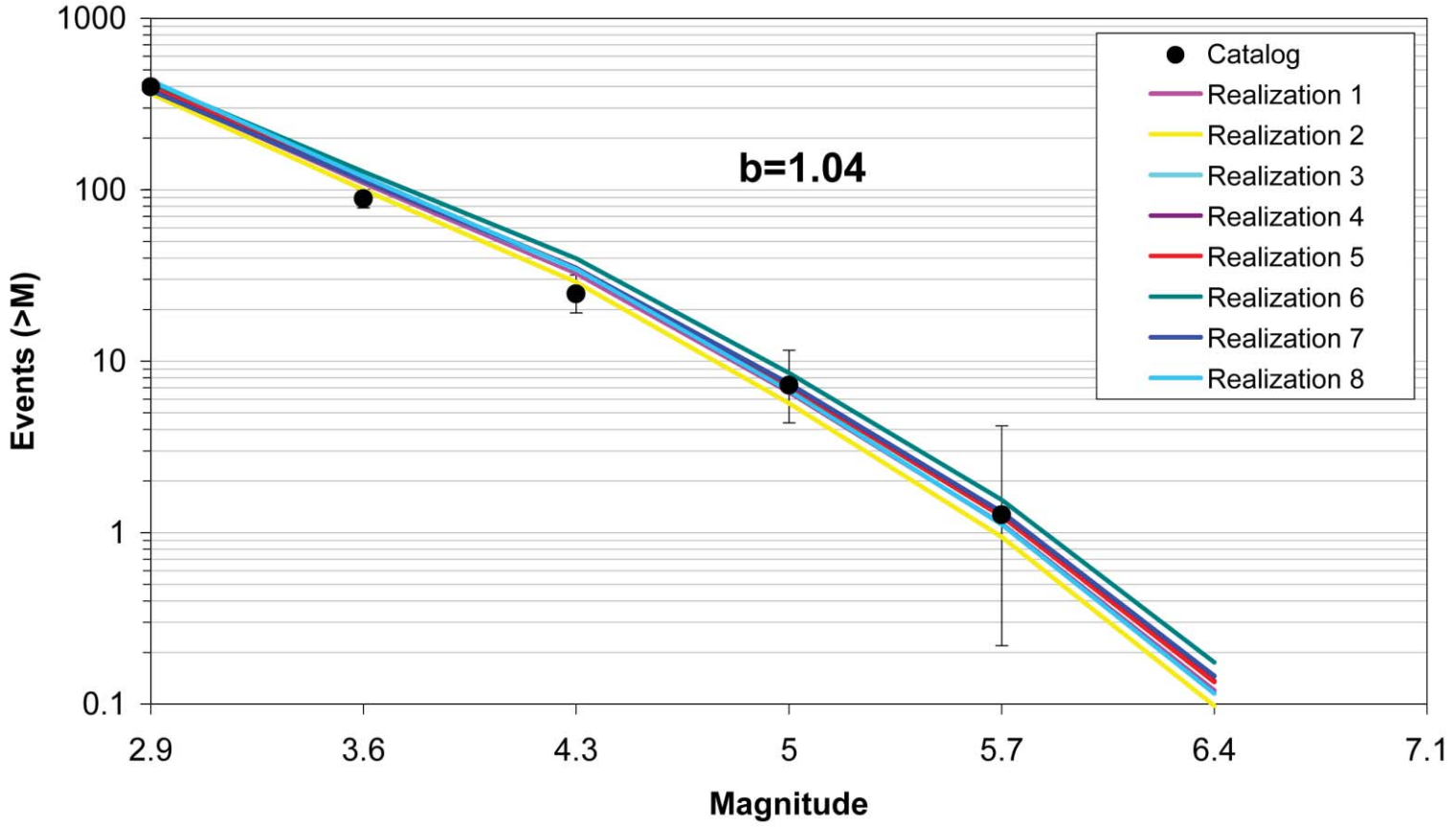

Figure 7.5.2-40
Comparison of model-predicted earthquake counts for PEZ_W using Case A magnitude weights. Error bars as in Figure 7.5.2-4.

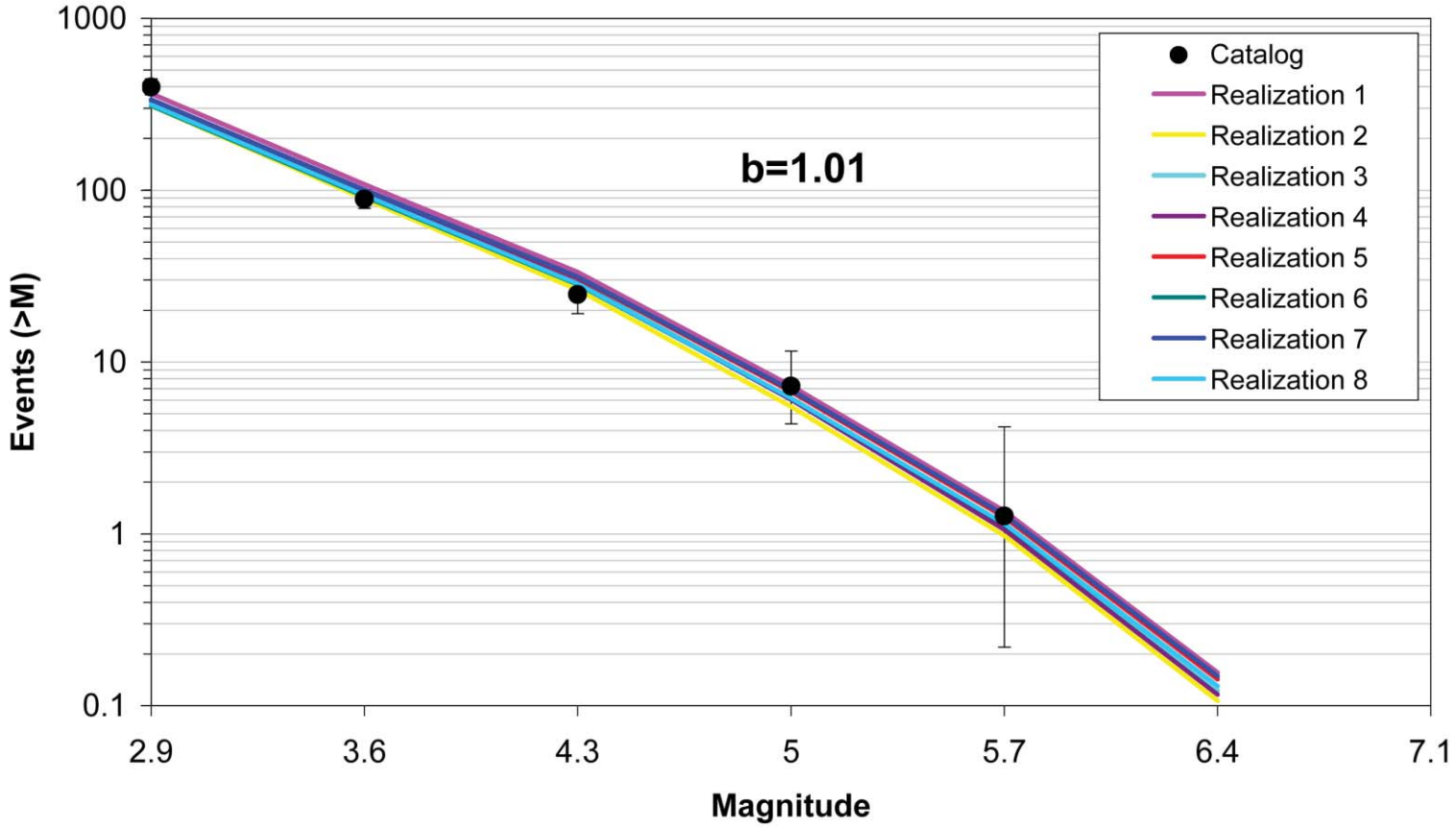

Figure 7.5.2-41
Comparison of model-predicted earthquake counts for PEZ_W using Case B magnitude weights. Error bars as in Figure 7.5.2-4.

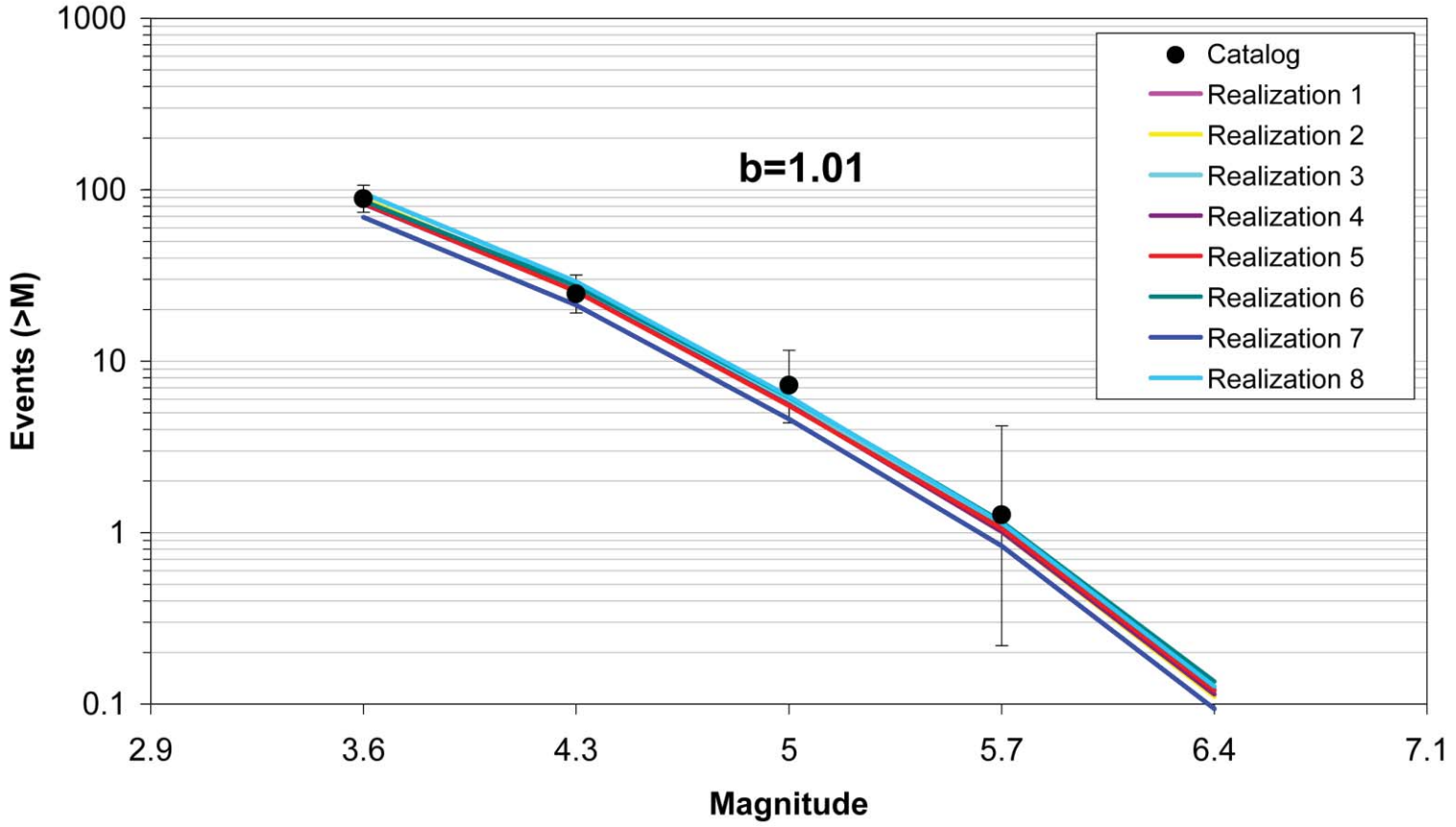

Figure 7.5.2-42
Comparison of model-predicted earthquake counts for PEZ_W using Case E magnitude weights. Error bars as in Figure 7.5.2-4.

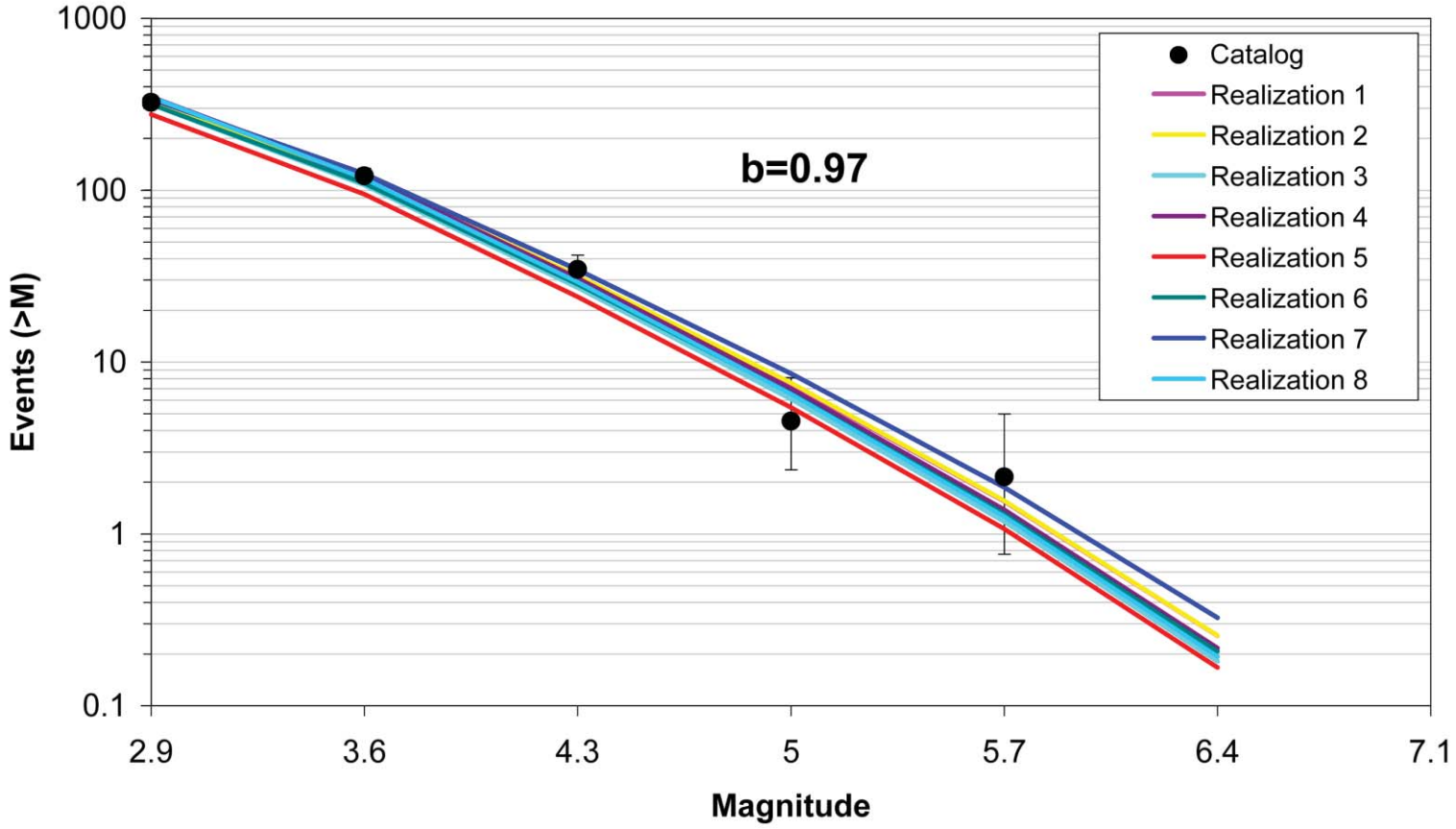

Figure 7.5.2-43
Comparison of model-predicted earthquake counts for RR using Case A magnitude weights. Error bars as in Figure 7.5.2-4.

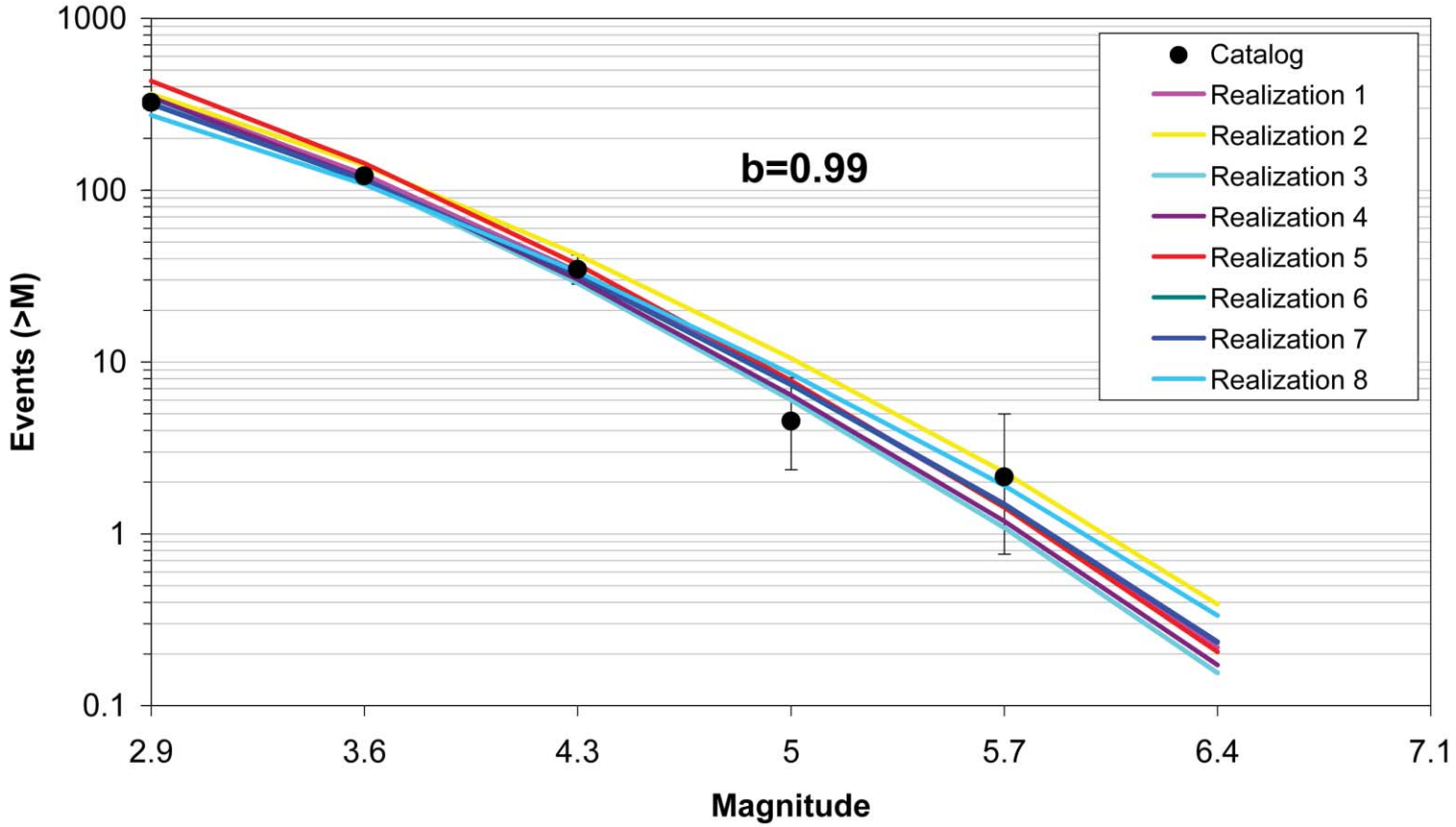

Figure 7.5.2-44
Comparison of model-predicted earthquake counts for RR using Case B magnitude weights. Error bars as in Figure 7.5.2-4.

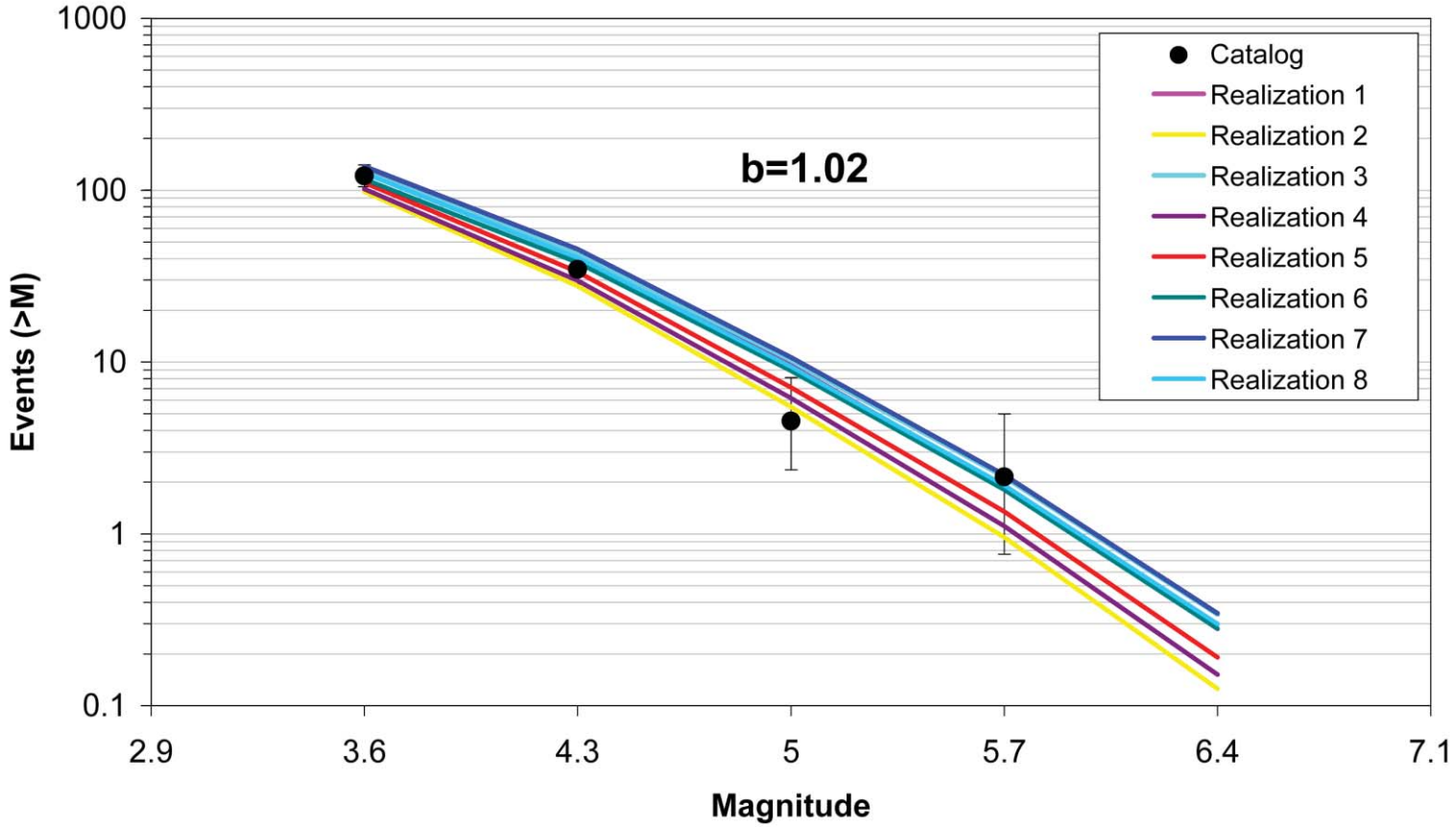

Figure 7.5.2-45
Comparison of model-predicted earthquake counts for RR using Case E magnitude weights. Error bars as in Figure 7.5.2-4.

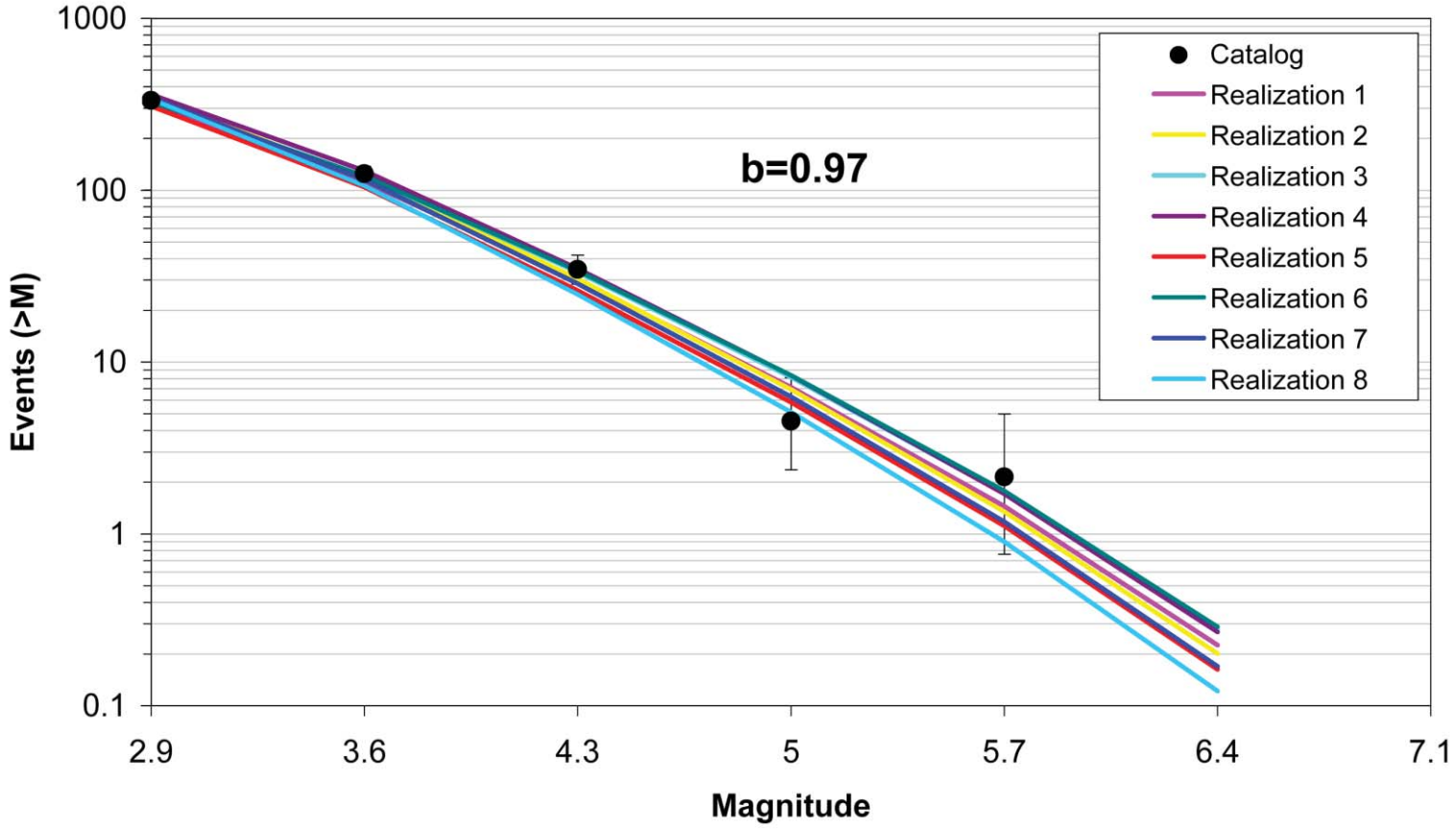

Figure 7.5.2-46
Comparison of model-predicted earthquake counts for RR_RCG using Case A magnitude weights. Error bars as in Figure 7.5.2-4.

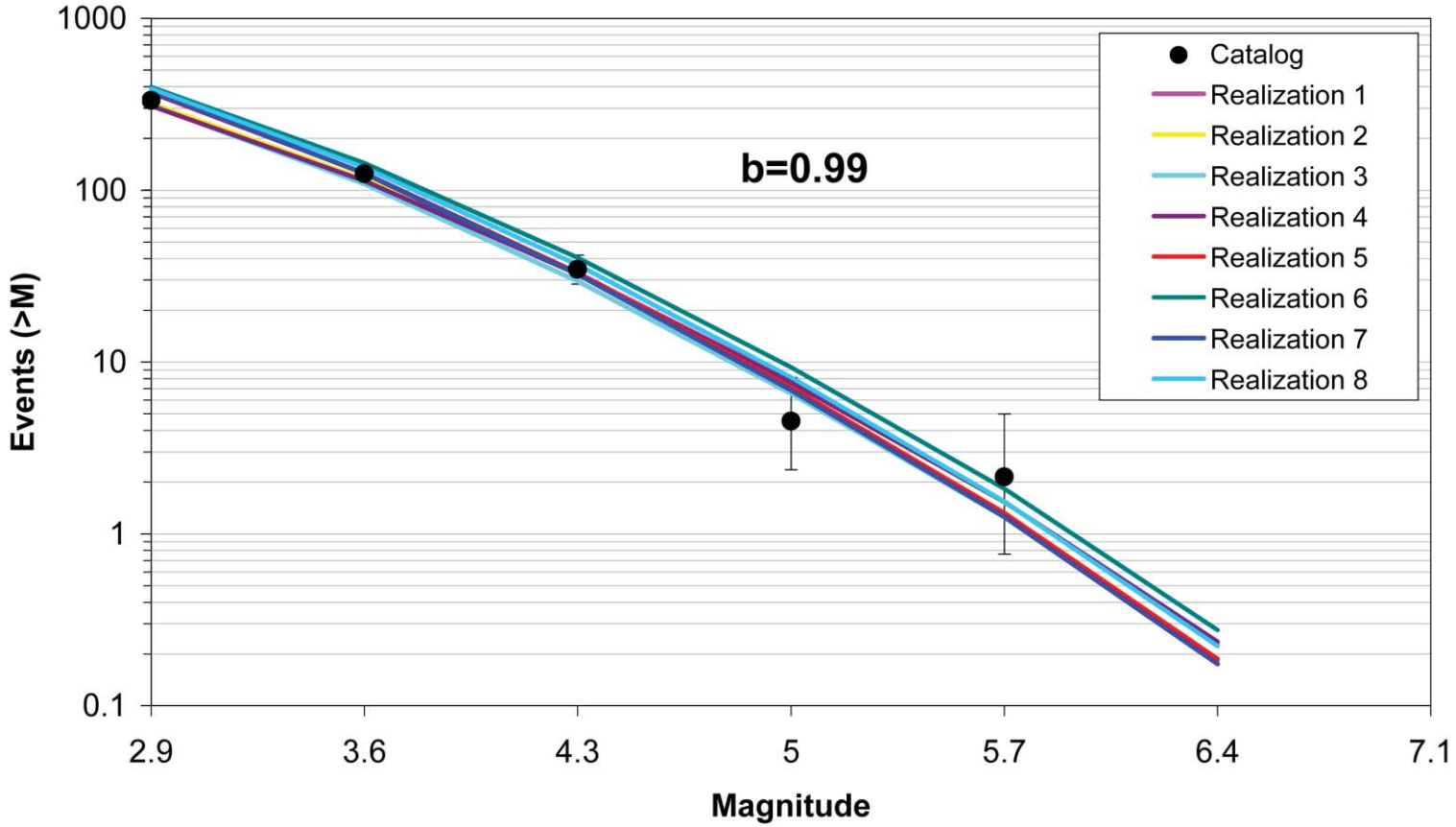

Figure 7.5.2-47
Comparison of model-predicted earthquake counts for RR_RCG using Case B magnitude weights. Error bars as in Figure 7.5.2-4.

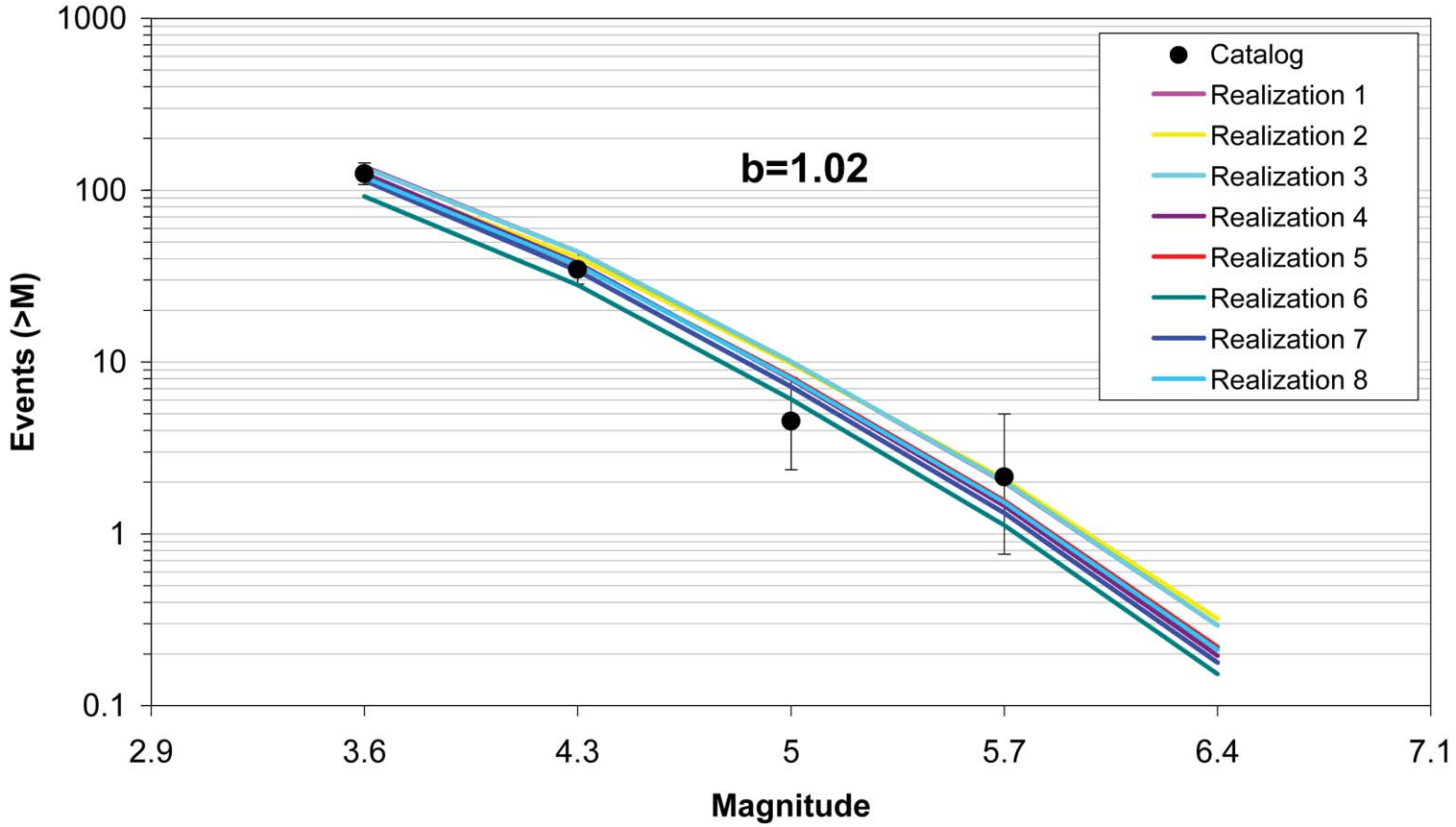

Figure 7.5.2-48
Comparison of model-predicted earthquake counts for RR_RCG using Case E magnitude weights. Error bars as in Figure 7.5.2-4.

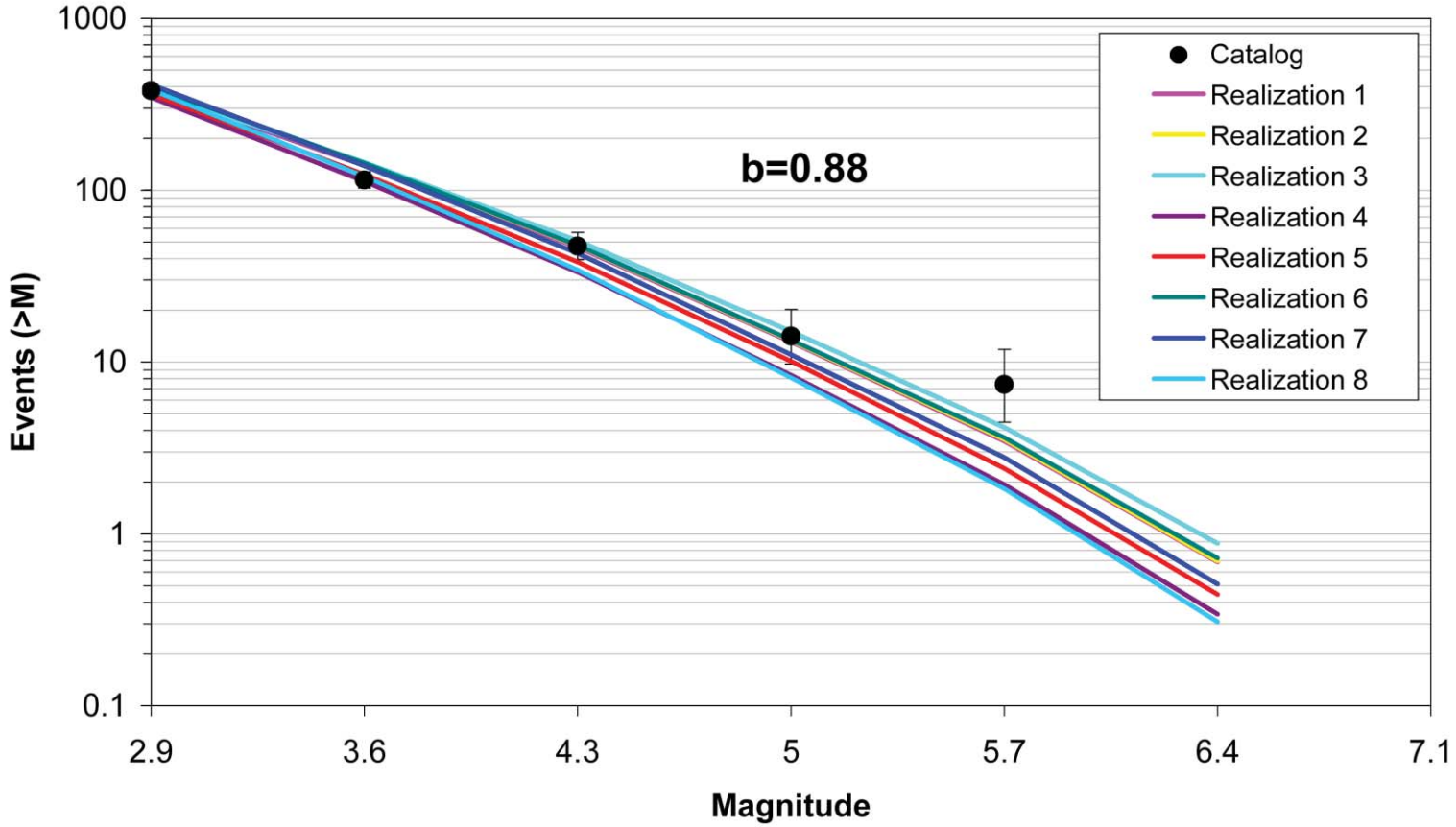

Figure 7.5.2-49
Comparison of model-predicted earthquake counts for SLR using Case A magnitude weights. Error bars as in Figure 7.5.2-4.

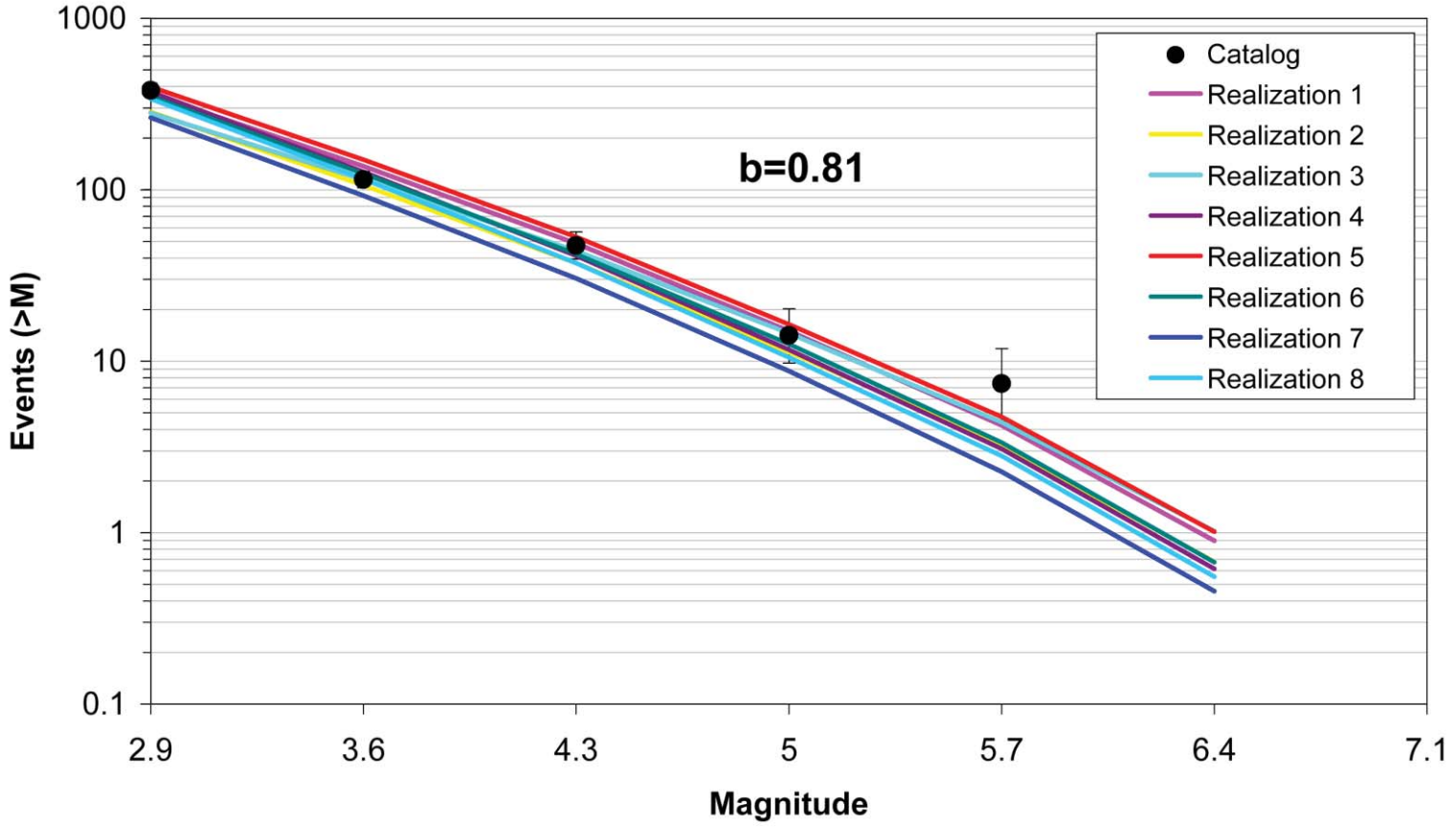

Figure 7.5.2-50
Comparison of model-predicted earthquake counts for SLR using Case B magnitude weights. Error bars as in Figure 7.5.2-4.

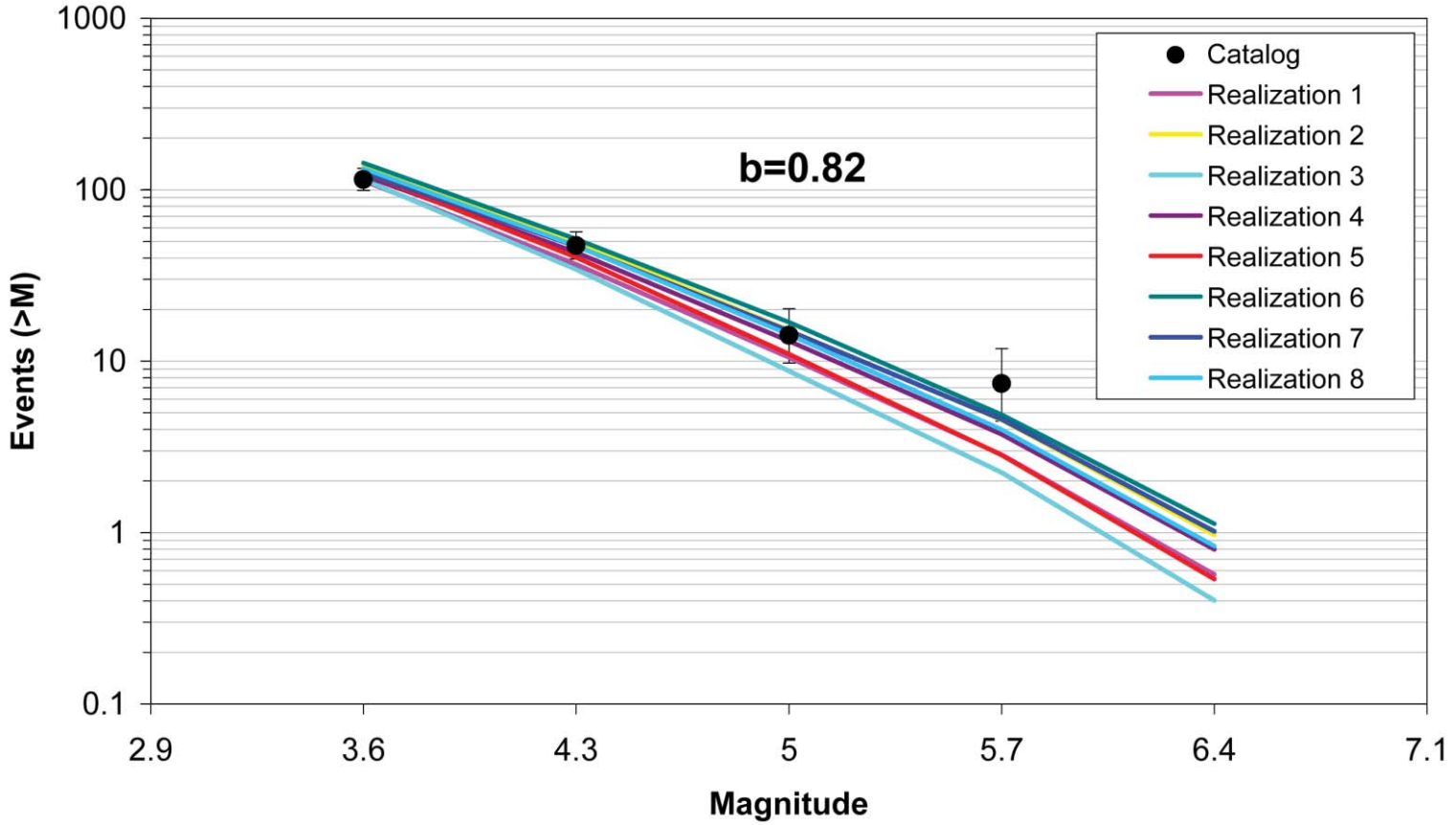

Figure 7.5.2-51
Comparison of model-predicted earthquake counts for SLR using Case E magnitude weights. Error bars as in Figure 7.5.2-4.